

Non-invasive high throughput monitoring of the exon-specific expression
of p53 isoforms identifies novel p53-tailored strategies for the treatment
of colorectal cancer



Dissertation
zur Erlangung des Doktorgrades
der Biomedizinischen Wissenschaften
(Dr. rer. physiol.)

der
Fakultät für Medizin
der Universität Regensburg

vorgelegt von
Deniz Tümen
aus
Bad Säckingen

Im Jahr
2023

Non-invasive high throughput monitoring of the exon-specific expression
of p53 isoforms identifies novel p53-tailored strategies for the treatment
of colorectal cancer



Dissertation
zur Erlangung des Doktorgrades
der Biomedizinischen Wissenschaften
(Dr. rer. physiol.)

der
Fakultät für Medizin
der Universität Regensburg

vorgelegt von
Deniz Tümen
aus
Bad Säckingen

Im Jahr
2023

Dekan: Prof. Dr. med. Dipl. Phys. Dirk Hellwig

Betreuer: PD. Dr. rer. nat. Karsten Gülow

Tag der mündlichen Prüfung:

„Wer es einmal so weit gebracht hat, dass er nicht mehr irrt, der hat auch zu arbeiten aufgehört.“

- Max Planck -

Content

1. Introduction	6
1.1 The Colon	6
The cecum and the appendix.....	6
The colon	6
The rectum	7
1.2 Colorectal Cancer	8
1.3 Therapeutic Strategies.....	11
Chemotherapy.....	11
Targeted therapies	11
Immune checkpoint inhibition.....	15
1.4 Tumor suppressor p53.....	17
1.5 Gene Editing	20
CRISPRs.....	21
Non-homologous end joining (NHEJ).....	22
Homology-directed repair (HDR).....	23
1.6 The Triple-EXSISERS Reporter System	24
Bioluminescence	24
Inteins.....	25
EXSISERS	27
Advantages over state-of-the-art methods.....	28
1.7 Objectives	29
2. Material and Methods	31
2.1 Molecular Cloning	31
Primer- and gene-fragment design.	31
PCR for molecular cloning.	31
DNA digestion with restriction endonucleases.	31
DNA agarose gel electrophoresis.	31
DNA ligation and Gibson assembly.....	32
Bacterial transformation and cultivation.	32
Bacterial strains used for DNA plasmid transformation.....	33
Plasmid DNA purification and Sanger sequencing.	33
p53 protein isoform overexpression in BL21 <i>E. coli</i>	33
2.2 Mammalian Cell Culture.	34
Cell lines and maintenance.....	34
Patient fibroblast isolation and maintenance.....	34

Content

Mycoplasma test.....	35
Seeding cell lines.....	35
Plasmid transfection.....	35
Overview of generated cell lines.....	35
Generation of stable EXSISERS cell lines with CRISPR-Cas9.....	36
p53-directed knock-out using CRISPR-Cas9.....	38
Gene expression manipulation using dCas9-VPR.....	40
Organoid generation and maintenance.....	40
Seeding colon organoids.....	41
Therapeutic treatment of cell lines, fibroblasts, and organoids.....	41
2.3 Protein Biochemical Analysis.....	43
Immunoblot analysis.....	43
Immunoprecipitation.....	44
p53 transcription factor binding assay.....	45
p53 transcription factor activity assay.....	45
Mass spectrometry sample preparation.....	46
Liquid Chromatography-Tandem Mass Spectrometry (LC-MS/MS analysis).....	46
2.4 DNA Design and Analysis.....	47
T7 Endonuclease assay.....	47
Genomic DNA isolation and genotyping.....	48
Design of EXSISERS constructs.....	48
2.5 RNA Analysis.....	49
Isolation of mRNA and generation of cDNA.....	49
Real-time quantitative PCR.....	49
Analytical PCR.....	50
2.6 Cellular and Molecular Imaging.....	50
Cell viability assay.....	50
Cell death assay.....	50
Immunofluorescence microscopy of cell lines.....	51
LIVE/DEAD staining/imaging of organoids.....	52
Live cell/real-time bioluminescence quantification.....	53
Computational differentiation of p53 isoforms.....	54
Anti-cancer drug library screening.....	55
2.7 Software.....	55
2.8 Contribution.....	56
3. Results.....	57
3.1 Establishment and optimization of a novel triple EXSISERS reporter system.....	57
3.2 Creation of a stable HCT116 triple-EXSISERS cell line by CRISPR/Cas9.....	66

Content

3.3 Functional integrity of tumor suppressor p53 and the EXSISERS reporters.	73
3.4 Experimental setup of the triple EXSISERS reporter system for real-time and live-cell quantitative measurements.....	77
3.4 Comprehensive analysis of the mutual interplay of FLp53, Δ40p53 and Δ133p53+ Δ160p53 in response to clinically established CRC-therapeutics.	78
3.5 Established protein analysis methods face challenges in detecting and quantifying the specific p53 protein isoforms.	82
3.6 Detection and quantification of p53 isoforms via multiple reaction monitoring mass spectrometry	86
3.7 High-throughput screening of differential p53 isoform expression in response to 4,863 anti-cancer compounds.	90
3.8 Identification of toxic anti-cancer compounds acting in an opposite p53-dependent manner.....	98
3.9 Complex-I inhibitor IACS-010759 specifically targets colon cancer and is innocuous to healthy and surrounding colon tissue.	104
4. Discussion	108
4.1 The journey towards an optimized triple-EXSISERS reporter system in <i>TP53</i>	109
4.2 Established protein analysis methods are challenging in terms of detection and quantification of the specific p53 isoforms.	112
4.3 Enhancing insights into p53's expressional behavior through high-throughput screening of over 4,863 anti-cancer compounds with EXSISERS	115
4.4 USP1 specific inhibitor SJB2-043 as a therapy for tumors with wildtype p53.	118
4.5 Mitochondrial respiratory chain complex I inhibitor IACS-010759 as a therapy for p53-mutated tumors.....	120
4.6 Future perspectives	122
5. Zusammenfassung.....	123
6. Abbreviations	125
7. References	129
8. Appendix	147
9. Declaration of Independence	154
10. Acknowledgement.....
11. Curriculum vitae
12. Publications

1. Introduction

1.1 The Colon

The colon is a crucial part of the digestive system in higher multicellular organisms, including humans [1]. It is located between the small intestine and the rectum. Primarily, the large intestine absorbs water and electrolytes from undigested food, consolidates waste materials, and facilitates the elimination of solid waste from the body [2,3]. The tube-like colon typically measures about 1.5 to 1.6 meters in length in adults. It is subdivided into the following functional parts: the cecum (including the appendix); the colon; the rectum; and the anal canal [4].

The cecum and the appendix are two distinct anatomical structures located at the lower right quadrant of the abdomen (Fig. 1). The cecum is the pouch-like structure that designates the start of the large intestine [5]. It receives undigested food material from the small intestine. The cecum serves as the reservoir for the arriving material, allowing for further absorption of water and electrolytes and the fermentation of certain vegetable fibers by the resident gut microbiota [6]. The appendix, on the other hand, is a small, finger-like projection that extends from the cecum. Although often considered a vestigial organ with no apparent function, studies suggest the appendix plays an important role in the immune system [7]. The appendix has been shown to have high concentrations of lymphatic cells and, therefore, is believed to constitute a part of the gut-associated lymphoid tissue [8]. It is also hypothesized that the appendix serves as a reservoir for gut bacteria, allowing for the recolonization of the intestine after infections or disruptions during an immune reaction [6].

The colon, which constitutes the largest portion of the large intestine, plays a prominent role in the reabsorption of water and vital nutrients from fecal matter. The mucosa, the innermost layer of the colon, consists of a surface lined with enterocytes, specialized epithelial cells that possess microvilli, increasing the absorptive and secretory surface area [9]. These cells collectively form a crypt-like macrostructure, further expanding the colon's surface area. Overlying the epithelial cell layer is a mucus layer primarily composed of densely packed glycoproteins called mucins. Goblet cells secrete mucins, which form a gel-like matrix that aids in the movement of intestinal contents. The closely packed epithelial cells and the mucus layer act as a physical barrier, safeguarding the interstitial space and neighboring organs from direct contact with luminal contents and microorganisms [10]. Beneath the mucosa lies the

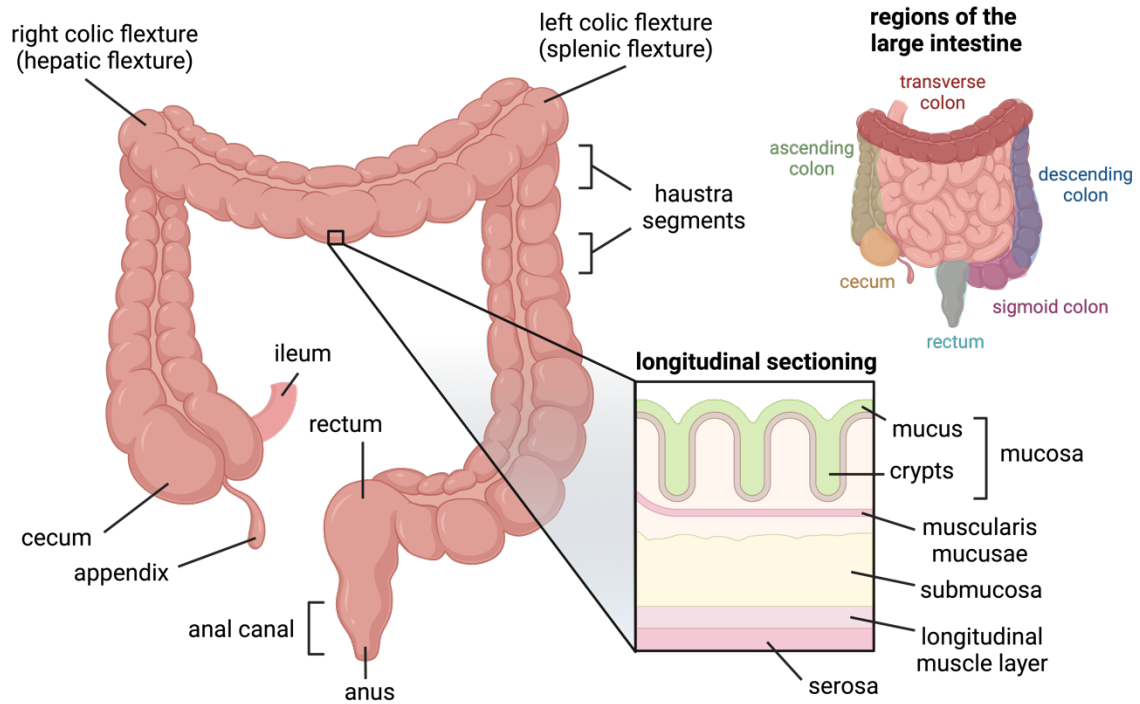


Figure 1: Structural schematic of the large intestine as part of the digestive system. The large intestine is structured in roughly 4 sections: ascending colon, transverse colon, descending colon, and sigmoid colon (upper right corner). Additionally, the large intestine is further subdivided into functional units with their own corresponding task (left image). From a histological point of view, the intestine's interior is spanned by so-called microvilli, which are filamentous protrusions of the cell membrane. These structures are mainly responsible for nutrition uptake. Due to the dense arrangement and strong cell-cell contacts, these cells form an impermeable barrier for noncorporeal particles and microorganisms (bottom right corner). This figure was created with BioRender.

submucosa, a layer of connective tissue housing blood vessels, lymphatic vessels, and nerves. These elements innervate the colon and ensure an adequate supply of nutrients. The muscularis layer is a vital component of the digestive system responsible for the rhythmic contractions of the large intestine. Comprising two distinct layers of smooth muscle, the muscularis plays a crucial role in the peristaltic movements that facilitate the efficient absorption of water and electrolytes while consolidating fecal matter for elimination [5].

The rectum serves as a temporary storage reservoir for fecal matter and plays a crucial role in the regulated elimination of waste from the body. Its ability to sense rectal fullness, coordinate defecation, and facilitate water reabsorption contributes to the overall efficiency of the digestive system.

Despite its vital functions, the colon is susceptible to various disorders and diseases. Common conditions affecting the colon include colorectal cancer, diverticulosis, inflammatory bowel disease (such as Crohn's disease and ulcerative colitis), and irritable bowel syndrome [11]. Regular screenings, such as colonoscopies, are recommended to detect early signs of abnormalities and prevent the progression of serious conditions [12,13].

1.2 Colorectal Cancer

Globally, colorectal cancer (CRC) ranks as the third most frequently diagnosed cancer (1.93 million/year) and the second leading cause of cancer-related deaths (935,173/year) worldwide [14]. The development of CRC occurs via three primary pathways, namely the adenoma-carcinoma sequence, serrated pathway, and inflammatory pathway [15]. It may arise from different etiology and molecular and genetic alterations (Fig. 2) [16]. Most cases are sporadic and largely influenced by environmental factors associated with Western lifestyle, including obesity, sedentary behavior, unhealthy diets, alcohol consumption, and smoking. The consequence of harmful environmental stimuli is the accumulation of induced mutations, which in turn promote the emergence and development of CRC [17].

During CRC progression, cancer cells usually pass four stages: initiation, promotion, progression, and metastasis [18]. Initiation is triggered by irreversible genetic damage, such as DNA adducts, which make the affected cells more susceptible to cancer development. The promotion stage is characterized by higher proliferation rates, resulting in abnormal cell growth (neoplasm). Subsequently, cancer cells progress through further genetic and epigenetic alterations and attain selective growth advantages. At this point, benign tumors usually transform into cancer cells and obtain aggressive metastatic potential. Metastasis represents the last and most dangerous stage, defined by the cell's ability to detach from the original tissue and spread into other organs through the blood or lymphatic system [18]. Colorectal cancer cells are known for their genetic instability, which is one of the primary reasons for CRC's aggressiveness and fast progressiveness. The three major genetic and epigenetic abnormalities include chromosomal instability (CIN), CpG island methylator phenotype (CIMP), and microsatellite instability (MSI) [19].

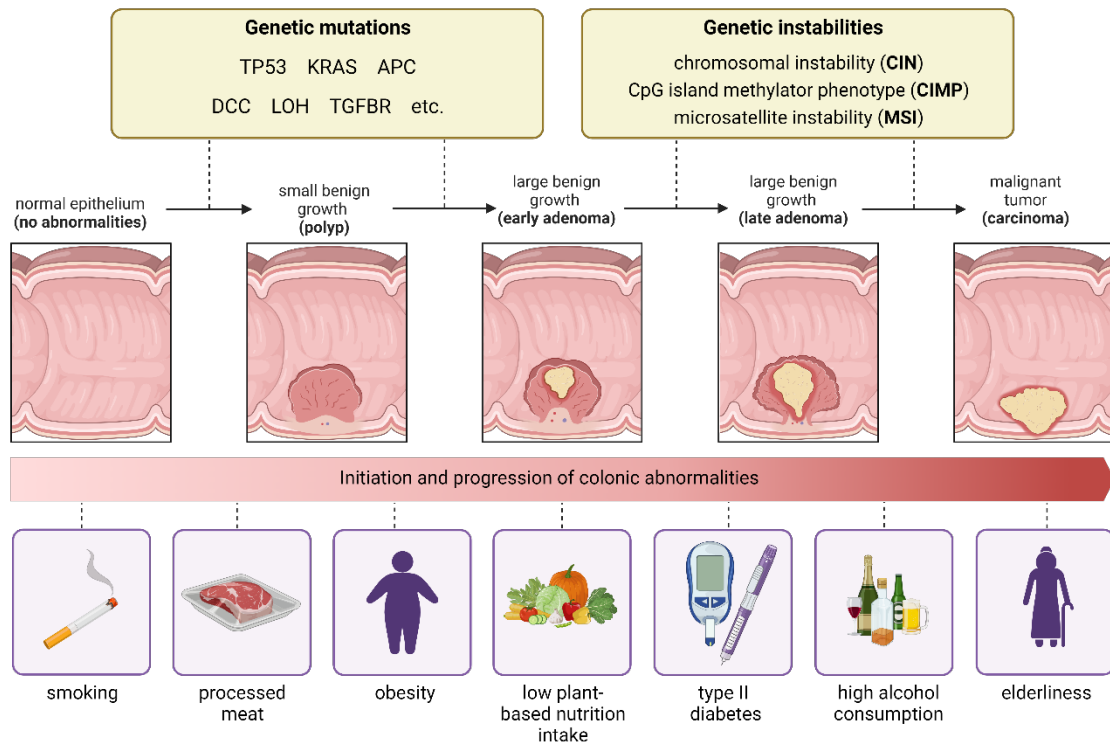


Figure 2: Causes and progression of colorectal cancer (CRC). Initiation and progression of CRC is a multi-stage process involving the aberrant transformation of healthy tissue into pathological tissue. The initiation and progression of CRC can be facilitated by multiple factors, including genetic instabilities, random or induced gene mutations, and etiological environmental factors. This illustration was created using BioRender.

CIN emerges from alterations in the structure and the copy number of chromosomes. These abnormalities arise from processing errors during mitosis [20]. CIMP refers to hypermethylation at specific regions of the DNA, called CpG islands, mainly located in promoter regions. Especially CpG-hypermethylation of tumor suppressor genes leads to the silencing of tumor suppressive abilities [21]. MSI is characterized by alterations in the DNA microsatellite length, often caused by the functional loss of genes responsible for DNA mismatch repair [22].

Due to these abnormal cellular processes, accumulation of mutations is often observed in specific genes. For instance, the initial stages of the sporadic CRC progression pathway often involve a loss of the Adenomatous-polyposis-coli (*APC*) gene. Disruption of the *APC* gene through genetic alterations or hypermethylation of its promoter region leads to the activation of the Wnt/ β -catenin signaling pathway [23]. This activation is considered a crucial event in the initiation of adenomas [24,25]. Mutant *APC* protein stabilizes β -catenin, resulting in its accumulation within the cytoplasm and subsequent translocation into the nucleus. Consequently, this process

Introduction

activates a set of genes involved in cell proliferation and growth [26]. Furthermore, the observation that many CRCs (50%) exhibit intact *APC* genes but a high frequency of activating mutations in β -catenin demonstrates the significance of Wnt/ β -catenin signaling in CRC development [27].

The *KRAS* pathway is another significant genetic pathway contributing to chromosomal instability in CRC. The *KRAS* gene belongs to the RAS family of oncogenes and is mutated in approximately 30-50% of CRC cases [28]. RAS proteins play critical roles in cellular processes, including cell division, differentiation, and apoptosis. A well-characterized pathway regulated by the RAS family is the Raf-mitogen-activated protein kinase (MAPK)-extracellular signal-regulated kinase (ERK) pathway, which mainly governs cell cycle progression [29]. Mutations in the *KRAS* gene impair its inherent GTPase activity, causing its accumulation in the active, GTP-bound conformation, consequently leading to the constitutive activation and stimulation of downstream pro-proliferative signaling pathways [30].

Another gene frequently mutated in all types of cancer is the tumor suppressor gene *TP53*, which is diagnosed specifically for CRC in about 60 % of all cases [31]. These mutations predominantly occur in exons 5 to 8, which comprise the DNA binding domain. Different types of p53 mutations play a pivotal role in determining the biological behavior of CRC, including factors such as invasive depth, metastatic sites, and patient prognosis. p53 mutations are associated with lymphatic invasion in proximal colon cancer and significantly correlate with lymphatic and vascular invasion in distal CRC[32]. In an international collaborative study on *TP53* in colorectal cancer, it was observed that patients with mutant p53 in exon 5 had worse outcomes, specifically in proximal colon cancer [32]. Furthermore, inactivating mutations of p53 occurred more frequently in advanced-stage tumors and were negatively associated with survival [33,34].

As Westernization progresses, the burden of CRC is increasingly shifting towards low- and middle-income countries. For 2040, the CRC burden is predicted to increase to 3.2 million new cases per year, approximately twice the current incidence rate [35]. Therefore, new therapeutic strategies are urgently required to prevent the associated mortality rates from rising along with the yearly increasing incidences.

1.3 Therapeutic Strategies

Due to advances in primary and adjuvant therapy, the survival rates for CRC have shown progressive improvement [36]. Ideally, the primary approach for CRC treatment provides complete tumor and metastasis removal, typically requiring surgical intervention [37]. However, approximately 25% of all cases are diagnosed at advanced stages with metastases. Additionally, 20% of the remaining cases may experience metachronous metastases, posing challenges for curative surgical control and leading to tumor-related deaths [15,38,39]. For patients with unresectable lesions or ineligible for surgery, the primary objective is to aim for tumor size containment and inhibition of proliferation. Radiotherapy and chemotherapy are the predominant therapeutic strategies for these patients with unresectable lesions [40,41].

Chemotherapy options for CRC include single-agent- or combined-agent therapy (Fig. 3) [36]. Single-agent treatment, mainly based on fluoropyrimidine (5-FU), remains the first-line therapeutic strategy. However, combined-agent strategies with additional chemotherapeutics have shown significant benefits in terms of overall survival [42,43]. Most commonly used chemotherapeutic regimens are drug combinations such as FOLFOX (folinic acid (FOL), 5-FU, and oxaliplatin (OX)), FOXFIRI (5-FU, OX, and irinotecan (IRI)), CAPOX (capecitabine (CAP)+OX), and CAPIRI (CAP+IRI) [36,44]. Further multiple agent regimens, including FOLOXIRI (folinic acid, 5-FU, OX, and IRI), are infrequently administered since increasing numbers of combined chemotherapeutics may lead to higher toxicity [45,46]. Multiple studies have demonstrated that the utilization of chemotherapy, particularly in patients with CRC and metastases, has significantly extended their overall survival (OS) time to nearly 20 months [47,48]. However, these treatments show severe drawbacks, including systemic toxicity, insufficient response rates, emerging therapeutic resistance, and low tumor-specificity [18,49]. Moreover, the chemosensitivity of CRC to 5-FU and OX highly depends on the cellular p53 status [50–52].

Targeted therapies affect cancer cells by directly impeding cell proliferation, differentiation, and migration. Additionally, these therapies have the potential to modify the microenvironment of the tumor. Targeted therapies can induce structural remodeling of local blood vessels or even stimulate immune cells to recognize the aberrant nature of tumor cells. Small molecules, such as monoclonal antibodies, play a crucial role in targeted therapies [53,54]. These molecules possess a molecular

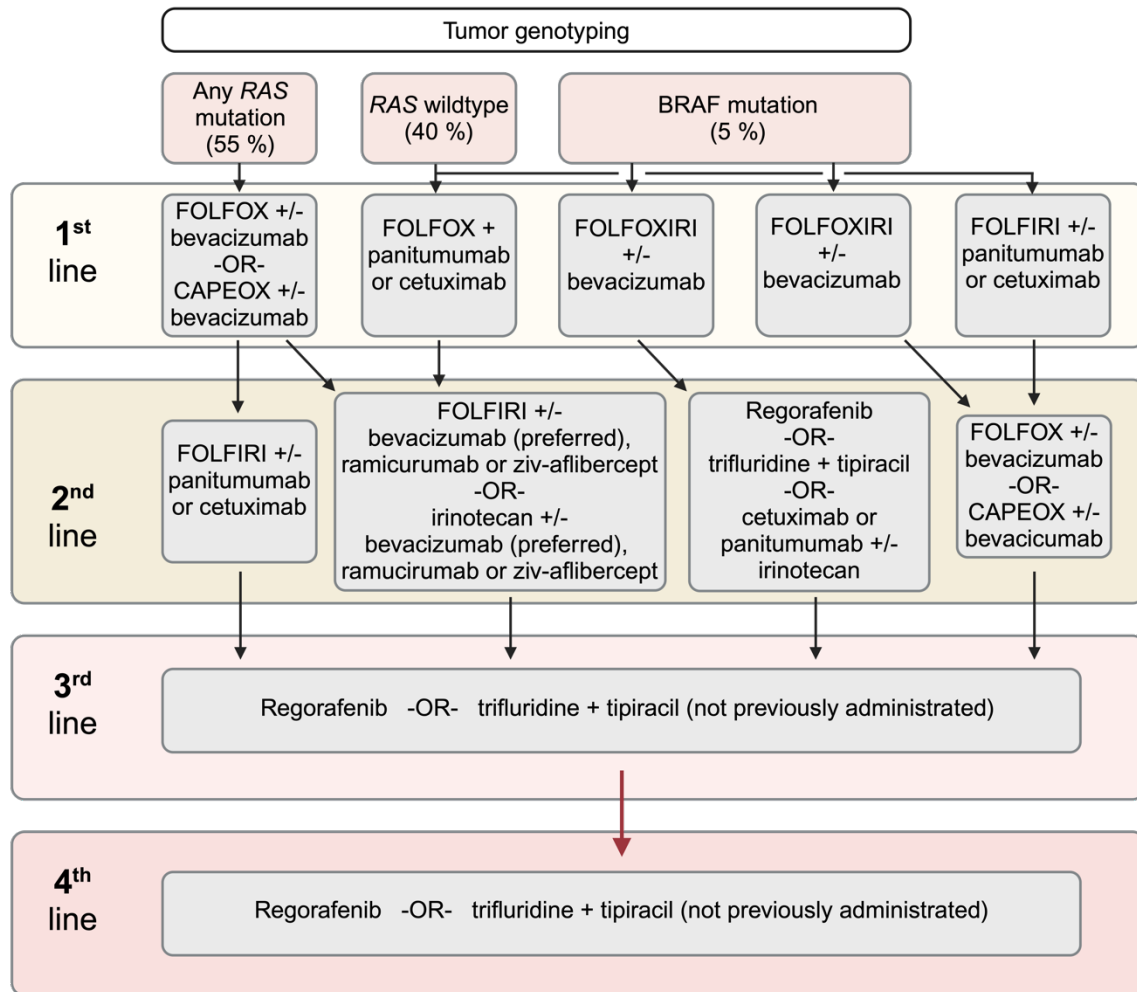


Figure 3: Treatment strategies of CRC. The establishment of a multi-sequence strategy for addressing CRC historically required numerous clinical studies to develop the optimal sequence of chemotherapeutic agents and targeted therapies. Depending on the genetic predisposition, different treatment strategies can be pursued. Often, dual combinations of chemotherapeutic agents along with EGF/R or VEGF/R inhibitors are used as initial therapy. In cases where patients exhibit suboptimal or refractory responses to first-line therapeutic modalities, a hierarchical succession of second line, third line, and fourth line therapeutic regimens is deployed. These therapeutic modalities were predicated upon empirically determined by the maximal probability of therapeutic responses. This illustration was created using BioRender.

weight of less than 900 Da, usually allowing to permeate cell membranes and predominantly exert their effects within the cell. By selectively inhibiting specific enzymes, small molecules can disrupt tumor cell growth or even trigger apoptosis [36,55,56].

The **EGFR pathway** belongs to the ErbB (erythroblastosis oncogene B)/HER (human epidermal growth factor receptor) family that comprises four members, namely ErbB1 (EGFR/HER1), uErbB2 (Neu/HER2), ErbB3 (HER3), and ErbB4 (HER4) [36]. These receptors require ligand-dependent homo- or heterodimerization to activate

subsequent intracellular signaling pathways. These include the RAS/RAF/MEK/ERK, PI3K/AKT, and JAK/STAT3 (Janus kinase/signal transducer and activator of transcription 3) pathways, which induce several cellular processes such as cell growth, cell survival, and cell migration [57,58]. There are several approaches to prevent the initiation or propagation of growth signals. Most commonly, receptor-targeted monoclonal antibodies or kinase inhibitors are applied in clinics [36]. Cetuximab, a chimeric immunoglobulin G (IgG) antibody, for instance, binds to the external domain of EGFR and induces its internalization and degradation [59]. Previous studies confirmed cetuximab treatment to prolong OS in patients who previously had received and failed first-line therapies, including 5-FU, IRI, and OX [60]. Due to the potential antibody-dependent and subsequent cell-mediated toxicity of murine-human chimeric antibody cetuximab, the fully humanized antibody panitumumab has been developed. Panitumumab targets EGFR and occupies its ligand-binding sites to prevent receptor dimerization. Both anti-EGFR agents are FDA-approved first-line therapeutics for CRC treatment. However, these drugs did not demonstrate any significant superior effects concerning OS of patients, which is why the chemotherapeutic regimens are still preferentially administered [61]. Furthermore, these anti-EGFR drugs have only beneficial effects in patients with *RAS*- and *BRAF*-wild-type tumors [62].

The **VEGF/VEGFR pathway** is another commonly targeted pathway for CRC and metastatic CRC treatment. Vascular endothelial growth factors (VEGFs) and vascular endothelial growth factor receptors (VEGFRs) are involved in the angiogenesis of the proximal tissue, which describes the reformation and neof ormation of blood vessels. The VEGF family encompasses five members, namely VEGF-A, -B, -C, -D, and placental growth factor (PlGF), which can be considered ligands of the tyrosine kinase VEGF receptors. VEGFRs are categorized into VEGFR-1, -2, and -3, alongside the non-tyrosine kinase coreceptors neuropilin-1 (NP-1) and NP-2. VEGF receptors are homo- and heterodimerized upon ligand-binding on the extracellular receptor domain, activating the intracellular kinase domain [63]. Pivotal clinical trials evaluating the potential of antiangiogenic therapy for CRC started in 2004.

The first FDA-approved and, by now, the most efficacious therapeutic agent is the humanized IgG monoclonal antibody bevacizumab, which specifically targets VEGF-A and has demonstrated significant improvements in both progression-free survival (PFS) and overall survival (OS) in metastatic CRC. Several trials investigating

Introduction

bevacizumab in combination with mono-chemotherapy or FOLFOX/FOXFIRI double-regimens exhibited only partial significant improvements in either OS or PFS [64–67]. In addition to its first-line application, the efficacy of bevacizumab has been validated in various trials for the second-line treatment. There are higher PFS-, OS-, and higher response rates when combining FOLFOX with bevacizumab compared to FOLFOX alone [68].

To date, the FDA has solely approved bevacizumab as a first- and second-line VEGF-targeted agent for CRC. However, many novel agents are currently emerging, with some obtaining approval for CRC's second-line treatment [36]. Aflibercept, for instance, is a recombinant fusion protein of the extracellular domain of VEGFR-1 and VEGFR-2. Thus, aflibercept acts as a ligand trap for VEGF-A, VEGF-B, and PlGF ligands, intercepting the ligand binding to their corresponding receptors [69]. In the first-line setting, the combination of aflibercept and FOLFOX did not yield significant benefits in terms of PFS and OS. The administration of aflibercept and FOLFOX after OX or bevacizumab first-line treatment demonstrated better response rates and longer PFS and OS. Therefore, aflibercept is recommended as the second-line CRC agent [70].

Ramucirumab, an FDA-approved drug for second-line treatment of metastatic CRC, is a fully-humanized monoclonal IgG antibody that targets VEGFR-2. The combination of ramucirumab and FOLFIRI significantly prolonged PFS and OS [71].

Tyrosine kinase inhibitors (TKIs) have emerged as an effective therapeutic option for patients with non-small cell lung cancer (NSCLC) resistant to anti-EGFR treatment. Concerning colorectal cancer (CRC), only a few drugs have demonstrated effectiveness. Regorafenib, a TKI with broad inhibitory effects, targets VEGFR, PDGFR (platelet-derived growth factor receptor), FGFR (fibroblast growth factor receptor), and BRAF [36]. It has received FDA-approval for the treatment of metastatic CRC. While first-line studies investigating the combination of regorafenib with FOLFOX treatment in CRC did not show any improvements compared to FOLFOX with placebo [72], regorafenib alone demonstrated superior median OS and PFS in refractory CRC compared to placebo [73].

The **HGF/c-MET pathway** comprises the hepatocyte growth factor (HGF) and its corresponding receptor, the mesenchymal-epithelial transition factor (c-MET or MET). Both factors are pivotal in governing various aspects of tumor biology, including

proliferation, cell survival, metastasis, and the development of acquired drug resistance [74,75]. Mesenchymal tissues predominantly secrete HGF. It was shown that patients with advanced CRC exhibit elevated HGF levels, which subsequently decrease after tumor resection [36].

The initiation of MET signaling begins upon HGF binding to the plasma membrane-resident MET receptor. Ligand binding induces the formation of an intracellular multifunctional docking site via phosphorylation of two tyrosine residues, subsequently facilitating the recruitment of downstream factors. The activated HGF/MET pathway triggers a cascade of signal transduction events involving the MAPK/ERK, PI3K/AKT, STAT/JAK pathways, and NF- κ B signaling. These signaling pathways collectively govern crucial physiological processes, such as hematopoiesis, organ regeneration, and wound healing [76]. Over 50 % of the CRC samples analyzed demonstrated a significant overexpression of HGF/c-MET, identifying this pathway as highly promising for targeted therapies [77–79]. Several strategies have been explored to impede the maturation process of pro-HGF or block its interaction with its respective receptors. One effective method involves the application of a humanized monoclonal antibody known as rilotumumab. This specific antibody has proven to prevent the binding of pro-HGF to its corresponding receptors, thus offering a potential avenue for therapeutic intervention [80].

Immune checkpoint inhibition recently crystallized as a novel targeting pathway to enhance immunorecognition and initiation of immune responses to cancer cells. Neoplastic malignancies characterized by a multitude of genetic and epigenetic alterations lead to the expression of aberrant antigens. These neo-antigens are processed and loaded on major histocompatibility complexes (MHC), which are recognized by T-cells of the host immune system. Secondary signaling events are orchestrated through the engagement of costimulatory or inhibitory receptors, which critically influence the activation and tolerance of T-cells [81,82]. This two-step verification serves as a pivotal control-mechanism in both physiological settings to avoid excessive immune responses and in pathological conditions, enabling the targeted elimination of abnormal cells [83].

Introduction

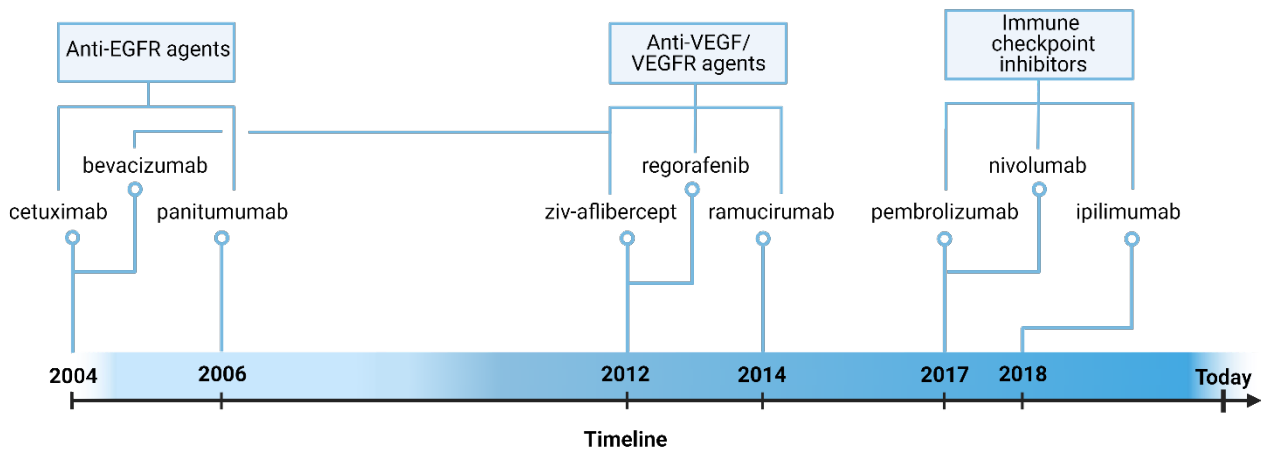


Figure 4: Timeline of approved targeted therapies for the treatment of colorectal cancer. Next to the preexisting chemotherapeutic agents, the FDA approved targeted therapies in 2004 as efficacious interventions for colorectal cancer. From 2004 to 2014, two strategies were primarily pursued, namely the antibody-based inhibition of EGFR and VEGFR. Subsequent to the revelation of tumor cells' capacity for checkpoint inhibition of the immune system, novel antibody-based therapies were developed and first authorized in 2017 to suppress this checkpoint inhibition, thereby, sensitizing the body's own immune response against tumor cells. This illustration was created by using BioRender.

"Immune escape" describes cancer cells' ability to evade this immune recognition. This behavior has been extensively observed across various types of cancer [84]. Immune evasion is attributed to several cellular response-reactions, including the secretion of immunosuppressive factors, such as TGF- β and IL-6, the recruitment of immunosuppressive cells, and the downregulation of MHC-I with the associated loss of immunogenicity [85,86]. Another significant mechanism contributing to immune escape involves T-cells' tumor-related inactivation and exhaustion, which is mediated by activating coinhibitory receptors, commonly known as immune checkpoint receptors. Such receptors located at the surface of T-cells include programmed cell death protein-1 (PD-1) and cytotoxic T lymphocyte antigen 4 (CTLA-4). PD-1 binds to its ligand PD-L1, representing a peripheral immune checkpoint on tumor, stromal, and immune cells [82,87]. CTLA-4 binds to its ligands CD80/CD86, depicting a central immune checkpoint on antigen-presenting cells (APCs). CTLA-4 activation **1.** leads to decreased IL-2 secretion, and **2.** competes for binding with B7-1/B7-2, thus reducing the stimulatory effect of CD28 on T cells. The activation of PD-1 results in the inhibition of downstream pathways, including the PI3K/AKT pathway, causing **1.** an absence in T-cell proliferation and **2.** an eventual development of immune anergy [88].

The objective of immune checkpoint targeted therapy is to support the immune system's ability to suppress and block the evasion of cancer cells. Current checkpoint inhibitors have been extensively investigated in various solid tumors. The first FDA-

approved therapeutic ipilimumab is a CTLA-4 inhibitor [89]. Further immune checkpoint inhibitors blocking PD-1/PD-L1 interaction are nivolumab and pembrolizumab [90–94]. The humanized IgG4 antibodies pembrolizumab and nivolumab were approved by the FDA in 2017 for metastatic CRC treatment (Fig. 4). Current first-line therapy approaches involve the utilization of either immunotherapies or combinational chemotherapy. The choice of the appropriate therapy depends on whether the tumor exhibits high/low microsatellite instability (MSI-H/L) and deficiencies in mismatch repair (MMR) mechanism. If CRC tumors exhibit high microsatellite instability (MSI-H) and deficient mismatch repair (dMMR), pembrolizumab alone or a combination of nivolumab and ipilimumab are administered first-line. Vice versa, low MSI (MSI-L) and proficient MMR (pMMR) CRC patients receive chemotherapy regimens [95]. Nowadays, medicine is increasingly embracing personalized approaches, which is exemplified by the extended first-line therapeutic options. In the case of chemotherapeutic administration, these therapies are often associated with severe drawbacks, including systemic toxicity, insufficient response rates, emerging therapeutic resistance, and low tumor specificity [18,49]. Moreover, the chemosensitivity of CRC to 5-FU and OX highly depends on the genetic p53 status [50,51]. For this reason, there is a greater need for p53-tailored and personalized medicine.

1.4 Tumor suppressor p53

The tumor suppressor p53, often referred to as the "guardian of the genome" [96], plays a crucial role in regulating cellular metabolism, proliferation, and viability [97–100]. Cellular abundance and activity of p53 are precisely regulated by its E3 ubiquitin-protein ligase Mdm2, which responds to a spectrum of intrinsic and extrinsic cellular stressors [101]. Under physiological conditions, Mdm2 binds to p53 and covalently transfers ubiquitin units designating p53 for proteasomal degradation. The suppression of Mdm2 activity (due to stress signals) leads to an extension in the half-life of p53 and triggers its transcriptional activation [97]. Activated p53 orchestrates the transcription of a large repertoire of genes involved in tumor suppression (Fig. 5). It encompasses activation of pathways shutting down proliferative and metabolic activity in case of pathophysiological changes and cellular damages [102]. Moreover, p53 activation triggers cell cycle arrest in response to DNA damage and initiates apoptosis [103] by either directly interacting with pro- (Bax, Bak) and anti-apoptotic BCL-2 family

members (Bcl2, Bcl-xL) [104] or stimulating the transcription of downstream pro-apoptotic target genes (PUMA, APAF1) [105–107].

Contrarily, p53 also has the potential to induce pro-survival pathways by transcriptionally activating downstream target genes that counteract apoptosis [108]. Cell fate and the predominantly activated pathway highly depend on the differentially expressed p53 protein isoforms and their respective cellular ratios [109,110].

Traditionally, the scientific community adhered to the notion that one gene corresponds to one protein product. However, human genome sequencing disrupted this long-held dogma, revealing that approximately 98% of human genes undergo alternative splicing and harbor multiple transcriptional products [111]. *TP53* is located on the human chromosome 17p13.1 and comprises 13 exons, with the first exon being non-coding. The subsequent exons are coding sequences that additionally underlie differential exon usage. Due to multiple alternative splicing events, alternative promoter usage, and alternative translation start sites, *TP53* expression results in 13 different p53 protein isoforms, including Full Length (FL)p53 α , FLp53 β , FLp53 γ , p53 Ψ , Δ 40p53 α , Δ 40p53 β , Δ 40p53 γ , Δ 133p53 α , Δ 133p53 β , Δ 133p53 γ , Δ 160p53 α , Δ 160p53 β , and Δ 160p53 γ . p53 α -, p53 β -, p53 γ -, and p53 Ψ -isoforms originate from alternative splicing events. FLp53, Δ 40p53, Δ 133p53, and Δ 160p53 differ in their N-terminal length and are generated through alternative promoter usage and alternative translation start sites [110]. The subsequent sections focus on the N-terminally varying isoforms FLp53, Δ 40p53, Δ 133p53, and Δ 160p53. These specific isoforms and their cellular ratio have been established to serve as the principal determinants in differential pathway initiation and subsequent cell fate determination [111–114].

FLp53 consists of three functional domains: 1. transactivation domain (subdivided into TAD I and TAD II), 2. conserved DNA binding domain (DBD), and 3. oligomerization domain (OD) encompassing a nuclear localization signal (NLS) [115]. FLp53 induces transcription of downstream genes responsible for cell cycle arrest, apoptosis, and metabolic regulation [16]. Δ 40p53 is an N-terminally truncated isoform lacking TAD I (1–40 aa), thus representing a transcriptionally inactive protein isoform [116]. Elevated Δ 40p53:FLp53 ratios are linked to increased apoptosis and lower tumor recurrence rates [117,118]. Δ 133p53 and Δ 160p53 are N-terminally truncated isoforms lacking TAD I and II. Both isoforms are known for their pro-survival abilities [119,120].

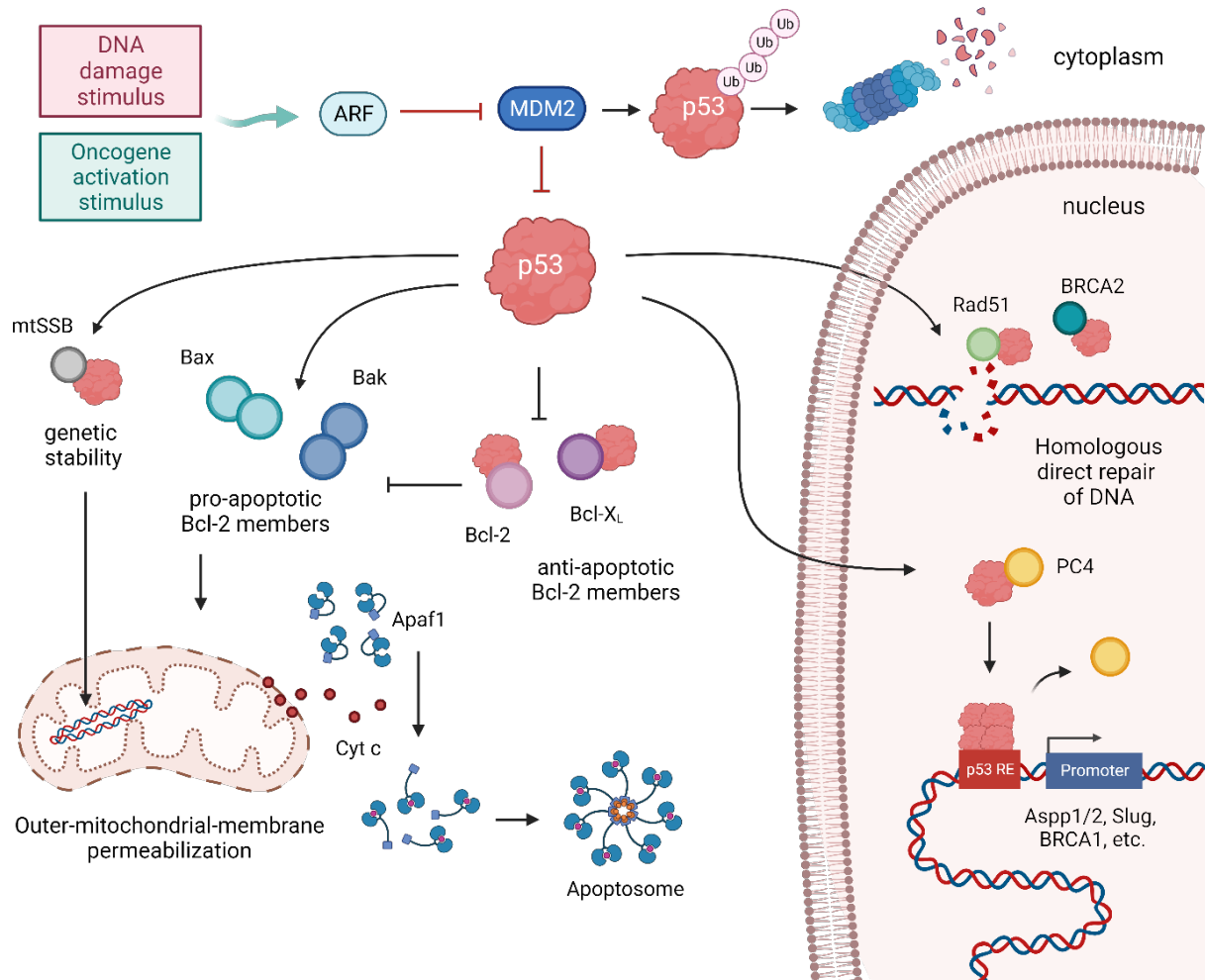


Figure 5: The tumor suppressor p53 is subject to rigorous regulation due to its capability to govern a multitude of pivotal cellular processes. The activation of p53 is triggered by DNA damage stimuli or oncogene-activating stimuli, which in turn decrease the interaction capability between p53 and its E3 ubiquitin ligase MDM2. p53 has a multitude of modalities. It can either function as a nuclear transcription factor to target and promote various downstream genes, or directly bind protein interaction partners that are either involved in DNA damage recognition and DNA repair or in the initiation of intrinsic apoptosis. This illustration was created by using BioRender.

Precise prediction of a treatment-dependent clinical outcome is challenging, particularly in tumors in which the genetic status of p53 exhibits substantial variability. Depending on the tumor type, the p53 mutational rate can be up to 50 % [121]. Most mutations are silent or missense mutations, not altering p53's transcriptional activity. Notably, approximately 30 % of all missense mutations mainly affect 5 residues (Arg273, Arg248, Arg175, Arg282, and Gly245), suggesting their functional significance for the regulatory role of p53 [122]. The residual mutations may not directly affect the functional integrity of p53 but can manifest within intronic regions, subsequently influencing alternative splicing or affecting promoter regions. These alterations often lead to imbalances in the expression of the p53 isoforms,

consequently influencing the regulation of essential cellular pathways [123]. Tumors with high genetic instabilities, such as colorectal cancer (CRC), demonstrate increased p53 alterations [124]. Consequently, we employ CRC as the tumor model for exploring the intricacies of p53 isoform regulation. To this aim, we stably integrated an exon resident and intein-luciferase reporter system to measure the differential exon usage during *TP53* expression. The process of stably integrating exogenous DNA (e.g., coding for reporter systems) into a host genome is called “gene editing.”

1.5 Gene Editing

Biotechnologists have long been focused on the development of tools for effective gene targeting and manipulation. Over the past decade, genome editing has made rapid advancements [125]. The first category of genome editing enzymes executed in prokaryotes is referred to as homing endonucleases, also known as 'meganucleases.' These proteins can recognize specific double-stranded DNA motifs of 20 to 30 base pairs through specific protein-DNA interactions [126]. Another notable development involves the successful editing of eukaryotic genomes using synthetic fusion proteins that combine the dsDNA recognition of zinc finger domains (3 base pairs per ZF domain) and the dsDNA cleavage activity of the catalytic domain of FokI, a type IIS restriction enzyme [127]. These engineered zinc finger nucleases (ZFNs) have demonstrated their efficacy in cleaving specific target sites and performing subsequent edits in the genomes of eukaryotic model organisms such as animals, plants, and human stem cells [128]. A similar approach involves the use of transcription activator-like enhancer nucleases (TALENs), where the FokI nuclease domain is fused to the TALEN protein, which typically possesses an 11-domain dsDNA recognition domain [129,130]. Both ZFNs and TALENs generate dsDNA cleavage and function as dimeric nucleases. Despite their long-lasting success, ZFNs, TALENs, and homing endonucleases have a practical drawback, as their DNA-binding domains must be adjusted according to the target sequence. This procedure is an elaborate process that requires multiple steps in protein engineering.

The first instance of utilizing guide molecules consisting of nucleic acids that target their complementary nucleic acid sequences was accomplished using Argonaute proteins. As part of the eukaryotic RNA interference (RNAi) pathway, the eukaryotic Argonaute (eAgo) proteins harbor short RNA guides to locate a matching mRNA sequence. This process can lead to the binding or cleavage of the mRNA transcript,

resulting in the silencing of gene expression [131,132]. Gene editing has reached a new era with the discovery of clustered regulatory interspaced short palindromic repeats (CRISPR) and the associated nuclease (Cas). The CRISPR/Cas system is the most efficient tool for direct dsDNA targeting and gene engineering. The first instances of programmable DNA cleavage by the Cas9 nuclease [133,134], as well as subsequent early demonstrations of its ability to achieve targeted genome modifications in living eukaryotic cells, sparked a significant increase in exploring, developing, and using CRISPR-Cas as a genome editing tool [135–139].

CRISPRs were first identified in *Escherichia coli* (*E. coli*) in 1987 when scientists accidentally cloned an unusual series of repeated sequences interspersed with spacer sequences [140]. The same sequences were found in numerous other bacterial and archaeal genomes. For the first time, these sequences were referred to as CRISPRs [141]. During the early 2000s, scientists observed the similarity between the spacer sequences found in bacteria to those in bacteriophages, viruses, and other bacterial plasmids. Further investigation revealed that bacteria carrying these homologous spacer sequences were resistant to infection by corresponding viruses. This finding strongly suggested the involvement of CRISPR in the adaptive immune system of prokaryotes [142]. Upon viral infection, the CRISPR spacer sequences undergo transcriptional activation, producing short CRISPR RNA (crRNA) molecules directing Cas protein to cleave viral DNA or RNA sequences complementary to the crRNA. Consequently, the CRISPR/Cas system serves as a robust defense mechanism, preventing recurrent infections by the same virus [143]. CRISPR-Cas systems have been categorized into two main groups: class 1, which utilizes multiprotein complexes for nucleic acid cleavage, and class 2, which employs single-protein effector domains for cleavage [144,145]. Due to the advantages offered by single-protein effector domains, class 2 systems are the most widely used CRISPR tools in biological research and translational applications [146]. Among class 2 proteins, the Cas9 protein has found the highest utilization in laboratory settings. Cas9 exhibits RNA-guided endonuclease activity, which enables the generation of double-stranded breaks (DSBs) at target DNA sequences [147]. In their original environment, Cas9 nucleases are guided by CRISPR RNAs (crRNAs) that form base-pair interactions with trans-activating crRNAs (tracrRNAs), facilitating the assembly of ribonucleoprotein complexes [148]. However, for most Cas9 genome editing applications, single guide RNAs (sgRNAs) are employed. These sgRNAs are artificially

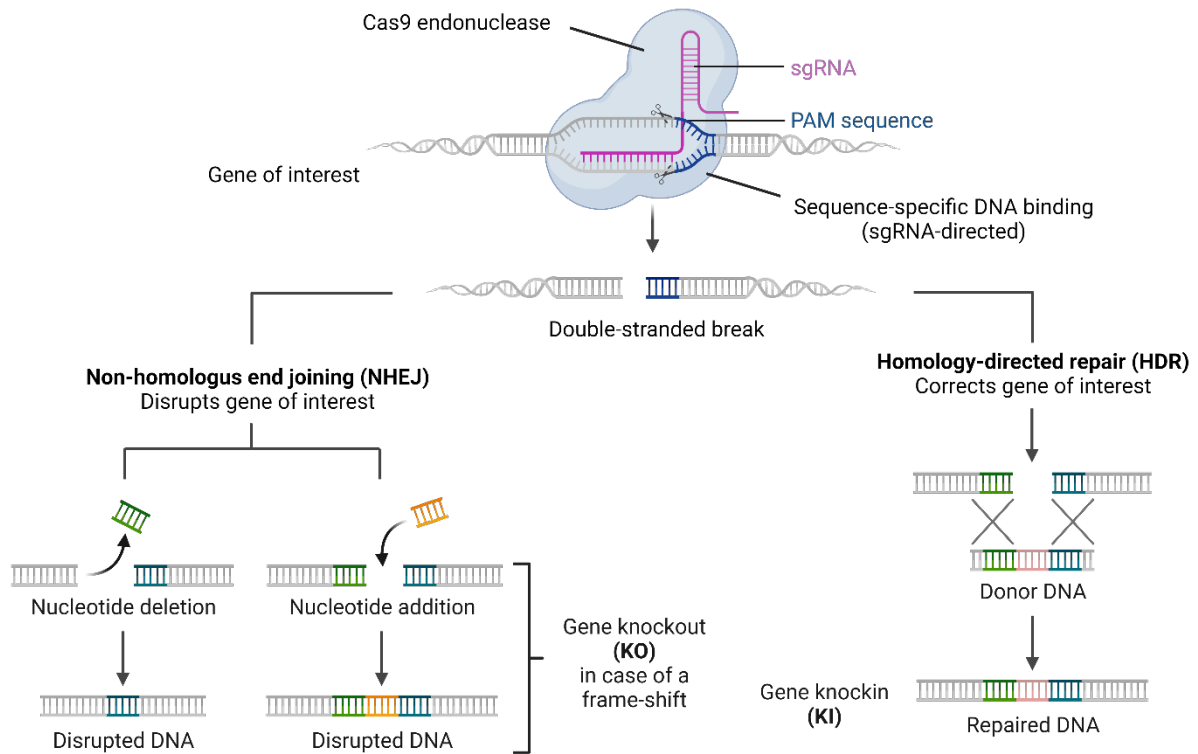


Figure 6: CRISPR/Cas9-mediated gene-editing. The Cas9 endonuclease is directed by a sgRNA to a complementary target sequence. Once directed, Cas9 generates a sequence-specific double strand break (DSB) and initiates cellular DNA repair mechanisms. In this context, two distinct repair mechanisms can be activated: 1. Non-Homologous End-Joining (NHEJ) is referred to as “non-homologous” due to the indiscriminate ligation of the broken DNA ends with minimal DNA reference. Without providing an appropriate template DNA, the cell shifts towards NHEJ and often generates gene knockouts (KO). 2. Homology-directed repair (HDR) is an intrinsic DNA repair mechanism that relies on DNA sequence homology to perform precise repair of double-strand break (DSB) damage at the accurate genomic site. In contrast to NHEJ, this repair mechanism requires a DNA template. This repair strategy is used by many researchers for generating gene-knock-ins (KI) with exogenous DNA sequences. This illustration was created by using BioRender.

engineered RNA molecules by combining the crRNA and tracrRNA sequences into a single RNA molecule [133]. A protospacer adjacent motif (PAM) subsequently 3' of the protospacer sequence is obligatory for the Cas9 nucleases to generate a targeted DNA double-strand break (DSB). In general, DNA-DSB caused by Cas9 is blunt-ended and occurs 3 bp upstream of the PAM within the protospacer sequence. As a result of DNA damage, various cellular repair mechanisms are activated within the cell. DNA can be repaired either by non-homologous end-joining or homology-directed repair.

Non-homologous end joining (NHEJ) is referred to as “non-homologous” due to the indiscriminate ligation of the broken DNA ends with minimal DNA reference (Fig. 6). Inaccurate DNA repair may lead to the deletion or insertion of a small number of nucleotides (INDELs), capable of generating frameshift mutations and premature stop

codons, resulting in the effective knockout (KO) of a specific gene. Therefore, DSBs conducted by Cas9 to initiate NHEJ is best used by scientists to induce gene KO [149].

Homology-directed repair (HDR) is an intrinsic DNA repair mechanism that relies on DNA sequence homology to precisely repair double-strand break (DSB) damage at the accurate genomic site. In contrast to non-homologous end joining (NHEJ), which rejoins any two broken DNA ends, HDR pathway proteins identify homologous DNA sequences (from a sister chromatid, a donor homology plasmid, single-stranded oligonucleotides, etc.) in the vicinity of the DSB region and utilize these homologous regions as a template for the accurate "correction" of the damage. Taking advantage of these circumstances, exogenous DNA sequences with specified homology arms (identical to the host DNA subsequently upstream and downstream of the DSB) can be used to stably integrate any DNA of interest at any specific DNA locus within an organism's genome. This procedure, called gene knock-in (KI), is now feasible without significant effort [150].

Due to the high gene-editing efficiency of CRISPR/Cas technology, it has become a firmly established tool for diagnostic and therapeutic procedures. Similarly, this applies to cancer research, where CRISPR-based approaches elucidated novel facets of cancer biology that were previously challenging to investigate. These include the identification of coding and noncoding cancer drivers, comprehension of tumor heterogeneity and evolution dynamics, and improvements in cancer diagnosis and therapeutic strategies [151]. As already stated, we aim to explore the regulative nature of p53 protein isoforms in response to various CRC therapeutics. By comprehending the mechanisms of action of the individual p53 protein isoforms, we can study their impact on distinct cellular pathways and systematically search for therapeutics that induce differential p53 isoform expression to trigger cell death in tumor cells efficiently. Using CRISPR/Cas9, we successfully integrated several exon-specific isoform expression reporter systems (EXSISERS) into *TP53*. This novel reporter system allows for easy and fast luminescence-based protein isoform quantification while the reporter systems post-translationally excise out of the nascent p53-polypeptide, leaving behind unaffected and fully functional p53 protein isoforms [152].

1.6 The Triple-EXSISERS Reporter System

The exon-specific isoform expression reporter system (EXSISERS) generally consists of a luciferase flanked by self-excising split-intein units. Genetic integration of EXSISERS into coding sequences of *TP53* results in the co-expression of the reporter together with the host protein (Fig. 7a, b). To simultaneously analyze multiple p53 protein isoforms, we expanded the subset of different EXSISERS reporters with three compatible luciferases, each flanked by distinct split-inteins. The following section delves deeper into the biology of luciferases and split inteins:

Bioluminescence, which refers to the emission of visible light by living organisms, involves a biochemical reaction requiring at least three key components: a luciferin substrate, an oxygen derivative, and a specialized luciferase enzyme. At the molecular level, bioluminescence arises due to the oxidation of the luciferin substrate catalyzed by the luciferase enzyme. The electronically excited product, oxyluciferin, emits light as it undergoes relaxation to its lower energy ground state [153]. The ability of emitting light due to a biochemical reaction has evolved in multiple organisms simultaneously. Consequently, there is a huge diversity of luciferase enzymes, each catalyzing individual luciferin substrates. Upon their discovery, scientists have capitalized on their usability and, since then, have been developing various optogenetic reporter systems to elucidate the cell's molecular biology.

For our purpose, we used both naturally occurring and artificially engineered luciferases. The **Firefly luciferase (FLuc)**, for instance, was the first luciferase identified and isolated by Raphaël Dubois from the organism *Photinus pyralis* (click beetle) [154]. FLuc is an enzyme catalyzing the hydrolysis of ATP and the decarboxylation of its corresponding substrate. For its bioluminescent activity, FLuc uses D-luciferin substrate (D LH2) containing a carboxylic acid residue, ATP, and oxygen [155]. The substrate conversion into oxyluciferin promotes the emission of photons at a specific wavelength, which, in the case of FLuc, corresponds to 565 nm.

Another widely used luciferase, Cypridina luciferase (CLuc), was first identified and characterized by Osamu and Akemi Shimomura in 1966 from the organism *Vargula hilgendorfii*, a Japanese sea firefly [156]. CLuc is a naturally secreted luciferase and inherently stable due to multiple disulfide bonds [157]. CLuc oxidizes its corresponding luciferin Vargulin to the energetically lower oxyluciferin product and, during this catalytic process, emits photons at a wavelength of 465 nm.

Introduction

The third luciferase for creating the triple EXSISERS reporter system is the artificially designed **Nano Luciferase (NLuc)** by Promega in 2012 [158]. NLuc originates from the deep-sea shrimp *Oplophorus gracilirostris*, and its luminescence output was enhanced through three successive rounds of mutagenesis. With a molecular weight of 19.1 kDa, this enzyme depends on the substrate furimazine, converted to the energetically lower furimamide to generate intense, glow-type luminescent signals at 460 nm [159].

The choice of these three luciferases was dependent on their substrate specificities. Similarities in structural motifs among the substrates often give rise to crosstalk reactions, obscuring luciferase differentiation [160]. However, FLuc, CLuc, and NLuc each employ distinct substrates (D-Luciferin, Vargulin, and Furimazine) to avert cross-reactivity. This makes the luciferases viable candidates for incorporation into EXSISERS reporters, enabling unambiguous differentiation of the three p53 isoform groups: FLp53, $\Delta 40$ p53, and $\Delta 133+\Delta 160$ p53. To complement the EXSISERS reporters, the selected luciferases need to be embedded into so-called split inteins.

Inteins mediate a biological process called protein trans-splicing, wherein two protein fragments interact to create a catalytically active enzyme, eventually catalyzing their excision and the ligation of their surrounding protein sequences. Since their identification, chemists and biologists have used split inteins in exogenous settings for various biotechnological applications [161]. Originally, inteins or rather protein splicing was first observed in the baker's yeast (*Saccharomyces cerevisiae*) in 1990, discovering the *VMA1* gene to be translated into one protein, but post-translationally being separated into two proteins by auto-catalyzation [162]. Since then, such trans-splicing events have consistently been discovered in various proteins and organisms, substantially expanding the intein-toolbox for protein engineering [163]. The idea of split-inteins arose when researchers found that inteins can be artificially split into two protomers that can spontaneously reassemble to catalyze their own protein trans-splicing. As for the luciferases, there are either naturally occurring or artificially engineered split-inteins, each having distinct splicing efficacies [163].

For instance, the split-intein **gp41-1** is a naturally fragmented intein originating from a functional replication helicase of bacteriophage T4 [164]. It was found as a result of metagenomic sequencing [165]. This intein, which is noted as one of the smallest reported split-inteins, displays a remarkably fast trans-splicing activity ($k = 2.2 \pm$

Introduction

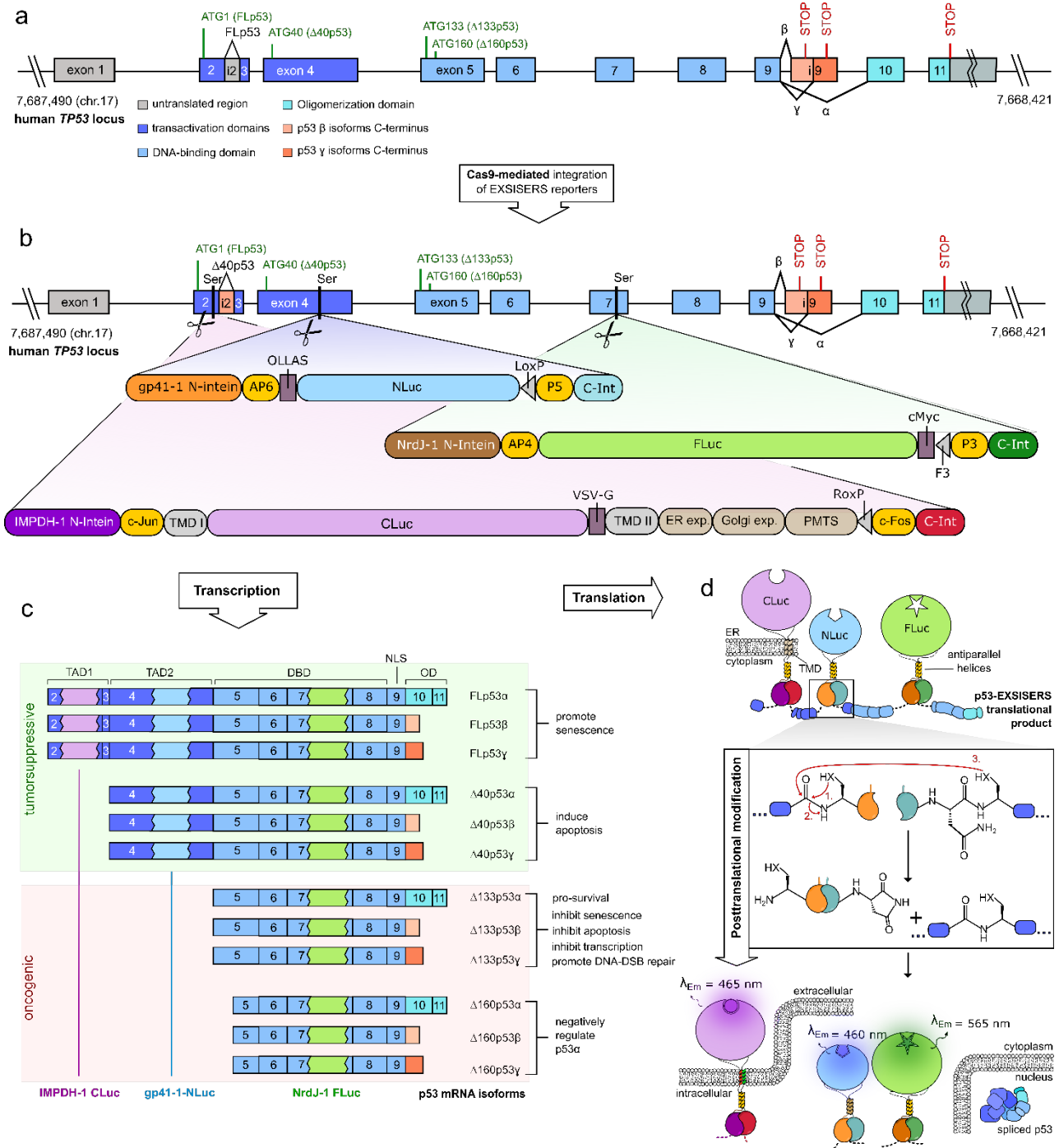


Figure 7: Integration into *TP53* and stable co-expression of the triple EXSISERS reporter system in HCT116 cells. **a)** Schematic representation of the tumor suppressor gene *TP53* with its corresponding domains (color-coded). **b)** Schematic representation of CRISPR/Cas9 mediated knock-in of EXSISERS-reporters IMPDH-1 Cypridina Luciferase (IMPDH-1-CLuc), gp41-1 Nano Luciferase (gp41-1-NLuc), and NrdJ-1 Firefly Luciferase from *Photinus pyralis* (NrdJ 1 PpyFLuc) into exon 2, 4, or 7 of the tumor suppressor gene *TP53*. **c)** Conservation of the p53 reading frame upon EXSISERS knock-in allows co-translation of corresponding reporter proteins in combination with p53. Depending on which p53 protein isoform is expressed (full length p53α/β/γ, Δ40p53α/β/γ, Δ133p53α/β/γ, Δ160p53α/β/γ), either three reporters (IMDPH 1 CLuc, gp41 1 NLuc, NrdJ 1 FLuc), two reporters (gp41 1 NLuc, NrdJ 1 FLuc), or one reporter (NrdJ 1 FLuc) are co-transcribed. **d)** Translation of the corresponding p53 mRNA which includes EXSISERS-reporters. Associated split-inteins (e.g., gp41-1-N-intein and gp41-1-C-intein) interact with each other to place the flanking p53 sequences (exteins) into close proximity and initiate intein-luciferase excision as well as p53-extein ligation. Subsequently, two EXSISERS-reporters (gp41 1 NLuc and NrdJ 1 FLuc) remain in the cytosol, while IMPDH 1 CLuc is transported and anchored to the plasma membrane. After protein-splicing, p53 is transported into the nucleus. Of note, the integrity of the p53 protein isoforms is completely conserved.

0.7×10^{-4} s) [166]. It comprises an 88-residue N-terminal and a 37-residue C-terminal fragment. Due to its compact size and robust protein splicing, it is an attractive split-intein candidate for protein engineering purposes. Notably, the gp41-1 intein employs serine as its catalytic residue found on position +1 as the first extein residue subsequently following the intein sequence. The significantly higher frequency of serines over cysteines allows a broader spectrum of recombinant insertion of gp41-1 split-intein into pro- and eukaryotic protein sequences [167].

NrdJ-1 is another naturally occurring split-intein that was also found as a result of metagenomic sequencing [165]. It originates from the catalytic subunit of the class II ribonucleotide reductase (RNR) of *Streptomyces avermitilis* [165]. The N-terminal fragment of NrdJ-1 consists of 103 residues, while the C-terminal fragment encompasses 40 residues. Like gp41-1, NrdJ-1 employs serine as a catalytic residue for the initial intein-rearrangement and subsequent intein-splicing. NrdJ-1 shows remarkably high splicing rates ($k = 2.4 \pm 0.1 \times 10^{-4}$ s), making it suitable for protein engineering [166].

The third split-intein we considered for designing the triple EXSISERS reporter system is **IMPDH-1**. As part of a nucleotide metabolism enzyme, namely inosine-5'-monophosphate dehydrogenases (IMDPH), the split-intein was found as an event of a self-fracturing IMPDH enzyme [165]. The N-terminal fragment of NrdJ-1 consists of 101 residues, while the C-terminal fragment encompasses 40 residues. IMPDH-1 also uses serines as catalytic intein-splicing residues and demonstrates relatively fast splicing-rates ($k = 7.7 \pm 1.6 \times 10^{-4}$ s) [166].

Incorporating each luciferase into a specific split-intein creates three functional reporter units capable of scarless excision from any target host protein, providing a serine residue essential for catalyzing the active splicing process.

EXSISERS describes a reporter system genetically integrated into the coding sequence of a specific protein of interest to be co-translated and autocatalytically spliced out of the host protein. Depending on the locus in which EXSISERS is stably incorporated, it quantitatively reflects the exon usage of an expressed gene. In the case of alternative mRNA-splicing events, and depending on the number of integrated EXSISERS reporters, this method can simultaneously capture the expression of multiple protein isoforms (Fig. 7c, d). Given the fact that the expression of the *TP53* gene results in multiple protein isoforms and since their respective cellular ratio can

determine the activation of crucial pathways [109,117], EXSISERS constitutes the ideal method for investigating p53 isoform-dependent signaling pathways under the influence of diverse exogenous stimuli, such as CRC therapeutics. Here, we integrated an individual EXSISERS-reporter into each domain: TAD I (representing FLp53), TAD II (FLp53 + Δ 40p53), and DBD (all p53 isoforms) of p53. Depending on the specific p53 isoform expressed, either all three luciferases for FLp53, gp41-1-NLuc, and NrdJ-1-FLuc for FLp53+ Δ 40p53 or NrdJ-1-FLuc alone for total p53 are co-translated. The quantity of the Δ 40p53 isoform is determined by subtracting the relative luminescence signals of IMPDH-CLuc from those of gp41-1-NLuc. Correspondingly, the amounts of Δ 133+ Δ 160p53 are calculated by subtracting the relative signals of gp41-1-NLuc from those of NrdJ-1-FLuc. The combined detection of three EXSISERS luciferase signals provides a method for non-invasive and longitudinal quantification and differentiation of constitutive expressed p53 protein isoforms (FLp53, Δ 40p53, Δ 133p53 + Δ 160p53) in living cells.

Advantages over state-of-the-art methods

Luminescence-based protein isoform analysis with EXSISERS allows for 1. translational quantification of the target protein, 2. differentiation of specific protein isoforms, 3. acquisition of time-series data, 4. measurement in living cells, and 5. high scalability with high-throughput screening applicability. EXSISERS stands as an innovative and revolutionary technique for relative protein quantification, concurrently complementing pre-existing mRNA (RT-qPCR, smFISH, RNAseq [168]) and protein-based single time-point strategies (immunoblot analysis, immunofluorescence). Transcriptional and translational regulation of genes does not necessarily coincide, as protein production is also influenced by several factors, including translationally arrested mRNA[169], ribosomal frameshift regulation [170], and local mRNA translation [152,171,172]. Current protein-based methods are highly dependent on the availability of exon-specific antibodies, while mRNA-based methods are usually elaborate and prevent longitudinal and large-scale experiments. The non-invasive, longitudinal live-cell analysis with EXSISERS allows for differential p53 protein isoform detection in CRC cell lines exposed to clinically established chemotherapeutics. Understanding the tumor suppressor's regulative mechanisms is paramount for drugging p53 [121], especially in cancer cells with different p53 mutational backgrounds [173]. This study introduces a novel method for detecting and quantifying

p53 isoforms. We aim to provide a better understanding of the intricacies of p53 isoform regulation and function to enhance therapeutic strategies for CRC.

1.7 Objectives

This doctoral thesis aims to elucidate the fundamental principles governing the regulation of p53 protein isoforms. As emphasized multiple times, the cellular ratio of isoforms — FLp53, $\Delta 40$ p53, $\Delta 133$ p53, and $\Delta 160$ p53 — is crucial for triggering fundamental pathways. Under the influence of specific therapeutics used for treating colorectal carcinoma, the existing isoform ratio can decisively influence the response to therapy and, ultimately, the patient's survival.

To quantitatively measure the expression of p53 protein isoforms—FLp53, $\Delta 40$ p53, $\Delta 133$ p53, and $\Delta 160$ p53—in real-time and live cells under the influence of therapeutics already established in clinical practice (e.g., 5-Fluorouracil, oxaliplatin, etc.), we have integrated and significantly advanced the novel method EXSISERS into the tumor suppressor gene *TP53*. Understanding the basic principles of p53 isoform regulation is imperative to develop novel therapeutic strategies for tumor treatment.

This thesis has achieved the following milestones, which will be elaborated in-depth in the "Results" section:

- Advancement of the EXSISERS technology allows for multiplexing luminescence screenings of Nano luciferase, Firefly luciferase, and Cypridina luciferase and, therefore, quantification of up to three protein isoforms simultaneously.
- Stable integration of EXSISERS reporters into tumor suppressor p53 for live-cell and real-time quantification of p53 protein isoforms including FLp53, $\Delta 40$ p53, and $\Delta 133$ + $\Delta 160$ p53.
- Study of the dynamic regulation of p53 isoforms and their respective activated signaling pathways: FLp53: cell-cycle arrest, $\Delta 40$ p53: cell death induction, $\Delta 133$ p53, and $\Delta 160$ p53: negative regulators of FLp53 and acceleration of $\Delta 40$ p53-mediated cell death.
- Non-invasive high-throughput screening of p53 isoform expression in response to 4,863 anti-cancer compounds. Identification of deubiquitinase inhibitor SJB2-043, which strongly enhances tumor suppressive properties of p53. Thus,

Introduction

it represents a potential treatment option for tumors encompassing wild-type p53.

- Identification of mitochondrial respiratory chain complex I inhibitor IACS-010759 amplifying tumor suppression in p53-mutated cells. Thus, IACS-010759 represents a potential treatment option for tumors displaying p53 mutations or deletions.
- Verification of IACS-010759 as a highly effective and tumor-specific therapeutic for treating colorectal cancer (CRC).

2. Material and Methods

2.1 Molecular Cloning

Primer- and gene-fragment design. DNA oligo primer and gBlocks gene fragments were obtained from Integrated DNA Technologies (IDT). Primers for sequencing or molecular cloning, gene fragments, and DNA plasmids were designed using the Geneious Prime Software. Lyophilized DNA oligo primers were dissolved in nuclease-free water (Carl Roth) to a stock concentration of 100 μM . Lyophilized gBlocks gene fragments were dissolved in nuclease-free water to a stock concentration of 10 $\text{ng } \mu\text{l}^{-1}$. DNA plasmids used for molecular cloning were dissolved in nuclease-free water, whereas DNA plasmids used for mammalian cell culture experiments were dissolved in elution buffer (EB-buffer, QIAGEN).

PCR for molecular cloning. Single-stranded oligo-primer deoxyribonucleotides (Integrated DNA Technology, IDT) were diluted in nuclease-free water to a stock concentration of 100 μM . Fifty microliter PCR reactions with plasmid- and genomic DNA templates were performed using Q5 Hot Start High-Fidelity 2 \times Master Mix (New England Biolabs, NEB). PCR conditions were used according to the manufacturer's protocol for PCR amplification from plasmid DNA templates (1 ng). For PCR amplification from genomic DNA templates (500 ng), initial denaturation was set to 98 $^{\circ}\text{C}$ for 2 min, and the cycle number to 40 cycles. Samples were purified by DNA agarose gel electrophoresis followed by gel extraction purification using the QIAquick Gel Extraction Kit (QIAGEN).

DNA digestion with restriction endonucleases. According to the manufacturer's protocol, samples were digested with NEB restriction enzymes in a total reaction volume of 40 μl and 3 μg of plasmid DNA. Digested fragments were separated according to their molecular weight by DNA agarose gel electrophoresis followed by gel extraction purification using the QIAquick Gel Extraction Kit (QIAGEN). The concentration of eluted and purified DNA fragments was determined using a Nanophotometer with LG100-UV-G quartz cuvette (IMPLEN).

DNA agarose gel electrophoresis. Depending on the expected fragment size, gels were prepared with 0.5 % agarose (> 8 kb), 1 % agarose (between 1 and 8 kb), and

Material and Methods

2 % agarose (< 1 kb). Agarose powder (Biozym LE Agarose) was dissolved in 1x TAE buffer and 1:10.000 SYBR Safe stain (Thermo Fisher Scientific) was added. Gels were left running for 1 h at 120 V. 6 µl GeneRuler 1 kb DNA-ladder was used for analysis. Samples were mixed with 6x Purple Loading Dye (NEB) in a 1:6 ratio before loading on gel.

DNA ligation and Gibson assembly. Digested plasmid-backbone and DNA fragments with appropriate overhangs were mixed and ligated equimolarly for DNA ligation. We used the Quick Ligation Kit (NEB) and conducted ligation according to the manufacturer's protocol. After incubation, DNA ligase was heat-inactivated at 65°C, and the ligase-DNA mix was transformed into 10-beta competent *E. coli* (NEB). For Gibson assembly, digested DNA fragments and a plasmid-backbone with double-stranded overlap sequences ($T_m \sim 65^\circ\text{C}$) were mixed on ice in an equimolar manner. NEBuilder HiFi DNA Assembly (NEB) was used according to the manufacturer's protocol. Subsequently, after incubation, 7 µl of DNA assembly master mix was dialyzed against distilled water for 10 min. 5 µl was transformed into NEB Turbo electrocompetent *E. coli* (NEB).

Bacterial transformation and cultivation. DNA plasmids ligated or assembled with the corresponding reaction mix, intended to be transformed into NEB Turbo electrocompetent *E. coli* via electroporation, were first dialyzed against distilled water for 10 min. After that, 1-5 µl of dialysate was mixed with 50 µl of thawed electrocompetent cells (on ice) and transferred into precooled electroporation cuvettes (2 mm, Merck). Cuvettes containing plasmid - *E. coli* mix were pulsed at 2.5 kV with the Gene Pulser II (Bio-Rad) and immediately mixed with 950 µl SOC-medium (NEB) and incubated for 1 h at 37°C with mild agitation (300 rpm). Ligated or assembled DNA plasmids (1-5 µl), intended to be transformed into 10-beta competent *E. coli*, were directly mixed with thawed chemocompetent cells and incubated for 30 min on ice. Subsequently, heat shock was conducted at 42°C for 30 s and incubated for another 5 min on ice. Transformed cells were mixed in 950 µl 10-beta stable outgrowth medium (NEB) and incubated for 1 h at 37°C with mild agitation (300 rpm). Transformed and incubated cells were plated on prewarmed agar plates containing the appropriate concentration of corresponding antibiotics. LB Agar plates were incubated overnight at 37°C or for 48 h at room temperature.

Bacterial strains used for DNA plasmid transformation. Ligated DNA plasmids for mammalian expression systems were transformed into 10-beta competent *E. coli* (NEB). Gibson assembled DNA plasmids were transformed into NEB Turbo electrocompetent *E. coli* (NEB). These plasmids contained an autonomously driven ampicillin resistance gene. 100 $\mu\text{g ml}^{-1}$ carbenicillin, dissolved in lysogeny broth medium (LB medium) or LB agar, was used as a selection agent. Assembled or ligated plasmids for bacterial protein expression were transformed into BL21 (DE3) competent *E. coli* (NEB). These plasmids contained an autonomously driven kanamycin resistance gene. 100 $\mu\text{g ml}^{-1}$ kanamycin was used as a selection agent.

Plasmid DNA purification and Sanger sequencing. After overnight incubation of transformed chemocompetent or electrocompetent *E. coli* on agar plates, grown bacterial clones were picked and transferred into 2.5 ml LB medium with appropriate antibiotics and incubated for 7 h (NEB Turbo competent *E. coli*) or overnight (10-beta competent *E. coli*). Plasmid DNA from 2 ml transformed bacterial culture, intended for sequencing or molecular cloning, was purified via QIAprep Plasmid MiniSpin (QIAGEN) according to the manufacturer's protocol. Purified plasmids were sent for Sanger sequencing (Eurofins, GATC services) for sequential quality control and analyzed with Geneious Prime software. Plasmid DNA from transformed bacterial clones intended to be used in mammalian cell culture experiments was purified from 200 ml of inoculated bacterial cell culture medium (containing appropriate antibiotics, 16 h, 37°C, 180 rpm) with QIAfilter Plasmid Maxi Kit (QIAGEN) according to manufacturer's protocol.

p53 protein isoform overexpression in BL21 *E. coli*. Bacterial strains containing the respective expression plasmids were inoculated into 50 mL LB medium containing 100 $\mu\text{g ml}^{-1}$ kanamycin and incubated at 37 °C and constant agitation (180 rpm) overnight. Main culture comprising 200 mL LB medium with 100 $\mu\text{g ml}^{-1}$ kanamycin was inoculated with 4 mL of overnight culture and incubated at 37°C until optical density (OD 600) reached 0.5-0.7. Protein expression was induced by adding 1 mM IPTG. Main culture was then incubated for another 16 h at 16 °C and under constant agitation. Cells were pelleted and lysed with sonication in appropriate lysis buffer.

2.2 Mammalian Cell Culture.

Cell lines and maintenance. HCT116 wild type (WT) (obtained from ATCC) and genetically modified cell lines were cultured in McCoy's 5A Media (Gibco, Thermo Fisher Scientific) supplemented with 10 % fetal bovine serum (FetalClone™II, HyClone™) and 100 µg ml⁻¹ of penicillin-streptomycin (Gibco, Thermo Fisher Scientific) and incubated at 37°C and 5 % CO₂. HCT15 and SW480 cell lines (ATCC) were cultured in RPMI media (Gibco, Thermo Fisher Scientific) supplemented with 10 % fetal bovine serum and 100 µg ml⁻¹ of penicillin-streptomycin and incubated at 37°C and 5 % CO₂. Caco-2 cell line was cultured in Minimal Essential Media (Gibco, Thermo Fisher Scientific) supplemented with 10 % fetal bovine serum, 100 µg ml⁻¹ of penicillin-streptomycin, and 1mM L-glutamine (Sigma Aldrich) and incubated at 37°C and 5 % CO₂. All cell lines were cultured in T75 flasks (Corning). Cell passage was conducted at 90 % confluency by discarding conditioned cell culture media and washing once with DPBS (Gibco, Thermo Fisher Scientific) and, after that, detaching mammalian cells from the flask surface with 2 ml accutase solution (Gibco, Thermo Fisher Scientific). Cells were incubated at room temperature for 5 -10 min with accutase solution. Accutase solution was inactivated by adding 8 ml of corresponding media (prewarmed) and cells were transferred at an appropriate density. For follow-up experiments, the detached cell suspension was counted in a TC20 Automated Cell Counter (Bio-Rad) and seeded at an adequate density on 6-well, 24-well, 48-well, or 96-well plates.

Patient fibroblast isolation and maintenance. Fibroblasts were isolated from patient-derived colonic biopsies (ethical vote N°: 00/14). Biopsies were transferred into a 15 ml Falcon tube pre-filled with 10 ml HBSS supplemented with 2 mM EDTA (Carl Roth) and incubated at 37°C at 300 rpm for 3 min. Biopsies were then transferred into a new tube and resuspended in digestion buffer (1 mg ml⁻¹ collagenase I (Merck), 0.3 mg ml⁻¹ DNase I (Roche), 2 mg ml⁻¹ hyaluronidase (Merck) dissolved in PBS containing Mg²⁺ and Ca²⁺). Biopsies were incubated at 37°C and 300 rpm agitation. Detached fibroblasts were pelleted by centrifuging at 300 x g and washing several times with PBS. Fibroblasts were cultured at 37°C and 10 % CO₂ in DMEM high glucose medium (Thermo Fisher Scientific) supplemented with MEM non-essential amino acids (100x Master Mix, Merck), 100 µM sodium pyruvate, MEM vitamin solution (100x Master Mix, Merck), 100 µg ml⁻¹ primocin (InvivoGen), 10 µg ml⁻¹ fungin

Material and Methods

(InvivoGen), and 10 % fetal bovine serum (Anprotec). Cell passage was conducted at 80 to 90 % confluency, cells were detached and passaged as described in the above section. For follow-up experiments, the detached cell suspension was counted in a TC20 Automated Cell Counter (Bio-Rad) and seeded at an appropriate density on 6-well, 24-well, 48-well, or 96-well plates.

Mycoplasma test. All CRC cell lines, and genetically edited HCT116 cell lines were tested for mycoplasma contamination using the Plasmotest Mycoplasma Detection Kit (InvivoGen) every 3 months according to the manufacturer's protocol.

Seeding cell lines. Cell lines ready for passaging were detached from the flask surface and counted as described in the section above (*cell lines and maintenance*). All cell lines were seeded on corresponding cell culture plates as follows: For 96-well-plates, 20,000 cells were seeded in 100 μ l per well. For 48-well-plates, 75,000 cells were seeded in 500 μ l per well. For 24-well-plates, 100,000 cells were seeded in 1 ml per well. For 6-well-plates, 400,000 cells were seeded in 3 ml per well. Plates were incubated for a minimum of 24 h at 37°C and 5 % CO₂ before using them for follow-up experiments.

Plasmid transfection. DNA plasmids were transfected into CRC cell lines via lipofection using X-treme GENE HP (Roche) according to the manufacturer's protocol. For cells seeded onto a 96-well plate, 100 ng DNA per well was used. For 48-well plates, an amount of 500 ng DNA, for 24-well plates an amount of 1 μ g DNA per well, and for 6-well plates, a total amount of 2.4 μ g DNA per well was used to transfect the cells contained therein. Across all experiments, DNA amounts were kept constant for all transient transfections in the appropriate well plates. If possible, supernatant was discarded 24 h post-transfection and replaced with fresh media.

Overview of generated cell lines. Genetically modified cells were exclusively generated from HCT116 wild-type (WT) cells (ATCC). Gene editing was conducted using expression plasmids with (CBh hybrid RNA polymerase II promoter-driven) mammalian codon-optimized Cas9 from *Streptococcus pyogenes* (*SpCas9*) with a tandem C-terminal SV40 nuclear localization signal (SV40 NLS) and (human U6 RNA polymerase III promoter-driven) single-guide-RNA (sgRNA) sequence. Therefore, we

used the scaffold sequence (F+E) designed by Chen et al. together with the corresponding spacer sequences for gene-directed knock-out and knock-in [174]. Starting from HCT116 WT, EXSISERS-reporters were sequentially integrated. HCT116 clone **2.A2** (EXSISERS_{TP53:7FLuc}) contains stably integrated NrdJ-1-FireflyLuc into coding exon 7 of *TP53* (conserved DNA-binding domain). Thereafter, HCT116 clone **5.D6** (EXSISERS_{TP53:4NLuc-7FLuc}), containing stably integrated gp41-1-NanoLuc within coding exon 4 of *TP53* (transactivation domain II), was derived from clone HCT116 2.A2. Ultimately, HCT116 clone **3.E9** (EXSISERS_{TP53:2CLuc-4NLuc-7FLuc}) carrying the third stable EXSISERS-reporter IMPDH-1-CLuc within coding exon 2 of *TP53* (transactivation domain I) was derived from clone HCT116 5.D6. Further, we created distinct p53-deficient HCT116 cell lines either continuously expressing p53 but missing essential parts of the DNA-binding domain (clone **3.C7**) or completely lacking p53 (clone **1.E8**).

Generation of stable EXSISERS cell lines with CRISPR-Cas9. To create stable cell lines carrying EXSISERS-reporters in the exon of interest (EOI), expression-plasmids coding for dCas9 protein and for corresponding sgRNAs (constructs are described in section: *Overview of generated cell lines*) were transfected into HCT116 WT cells to promote DNA-double strand breaks (DNA-DSB) and homologous direct repair (HDR) at the desired loci. Spacer sequences for directed DNA-DSB consisted of 20 bp (*TP53* exon 2 sgRNA 2 (between Phe19 and Ser20): AGGAAACATTTTCAGACCTA; *TP53* exon 4 sgRNA 2 (between Lys93 and Ser94): GACAGAAGATGACAGGGGCC; *TP53* exon 7 sgRNA 2 (between Asn239 and Ser240): CATGTGTAACAGTTCCTGCA) complementary sequence of the targeting locus. The efficiency of Cas9 nuclease activity depending on the sgRNA spacer sequence was determined by a T7 endonuclease I assay (NEB) carried out according to the manufacturer's protocol. As indicated, the EXSISERS insertion site was set subsequently upstream of serine, which is needed for post-translational excision-processing of inteins. NetGene2 (v.2.42) [175] was used to avoid inserting cryptic splice sites and deleting potential regulatory elements within the tumor suppressor gene *TP53*. In case of stable knock-in events, an i53 protein (53bp1 inhibitor) [176] is also encoded on the Cas9 expression plasmid, driven by the same CBh promoter but translationally separated by a p2A peptide. Co-expression of i53 should optionally enhance homologous recombination after Cas9-mediated DNA-DSB at the EOI. For HDR and stable genomic integration,

Material and Methods

a donor DNA plasmid carrying the EXSISERS construct, including an (EF1 α promoter-driven and mRNA self-processing) selection-cassette and two homology arms of at least 1000 bp flanking the integrable moiety are required to be co-transfected into the modifiable cell line. The selection-cassette contains coding sequences for puromycin-N-acetyl-transferase (PuroR) and herpes simplex virus thymidine-kinase (HSVtk) driven by the same promoter but translationally separated by a p2A peptide. 48 h post-transfection (6-well plate format), cell culture media were replaced by 50 $\mu\text{g ml}^{-1}$ puromycin-dihydrochloride (Merck) containing media. Selective media were repeatedly changed every 72 hours. The selection procedure was conducted for at least 1 to 2 weeks. Surviving cells were detached with accutase solution (Gibco, Thermo Fisher Scientific) and monoclonalized by FACS sorting (BD FACS Aria III) into 96-well plates. Cells were cultured in conditioned media (50 % conditioned and sterile-filtered media from appropriate cells, 50 % fresh media supplemented with 20 % fetal bovine serum, and 100 units ml^{-1} Pen/Strep) for 1 week and thereafter supplemented with an additional 100 μl of fresh media per well and cultured for another week at 37°C and 5 % CO_2 . As soon as colonies reached an accumulation of at least 100 cells, cells were detached with accutase solution and expanded onto a 48-well plate. As soon as a confluency of 90 % was reached, cells were carefully detached and passaged at a 1:5 ratio into a new 48-well plate, while the remaining cell suspension was used for genotyping the corresponding colonies. Please refer to section *Genomic DNA isolation and genotyping* for a detailed genotyping procedure. Cell clones having integrated EXSISERS at the EOI in a homozygous manner were expanded and prepared to remove the co-integrated selection-cassette. Therefore, cells were seeded on a 6-well plate and transfected 24 h afterward with DNA expression plasmids coding for mammalian codon-optimized Flp-, Cre-, or Dre-recombinases. These expression plasmids are designed to express a modified green fluorescent protein, Xpa H62Q, under the control of the CAG-promoter. The CAG-promoter is a synthetic promoter created by combining elements from different genes, including the cytomegalovirus (CMV) early enhancer element, the first exon and intron of the chicken beta-actin gene, and the splice acceptor from the rabbit beta-globin gene [177]. Importantly, the Xpa H62Q and other proteins coded on the plasmid are driven by the same promoter but translationally separated by a p2A peptide. After 48 hours following the transfection of these plasmids into cells, a process known as FACS pre-sorting is conducted. This method employs flow cytometry to identify and isolate cells that exhibit green

Material and Methods

fluorescence, effectively increasing the proportion of cells that have successfully taken up and expressed the transfected plasmids. This is a common procedure used in molecular and cell biology to enhance the population of cells expressing the target gene, in this case, the Xpa H62Q green fluorescent protein. Thereafter, cells were cultured in selection media containing 100 μ M ganciclovir and cultured for at least 2 weeks. After ganciclovir selection, cells were FACS-sorted once more to monoclonalize into 96-well plates. Cells were then cultured in 100 μ L conditioned media (composition as described above) for 1 week and thereafter supplemented with additional 100 μ l fresh media per well. As soon as colonies reached an accumulation of at least 100 cells, cells were detached with accutase solution and expanded into a 48-well plate. As soon as confluency of 90 % was reached, cells were carefully detached and passaged at a 1:5 ratio into a new 48-well plate, while the remaining cell suspension was used for genotyping the corresponding colonies. Cell clones that carried the EXSISERS-reporter stably integrated at the EOI and that had undergone successful homozygous exclusion of the selection-cassette were considered for expansion, further gene-editing, or live-cell luminescence quantification experiments. Homozygous targeting is not required in general, but we have previously shown that choosing homozygous clones is better for confirming minimal invasiveness without confounders from WT alleles [152].

p53-directed knock-out using CRISPR-Cas9. p53 KO was conducted by multiplexed Cas9-sgRNA targeting and functional deletion of the DNA-binding-domain (DBD) without altering the reading-frame and without evoking a complete loss of p53. Hence, p53 is still expressed but incapable of binding DNA-response elements (p53-RE) or establishing protein-protein interactions. HCT116 cells were transfected with mammalian codon-optimized expression plasmids for dCas9 protein and for corresponding sgRNAs to promote DNA-DSB and homologous direct repair (HDR) at the desired loci. For multiplexed gene targeting, we redesigned the U6 promoter-driven sgRNA transcripts (description in section: *Overview of generated cell lines*) by inserting a second sgRNA sequence with identical tracrRNA but different spacer sequence (*TP53* exon 7 sgRNA 2 (between Asn239 and Ser240): G+ATGTGTAACAGTTCCTGCAT; *TP53* exon 8 sgRNA 2 (between Gly302 and Ser303): G+CTCACCACGAGCTGCCCCCA), and sequentially separated by a tRNA scaffold spacer [178]. The sgRNA-tRNA-sgRNA transcript is post-transcriptionally

Material and Methods

processed by RNase P (5' of tRNA) and RNase Z (3' of tRNA), causing a digestive release of one tRNA and two spatially separated sgRNA molecules, driven by the same U6 promoter. The efficiency of Cas9 nuclease activity depending on the sgRNA spacer sequences was determined by a T7 endonuclease I assay (NEB) carried out according to the manufacturer's protocol. i53 protein (53bp1 inhibitor) [176] is also encoded on the Cas9 expression plasmid, driven by the same CBh promoter but translationally separated by a p2A peptide. Co-expression of i53 should optionally enhance homologous recombination after Cas9-mediated DNA-DSB at the EOI. Before p53 functional KO, we stably inserted an EF1 α promoter-driven and mRNA self-processing selection cassette (consisting of the coding sequences for puromycin-N-acetyl-transferase (PuroR) and mNeonGreen (mNG) translationally separated by p2A) by replacing the coding sequence for a part of the p53-DBD between Asn239 and Ser303. This co-transfected DNA-donor plasmid contained two homology arms flanking the selection cassette, each identical to the upstream or downstream *TP53*-insertion site sequence and at least 1000 bp in length. 48 h post-transfection (6-well plate format), cell culture media were replaced by 50 $\mu\text{g ml}^{-1}$ puromycin-dihydrochloride (Merck) containing media. Selective media were repeatedly changed every 72 hours. The selection procedure was conducted for at least 1 to 2 weeks. Thereafter, surviving cells were detached with accutase solution (Gibco, Thermo Fisher Scientific) and monoclonalized by a FACS sorter (BD FACS Aria III) into 96-well plates. Cells were cultured in conditioned media (50 % conditioned) for 1 week, supplemented with an additional 100 μl of fresh media per well, and cultured for another week at 37°C and 5 % CO₂. As soon as colonies reached an accumulation of at least 100 cells, cells were detached with accutase solution and expanded into a 48-well plate. As soon as a confluency of 90 % was reached, cells were carefully detached and passaged at a 1:5 ratio into a new 48-well plate, while the remaining cell suspension was used for genotyping the corresponding colonies. Cells that integrated the selection cassette in a homologous manner were expanded and prepared for Flp-recombinase-mediated excision. For this purpose, cells were seeded in a 6-well plate and transfected 24 h afterward with DNA expression plasmids coding for mammalian codon-optimized Flp-recombinase. 48 h post-transfection, cells were FACS-sorted (BD FACS Aria III) and monoclonalized into a 96-well plate. Cells were cultured in conditioned media (50 % conditioned) for 1 week, supplemented with an additional 100 μl of fresh media per well, and cultured for another week at 37°C and 5

Material and Methods

% CO₂. Cell colonies were screened via fluorescence microscopy. Colonies having lost their fluorescent property and consisting of at least 100 cells were detached with accutase solution and expanded into a 48-well plate. As soon as a confluency of 90 % was reached, cells were carefully detached and passaged at a 1:5 ratio into a new 48-well plate while the remaining cell suspension was used for genotyping *TP53*. Cell clones missing the selection cassette and an essential part of the p53 DBD in a homozygous manner were considered for expansion and further experimental procedures. p53 DBD-deficient cells were additionally validated by immunoblot analysis.

Gene expression manipulation using dCas9-VPR. Artificial gene induction of *TP53* in HCT116 cell lines was conducted by co-transfection of CAG-promoter-driven mammalian-codon optimized nuclease-defective *S. pyogenes* Cas9 (D10A, H840A) fused to a tripartite trans-activation domain VP64-p65-Rta (VPR) and SV40 NLS [152,179] and a plasmid mix expressing (human U6 promoter-driven) sgRNA molecules targeting the 5' upstream region of the *TP53* transcription start site (*TP53* sgRNA 1: G+TTGCTACCCAGCACTGATAT;
sgRNA 2: G+TAAATCTTATCAGAGTGATA;
sgRNA 3: G+AACGTTAGGGTGTGATATTA;
sgRNA 4: G+CTTCATATTTGACACAATGC;
sgRNA 5: G+CAATTCTGCCCTCACAGCTC;
sgRNA 6: G+AGTCAGGATTCTCGCCGACC).

Control samples were transfected with a dCas9 expression plasmid and an empty sgRNA cloning plasmid.

Organoid generation and maintenance. Colon cancer organoids PDM-46 (HCM-SANG-0269-C18), PDM-47 (HCM-SANG-0270-C20), and PDM-50 (HCM-SANG-0273-C18) were obtained from ATCC and cultured accordingly to the recommendations of the manufacturer. Patient-derived colonic biopsies (ethical vote N°: 18-982-101) were cut into smaller pieces with surgery scissors and transferred into digestion buffer (0.5 mg ml⁻¹ collagenase (Merck), 2 mg ml⁻¹ collagenase IV (Merck), 1 mg ml⁻¹ hyaluronidase (Merck), 10 µM Y-27632 (Merck) dissolved in DMEM/F12 media (Gibco, Thermo Fisher Scientific) and incubated at 37°C and 200 rpm for 45 min. Biopsies / detached cells were centrifuged at 300 x g for 5 min and carefully washed

Material and Methods

twice with ice-cold PBS supplemented with 1 % BSA to stop the digestive reaction. Pelleted cells were resuspended in 100 μ l Matrigel (Corning) and pipetted in 10 μ l Matrigel domes onto a pre-warmed 24-well plate. Subsequent up-side down incubation at 37°C for 10 min was performed to harden the Matrigel. Plates containing cell-Matrigel domes were flipped and cultivated in 300 μ l 3dGRO™ Human Colon Organoid Expansion Media (Merck) supplemented with 10 μ M Y-27632, 100 μ g ml⁻¹ primocin (invivogen), and 10 μ g ml⁻¹ fungin (invivogen) in each well (37 °C, 5 % CO₂). After 24 h, media were replaced and cultivated with Human Colon Organoid Expansion Media without Y-27632. All our studies were conducted according to ethical guidelines at our institution as well as to the Helsinki Declaration and were approved by the ethics committee of the University Hospital of Regensburg.

Seeding colon organoids. For most of the experiments, removing the Matrigel (Corning) and harvesting solely colon organoids to seed them onto appropriate 96-well-round-bottom plates was necessary. Therefore, the media for culturing Matrigel-organoid domes was discarded and replaced by ice-cold Gentle Dissociation Reagent (Stemcell). After 2 min of incubation, domes were vigorously pipetted up and down and transferred into a reaction tube for 500 x g, 4 min centrifugation at 4°C. Supernatant was discarded, and organoids were washed twice with DMEM/F12 media to remove residual Matrigel. Organoids were seeded without Matrigel onto minimal-adherent 96-well bottom plates (Thermo Fischer Scientific) and cultured in 3dGRO™ Human Colon Organoid Expansion Media at 37°C and 5 % CO₂ for 24 h before continuing with further experiments.

Therapeutic treatment of cell lines, fibroblasts, and organoids. For treatment, corresponding cell lines, primary colon fibroblasts, or colon organoids were seeded onto an appropriate well-plate at least 24 h in advance. Chemotherapeutics and targeted therapies used for this study were dissolved in DMSO (IACS-010759.HCl (MedChemExpress (MCE), stock conc.: 10 mM), JNJ-64619178 (MCE, stock conc.: 10 mM), BLM-IN-1 (MCE, stock conc.: 10 mM), SJB2-043 (MCE, stock conc.: 10 mM), bleomycin (TargetMol, stock conc.: 10 mM), doxorubicin (TargetMol, stock conc.: 10 mM)) or ddH₂O (5-Fluorouracil (MCE, stock conc.: 10 mM), oxaliplatin (intern, stock conc.: 5 mg ml⁻¹)). For **cell-viability** experiments, HCT116 WT (ATCC), HCT116 p53-DBD^{-/-}, HCT116 p53^{-/-}, HCT15 WT (ATCC), SW480 WT (ATCC), and

Material and Methods

Caco-2 WT (ATCC) cells were cultured in 96-well plates (20,000 cells per well in 100 μ l) for 24 h and afterwards treated with varying therapeutic concentrations ranging from 0.05 nM to 5 μ M. For treatment, the supernatant was discarded and replaced with fresh cell culture media supplemented with drugs in the appropriate therapeutic dilution. Cells were cultured at 37°C and 5 % CO₂ for another 48 h before measuring cell viability. For peptide quantification via **mass spectrometry**, HCT116 WT cells were cultured in 6-well plates (400,000 cells per well in 3 ml) for 24 h and treated with either 20 μ M 5-FU or 20 μ g ml⁻¹ OX. The supernatant was discarded and replaced with fresh cell culture media supplemented with the appropriate therapeutic dilution. Cells were cultured at 37°C and 5 % CO₂ for another 24 h before detaching with accutase solution and generating RIPA lysates. For p53 protein-isoform quantification, EXSISERS_{TP53:2CLuc-4NLuc-7FLuc} cells were cultured in 96-well plates (20,000 cells per well in 100 μ l) for 24 h and subsequently treated with either 20 μ M 5-FU, 20 μ g ml⁻¹ OX, 50 nM IACS-010759.HCl, 1 μ M JNJ-64619178, 5 μ M BLM-IN-1, 1 μ M SJB1-043, 20 μ M bleomycin, or 100 nM doxorubicin. Supernatant was discarded and replaced with fresh cell culture media supplemented with appropriate therapeutic and luciferase substrate dilution. Cells were cultured at 37 °C and 5 % CO₂ for 48 h with 3 h measuring intervals. For immunoblot analysis or flow-cytometry (FC)-based cell death assays, HCT116 WT, EXSISERS_{TP53:4NLuc-7FLuc}, EXSISERS_{TP53:2CLuc-4NLuc-7FLuc}, HCT116 p53-DBD^{-/-}, HCT116 p53^{-/-}, HCT15, Caco-2 cell lines and primary colon fibroblasts were cultured in 24-well plates (100,000 cells per well in 1 ml) for 24 h and, thereafter, treated with either 20 μ M 5-FU, 20 μ g ml⁻¹ OX, 50 nM IACS-010759.HCl, or 1 μ M SJB1-043. The supernatant was discarded and replaced with fresh cell culture media supplemented with appropriate therapeutic dilution. Cells were cultured at 37°C and 5 % CO₂ for 24 h or 48 h before generating RIPA lysates for immunoblotting or before staining cells with DAPI and Annexin-V-FITC for subsequent FC-based cell death assay. For **LIVE/DEAD** determination via fluorescent microscopy, patient-derived primary colon organoids (ethical vote N°:18-982-101) were cultured in BIOFLOAT FLEX coating solution (feCellitate, F202005, for low adhesion) treated 96-well plates (Thermo Fisher Scientific) (3-4 colon organoids per well in 100 μ l) for 24 h. For drug treatment, 100 μ l fresh cell culture media supplemented with appropriate therapeutic dilution (0.0005 % DMSO, 50 nM IACS-010759) were added without discarding supernatant. Cells were cultured at 37°C and 5 % CO₂ for another 48 h before analysis by fluorescence microscopy.

2.3 Protein Biochemical Analysis.

Immunoblot analysis. Cells were detached with accutase solution (Gibco, Thermo Fisher Scientific) or cell scraper (Sarstedt). Samples were centrifuged at 13,000 x g for 30 sec to pellet cells and discard the supernatant. Approximately 1 million cells were lysed in 100 μ l RIPA buffer (Merck) supplemented with protease inhibitors (c0mplete Tablets Mini EDTA free, Roche) and, if necessary, phosphatase inhibitors (PhosSTOP, Roche) according to the manufacturer's protocol. Samples were incubated for 20 min on ice and centrifuged at 13,000 x g for 20 min. Supernatant was transferred to new reaction tubes. Protein concentration of clear lysates was measured using Pierce Rapid Gold BCA Protein Assay Kit (Thermo Fisher Scientific) according to the manufacturer's protocol, and absorbance was measured at 492 nm in a transparent 96-well plate with the EMax Plus Microplate Reader (Molecular Devices). Cell lysates were normalized to the lowest concentrated sample by the addition of RIPA buffer. Lysates were prepared for SDS-PAGE by mixing samples in 6x Laemmli SDS sample buffer (Thermo Fisher Scientific) supplemented with 50 μ M DTT (Merck) and subsequently incubated at 95°C with mild agitation for 10 min. The SDS-PAGE chamber (Mini-PROTEAN Tetra System, Bio-Rad) was filled up with SDS buffer (25 mM Tris (Carl Roth), 250 mM glycine (Carl Roth), 5 mL of 20 % SDS (Carl Roth) in 1 L MilliQ water) and equipped with Mini-PROTEAN TGX gels (4-20 % gradient 10 wells, Bio-Rad). Samples were loaded on the gel and electrophoresis was run at 150 V for 40 min. A protein marker (PageRuler Prestained Protein Ladder, Thermo Fisher Scientific) was also applied to the gel to compare the molecular mass. Subsequently, an immunoblot was generated by transferring the sample from the gel to a PVDF Transfer Membrane (Thermo Fisher Scientific) with a semi-dry blotting system (TE77XP, Hoefner). For this, PVDF membrane and Whatman paper (GE Healthcare) were cut to the size of the gel and placed on top of each other in the following order: 1. Whatman paper wetted in buffer A (300 mM Tris base, 100 ml Methanol (Carl Roth), 400 ml MilliQ water), 2. two Whatman papers wetted in buffer B (25 mM Tris base, 100 ml methanol, 400 ml MilliQ water), 3. PVDF membrane wetted in methanol, 4. SDS-polyacrylamide gel with loaded samples, 5. three Whatman papers wetted in buffer C (25 mM Tris base, 40 mM aminocaproic acid, 100 ml methanol, 400 ml MilliQ water). Blots were run for 50 min at 80 mA per gel. Thereafter, PVDF membranes were blocked in blocking buffer containing 5 % skimmed milk (Carl Roth) dissolved in TBS-T

Material and Methods

buffer containing 0.05 % Tween 20 (Merck) for 1 h at room temperature under mild agitation. Primary antibodies (ab) were diluted in blocking buffer with the indicated dilution factor and either incubated on the membrane for 2 h at room temperature or overnight at 4°C. After the appropriate antibody incubation time, blots were washed with TBS-T at room temperature for 5 rounds, each lasting for 5 min under mild agitation. Secondary HRP-conjugated antibodies were diluted in blocking buffer with the indicated dilution factors and incubated on the membrane for another 2 h at room temperature. HRP was detected using 0.01 % H₂O₂ mixed in ECL solution (1 mM luminol sodium salt (Merck), 0.36 mM p-coumaric acid (Merck), 100 mM Tris base in MilliQ water) directly applied on the antibody-treated membrane, and measured in a ChemiDoc XRS+ Imaging system (Bio-Rad). Primary and secondary antibodies were used as follows: M2 mouse anti-Flag (1:1,000, F3165-1MG, Merck), anti-VSV-G-tag (1:5,000, PA1-30138, Invitrogen), anti-OLLAS-tag (1:5,000, NBP1-06713, NovusBio), anti-Myc-tag (1:1,000, ab32, abcam), DO1 anti-p53 (1:1,000, sc-126, Santa Cruz), ab26 anti-p53 (1:1,000, ab26, abcam), DO-12 anti-p53 (1:1,000, 153403, ximbio), PAb421 anti-p53 (1:1,000, OP03, Merck), PAb240 anti-p53 (1:1,000, CBL404, Merck), anti-p53 phospho S15 (1:1,000, ab1431, abcam), anti-p53 phospho S315 (1:1000, sc-135772, Santa Cruz) anti-p21 (1:1,000, ab188224, abcam), anti-PARP (1:1,000, 46D11, Cell Signaling), anti-beta actin HRP-conjugated (1:10,000, ab49900, abcam), anti-mouse IgG HRP-conjugated (1:2,500, ab6728, abcam), anti-rabbit IgG HRP-conjugated (1:20,000, 31460, Thermo Fisher), anti-rat IgG HRP-conjugated (1:5,000, ab97057, abcam). Re-Blot Plus Strong Solution (MilliQ) was used for 20 min at room temperature and mild agitation to remove bound antibodies and re-use the PVDF membrane. Subsequently, the membrane was washed with MilliQ water, blocked in blocking solution for 1 h at room temperature, and retreated with a new primary antibody. Beta-actin signals were used for normalization purposes. Densitometric analysis was performed with ImageJ.

Immunoprecipitation. Cell lysates were prepared as described for immunoblot analysis (see section *Immunoblot analysis*). If cleared cell lysate was still viscous, incubation at 95°C for 10 min and mild agitation was performed. Cell lysates were pre-cleared by adding approximately 10 µg of isotope- and species-specific antibody control to 1 ml cell lysates and incubating samples for 1 h on ice. Thereafter, 100 µL of protein G-conjugated agarose bead (Merck) slurry was added to each sample and

Material and Methods

incubated for another 30 min on ice. The cell lysate-antibody-agarose bead mix was centrifuged at 14,000 x *g* for 10 min, and supernatant was saved in a new reaction tube while the bead pellet was discarded. Preclearing is unnecessary, but we recommend this step as it may reduce background signal. 100 μ l Protein G-conjugated agarose beads were mixed with 10 μ l primary antibody at the recommended dilution factor and incubated at 4°C for 4 h. Antibody-coupled beads were centrifuged at 2,000 x *g* for 2 min, and supernatant was discarded. The antibody-bead mixture was washed with RIPA lysis buffer twice before adding 10 - 50 μ g of cell lysate and incubating at 4°C overnight under rotatory agitation. Samples were centrifuged at 2,000 x *g* for 2 min, and the supernatant was removed (stored at -80 °C for IP control). Bead pellets were washed with RIPA lysis buffer at least three times. Thereafter, specifically bound proteins were eluted in an appropriate volume of 0.2 M glycine (pH 2.6) by incubating beads for 10 min under mild agitation. This elution procedure prevents non-covalent antibody complexes from being co-eluted. Subsequently, eluted samples were neutralized with an equal volume of Tris (pH 8.0). Samples were analyzed via immunoblotting.

p53 transcription factor binding assay. This assay was applied on HCT116 WT and genetically edited HCT116 p53DBD^{-/-} and HCT116 EXSISERS cell lines. Cells were harvested from a 75 cm² flask by scraping cells with a cell scraper (Sarstedt) and 10 ml ice-cold PBS off the surface and pelleted in a reaction tube by centrifuging at 13,000 x *g* for 30 sec. We isolated the nuclear extracts for HCT116 WT, EXSISERS^{TP53:7FLuc}, EXSISERS^{TP53:4NLuc-7FLuc}, HCT116 3.E7, and HCT116 p53 DBD^{-/-} cells by adding 1 mL of ice-HB buffer, incubating for 15 min on ice and adding 50 μ L of NP-40 (stock conc.: 10 %, Merck). Cell lysates were centrifuged at 13,000 x *g* for 30 sec, and supernatant was discarded while nuclear pellets were lysed with 50 μ L complete lysis buffer (provided by assay). p53 transcription factor binding assay (ab207225, Abcam) was conducted according to the manufacturer's protocol. Absorbance was measured at 450 nm with EMax Plus Microplate Reader (Molecular Devices).

p53 transcription factor activity assay. A transiently transfected reporter plasmid with fluorescent output measured the transcriptional activity of p53 in HCT116 WT and EXSISERSTP53:4NLuc-7FLuc cells. Therefore, corresponding cells were seeded into black 96-well plates with clear bottom (Berthold) for optimal fluorescent quantification.

After 24 h, cells were transfected with reporter plasmids consisting of the coding sequence for mNeonGreen (mNG) driven by the promoter sequence of the *p53RFP* gene. The promoter region reveals multiple p53 response elements (p53-RE), which can be targeted and induced by the transcriptional activation of p53. As a control plasmid, we created another reporter plasmid coding the same green fluorescent mNG, but this time driven by the upstream sequence of the *LMF* gene carrying none of the p53RE. Cells were either transfected with inducing constructs (dCas9-VPR + *TP53* sgRNA 6: G+AGTCAGGATTCTCGCCGACC vs. empty sgRNA) or treated with p53 inducing agents (e.g., 5-FU). Fluorescent signals were measured with the TriStar² LB 942 Multimode Reader (Berthold).

Mass spectrometry sample preparation. HCT116 WT cells were seeded into 6-well plates in triplicates at a cell density of 600,000 in 3 ml of appropriate medium per well. After 24 h of culturing, cells were either treated with DMSO (control), 20 mJ cm⁻² UV-light, 20 μM 5-FU, or 20 μg ml⁻¹ oxaliplatin and cultured for another 24 h. Thereafter, cells were detached from the plate surface with a cell scraper (Sarstedt) and transferred into reaction tubes. Cells were pelleted by centrifugation (13,000 x g, 30 sec), washed once with ice-cold PBS, and lysed with 200 μl RIPA buffer (Merck) supplemented with protease inhibitors (cOmplete Tablets Mini EDTA free, Roche). Protein concentration was determined using Pierce Rapid Gold BCA Protein Assay Kit (Thermo Fisher Scientific) according to the manufacturer's protocol, and absorbance was measured at 492 nm in a transparent 96-well plate with the EMax Plus Microplate Reader (Molecular Devices). For absolute p53 protein isoform quantification via multiple reaction monitoring (MRM) mass spectrometry, 5 μL of protein lysate was spiked with 80fmol ¹⁵N-labelled-recombinant p53 protein (PolyQuant GmbH). Protein digestion was performed according to the FASP protocol [180].

Liquid Chromatography-Tandem Mass Spectrometry (LC-MS/MS analysis). Multiple reaction monitoring (MRM) analyses were performed on a triple quadrupole mass spectrometer with a nano-electrospray ion source (TSQ Vantage, Thermo Scientific). Chromatographic separation of the peptides was performed by liquid chromatography on a nano-UHPLC system (Ultimate 3000 RSLC, Dionex) using a nano-LC column (Acclaim PepMap100 C18, column i.d. 75 μm, column length 500 mm, particle size 3 μm, pore size 100 Å, Dionex). Samples were injected from a

cooled autosampler (5 °C) and loaded onto a trap column (μ Precolumn cartridge, Acclaim PepMap100 C18, column i.d. 300 μ m, column length 5 mm, particle size 5 μ m, pore size 100 Å, Dionex) at 4 μ g total protein digest using the μ L-pickup method with 0.1 % v/v formic acid as a transport liquid. Peptides were separated on the nano-LC column using a linear gradient from 3-60 % v/v acetonitrile plus 0.1% v/v formic acid in 100 min at a flowrate of 300 nL/min.

The mass spectrometer was operated in the positive mode at a spray voltage of 1500 V, a capillary temperature of 270 °C, a half maximum peak width of 0.7 m/z for Q1 and Q3, a collision gas pressure of 1.2 mTorr and a cycle time of 1.2 ms. Optimal collision energies (CE) were predicted using the following linear equations: $CE = 0.03 \times m/z$ of precursor ion + 2.905 for doubly charged precursor ions, and $CE = 0.03 \times m/z$ of precursor ion + 2.467 for triply charged precursor ions. For each of the peptides, the optimal precursor charge and up to three optimal transitions were selected after screening with the concatemers. Isolation windows of 10 min were used, centered at the observed retention times of the peptide precursor. (This protocol was kindly provided by Dr. Florian Sigloch from Polyquant, Bad Abbach, Germany)

2.4 DNA Design and Analysis.

T7 Endonuclease assay. For analysis of genome targeting efficiency, HCT116 WT cells were seeded into 6-well plates (one well for each sgRNA with a different spacer sequence). Cells were transfected with expression plasmids coding for (CBh hybrid RNA polymerase II promoter-driven) mammalian codon-optimized Cas9 from *Streptococcus pyogenes* (*SpCas9*), including a tandem C-terminal SV40 nuclear localization signal (SV40 NLS) and a (human U6 RNA polymerase III promoter-driven) single-guide-RNA (sgRNA) sequence. 48 h post-transfection, cells were detached with 1.5 ml PBS and cell scraper (Sarstedt) and centrifuged at 13,000 $\times g$ for 30 sec. Supernatant was discarded, and genomic DNA was purified with Wizard Genomic DNA Purification Kit (Promega) according to the manufacturer's protocol. Primer sequences were designed to bind 300 – 500 bp upstream and downstream of the DNA-DSB-site. PCR amplification was conducted with Q5 HS Polymerase Master Mix (NEB), and PCR amplicons (600 – 1000 bp) were purified using PCR Clean-Up Kit (NEB). T7 Endonuclease Assay was performed according to the manufacturer's protocol using T7 Endonuclease I (NEB). Genome targeting efficiency for specific sgRNA spacer sequences was given in percent.

Genomic DNA isolation and genotyping. To sequence the gene-edited locus, corresponding cells were detached from the cell culture flask with accutase solution (Thermo Fisher Scientific) and split into a new cell-culture flask at a 1:5 ratio. The residual cell suspension was centrifuged at 13,000 x *g* for 30 sec, and supernatant was discarded. According to the manufacturer's protocol, genomic DNA was isolated using the Wizard Genomic DNA Purification Kit (Promega). Genomic DNA was resuspended into 30 – 50 μ l nuclease-free water, and DNA concentration was measured using a Nanophotometer with the corresponding LG100-UV-G quartz cuvette (IMPLEN). 500 ng of corresponding genomic DNA samples were used for PCR amplification. Primers were designed to bind 500 bp upstream and downstream of the modified genomic locus. Q5 HS polymerase Master Mix (NEB) was used to run the PCR amplification reaction. PCR reaction was loaded on an agarose gel for gel electrophoresis to verify the successful amplification of the desired locus. Agarose gels were analyzed using the ChemiDoc XRS+ Imaging system (Bio-Rad) before cutting out the desired bands and purifying the DNA amplicons with a gel extraction kit (QIAGEN). DNA concentration of DNA amplicons was measured and diluted to a final of 100 ng μ l⁻¹. Samples were sent for sequencing using the GATC-services from Eurofins genomics.

Design of EXSISERS constructs. Plasmids and primers were designed with Geneious Prime software. All DNA-donor plasmids for HDR-mediated knock-in of the EXSISERS-reporters into p53 are provided in the supplement information as vector cards. EXSISERS-reporters consist of a central luciferase (either *Firefly* luciferase from *Phytinus pyralis* (PpyFLuc), *Nano* luciferase (NLuc, Promega), or *Cypridina* luciferase (CLuc)), flanked by antiparallel helices (either AP3 and AP4, AP5 and AP6, or helical domains of c-Jun and c-Fos), in turn, flanked by split-inteins (either N- and C-terminal NrdJ-1, N- and C-gp41-1, or N- and C-IMPDH-1). Split-inteins initiate co-translational excision of the EXSISERS-reporter out of the flanking amino acid sequences (exteins) of p53 in an auto-catalytical manner. In proximity to the split-inteins located antiparallel helices were shown by Truong et al. to accelerate the splicing process by efficiently guiding the split-inteins in spatial proximity [152]. IMPDH-1-CLuc additionally consists of a start-transfer signal (placed between N-IMPDH-1 intein and CLuc) and a stop-transfer signal (placed between CLuc and C-IMDPH-1 intein). These transfer signals enable CLuc to be translocated into the lumen of the endoplasmic reticulum (ER) while

both split-inteins and p53 exteins remain in the cytoplasm. During intein-splicing, p53 is spatially separated from ER membrane-anchored IMPDH-1-CLuc. Additional consecutive transport and export signals, including ER export signal, Golgi export signal, and plasma membrane trafficking signal (located between stop transfer signal and C-IMPDH-1 intein) enable efficient transport of IMPDH-1-CLuc to the plasma membrane. EXSISERS-reporters were placed upstream of a serine or cysteine to provide the requirements for co-translational processing of inteins and subsequent junction of the flanking p53 exteins. EXSISERS-reporters also carry recombinant tags to be efficiently detected in immunoblot and immunofluorescence analyses. These include an OLLAS-tag (gp41-1-AP6/5-NLuc), a c-Myc-tag (NrdJ-1-AP4/3-FLuc), and a VSV-g-tag (IMPDH-1-c-Jun/Fos-CLuc).

2.5 RNA Analysis.

Isolation of mRNA and generation of cDNA. HCT116 WT or gene-edited cell lines (EXSISERS_{TP53:7FLuc}, EXSISERS_{TP53:4NLuc-7FLuc}, and EXSISERS_{TP53:2CLuc-4NLuc-7FLuc}) intended for p53 transcription analysis (either alone or including stable integrated EXSISERS-reporters), were detached from the cell culture flask with accutase solution and transferred to a reaction tube to be centrifuged at 13,000 x g for 30 sec. Supernatant was discarded while the remaining cell pellet was washed with PBS and centrifuged. PBS-supernatant was discarded, cell pellet was lysed and processed for mRNA isolation with Monarch Total RNA Miniprep Kit (NEB) according to the manufacturer's protocol. Total RNA was eluted in approximately 30 µl of nuclease-free water. Concentration was measured with a Nanophotometer using the LG100-UV-G quartz cuvette (IMPLEN). 1 µg of total RNA was used for reverse transcription into cDNA. Reverse transcription was conducted with Reverse Transcription System (Promega) according to the manufacturer's protocol. The concentration of reverse-transcribed cDNA was measured with the nanophotometer. Depending on the subsequently applied method (e.g., PCR, gel-electrophoresis, RT-qPCR), 1 – 4 µl of the previously generated cDNA solution was utilized.

Real-time quantitative PCR. 1 µl of cDNA generated from isolated and reverse transcribed mRNA was used for the follow-up real-time quantitative PCR. 1 µl of cDNA, 0.5 µl of corresponding forward and 0.5 µl of the reverse primer (stock conc. 100 µM), 5 µl Brilliant III Ultra-Fast SYBR Green qPCR Master Mix (Agilent), and 3 µl nuclease-

free water were mixed in a LightCycler 480 Multiwell Plate 384 (Roche). The plate was centrifuged at 1,000 x g for 1 min to ensure the reaction mixture settled at the well's bottom. RT-qPCR reactions were run with a LightCycler 480 (Roche), and Ct-values were determined with the corresponding software. Additional RT-qPCR reactions were run as a normalization control to determine the Cp-values of housekeeping genes, including GAPDH and β 2m (forward and reverse primer obtained from metabion). $\Delta\Delta$ Ct values were calculated based on the double-cycle threshold method for each replicate.

Analytical PCR. For analytical visualization of certain cDNA-transcripts via agarose gel electrophoresis, 2 - 4 μ l of reverse-transcribed cDNA were mixed with corresponding forward and reverse primer (working conc.: 500 nM), and 25 μ l Q5 Polymerase Master Mix (NEB) and filled up with nuclease-free water to a total volume of 50 μ l. PCR reactions were run on a non-quantitative ThermoCycler. PCR reaction was loaded on a 1 % agarose gel, and electrophoresis was conducted with 120 V and 400 mA for 1 h. Gels were analyzed on a ChemiDoc XRS+ Imaging system. p53 transcriptional activity was determined using the $\Delta\Delta$ Ct method. Differential isoform expression of FLp53, Δ 40p53, and Δ 133+ Δ 160p53 was determined using the formula given in the section *Computational differentiation of p53 isoforms*. All primer sequences are included in the supplementary information.

2.6 Cellular and Molecular Imaging.

Cell viability assay. Colorectal cancer cell lines were seeded on black 96-well plates with clear bottom (Berthold) with a cell density of 20,000 in 100 μ l per well. Seeded cells were cultured at 37 °C and 5 % CO₂ for 24 h before replacing the supernatant with fresh cell culture media supplemented with specific therapeutic in an appropriate concentration. Therapeutic treatments were conducted for 48 h before adding an equal volume of CellTiter-Glo 2.0 (Promega) into each well. Cell viability assay was performed according to the manufacturer's protocol. A TriStar2 LB 942 Multimode Reader (Berthold) measured luminescent signals representing cell viability. Raw data was normalized to blank wells and relativized to non- or DMSO-treated cells.

Cell death assay. Distinct CRC-cell lines and non-/inflamed fibroblasts were seeded into 24-well plates with a cell density of 100,000 in 1 ml per well. Seeded cells were

Material and Methods

cultured at 37 °C and 5 % CO₂ for 24 h before replacing the supernatant with fresh cell culture media supplemented with specific therapeutic in an appropriate concentration. Treatments were conducted for 24 h and 48 h before transferring supernatant and detached cells (with accutase solution) into new reaction tubes. Live and potentially dead cells were centrifuged at 500 x g for 3 min, and the supernatant was discarded while pelleted cells were resuspended into PBS. After repeated centrifugation and supernatant removal, cells were resuspended and incubated in 500 µl of Ca²⁺ and Mg²⁺ containing ice-cold PBS supplemented with 5 µl (1:100 dilution) FITC-Annexin V (556419, BD) and 100 nM DAPI (564907, BD). Thereafter, stained cells were pipetted through a cell strainer cap into round-bottom polystyrene tubes (Thermo Fisher Scientific) and were measured and analyzed with an LSRFortessa (BD) and the corresponding FACSDiva™ software (BD) concerning Pacific Blue and FITC fluorescent signal. Quadrant 4 (Q4) represents living cells, Q3 represents early apoptotic cells, and Q2 represents late-apoptotic or necrotic cells. Quadrant fractions were specified by using the FlowLogic software. Specific cell death was calculated using the following equation [181]:

$$\frac{\% \text{ Cell death}_{\text{treated}} (Q2 + Q3) - \% \text{ Cell death}_{\text{control}} (Q2 + Q3)}{100 - \% \text{ Cell death}_{\text{control}} (Q2 + Q3)}$$

Immunofluorescence microscopy of cell lines. Cells (either transfected HCT116 WT or stable EXSISERS_{TP53:2CLuc-4NLuc-7FLuc}) considered for immunostaining and fluorescence-microscopy were seeded onto black 24-well µ-plates (ibidi) with a cell density of 100,000 in 1 ml per well. Seeded cells were either cultivated for 24 h at 37 °C and directly prepared for immunostaining or first incubated for 24 h at 37 °C, then transfected with mammalian expression DNA plasmids and ultimately incubated for another 48 h before preparing cells for immunostaining. Therefore, the supernatant was discarded, and cells were washed with 1 ml of ice-cold PBS containing Mg²⁺ and Ca²⁺ (Thermo Fisher Scientific). For cell fixation, cells were incubated with 4 % paraformaldehyde solution (Thermo Fisher Scientific) for 5 min at RT. Cells were washed three times with 1 ml of ice-cold PBS (Mg²⁺ and Ca²⁺) and afterward incubated with 95°C prewarmed unmasking buffer (10 mM Tris base (Carl Roth), 1 mM EDTA (Carl Roth), 0.05 % Tween 20 (Carl Roth), pH 9.0) for 10 min. Cells were washed three times with PBS and incubated with permeabilization buffer (0.25 % Triton X-100 (Carl

Material and Methods

Roth) dissolved in PBS) for 10 min at RT. Cells were washed three times with 1 ml of ice-cold PBS (Mg^{2+} and Ca^{2+}) to be subsequently incubated with blocking buffer (either in 1 % bovine serum albumin (BSA, Carl Roth) or 1 % skimmed milk and 0.1 % Tween 20 dissolved in PBS) for 30 min. Primary antibodies were diluted in blocking buffer in a suitable concentration as specified by the manufacturer. Blocking buffer was replaced with a primary antibody-containing blocking buffer and incubated for 2 h at 37°C. Cells were washed three times with ice-cold PBS and incubated with fluorophore-conjugated secondary antibody (diluted accordingly in blocking buffer) for 2 h at 37°C. Cells were subsequently washed three times with ice-cold PBS again and incubated with a 300 nM DAPI solution (diluted in PBS) for 7 min at RT. Cells were washed three times with ice-cold PBS and stored in PBS (with Mg^{2+} and Ca^{2+}) at 4 °C until further use. Fluorescence microscopic images were taken with a BZ-X800 fluorescence microscope (Keyence) and analyzed with the corresponding software. Primary and secondary antibodies were used as follows: anti-VSV-G-tag (1:250, PA1-30138, invitrogen), DO1 anti p53 (1:250, sc-126, Santa Cruz), anti-calreticulin – ER marker (1:250, PA1-902A, Thermo Fisher Scientific), anti-GM130-AF488-conjugated – Golgi marker (1:100, ab52649, abcam), anti-mouse-AF488-conjugated (1:400, ab150117, abcam), anti-rabbit IgG-AF488, anti-chicken IgY-AF488 conjugated (1:250, A11039, Thermo Fisher Scientific).

LIVE/DEAD staining/imaging of organoids. Organoids were generated from epithelial cells of patients' colon biopsies (see section *Organoid generation and maintenance*). After successful expansion, a predetermined amount of colon organoids was extracted from Matrigel (Corning), seeded onto 96-well-round-bottom plates (Thermo Fisher Scientific), and cultured in 100 μ l 3dGRO™ Human Colon Organoid Expansion Media (Merck) at 37 °C and 5 % CO₂ for 24 h. Thereafter, an equal volume of 3dGRO™ supplemented with an appropriate concentration of therapeutic compound (IACS-010759.HCl working concentration on organoids: 500 nM) was added to the existing media and cultured for another 48 h. For LIVE/DEAD staining, 100 μ l of the excess medium was discarded, and the remaining 100 μ l, including the organoids were carefully transferred with wide bore filtered pipette tips (Merck) into a 96-well microtiter plate applicable for fluorescence microscopy. LIVE/DEAD staining Kit (R37601, Thermo Fisher Scientific) consisting of Calcein-AM (live-cell staining) and propidium iodide (dead-cell staining) was used to stain organoids according to the manufacturer's

Material and Methods

protocol. Both staining solutions were thawed at RT and mixed to generate a 2X concentrated stock solution. Equal volumes of mixed staining solution (100 μ l) were added to the 96-wells containing 3dGRO media and the corresponding colon organoids. Staining solution was incubated for 10 min, and organoids, including LIVE and DEAD fluorescent signals, were subsequently analyzed and quantified with a BZ-X800 fluorescence microscope (Keyence). Integration times (FITC-, Texas Red-channel) were defined for each organoid type (healthy: No.76, No.77, No.92; tumor: No.80, No.86, C18, C20) but kept constant between DMSO control and IACS-010759 treatment. Fluorescent signal intensities were quantified using the corresponding analysis software and set into ratio (LIVE (green fluorescence intensity): DEAD (red fluorescence intensity)). LIVE : DEAD ratios of DMSO control samples were set to 1, while LIVE : DEAD ratios of IACS-010759 treated samples were relativized to the DMSO control ratios.

Live cell/real-time bioluminescence quantification. EXSISERS-reporters IMPDH-1-CLuc, gp41-1-NLuc, and NrdJ-1-FLuc convert their specific substrates vargulin (#305-10, NanoLight Technology), furimazine, and D-luciferin (E2920, DualGlo Assay, Promega), respectively, into the oxidated equivalent and, thereby, show emission maxima at specific wavelengths (CLuc λ_{Em} = 465 nm, NLuc λ_{Em} = 460 nm, FLuc λ_{Em} = 565 nm). These reporters reflect the cellular p53 protein isoform abundance and enable the relative quantification of individual p53 protein isoform groups. Applying membrane-permeable substrates such as D-luciferin ethyl ester (ab275489, abcam) and Endurazine (furimazine analogon, N2570, Promega) also allows quantitative measurements in a live-cell and *real-time* manner. IMPDH-1-CLuc is anchored and exposed to the plasma membrane and, therefore, accessible to membrane-impermeable vargulin. Since CLuc and NanoLuc display emission maxima at similar wavelengths, luminescence signals for each luciferase were measured on separate plates. For measuring, EXSISERS_{TP53:2CLuc-4NLuc-7FLuc} cells were seeded on white 96-well plates with clear bottom (Berthold) with a cell-density of 20,000 in 100 μ l of appropriate media per well. Thus, at least three separate plates were seeded for each measurable condition. 96-well plates were cultured at 37 °C and 5 % CO₂ for 24 h. Thereafter, supernatant was discarded and replaced with fresh media, each supplemented with the appropriate luciferase-substrate (vargulin stock conc.: 50 mM in DMSO, working conc.: 50 μ M; D-luciferin ethyl ester stock conc.:

Material and Methods

100 mM in DMSO, working conc.: 100 μ M; Endurazine working concentration 1:100 dilution). IMPDH-1-CLuc luminescence was measured with a TriStar² LB 942 Multimode Reader (Berthold) immediately after substrate addition to record t_0 values (normalization control). NrdJ-1-FLuc and gp41-1-NLuc luminescence were measured after 20 min of incubation at 37 °C to enable the internalization of luciferase substrates. After recording t_0 values for all three luciferases, supernatant was discarded and replaced with fresh media, each supplemented with the appropriate luciferase substrate and the corresponding treatment (e.g., 20 μ g ml⁻¹ oxaliplatin, 20 μ M 5-FU, 50 nM IACS-010759.HCl, 1 μ M SJB2-043, 1 μ M JNJ-64619178, 5 μ M BLM-IN-1, 20 μ M bleomycin, 100 nM doxorubicin). New D-luciferin-ethyl ester was added every 12 h at the indicated concentration. Fresh vargulin was added before every measurement at the indicated concentration. Luciferase signals were recorded after 3 h, 6 h, 9 h, 12 h, 24 h, and 48 h of treatment ([Supplementary Fig. 8](#)). Absolute values were normalized to t_0 values and relativized to DMSO control recorded at the same timepoint.

Computational differentiation of p53 isoforms. The three EXSISERS-reporters either represent individual p53 protein isoform groups or an association of several p53 isoform groups. IMPDH-1-CLuc signals represent cellular FLp53 abundance. Gp41-1-NLuc signals represent all tumor suppressive isoforms, including FLp53 and Δ 40p53. NrdJ-1-FLuc signals count for total cellular p53 (including FLp53, Δ 40p53, Δ 133p53, and Δ 160p53). Accordingly, quantifying Δ 40p53 and oncogenic isoforms (Δ 133p53 + Δ 160p53) are obtainable by subtracting the relative luminescence values of selected luciferases. Luminescence signals are calculated as follows:

$$\text{Rel. luminescence} = \frac{\text{Luciferase signal}_{\text{treated (t=x)}}}{\emptyset(\text{Luciferase signal}_{\text{control (t=x)}} \text{ replicates})}$$

Consequently, the relative Δ 40p53 quantity is calculated as follows: $\text{Rel. } \Delta 40\text{p53} = (\text{NLuc}_{\text{rel.sig.}} - \text{CypLuc}_{\text{rel.sig.}}) + \text{NLuc}_{\text{rel.sig.}}$

And relative oncogenic p53 isoform (Δ 133p53 + Δ 160p53) quantity is calculated as follows:

$$\text{Rel. } \Delta 133 + \Delta 160\text{p53} = (\text{FLuc}_{\text{rel.sig.}} - \text{NypLuc}_{\text{rel.sig.}}) + \text{FLuc}_{\text{rel.sig.}}$$

Anti-cancer drug library screening. For the screening of differentially expressed p53 protein isoforms (tumor suppressive vs. oncogenic), upon treatment with an anti-cancer compound library comprising 4,863 different compounds (HY-L025, MedChemExpress, 2021), EXSISERS_{TP53:4NLuc-7FLuc} cells (including gp41-1-NLuc within coding exon 4 and NrdJ-1-FLuc within coding exon 7 in *TP53*) were seeded into white 96-well plates with clear bottom (Berthold) at a cell density of 20,000 in 100 μ l of appropriate media per well. Cells were cultured for 24 h before screening. As described in section *Live cell/real-time bioluminescence quantification*, t_0 luminescence was determined for each seeded well in advance (normalization control). All compounds were diluted to a working concentration of 5 μ M or 5 μ g ml⁻¹. Luminescent signal was measured on separate plates for each EXSISERS-reporter (gp41-1-NLuc and NrdJ-1-FLuc). Thus, an experimental setup was conducted twice. NrdJ-1-FLuc and gp41-1-NLuc signals were recorded with the TriStar² LB 942 Multimode Reader (Berthold) after 3 h, 6 h, 9 h, 12 h, 24 h, and 48 h of treatment. New D-luciferin-ethyl ester was added every 12 h at the indicated concentration. In addition, DMSO control-wells were measured to relativize the luminescent data captured for the therapeutic compounds. Relative luminescence signals for each EXSISERS-reporter were calculated as indicated in the section above. In some cases, calculated Δ 133p53 and Δ 160p53 abundances can fall below zero. Therefore, all relative p53 isoform values were converted and calculated in an exponential manner:

$$\text{Rel. FLp53} + \Delta 40\text{p53} = e^{\text{[NLuc}_{\text{rel.sig.}} - 1]}$$

$$\text{Rel. } \Delta 133 + \Delta 160\text{p53} = e^{\text{[(FLuc}_{\text{rel.sig.}} - \text{NLuc}_{\text{rel.sig.}}) + \text{FLuc}_{\text{rel.sig.}} - 1]}$$

The isoform ratio is calculated as follows:

$$\text{p53 isoform ratio}_{\text{tumor suppressive vs. oncogenic}} = \frac{\text{Rel. FLp53} + \Delta 40\text{p53}}{\Delta 133\text{p53} + \Delta 160\text{p53}}$$

2.7 Software.

Graphical plots and statistics were done using GraphPad Prism. Graphical figures were designed with Inkscape and Biorender.com. Densitometric analysis of immunoblots was conducted with ImageJ. Processing of immunoblots and agarose gels was done by ImageLab software. Plasmid maps were designed and viewed with Geneious Prime. Data collected by flow cytometry were analyzed with FlowLogic.

Material and Methods

Mass spectrometry data obtained from Polyquant (Bad Abbach, Germany) were viewed and analyzed with Skyline software. Protein structures were loaded from the Protein Data Base (PDB) and viewed with PyMol. For pathway analysis, a Python script was created to count the pathway abundance for all drugs depicted either in the anti-cancer compound library or in the Excel sheets created for the identified p53-TIEs and p53-OIEs. The Python script is shown in Supplementary Figure 5.

2.8 Contribution

The following “Result” section includes data, that were partially acquired with the assistance of the following persons: Elisabeth Aschenbrenner (Fig. 9, 10, 15, 16, 23, 27, 28, 30, 31, 32, 33), Manuela Gunckel (Fig. 35), Kirstin Pollinger (Fig. 31, 32, 33), Barbara Volz (Fig. 12, 27, 28, 30), Katja Neumeyer (providence of the HCT116 p53^{-/-} cell line, Fig. 27, 28, 30), Veruschka Albert (Fig. 11, 12), Kathrin Heider (Fig. 16), Mara Kießling (Fig. 16), Dr. Florian Sigloch (Polyquant) and Prof. Dr. Peter Oefner (Fig. 25, 26). Data was analyzed, edited, and plotted exclusively by me, Deniz Tümen.

3. Results

3.1 Establishment and optimization of a novel triple EXSISERS reporter system.

To establish, validate and optimize the triple-EXSISERS reporter system, we were obliged to identify the optimal pairing of split-inteins and luciferases since each combination can yield different splicing rates due to favourable or non-favourable steric factors. From previous studies, we already ascertained that gp41-1-NLuc and NrdJ-1-FLuc are optimal combinational reporters [152]. As we seek to broaden the scope of multiplexed quantitative measurements, we aspire to establish a new split-intein-luciferase as an EXSISERS reporter to show robust protein splicing and good compatibility with the other luciferases regarding substrate-specificity. In conjunction with the previously introduced gp41-1 and NrdJ-1 split-inteins, we chose additional naturally occurring split-inteins candidates for expanding the EXSISERS reporter repertoire, namely gp41-8 and IMPDH-1. These split-inteins have small molecular sizes and show fast splicing rates [166]. In comparison to coherent inteins, split-inteins can be expressed spatially separated. Consequently, the N-terminal and C-terminal parts of the split-inteins were placed on either side of the selected luciferase reporters (Fig. 8a). Initially, we used gp41-8 split-intein to be combined with the artificially engineered Green Renilla luciferase (GreenRLuc8.6) [182].

We determined its protein-splicing efficiency by introducing the gp41-8-GreenRLuc8.6 reporter system into a splitted fluorescent protein, namely split-mNeonGreen (mNG). For comparative analysis, we also incorporated gp41-1-NLuc and NrdJ-1-FLuc into split-mNeonGreen, each recombinantly designed in a separate mammalian expression plasmid. The EXSISERS reporters were positioned within the amino acid sequence of mNG, each preceding a serine or cysteine residue to ensure the catalytic prerequisites for protein splicing. As already described, a serine or cysteine subsequently after the EXSISERS reporter is obligatory for enabling the initial N-O or N-S acyl-shift to prepare for the subsequent intein-extein rearrangement.

If the splicing-process has undergone successfully, N- and C-terminal split-inteins incorporating the luciferase reporter autocatalytically excise out of the mNG. Thereby, both mNG parts are ligated together and reconstitute the fluorescence activity. A strong fluorescent signal directly correlates with a strong protein expression and efficient intein splicing. Previous studies have shown that adding two complementary anti-

Results

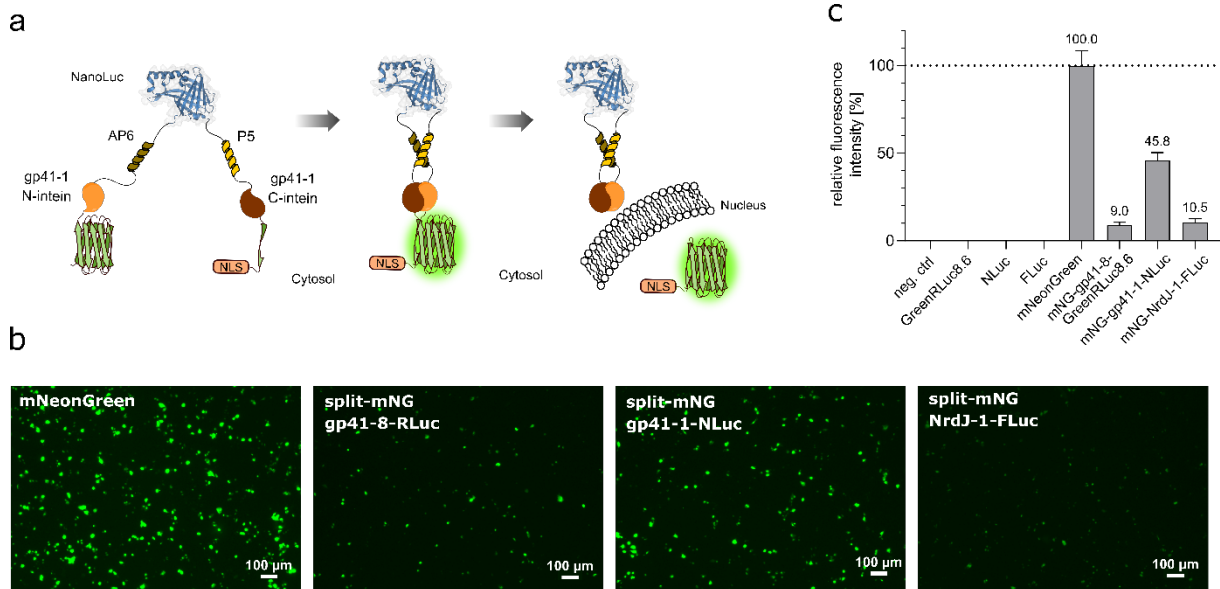


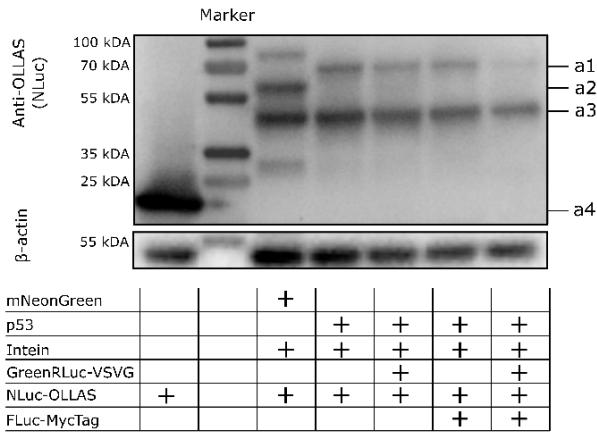
Figure 8: Determination of splicing-efficiency of distinct split-intein/luciferase combinations for assembly into functional EXSISERS reporters. **a)** Test-construct gp41-1-NLuc incorporated into mNG visualizes the process of protein-splicing, EXSISERS reporter excision and ligation of the mNG-extein halves. Split-mNG represents the two N- and C-terminal exteins flanking the central intein-luciferase reporter system (EXSISERS). The two antiparallel helices (e.g. AP5 and 6) placed in close proximity to each split intein-halve, significantly accelerates the splicing rate. **b)** Fluorescence-microscopy-images of cells overexpressing either functional mNG alone or one of three EXSISERS reporters embedded into split-mNG. Green fluorescence reveals working splicing process for the tested EXSISERS constructs. **c)** Fluorescent signals shown in b) were quantified with a Berthold TriStar² Fluorometer and absolute fluorescence values were normalized to the value measured for mNG alone and set to 100 %.

parallel helices in proximity to each split-intein significantly increases the split-intein splicing-rates [152]. Therefore, we designed the EXSISERS reporters to carry anti-parallel helices AP5 & AP6 in gp41-1-NLuc, AP3 & AP4 in NrdJ-1-FLuc, and interacting domains of the c-Jun & c-Fos leucine-zipper in gp41-8-GreenRLuc8.6 (Fig. 8a).

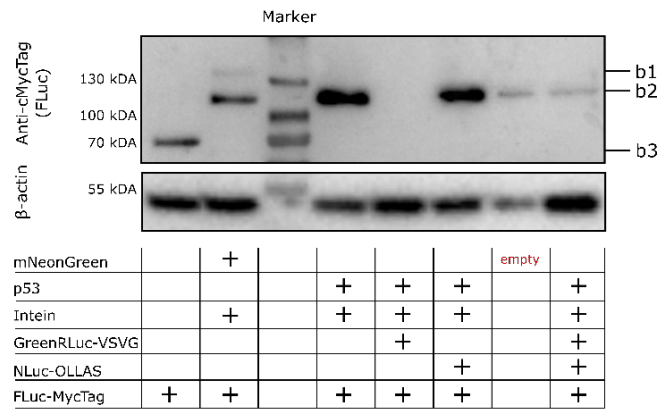
Compared to the control plasmid expressing mNG alone, intein-splicing of all EXSISERS reporters was able to reconstitute the fluorescence activity of mNG (Fig 8b). Since gp41-1 is known to possess the fastest splicing rates, EXSISERS reporters, including gp41-1-NLuc, reached the strongest mNG-fluorescence signals (up to 46 %) (Fig. 8c). The other EXSISERS reporters consisting of gp41-8-GreenRLuc8.6 and NrdJ-1-FLuc reached 9.0 and 10.5 % of reconstituted fluorescence activity. The lower signals are explainable by lower splicing rates of the gp41-8 and NrdJ-1 inteins and also by the larger protein sizes to be expressed by the cell (gp41-1-NLuc = 44.2 kDa; gp41-8-GreenRLuc8.6 = 62.6 kDa; NrdJ-1-FLuc = 88.7 kDa). Even though observing lower fluorescent signals for mNG, including the EXSISERS reporters, this experiment conclusively reveals the working autocatalytic excision of all EXSISERS reporters from

Results

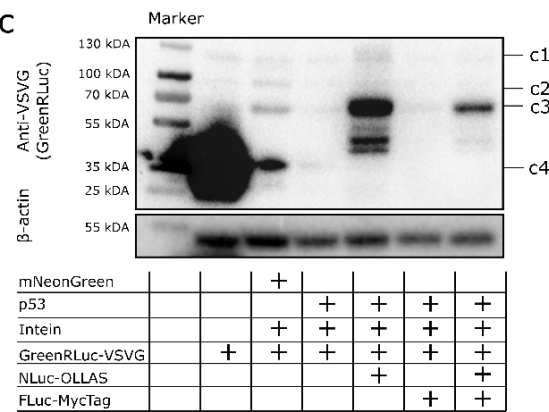
a



b



c

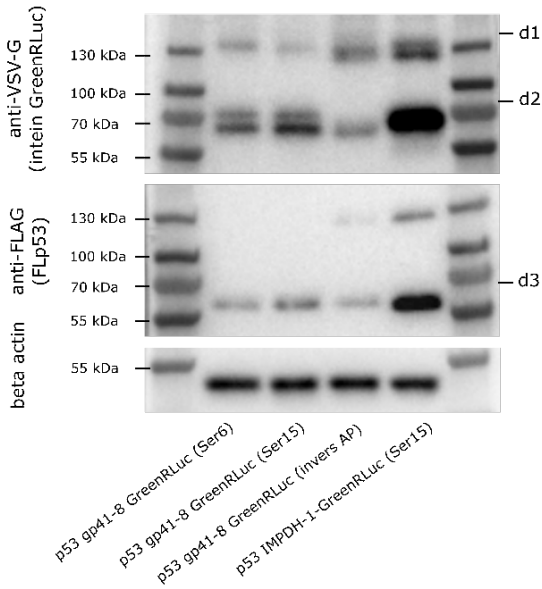


a1 p53 gp41-1 AP5/6 NLuc OLLAS-tag (unspliced) ~ 89 kDa
a2 mNG gp41-1 AP5/6 NLuc OLLAS-tag (unspliced) ~ 76 kDa
a3 gp41-1 AP5/6 NLuc OLLAS-tag (**spliced**) ~ 44 kDa
a4 NLuc OLLAS-tag ~ 21 kDa

b1 mNG NrdJ-1 AP3/4 FLuc cMyc tag (unspliced) ~ 120 kDa
b2 NrdJ-1 AP3/4 FLuc cMyc tag (**spliced**) ~ 89 kDa
b3 FLuc cMyc tag ~ 62 kDa

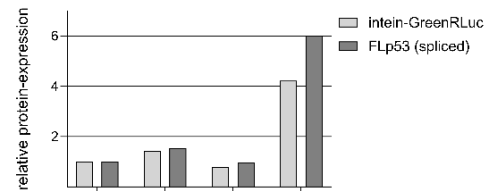
c1 p53 gp41-8 c-Jun/c-Fos GreenRLuc VSV-G tag (unspliced) ~ 107 kDa
c2 mNG gp41-8 c-Jun/c-Fos GreenRLuc VSV-G tag (unspliced) ~ 94 kDa
c3 gp41-8 c-Jun/c-Fos GreenRLuc VSV-G tag (**spliced**) ~ 62 kDa
c4 GreenRLuc VSV-G tag ~ 35 kDa

d

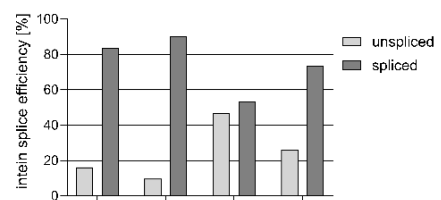


d1 unspliced gp41-8 or IMPDH-1 GreenRLuc = 107 kDa
d2 spliced gp41-8 or IMPDH-1 GreenRLuc = 62 kDa
d3 spliced and assembled p53 = 53 kDa

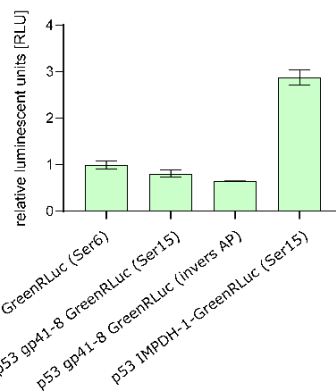
e



f



g



Results

Figure 9: Introduction of EXSISERS reporters into the respective integration sites of recombinant FLp53. Each EXSISERS reporter was placed into a predetermined integration site of recombinant FLp53 to assess the suitability of these integration sites for the final and stable knock in of the EXSISERS reporters into the human *TP53* gene. For each p53-EXSISERS combination, a distinct plasmid was designed, carrying either one, two, or three reporters at their designated integration sites simultaneously. Expression plasmids were transfected into HCT116 cells. Gp41-8 GreenRLuc8.6 was placed prior to Ser6 of FLp53, gp41-1 NLuc was placed prior to Ser94, and NrdJ-1 FLuc was placed prior to Ser240. **a)** The contents of each expression plasmid is indicated with a '+', specifying the host protein (mNG or FLp53) carrying a variable quantity of EXSISERS reporters. Gp41-8 GreenRLuc8.6 is tagged with a VSV-G tag, **b)** gp41-1 NLuc contained an OLLAS tag and **c)** NrdJ-1 FLuc is tagged with a c-Myc tag. RIPA lysates were generated 48 h post-transfection and analyzed via immunoblot. **d)** As a result of the previous immunoblot experiments, distinct intein-GreenRLuc8.6 alternatives were tested on an immunoblot concerning the expressed protein levels and intein-splicing efficacy. FLp53 was additionally tagged with a recombinant FLAG-tag. The alternative intein-GreenRLuc reporters encompassed either a different integration site within FLp53, inverted anti-parallel helices (APH), or the substitution of the gp41-8 intein with the IMPDH-1 intein. **e)** Densitometric analysis of spliced FLp53 and the respective intein-GreenRLuc alternatives. **f)** Intein splicing rates were determined as the ratio of spliced and unspliced intein-GreenRLuc densitometric signals. Signal intensities were determined by Image J. **g)** To evaluate the luciferase activity of each EXSISERS alternative, a luminescence assay was conducted. Therefore, HCT116 cells were transfected with the respective expression plasmids. 48 h post-transfection, cells were treated with the Renilla-Glo Luciferase Substrate (Promega) and analyzed with a TriStar² luminometer.

a protein of interest (POI), leading to the re-assembly of both extein-parts and consequently restoring full integrity of the POI.

To ascertain the proper expression and intein-splicing of the EXSISERS reporters within the designated insertion sites in TP53, we engineered a recombinant full-length p53 (FLp53) variant harboring six specific mutations (R175H, R196H, R213H, R248H, R273H, and R282H) to prevent inadvertent apoptosis induction [183]. Into this inactive p53 variant, gp41-8 GreenRLuc, gp41-1 NLuc, and NrdJ-1 FLuc were inserted into coding exons 2, 4, and 7, respectively. We designed individual expression plasmids for each p53-EXSISERS combination. The EXSISERS reporters were, therefore, inserted either individually or in combination with the other reporters at their designated p53 integration sites. Furthermore, each EXSISERS reporter was equipped with a distinct recombinant tag, facilitating the quantification of expression levels and splicing rates by immunoblotting.

Notably, gp41-1 NLuc exhibited the most robust expression and intein splicing either integrated alone in coding exon 4 of FLp53 or in tandem with the other EXSISERS reporters (Fig. 9a). A similar pattern was observed for NrdJ-1 FLuc when integrated either individually or in combination with gp41-1-NLuc (Fig 9b). However, the corresponding signals diminished upon the introduction of gp41-8 GreenRLuc. Intriguingly, gp41-8 GreenRLuc appeared to reduce the expression of itself (Fig. 9c) and the overall expression of p53 and all concomitant EXSISERS reporters (Fig. 9b, c).

Results

We postulate that an N-terminal insertion of gp41-8 GreenRLuc at positions Ser6 of FLp53 may disrupt protein folding, which leads to the rapid degradation of p53 and all concomitant EXSISERS reporters. Consequently, a downstream shift of the integration site within FLp53 for several amino acids can eliminate potential protein instabilities. Furthermore, enhancing splicing efficiency can also lead to increased protein stability. Therefore, we considered alternatively substituting gp41-8 with another split-intein, namely IMPDH-1.

Besides the original construct, we validated three alternatives, including the following changes:

- 1) Increasing the distance of the gp41-8 GreenRLuc insertion from amino acid position Ser6 to Ser15 of FLp53.
- 2) Excluding the possibility of a wrong orientation of the anti-parallel helices.
- 3) Substituting gp41-8 with IMPDH-1 intein to create an alternative IMPDH-1 GreenRLuc reporter.

HCT116 cells transfected either with original or alternative constructs were incubated for 48 h and, after that, lysed with RIPA buffer to determine the protein expression and splicing efficiency of the respective EXSISERS reporters within FLp53 by immunoblotting (Fig. 9d).

Exchanging gp41-1 with IMPDH-1 intein considerably increased p53 and intein-GreenRLuc expression by 4 to 6 fold (Fig. 9e). Also, shifting the insertion site several amino acids away from the N-terminus slightly increased protein splicing and protein expression for both p53 and the EXSISERS reporter (Fig. 9e, f). Improved protein stability and higher expressional rates for the alternative EXSISERS reporter IMPDH-1 GreenRLuc were also reflected with increased outputs of luminescent signals (Fig 9g).

As a result, we successfully identified the optimal insertion site in p53 and incorporated the split-intein system IMPDH-1 with higher splicing rates into the third EXSISERS reporter IMPDH-1 GreenRLuc.

EXSISERS represents a highly adaptable technology. Owing to the pivotal role of intein splicing in preserving protein structure and function, these reporters can be seamlessly incorporated into any protein of interest (POI). Given the crucial role of the other p53 family members, p63 and p73, in networking with p53 to execute their tumor suppressive role, we demonstrate that the EXSISERS reporters are integrable and

Results

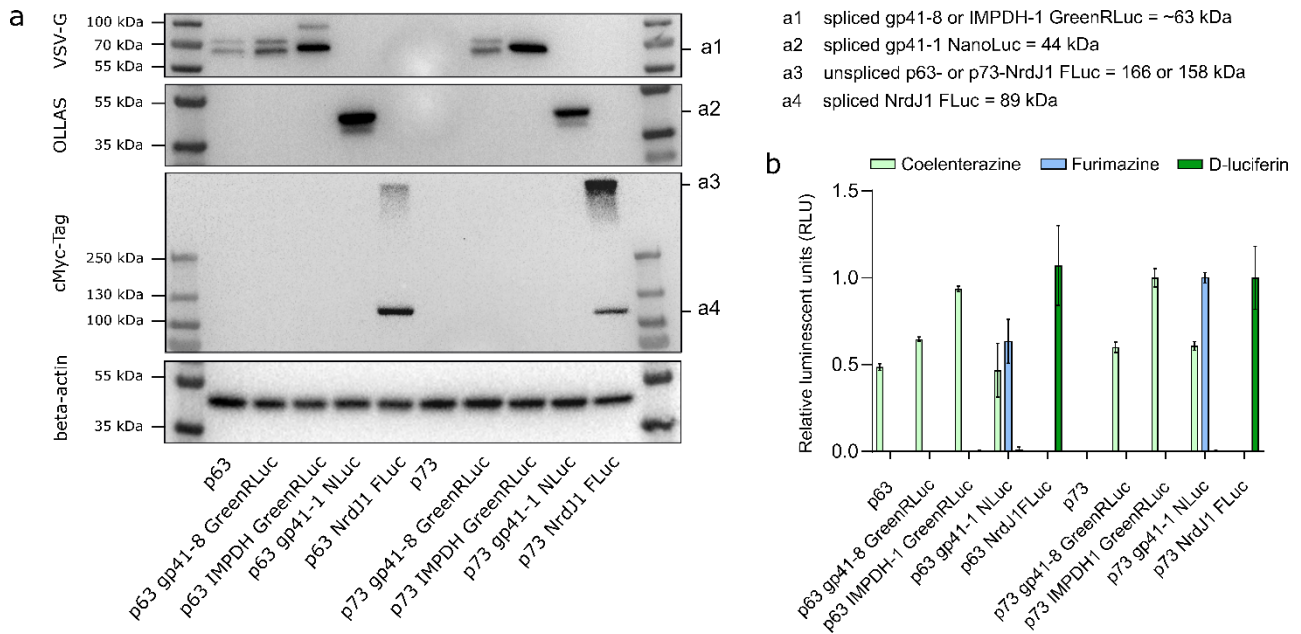


Figure 10: Original, as well as optimized EXSISERS reporters were introduced into FLP63 and FLP73. a) Immunoblotting analyses revealed expressional and intein splicing rates for the individual EXSISERS reporters in FLP63 and FLP73. HCT116 cells were transfected with the respective expression plasmids. 48 h post-transfection, RIPA-lysates were generated. **c)** A triple-luciferase assay was conducted with HCT116 cells transfected with the respective expression plasmids. Prior to analysis, transfected cells were incubated for 48 h. Each FLP63/FLP73-EXSISERS construct was supplemented either with coelenterazine (specific luciferin substrate for GreenRLuc), furimazine (specific luciferin substrate for NLuc), and D-luciferin (specific luciferin substrate for FLuc). Quantitative luminescence measurements were conducted with a TriStar² luminometer.

expressed individually. We individually integrated each EXSISERS reporter into coding exon 4 of recombinant FLP63 at amino acid position Ser154 and into coding exon 6 of recombinant FLP73 at Ser212. Determining the protein expression and splicing efficiency by immunoblot analyses, we intend to provide insights into the compatibility of the reporters incorporated in distinct host proteins. Regarding compatibility considerations, we aim to concurrently exclude any potential cross-reactivity of luciferases with non-specific luciferin substrates through a triple-EXSISERS reporter assay. Immunoblot analyses unveiled the protein abundance and proper intein-splicing of all EXSISERS reporters, regardless of the host protein they are embedded in (Fig. 10a). However, the triple EXSISERS reporter assay measuring the luminescent output of each reporter (each of which was supplemented with coelenterazine, furimazine, and D-luciferin), revealed an incompatibility between the quantitative measurement of GreenRLuc and NLuc (Fig 10b). Besides their specific luciferin substrate, GreenRLuc and NLuc co-accept and enzymatically convert furimazine and coelenterazine, respectively, making quantitative discrimination between these two luciferases impossible. That is because furimazine and coelenterazine exhibit a high

Results

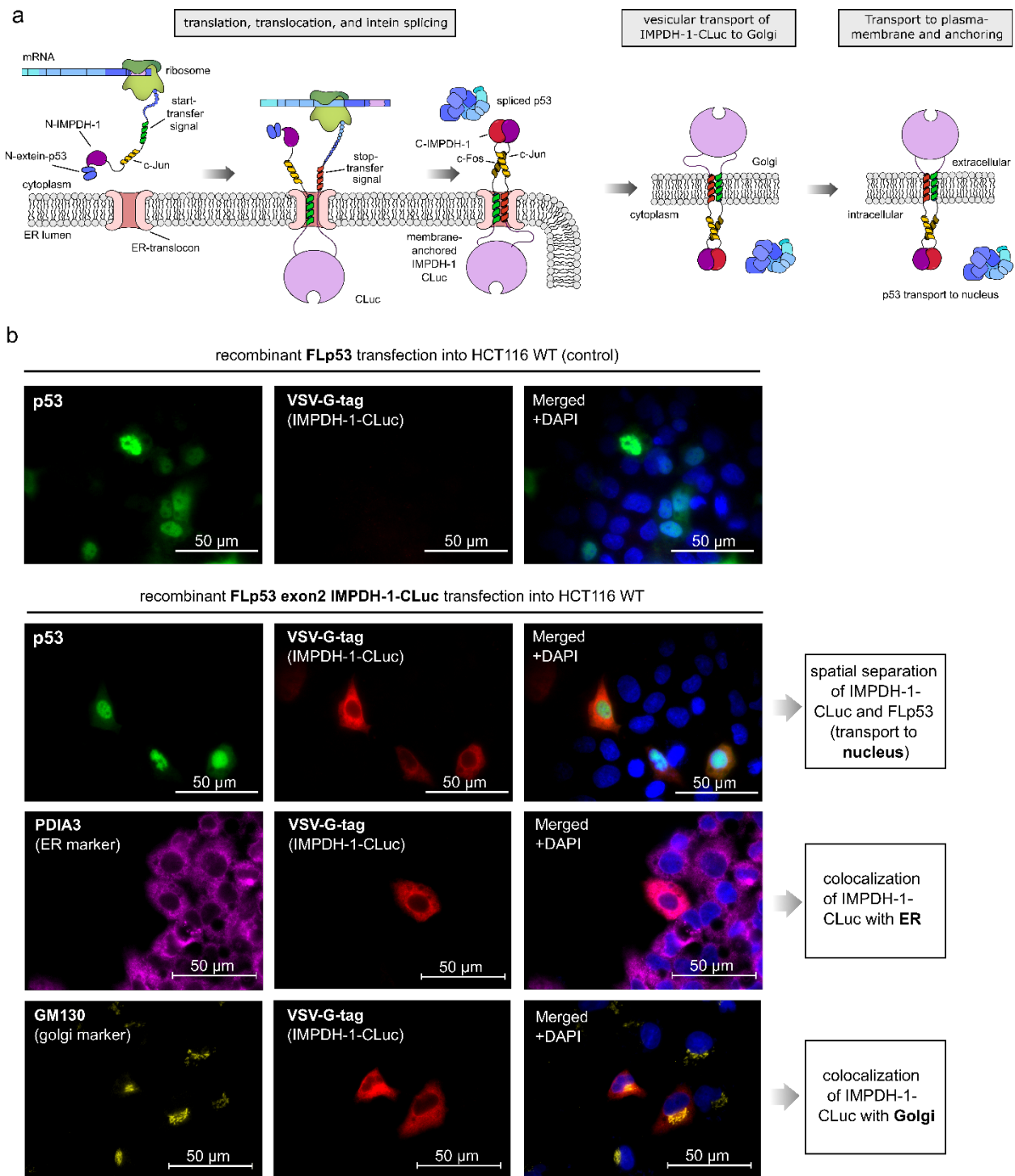


Figure 11: Design of a secretable and spatially separable IMPDPH-1-CLuc reporter. **a**) Schematic of co-translation and translocation of IMPDPH-1-CLuc to the ER membrane. Transmembrane domain 1 (TMD I, derived from Fcer2) and TMD II (derived from Glycophorin A) consist of a start transfer and a stop transfer signal, thus initiating and terminating the polypeptide-threading through the ER membrane into the ER lumen. IMPDPH-1-inteins initiate p53-excision into the cytosol. ER-membrane resident IMPDPH-1-CLuc is first transported to the Golgi and, thereafter, to the plasma membrane to be membrane-anchored and exposed to the exoplasm. **b**) Transfection of HCT116 WT cells with recombinant FLp53 either missing (ctrl.) or including IMPDPH-1-CLuc at coding sequence exon 2. Immunofluorescence microscopy 48 h post-transfection demonstrated spatial separation of p53 and IMPDPH-1-CLuc as well as colocalization of IMPDPH-1-CLuc reporter with the ER (marker: PDIA3) and the Golgi (marker: GM130). p53, PDIA3, and GM130 were detected with appropriate primary and AlexaFluor488-secondary antibodies. IMPDPH-1-CLuc was detected with appropriate primary and AlexaFluor594-secondary antibodies. Fluorescent images were acquired using a 20x objective lens. Scale bars represent 50 μ m.

Results

degree of structural similarity. Due to this circumstance, we substituted GreenRLuc with the Cypridina Luciferase (CLuc), in which we were highly confident that its specific substrate vagulin would have the requisite structural distinctions to prevent any cross-reactivity with the other luciferases, NLuc and FLuc. Unlike ordinary luciferases like NLuc and FLuc, which convert their substrate in the cytosol, CLuc is a secreted protein exclusively working in oxidative environments [184].

If we used CLuc, NLuc, and FLuc simultaneously as a triple-EXSISERS reporter system, we would mark the first instance in which these three luciferases are employed for multiplexed measurements. Nevertheless, it poses a challenge to integrate a secreted protein like CLuc into a nuclear protein like p53 that is expressed from the same promoter and initially undergoing translation as a single contiguous polypeptide. Intein splicing initially triggers spatial segregation into two functional proteins. While p53 is naturally endowed with a nuclear localization signal (NLS) and transported to the nucleus, IMPDH-1 CLuc is meant to be translocated into the ER and transported to the plasma membrane to be either anchored and exposed on the plasma membrane or to be secreted into the exoplasm. Therefore, we constructed IMPDH 1 CLuc to carry additional start- and stop-transfer signals. The recognition of these sites results in the translocation of CLuc into the ER lumen [152] (Fig. 11a). CLuc is anchored to the ER membrane and protrudes into the interior. It is then transported to the plasma membrane and exposed to the exoplasm. FLp53 IMPDH-1 CLuc was transformed into HCT116 wild-type (WT) cells, demonstrating efficient intein splicing. This is evident due to spatial separation of p53 and CLuc, which we could confirm by the colocalization of IMPDH-1-CLuc with ER and Golgi and the colocalization of p53 with the nucleus (Fig 11b). Furthermore, the translocation of p53 into the nucleus suggests the structural and functional integrity of p53 and CLuc since only structurally intact proteins can pass the interconnected compartment protein quality control [185,186].

Now the question arises: which system is the more suitable reporter for quantifying the FLp53 protein isoform? Due to membrane-resident protein recycling mechanisms [187], we postulate that plasma membrane-anchored IMPDH-1-CLuc represents a better approach to reflect the dynamic and tightly regulated expression of FLp53. In contrast to the secretory IMPDH-1-CLuc, which accumulates in the supernatant (Fig. 12a), the membrane-anchored reporter is susceptible to time-

Results

a

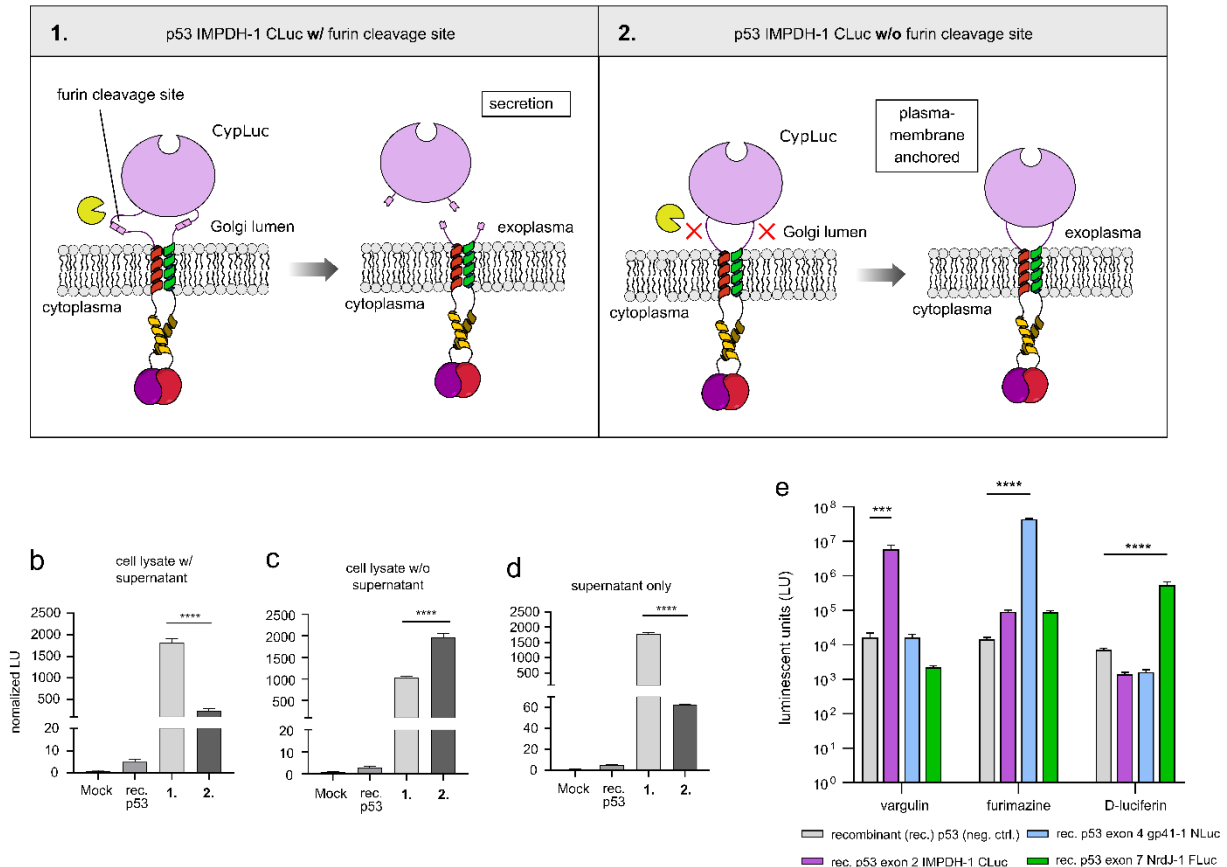


Figure 12: Comparison of Furin-protease cleavable and plasma membrane-anchored IMPDH-1-CLuc. **a)** Comparison between **1.** IMPDH-1-CLuc carrying furin cleavage sites for digestive membrane anchor-release and secretion into exoplasm, and **2.** novel plasma membrane anchored IMPDH-1-CLuc without furin cleavage sites. **b)** Normalized luminescence measurements (n=3) 48 h post-transfection of **1.** secretable and **2.** membrane-anchored IMPDH-1-CLuc reporter transfected into HCT116 WT cells. Quantifications were conducted for cell lysate + supernatant, **c)** cell lysate only or **d)** supernatant only. Group means between cleavable and membrane-anchored IMPDH-1-CLuc were compared by Student's t-test (****p<0.0001). **e)** Immunofluorescence microscopy of genetically modified HCT116 (EXSISERS_{TP53:2CLuc-4NLuc-7FLuc}) cell lines comprising three EXSISERS in p53 at their corresponding locus in TP53 to localize plasma membrane anchored IMPDH-1-CLuc. Fluorescent images were taken with a 40x lens. Scale bars represent 100 μ m. **c)** Transient transfection of recombinant p53-EXSISERS into HCT116 WT cells. Each reporter was cloned into a p53 expression plasmid at its designated integration site (see Fig 1b). 48 h post-transfection, luminescence was measured for each expression system, having been individually exposed to each luciferase substrates (varguline, furimazine, and D-luciferin) (n=3). Statistical significances were calculated using one-way ANOVA (***p<0.0005; ****p<0.0001).

dependent internalization and degradation (Fig. 12a, b, c, d) and thereby allows for a more sensitive readout. Furthermore, supplementing EXSISERS-transfected HCT116 cells with either vargulin, furimazine, or D-luciferin demonstrates that only the respective luciferases can respond to their specific luciferin substrates (Fig. 12e). Thus, we have shown the three luciferases CLuc, NLuc, and FLuc, to be combinable. In summary, combining IMPDH-1-CLuc with gp41-1-NLuc and NrdJ-1-FLuc completes the triple-EXSISERS-reporter system and allows for the simultaneous quantification of FLp53, Δ 40p53, and Δ 133+ Δ 160p53 in living cells.

3.2 Creation of a stable HCT116 triple-EXSISERS cell line by CRISPR/Cas9.

For all experiments conducted thus far, we employed recombinant expression plasmids introduced transiently into the cells. Now that we have validated the integrity and compatibility of all intein luciferases, we have proceeded with stable genomic integration into *TP53* using CRISPR/Cas9 technology.

The first stable knock-in involved the integration of NrdJ-1 FLuc into TP53 coding exon 7. Since exon 7 is consistently expressed and available in all p53 protein isoforms, the readout from NrdJ-1 FLuc enables the detection and quantitative determination of the entire p53 population. To achieve stable integration of the EXSISERS reporters into *TP53*, we previously identified appropriate sgRNA sequences (complementary to the Cas9 targeting sequence) that induce sufficient Cas9 nuclease activity to create sequence-specific DNA-DSB efficiently (Fig. 13). These DNA damages initiate two distinct repair mechanisms within the cell. The repair mechanism we aim to activate is homology-directed repair (HDR), in which the second allele acts as the template for the damaged DNA. This repair mechanism can be exploited by introducing a recombinant DNA fragment containing exogenous sequences flanked by 1 kb long endogenous homology sequences. These homology arms (HAs) are identical to the genomic DNA and are located upstream (5' HA) and downstream (3' HA) of the generated DSB.

In addition to the 5'HA and 3'HA sequences and the coding sequences for the EXSISERS reporters, each recombinant DNA template also includes a selection cassette containing coding sequences for Hepatitis Simplex Virus thymidine kinase (HSVtk) and puromycin-N-acetyltransferase (PuroR) (Fig. 14a). Both genes are under the control of the same EF1 α promoter and are translationally separated by a 2A peptide. A concentration of 50 $\mu\text{g ml}^{-1}$ puromycin was employed for the 'positive selection' of cells that had successfully integrated the EXSISERS reporters into the designated integration site in a homologous manner.

We flanked these sequences with distinct recombinase recognition sites to remove the stably co-integrated selection cassettes. The DNA template carrying NrdJ-1 FLuc was equipped with FRT sites (recognized by flippase recombinase), flanking the selection cassette. The DNA template containing gp41-1 NLuc utilized the Cre/LoxP system for

Results

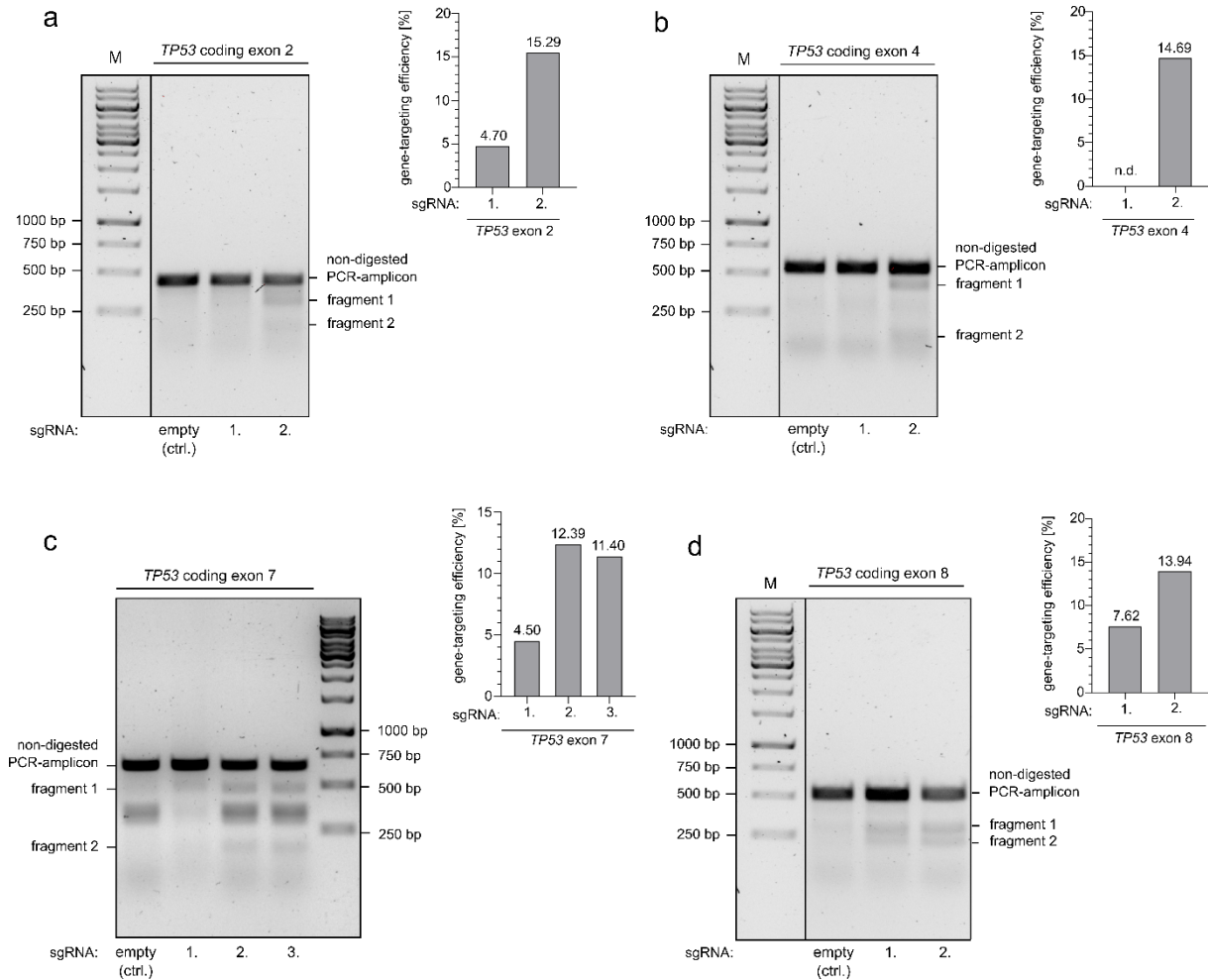


Figure 13: Determination of sgRNA dependent gene targeting efficiency by T7 endonuclease assay. Before conducting Cas9 mediated DNA double strand breaks for stable integration of EXSISERS-reporters into human *TP53* locus of HCT116 WT, sgRNA dependent gene targeting efficiencies (evoked by the variable spacer sequences within the sgRNA molecules) were determined with T7 endonuclease I assay. Gene targeting efficiencies were specified for different sgRNAs either targeting a) *TP53* coding exon 2, b) *TP53* coding exon 4, c) *TP53* coding exon 7, or d) *TP53* coding exon 8. Each sgRNA specific gene targeting efficiency was normalized to the corresponding negative ctrl. (sgRNA with empty spacer sequence) and given into percentage, which was calculated according to the manufacturers protocol.

removing the selection cassette. The IMPDH-1 CLuc DNA template encompassed the Dre/RoxP system (Fig. 14a). Consequently, the transfection of the expression plasmids encoding the respective recombinase led to the excision of EF1 α -PuroR-P2A-HSVtk-bpA selection cassette and joining of the EXSISERS reporters. Only cells lacking the HSVtk gene could survive the subsequent ‘negative selection’ with 25.5 $\mu\text{g ml}^{-1}$ ganciclovir. The systematic integration of the EXSISERS reporters and selection of the genetically engineered HCT116 cells led to the creation of a modified *TP53* gene carrying IMPDH-1 CLuc in coding exon 2, gp41-1 NLuc in coding exon 4,

Results

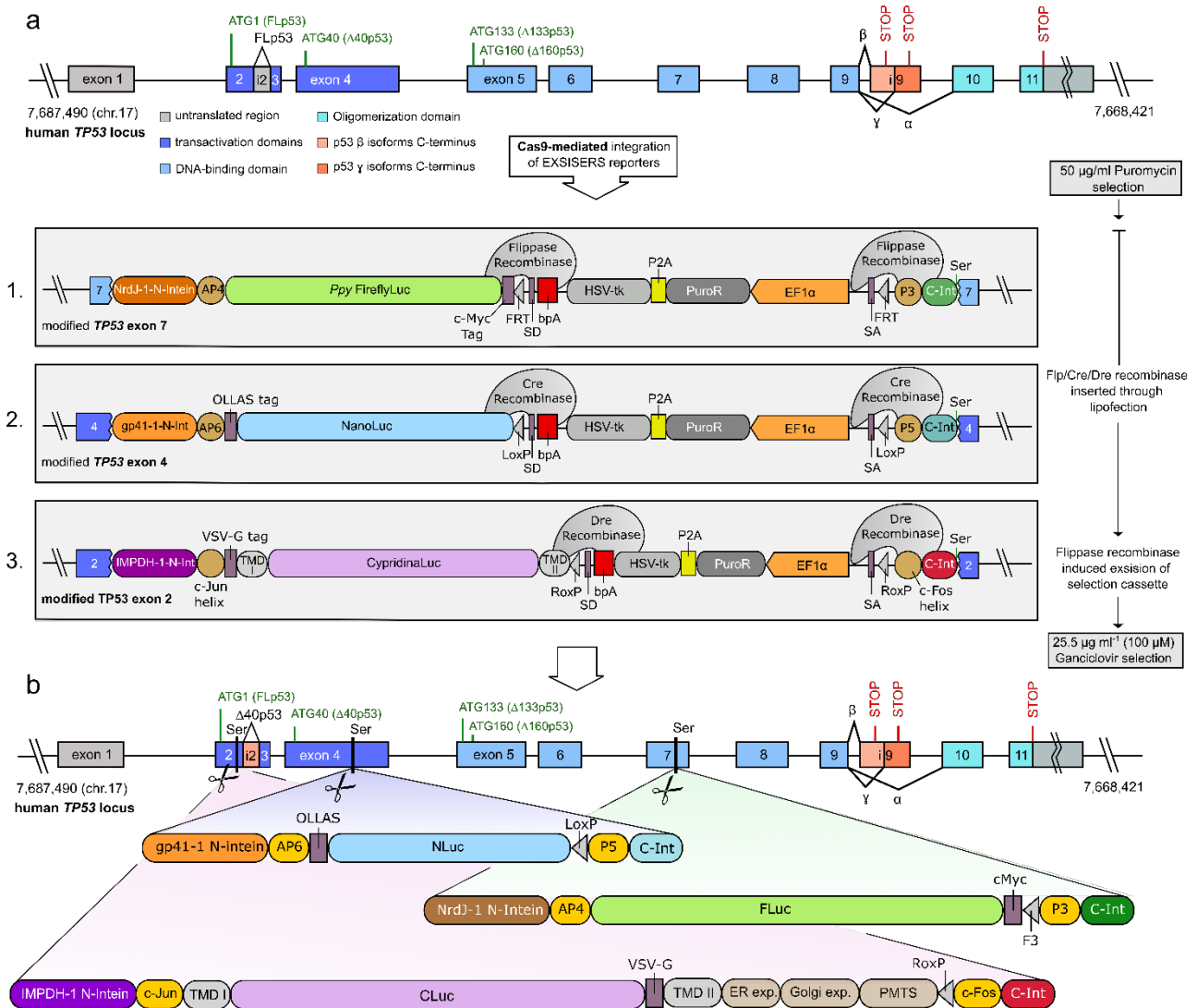


Figure 14: Generation of a HCT116 cell line two-step selected and stably expressing EXSISERS.

a) Schematic representation of CRISPR/Cas9 mediated knock-in of EXSISERS-reporters IMPDH-1 Cypridina Luciferase (IMPDH-1-CLuc), gp41-1 Nano Luciferase (gp41-1-NLuc), and NrdJ-1 Firefly Luciferase from *Photinus pyralis* (NrdJ-1-PpyFLuc) into exon 2, 4, or 7 of the tumor suppressor gene *TP53*. The donor plasmids containing coding sequences for the EXSISERS-reporters also harbor an autonomous selection cassette consisting of a constitutive EF1 α promoter, a puromycin-N-acetyltransferase gene (PuroR), and a herpes simplex virus-thymidine kinase gene (HSV-tk) translationally separated by a p2A peptide. After knock-in, the modified HCT116 cells were treated with 50 μ g/ml puromycin. Thereafter, cells were transfected with expression plasmids coding for Flp-, Cre-, or Dre-recombinase to remove the selection cassette by genomic recombination. Subsequent negative selection with 100 μ M ganciclovir ensured homozygote knock-in of EXSISERS-reporters without the selection cassette. **b)** Visualization of CRISPR/Cas9-mediated integration of EXSISERS-reporters into their respective *TP53* loci.

and NrdJ-1 FLuc in coding exon 7 (Fig. 14b and Fig. 16a). For this generated cell line, we use the terminology EXSISERS_{TP53:2CLuc-4NLuc-7FLuc}.

The availability of the EXSISERS technology for *TP53* allows for the quantitative distinction between the three isoform groups FLp53, Δ 40p53, and Δ 133+ Δ 160p53. Depending on the specific p53 isoform expressed, either all three luciferases for

Results

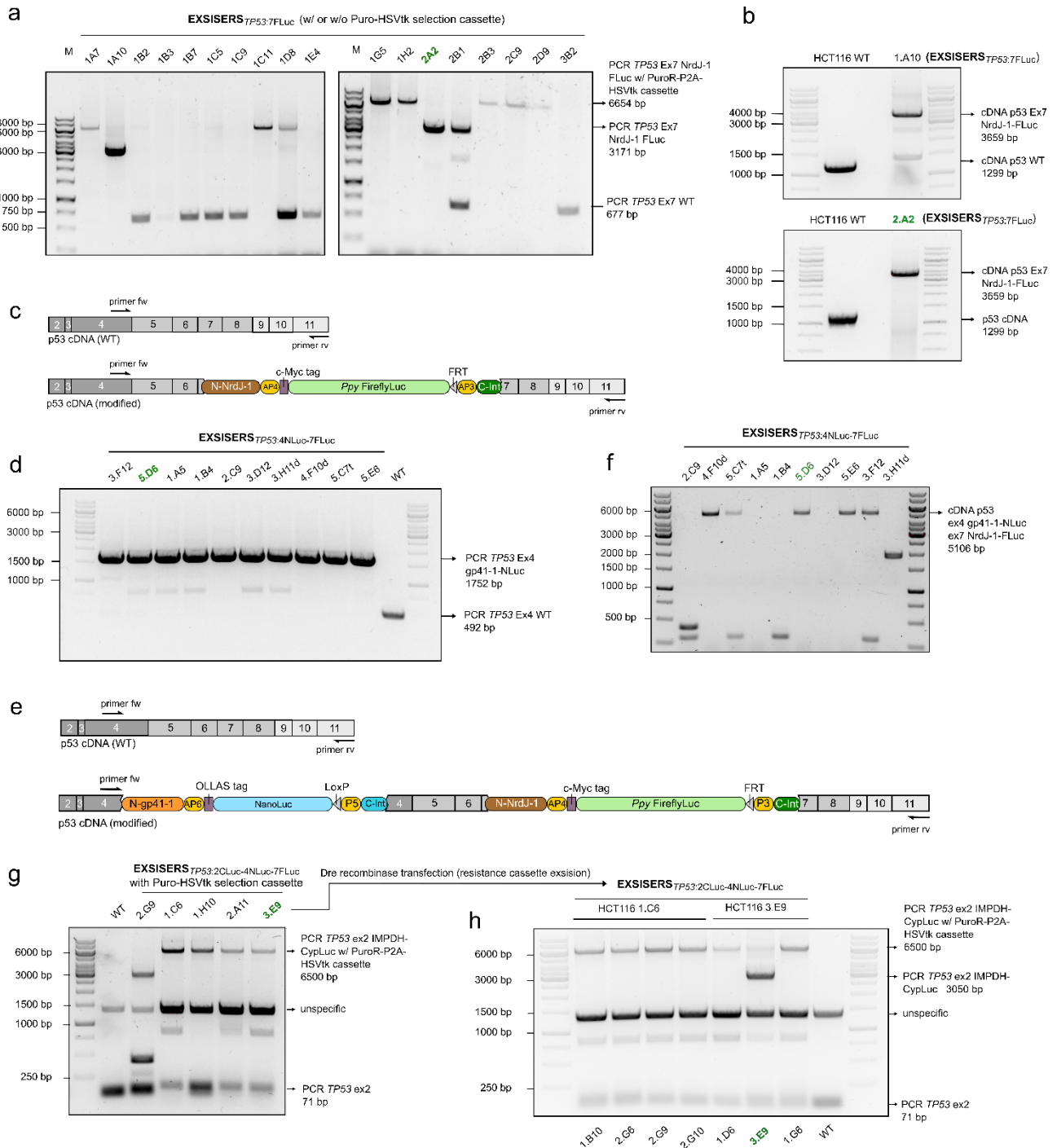
FLp53, gp41-1-NLuc, and NrdJ-1-FLuc for FLp53+ Δ 40p53 or NrdJ-1-FLuc alone for total p53 are co-translated. The quantity of the Δ 40p53 isoform is determined by subtracting the relative luminescence signals of IMPDH-1 CLuc from those of gp41-1 NLuc. Correspondingly, the amounts of Δ 133+ Δ 160p53 are calculated by subtracting the relative signals of gp41-1 NLuc from those of NrdJ-1 FLuc (Fig. 7c).

Stable integration of EXSISERS reporter NrdJ-1 FLuc into *TP53* exon 7 resulted in the generation of two distinct HCT116 clones. Clones EXSISERS_{TP53:7FLuc} 1.A10 and 2.A2 were initially identified through genotyping (PCR amplification of the genetically modified locus). The exclusive presence of bands at 3171 bp, without accompanying by-products, indicated successful and homozygous knock-in of NrdJ-1 FLuc (Fig. 15a). These clones were selected for further analysis. The PCR amplicons were purified and sequenced to exclude potential mutations. Nevertheless, integrating exogenous DNA fragments into a coding sequence may inadvertently disrupt post-transcriptional maturation processes. Therefore, we isolated and reversely transcribed total mRNA from clone EXSISERS_{TP53:7FLuc} 1.A10 and 2.A2 HCT116 into cDNA. Subsequent PCR amplification of the cDNA-converted transcript revealed a non-fragmented and NrdJ-1 FLuc-containing FLp53 species for both clones (Fig. 15b, c). These amplicons appeared at 3569 bp. As a control, FLp53 lacking NrdJ-1 FLuc displayed a PCR amplicon length of 1299 bp. Clone EXSISERS_{TP53:7FLuc} 2.A2 exhibited a consistent lane with minimal by-products.

Immunoblot analysis of both EXSISERS_{TP53:7FLuc} clones demonstrated robust protein production for endogenous FLp53 and EXSISERS reporter NrdJ-1 FLuc (Fig. 16b). In comparison to HCT116 WT, cell lysates from EXSISERS_{TP53:7FLuc} 1.A10 and 2.A2 cells revealed spliced NrdJ-1 FLuc product (c-myc tagged) with clone EXSISERS_{TP53:7FLuc} 2.A2 displaying significantly stronger signals. Consequently, clone EXSISERS_{TP53:7FLuc} 2.A2 was chosen for subsequent gp41-1 NLuc integration into *TP53* coding exon 4.

Therefore, we transfected these cells with expression plasmids coding for Cas9 and the appropriate sgRNA. Moreover, we provided a donor plasmid carrying the respective sequences for gp41-1 NLuc harboring the two selection markers PuroR and HSVtk (Fig. 14a). Passing the necessary selection procedures, we created the stable EXSISERS_{TP53:4NLuc-7FLuc} HCT116 cell line including NrdJ-1 FLuc and gp41-1 NLuc in a homozygous manner. Genotyping of clone EXSISERS_{TP53:4NLuc-7FLuc} 5.D6 revealed a strong and consistent band at 1752 bp (Fig. 15d). Also, re-transcription of total mRNA

Results



into cDNA and subsequent PCR amplification of FLP53 showed a non-fragmented transcript at 5106 bp, now carrying gp41-1 NLuc as well as NrdJ-1 FLuc (Fig. 15e, f). In an immunoblot experiment, clone EXSISERS_{TP53:4NLuc-7FLuc} 5.D6 displayed robust protein expression for EXSISERS reporters gp4-1 NLuc, NrdJ-1 FLuc. With these two stably integrated EXSISERS reporters, it is now possible to quantitatively determine and differentiate tumor suppressive p53 protein isoforms FLP53+Δ40p53 from anti-apoptotic p53 protein isoforms Δ133p53+Δ160p53. For the subsequent IMPDH-1 CLuc integration into TP53 coding exon 2, clone EXSISERS_{TP53:4NLuc-7FLuc} 5.D6 was chosen.

Results

Figure 15: Genotyping *TP53* after stable EXSISERS knock-in. **a)** Agarose gel electrophoresis of PCR amplification product from genomic DNA at *TP53* coding exon 7. Identified clones carry stably integrated NrdJ-1-FLuc after positive (puromycin) and negative (ganciclovir) selection. Clones still including the selection cassette show a PCR product at 6654 bp, while clones carrying final NrdJ-1-FLuc EXSISERS show a PCR amplicon at 3171 bp. *TP53* exon 7 without any genetic modification shows a PCR amplicon at 677 bp. Clone HCT116 2.A2 (EXSISERS_{*TP53:7FLuc*}) was considered for integration of further EXSISERS-reporters. **b)** Agarose gel electrophoresis of PCR amplification product from cDNA of HCT116 WT and genetically edited EXSISERS_{*TP53:7FLuc*}. **c)** Schematic of p53 cDNA of WT and genetically modified HCT116 cells (NrdJ-1-FLuc in *TP53* exon 7). **d)** Agarose gel electrophoresis of PCR amplification product from genomic DNA at *TP53* coding exon 4. Identified clones carry stably integrated gp41-1-NLuc and successfully passed positive (puromycin) and negative (ganciclovir) selection. Clones carrying final gp41-1-NLuc EXSISERS reveal a PCR amplicon at 1752 bp. *TP53* exon 4 without any genetic modification shows a PCR amplicon at 492 bp. Clone 5.D6 (EXSISERS_{*TP53:4NLuc-7FLuc*}) was considered for integration of further EXSISERS reporters. **e)** Schematic of p53 cDNA of WT and genetically modified HCT116 cells (w/ gp41-1-NLuc at exon 4 and NrdJ-1-FLuc at exon 7 of *TP53*). **f)** Agarose gel electrophoresis of PCR amplification product from cDNA of HCT116 WT and selected clones genetically edited and carrying two EXSISERS. **g)** Agarose gel electrophoresis of PCR amplification product from genomic DNA at *TP53* coding exon 2. Identified clones carry stably integrated IMPDH-1-CLuc and successfully passed positive (puromycin) selection. So far, clones were not transfected with Dre-recombinase and have not excluded the selection cassette. These clones (especially EXSISERS_{*TP53:2CLuc-4NLuc-7FLuc*}) show a PCR amplicon at 6500 bp. **h)** Genotyping of HCT116 clones after transfection with Dre-Recombinase. EXSISERS_{*TP53:2CLuc-4NLuc-7FLuc*} cell line was considered for further experiments.

To distinguish FLP53 from $\Delta 40p53$, we stably integrated IMPDH-1 CLuc into coding exon 2 of *TP53*. Genetic modification of EXSISERS_{*TP53:4NLuc-7FLuc*} 5.D6 cells was, again, conducted by CRISPR/Cas9-mediated DNA-DSB. First, IMPDH-1 CLuc was jointly integrated with a selection cassette. Genotyping of successfully modified cell lines resulted in bands at 6.500 bp (Fig. 15g). EXSISERS_{*TP53:2CLuc-4NLuc-7FLuc*} 3.E9 cells were transfected with plasmids expressing the Dre-recombinases to ultimately remove the selection cassette. The excision of PuroR and HSVtk, the homologous recombination of IMPDH-1 CLuc, and the selection with 25.5 $\mu\text{g ml}^{-1}$ ganciclovir resulted in the final creation of the triple-EXSISERS reporter cell line EXSISERS_{*TP53:2CLuc-4NLuc-7FLuc*}. Genotyping of these cells revealed consistent bands at 3050 bp (Fig. 15h). Immunoblot analysis of the triple EXSISERS reporter cell line revealed two bands representing spliced IMPDH-1 CLuc and unspliced FLP53-IMPDH-1 CLuc (Fig. 16d). Also FLP53 blotting displayed two bands, one for spliced FLP53, and the other for unspliced FLP53-IMPDH-1 CLuc. All other EXSISERS reporters still demonstrate consistent expression and efficient intein splicing. The fact,

Results

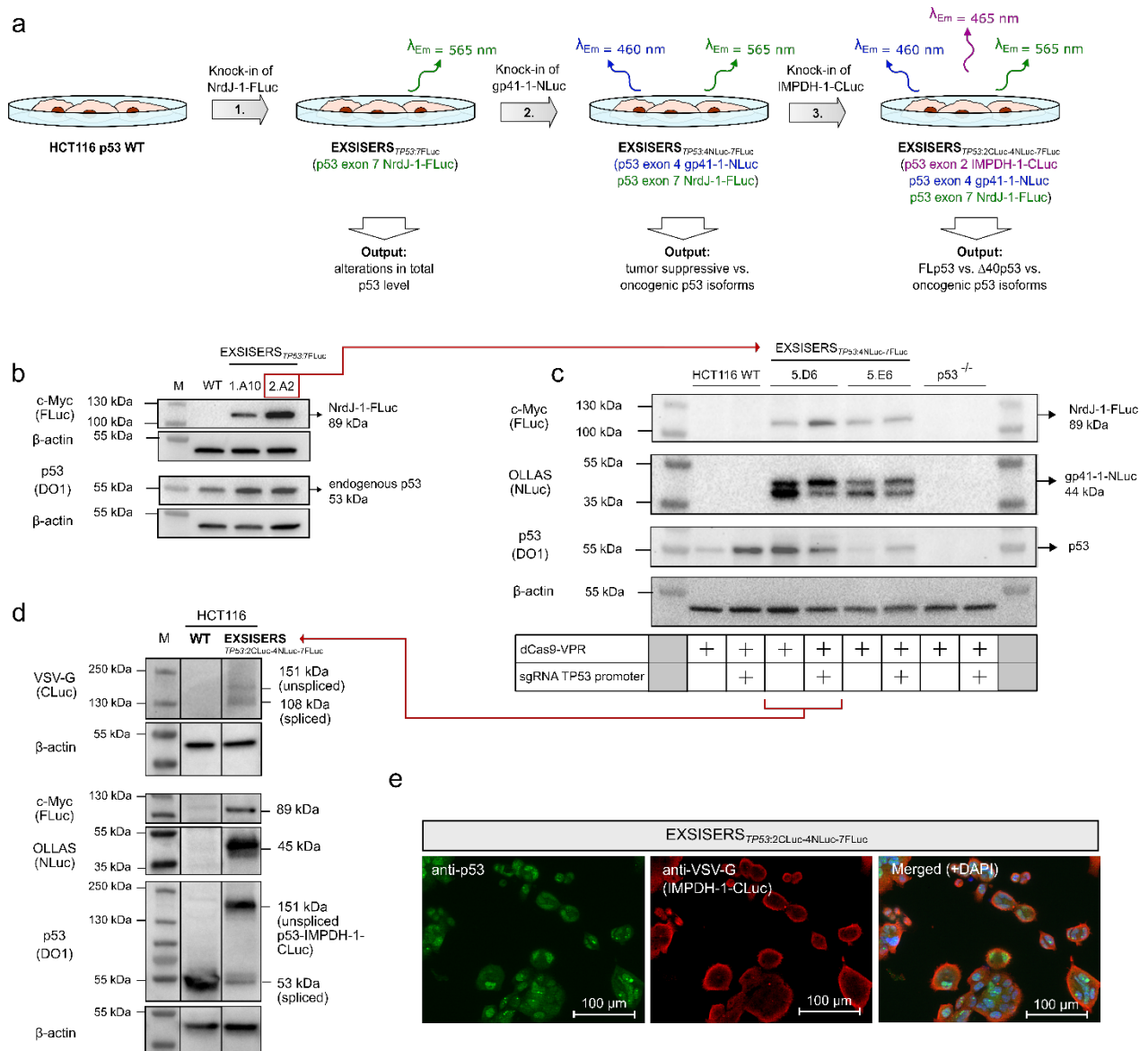


Figure 16: Establishment of stable triple EXSISERS reporter cell lines and validation of p53 functionality. **a**) Overview of sequentially generated stable cell lines carrying EXSISERS-reporters after first knock-in (NrdJ-1-FLuc in *TP53* exon 7), second knock-in (gp41-1-NLuc in *TP53* exon 4), and third knock-in (IMPDH-1-CLuc in *TP53* exon 2). **b**) Western blot (WB) analysis of HCT116 1.A10 and 2.A10 (EXSISERS_{TP53:7FLuc}) cell lines carrying NrdJ-1-FLuc (cMyc-tagged) within *TP53* exon 7. **c**) Second EXSISERS cell line generation obtained by modifying EXSISERS_{TP53:7FLuc} cells and stably integrating gp41-1-NLuc into *TP53* coding exon 4. WB analysis of clones 5.D6 and 5.E6 (EXSISERS_{TP53:4NLuc:7FLuc}) revealed stable integration of NrdJ-1-FLuc and gp41-1-NLuc (OLLAS-tagged) in *TP53*, robust expression, and correct splicing of p53. Third EXSISERS cell line generation obtained by modification of EXSISERS_{TP53:4NLuc:7FLuc} cells and stable integration of IMPDH-1-CLuc into *TP53* coding exon 2 (EXSISERS_{TP53:2CLuc:4NLuc:7FLuc}). **d**) HCT116 WT and the genetically modified EXSISERS_{TP53:2CLuc:4NLuc:7FLuc} cell line consisting of three EXSISERS reporters within *TP53* were compared by Western blot (WB) analysis. IMPDH-1-CLuc (VSV-G tag), gp41-1-NLuc (OLLAS tag), and NrdJ-1-FLuc (cMyc tag) were visualized with antibodies directed against the corresponding recombinant tags (see Fig. 7b). p53 was detected with DO1-anti-p53 antibody. **e**) Immunofluorescence microscopy of genetically modified HCT116 (EXSISERS_{TP53:2CLuc:4NLuc:7FLuc}) cell lines comprising three EXSISERS in p53 at their corresponding locus in *TP53* to localize plasma membrane anchored IMPDH-1-CLuc. Fluorescent images were taken with a 40x lens. Scale bars represent 100 μm .

that integration of IMPDH-1 CLuc resulted in reduced intein splicing, did not affect the expression of p53 and the other two EXSISERS reporters. Regardless of the IMPDH-1 intein splicing efficacy, as long as all EXSISERS reporters and all p53 protein isoforms were properly expressed, quantitative measurement of the p53 protein isoform groups FLp53, $\Delta 40$ p53, and $\Delta 133$ p53+ $\Delta 160$ p53 was still practicable. In addition, immunofluorescence microscopy of EXSISERS^{TP53:2CLuc-4NLuc-7FLuc} cells demonstrated persistent expression and effective segregation of p53 and IMPDH-1 CLuc into their predetermined cellular compartment.

3.3 Functional integrity of tumor suppressor p53 and the EXSISERS reporters.

We postulate that intein splicing-mediated excision of EXSISERS out of p53 does not influence the tumor suppressor's structural and functional integrity. Therefore, we tested the transcription factor's capability of binding to corresponding p53 response elements (p53-RE) and to be phosphorylated by kinases. These two experiments would conclusively demonstrate that genetic modification of *TP53* does not hinder p53 from executing its respective cellular tasks as a transcription factor.

An additional cell line was established to compare the behavior of non-functional p53 in a p53 transcription factor binding assay. This cell line contains a modified version of p53 in which the conserved DNA-binding domain (DBD) is absent, rendering it incapable of binding to the corresponding p53 RE (Fig. 17b). Of note, p53 continues to be expressed, albeit with entirely deactivated function. By deleting a selected portion of the DBD (amino acids 240-302), we not only effectively disrupted its interaction with genomic p53-RE, the DBD deletion also disrupted the direct interaction with members of the Bcl-2 protein family [104].

The targeted knockout of *TP53* in HCT116 cells was achieved through multiplexed sgRNA-mediated genome editing (Fig. 17a). Two sgRNA molecules carrying the spacer sequences 5' CATGTGTAACAGTTCCTGCA 3' (targeting *TP53* coding exon 7) and 5' TTACCTCGCTTAGTGCTCCC 3' (targeting *TP53* coding exon 8), were driven by a single U6-promoter and post-transcriptionally separated by an endogenous tRNA sequence. Typically, tRNA precursors undergo cleavage by RNase P and RNase Z to eliminate additional sequences at their 5' and 3' ends [188]. We placed an endogenous tRNA sequence between both sgRNA sequences, resulting in post-transcriptional maturation and segregation of the two *TP53*-targeting sgRNA molecules.

Results

coding for the flippase recombinase (targeting the two flanking FRT sites on either end of the selection cassette) finalized the *TP53* DBD KO cell line.

Genotyping of *TP53* DBD KO cells resulted in 500 bp truncated PCR amplicons of approximately 2265 bp fragment size (Fig. 17c). In contrast, PCR amplicons generated from HCT116 WT cells displayed a band at 2797 bp. Immunoblot analysis of *TP53* DBD KO clone HCT116 3.C7 revealed a signal at 36 kDa representing a truncated FLp53 protein (Fig. 17d, e). In contrast to a complete gene knockout, we created a p53 protein with a loss-of-function mutation. The presence of an emerging immunoblot signal indicates the ongoing cellular expression of p53 despite the DBD KO.

We have previously demonstrated that stable integration of EXSISERS reporters into *TP53* did not influence the structural integrity of p53. Since all co-translated EXSISERS reporters (IMPDH-1 CLuc, gp41-1 NLuc, and NrdJ-1 FLuc) contain self-excising split-inteins, we postulate that after post-translational processing, p53 remains in its native form and fulfills its task as a transcription factor. Therefore, we conducted a p53 transcription factor binding assay by isolating nuclear extracts from HCT116 WT and distinct EXSISERS cell lines, including EXSISERS_{TP53:7FLuc}, EXSISERS_{TP53:4NLuc-7FLuc}, and EXSISERS_{TP53:2CLuc-4NLuc-7FLuc}. Isolated nuclear extracts from these cell lines were loaded and incubated onto 96 well plates, carrying immobilized p53 RE on their plate surface. Structurally and functionally unaffected p53 proteins can bind these sequences. A subsequent ELISA using antibodies directed against p53 allows the spectrophotometric detection of the relative abundance of DNA-binding p53 within the nuclear extracts (Fig. 18a). HCT116 WT nuclear extracts with supplementation of mobilized p53 RE (DNA oligos), as well as nuclear extracts from HCT116 p53 DBD KO cells both yielded the lowest amounts of immobilized endogenous p53 (Fig. 18b). EXSISERS_{TP53:7FLuc} and EXSISERS_{TP53:4NLuc-7FLuc} revealed similar amounts of p53 as for the positive control with nuclear extracts from HCT116 WT cells. EXSISERS_{TP53:2CLuc-4NLuc-7FLuc} showed the lowest relative abundance of immobilized endogenous p53 besides the two negative controls. As seen before (Fig. 16d), integration of the third EXSISERS reporter caused lower splicing efficiencies, so p53 requires more time to be transported to the nucleus. Furthermore, a gene enlargement with three additional EXSISERS reporter sequences may also reduce overall p53 expression. However, the p53 protein isoforms are continuously expressed, allowing a relative isoform discrimination by EXSISERS. We further conducted

Results

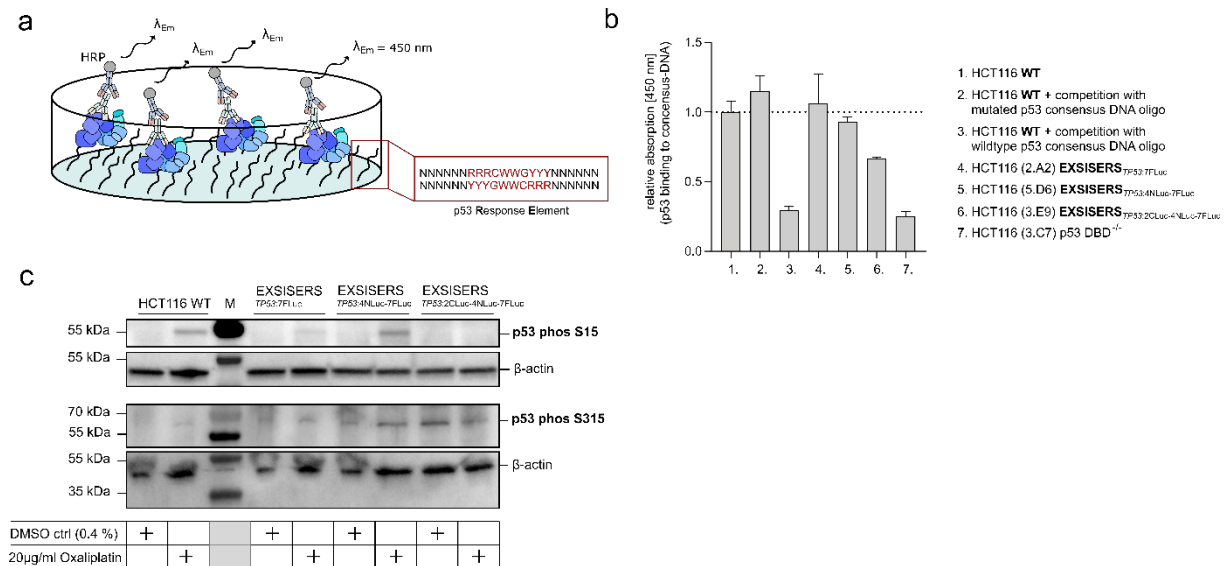


Figure 18: Preservation of p53 functional integrity with integrated EXSISERS reporters.

a) Schematic representation of p53 transcription factor binding to specific DNA consensus sequences (p53 response elements, p53 REs). Bound p53 proteins were detected by primary anti-p53 antibodies and horseradish peroxidase (HRP)-conjugated secondary antibodies. **b)** Measured relative absorbation at 450 nm represents p53 binding capacity of nuclear extracts derived from different HCT116 EXSISERS or HCT116 WT cell lines. Sample measurements were conducted in triplicates ($n=3$). Normalization of data points to previously measured protein concentrations (nuclear extracts). **c)** WB analysis of HCT116 WT, EXSISERS $_{TP53:7FLuc}$, EXSISERS $_{TP53:4NLuc-7FLuc}$, and EXSISERS $_{TP53:2CLuc-4NLuc-7FLuc}$ RIPA cell lysates. Prior to cell lysis, cells were either treated with DMSO control (0.4 %) or with 20 $\mu\text{g ml}^{-1}$ oxaliplatin. Phosphorylation of serine 15 and serine 315 confirmed induction of p53 activity upon drug-induced cell death.

an immunoblot experiment of RIPA-cell lysates derived from HCT116 WT and the distinct EXSISERS cell lines, including EXSISERS $_{TP53:7FLuc}$, EXSISERS $_{TP53:4NLuc-7FLuc}$, and EXSISERS $_{TP53:2CLuc-4NLuc-7FLuc}$, which were either treated with 0.4 % DMSO or 20 $\mu\text{g ml}^{-1}$ oxaliplatin (OX) for 48 h (Fig. 18c). We first analyzed the responsiveness of stimulated p53 through phosphorylation of Ser15. While HCT116 WT, EXSISERS $_{TP53:7FLuc}$, and EXSISERS $_{TP53:4NLuc-7FLuc}$ revealed robust p53 inducibility, EXSISERS $_{TP53:2CLuc-4NLuc-7FLuc}$ showed only minor signals in response to OX treatment. Other than HCT116 WT, EXSISERS $_{TP53:7FLuc}$, EXSISERS $_{TP53:4NLuc-7FLuc}$, the Ser15 phosphorylation status of EXSISERS $_{TP53:2CLuc-4NLuc-7FLuc}$ is highly dependent on the IMPDH-1 CLuc intein-splicing efficiency. IMPDH-1 CLuc was stably integrated between Lys14 and Ser15. Moderate IMPDH-1 intein-splicing may result in restricted accessibility for serine/threonine kinases and reduced Ser15-phospho-dependent p53 induction. For that reason, we additionally analyzed the phosphorylation inducibility of Ser315 to exclude any steric hindrance of EXSISERS reporters. In contrast to Ser15, Ser315 remains amenable to phosphorylation across all cell lines. Given that our primary focus lies in investigating the differential expression of the p53 protein isoforms

under the influence of distinct CRC therapeutics, the absence of p53 Ser15 inducibility is of non-essential significance to us.

3.4 Experimental setup of the triple EXSISERS reporter system for real-time and live-cell quantitative measurements.

Mentioning the investigation of the differential p53 protein isoform expression under the influence of distinct therapeutics, we first had to set up the experimental procedure of the triple EXSISERS reporter system. To enable real-time and live-cell luminescent measurements, we had to deviate from our previous approach of lysing the cells to make the EXSISERS reporters accessible to their specific substrates. Instead, we employed alternative plasma membrane-permeable luciferin substrates. D-luciferin-ethyl-ester, for instance, is a D-luciferin derivate that acquires the capacity to penetrate the plasma membrane due to the addition of hydrophobic ethylester residues (Fig. 19a). Endurazine was developed by Promega to be a membrane-permeable and highly thermostable NLuc substrate which allows the quantitative measurement of cytosolic gp41-1 NLuc. Vargulin, on the other hand, does not need to be membrane-permeable since IMPDH-1 CLuc was designed to be transported and exposed to the plasma-membrane. The special translocation-mechanism of IMPDPH-1 Cluc during spatial segregation from p53 makes the luciferase accessible to its specific substrate. After adding the respective luciferin substrates and therapeutics, the luminescent signals of CLuc are measured at 465 nm, the luminescent signals of NLuc are measured at 460 nm, and those of FLuc are measured at 564 nm. Since CLuc and NLuc emit luminescence at similar wavelengths, respective luciferin substrates have to be administered on different plates but have the same drug treatment (Fig. 19a). As already mentioned, the NLuc substrate Endurazine is reported to be highly thermostable and, therefore, has a half-life of approximately 72 h. We measured the signal decay of FLuc starting from the time point of substrate addition and, thus, estimated the half-life of D-luciferin-ethylester to be approximately 6 h (Fig. 19c). Therefore, it is advisable to renew the D-luciferin-ethylester substrate every 12 hours (Fig. 19d). Conversely, Vargulin is characterized by its thermolability, resulting in a rapid decline of the CLuc luminescent signal within a few minutes after substrate addition (Fig. 19b). Consequently, luminescence measurements for CLuc

Results

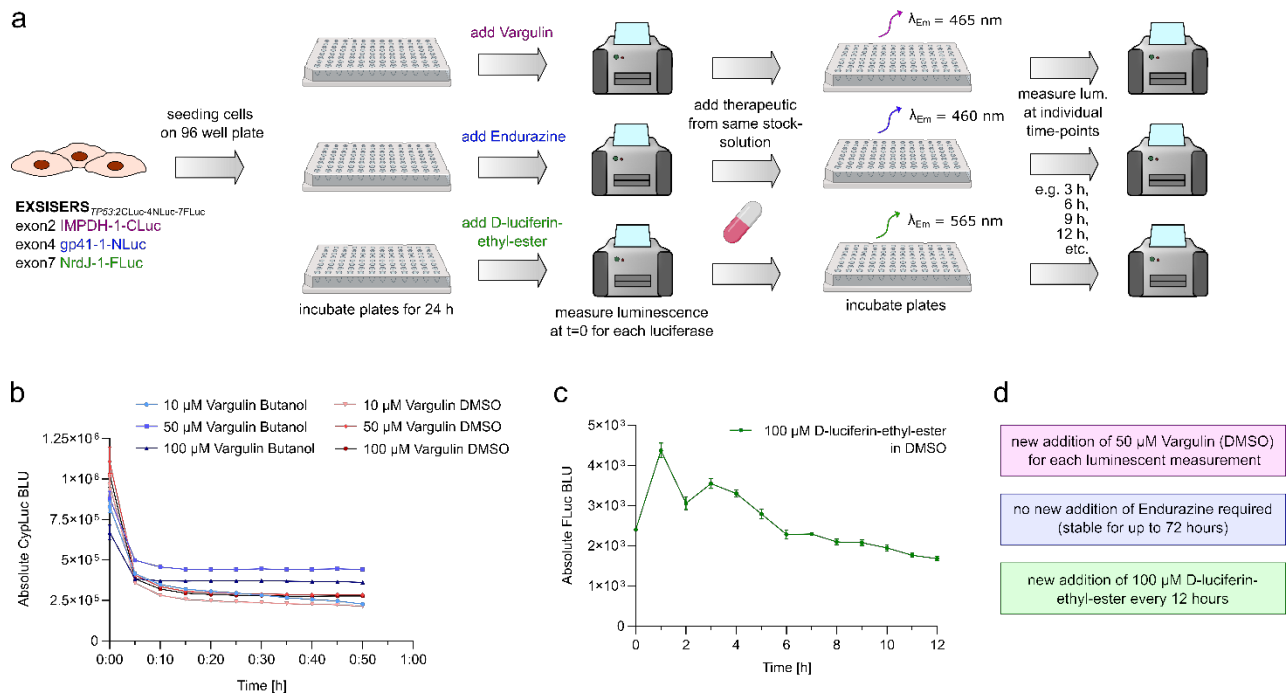


Figure 19: Experimental setup and evaluation of luciferase substrate stability. **a**) Schematic of experimental setup (including EXSISERS_{TP53:2CLuc-4NLuc-7FLuc} cell seeding, luciferase substrate addition, therapeutic drug treatment, and luminescence measurement) for relative p53 protein isoform quantification with EXSISERS-reporters. **b**) Determination of the stability of CLuc substrate vargulin either solved in Butanol or DMSO. Vargulin was applied on EXSISERS_{TP53:2CLuc-4NLuc-7FLuc} cells at the indicated concentrations (10 μM , 50 μM , 100 μM). Absolute CLuc luminescent signal was measured immediately after substrate addition for a total of 50 min in 5 min intervals. **c**) Determination of FLuc substrate stability D-luciferin-ethyl-ester solved in DMSO. FLuc-substrate was applied on EXSISERS_{TP53:2CLuc-4NLuc-7FLuc} cells at the indicated concentrations (100 μM). Absolute FLuc luminescent signal was measured immediately after substrate addition for a total of 12 h in 1 h intervals. **d**) Recommended time-points of new luciferase-substrate addition (determined from b and c; substrate stability) for the corresponding luciferase measurements.

must be promptly conducted, with replenishment of fresh substrate before each successive measurement (Fig. 19d).

3.4 Comprehensive analysis of the mutual interplay of FLP53, $\Delta 40\text{p53}$ and $\Delta 133\text{p53} + \Delta 160\text{p53}$ in response to clinically established CRC-therapeutics.

As already stated, p53 is referred to as one of the most important proteins in tumor recognition and tumor suppression, capable of shutting down whole proliferative and metabolic activities [102]. p53 induces cell-cycle arrest or apoptosis [103] by either interacting with pro-apoptotic BCL-2 family members (Bax, Bak, Bcl-xL) [104] or stimulating the transcription of downstream genes (*PUMA*, *APAF1*) [105–107,189]. Contrarily, p53 also activates pro-survival pathways by transcriptionally activating downstream genes that efficiently counteract apoptosis [108]. Thus, cell fate and the predominantly activated pathways highly depend on the differentially expressed p53

Results

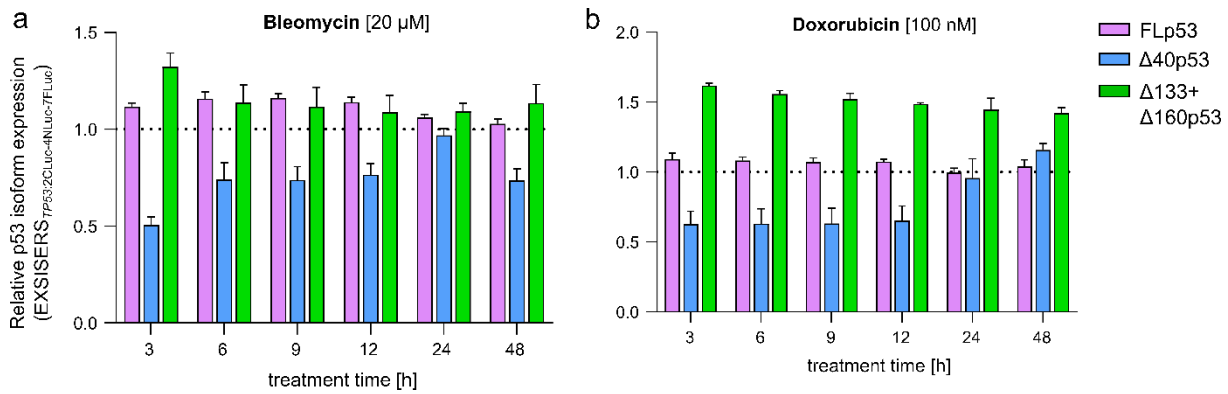


Figure 20: Study of the differential p53 isoform expression in EXSISERS_{TP53:2CLuc-4NLuc-7FLuc} cells in response to cell-cycle arresting agents. a) Real-time and live-cell quantification of p53 protein isoforms (FLp53, Δ40p53, and Δ133p53+Δ160p53) using EXSISERS_{TP53:2CLuc-4NLuc-7FLuc} cells. Relative p53 protein isoform quantification was performed for cell cycle arrest-inducing compounds bleomycin [20 µM] and **b)** doxorubicin [100 nM] at timepoints 3 h, 6 h, 9 h, 12 h, 24 h, and 48 h. t=0 was used as a normalization control. Luminescent signals in b) and c) were normalized to 0.2 % DMSO treatment. DMSO control was set to y=1 and displayed as a dashed line (y=1). Measurements were conducted in triplicates (n=3).

protein isoforms and their respective cellular ratios [116,117]. Especially the FLp53:Δ40p53 ratio is especially known to govern crucial tumor-suppressive pathways. Elevated FLp53 levels mainly influence the cell cycle and metabolism [190]. Δ40p53, on the other hand, lacks substantial parts of the TAD I domain (1 – 40 aa) and therefore represents a transcriptionally inactive isoform. Elevated Δ40p53:FLp53 ratios are linked to increased apoptosis and decreased tumor recurrence rates [117,118]. In light of successfully establishing the triple-EXSISERS reporter system in *TP53*, we can now efficiently investigate whether distinct tumor therapies with known mechanisms of action on tumor cells can induce the expected shifts in the p53 protein isoform ratio. Defined concentrations of bleomycin (20 µM) and doxorubicin (100 nM) are known to induce cell-cycle arrest in HCT116 cells efficiently. Real-time luminescence measurements with administration of 20 µM bleomycin onto EXSISERS_{TP53:2CLuc-4NLuc-7FLuc} cells showed a slight increase in FLp53 and Δ133+Δ160p53 at all measured time points (Fig. 20a). However, Δ40p53 is decisively downregulated at early treatment time points (3, 6, 9 h), which causes a significant FLp53:Δ40p53-ratio-shift towards FLp53. In conjunction with the modest upregulation of the anti-apoptotic Δ133+Δ160p53 isoforms throughout the entire treatment time, the induction of apoptosis is hindered while concurrently influencing a cell's proliferative and metabolic activity. The same was observed for the treatment with 100 nM doxorubicin. However, Δ133+Δ160p53 exhibited a higher upregulation (Fig. 20b). When predominantly considering the FLp53:Δ40p53 ratio, there is a pronounced shift

Results

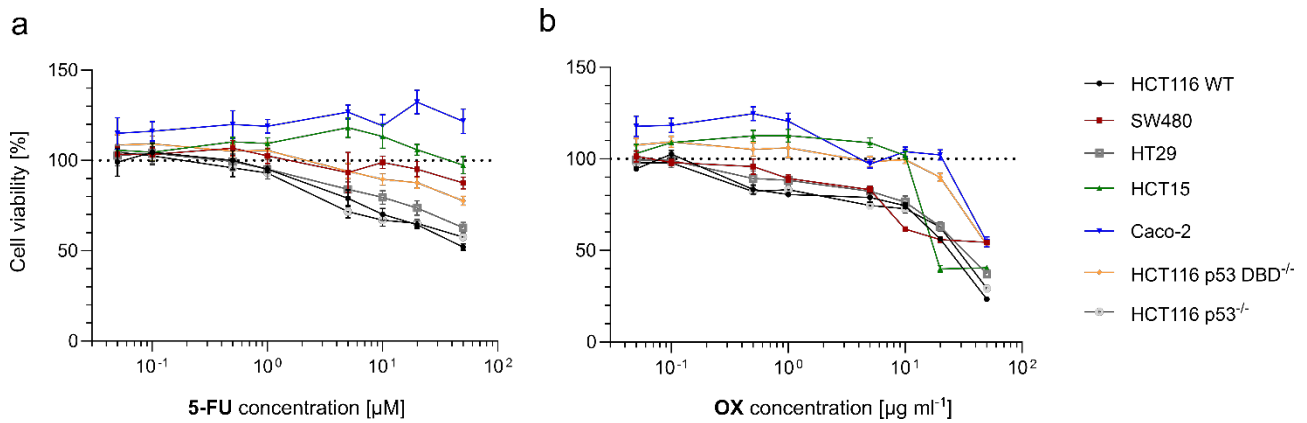


Figure 21: Clinically established chemotherapeutics induce moderate cell-death in CRC cell lines. Luciferase-based cell viability assay using clinical-relevant chemotherapeutics **a)** 5-Fluorouracil (5-FU) and **b)** oxaliplatin (OX) for the treatment of distinct CRC cell lines for 48 h (n=3). Drug concentrations were spanning from 50 nM to 50 μM or 50 ng ml^{-1} to 50 $\mu\text{g ml}^{-1}$, respectively. Cell viability of selected CRC cell lines was normalized to 0.5 % DMSO control, which was set to 100 % cell viability (dashed line at $y=100\%$). Luminescence values of respective therapeutical concentrations were measured in triplicates (n=3).

towards FLp53. By employing defined concentrations of bleomycin and doxorubicin, we identified FLp53 as the predominant protein isoform responsible for the induction of cell-cycle arrest, emphasizing its interaction with anti-apoptotic p53 protein isoforms.

To verify whether $\Delta 40\text{p}53$ is the protein isoform predominantly responsible for the induction of apoptosis, we sought to identify appropriate *in vitro* doses for chemotherapeutics 5-fluorouracil (5-FU) and oxaliplatin (OX), which are clinically applied for the treatment of CRC. Conducting a viability assay with varying drug-concentrations, we identified 20 μM 5-FU and 20 $\mu\text{g ml}^{-1}$ OX to induce only mild cytotoxic effects to provide optimal screening conditions for the quantification of p53 while minimizing the potential adverse impact of too intense treatment (Fig 21a,b). The utilization of multiple cell lines concurrently revealed that the therapeutic effects of 5-FU and OX are predominantly cell-type-specific.

We treated EXSISERS_{TP53:2CLuc-4NLuc-7FLuc} cells with 20 μM 5-FU and 20 $\mu\text{g ml}^{-1}$ OX and investigated the differential expression of FLp53, $\Delta 40\text{p}53$, and $\Delta 133+160\text{p}53$ isoforms. Following both treatments, we observed a temporary reduction in oncogenic $\Delta 133+160\text{p}53$ levels, accompanied by a significant shift in the FLp53: $\Delta 40\text{p}53$ ratio towards the pro-apoptotic $\Delta 40\text{p}53$ isoform after 24 and 48 h (Fig. 22f, g). Moreover, OX treatment led to an initial increase in FLp53 expression. To elucidate the relationship between the changes in p53 isoform ratios and the correspondingly activated signaling pathways, we assessed an immunoblot analysis with specific

Results

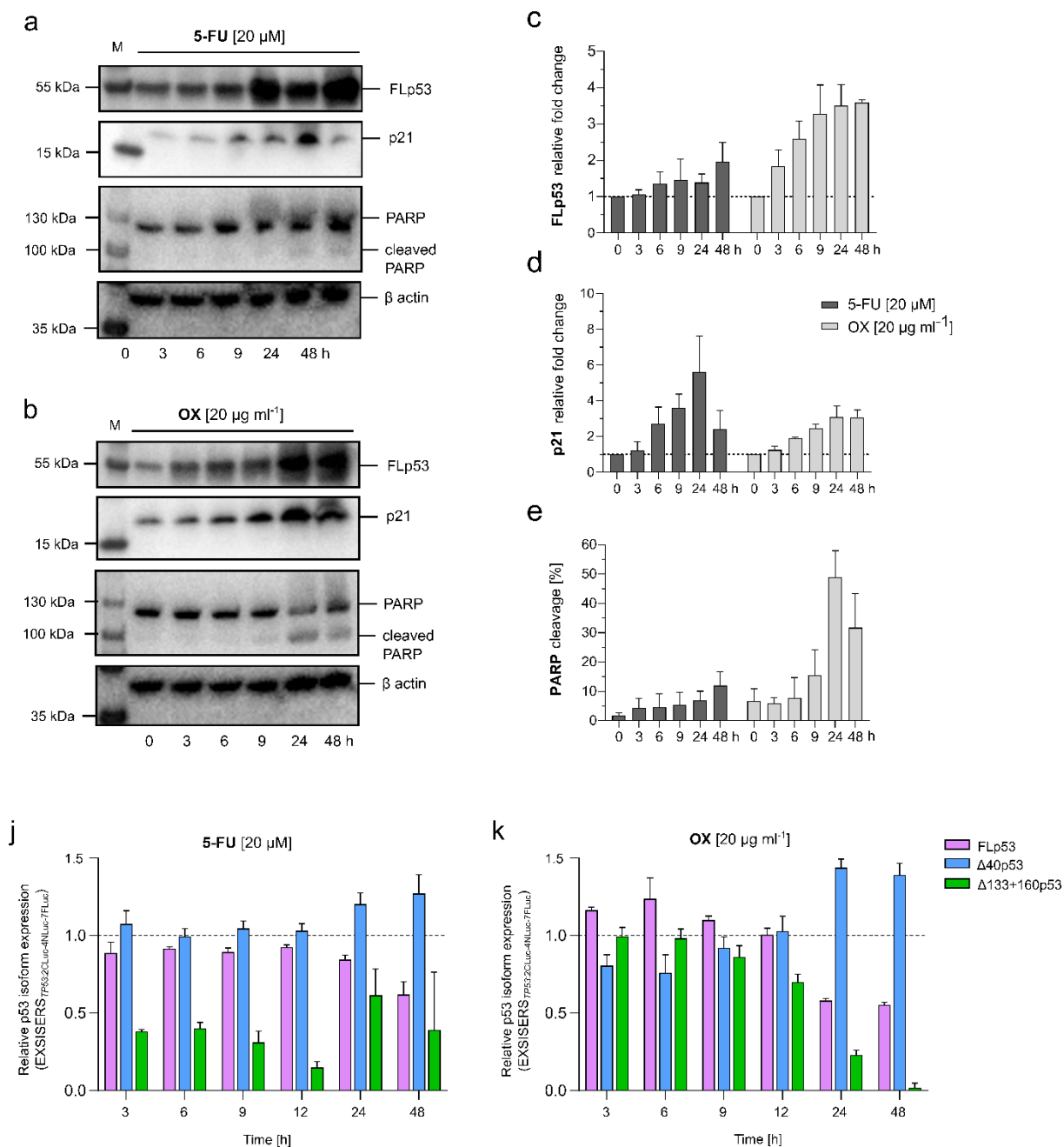


Figure 22: The triple EXSISERS reporter system reliably differentiates and quantifies p53 protein isoforms in living cells and in real-time. **a)** Western blot analysis of cell lysates from 5-FU [20 μ M] and **b)** OX [20 μ g ml⁻¹] treated HCT116 cells detecting cellular FLp53 and relevant markers for cell cycle arrest (p21) and apoptosis (PARP cleavage) at t=0, 3 h, 6 h, 9 h, 24 h, and 48 h. All Western blots were conducted in triplicates (n=3). Densitometric analyses of relative **c)** FLp53 expression, **d)** p21 expression, and **e)** PARP cleavage in percent. **e)** *Real-time* and *live-cell* quantification of corresponding p53 protein isoforms using EXSISERS. Relative p53 protein isoform quantifications were detected for **f)** 5-FU [20 μ M] and **g)** OX [20 μ g ml⁻¹] treatment at timepoints 3 h, 6 h, 9 h, 12 h, 24 h, and 48 h. t=0 was used as a normalization control. DMSO treated cells were used to normalize luminescent signals from treated cells. Measurements were conducted in triplicates (n=3).

protein markers for cell cycle arrest (p21) and apoptosis induction (PARP cleavage) in 5-FU- and OX-treated HCT116 WT cells (Fig. 22a, b). While p21 levels steadily increased over time (Fig. 22d), PARP cleavage was minimally detected after 5-FU treatment but clearly evident after OX treatment (Fig. 22e), corresponding to the

Results

increasing $\Delta 40p53$ expression measured by EXSISERS at 24 and 48 hours of 5-FU and OX treatment. Hence, we can affirm that the upregulation of $\Delta 40p53$ and the consequent alteration in FLp53: $\Delta 40p53$ isoform ratio can serve as potential mechanisms underlying p53-dependent induction of apoptosis.

Noteworthy, the time-dependent increase in FLp53 levels and the concurrent increase in p21 expression demonstrate that EXSISERS exclusively registers *de novo* p53 expression and does not detect post-translational stabilization effects that are common for p53 (Fig. 22c, g). EXSISERS is a potent tool for accurately assessing short- or long-term alterations in p53 isoform ratios and reflecting their associated cellular consequences, where conventional methods may fail.

3.5 Established protein analysis methods face challenges in detecting and quantifying the specific p53 protein isoforms.

To highlight the merits of the EXSISERS technology, we have applied diverse gold standard techniques for identifying and measuring protein isoforms for comparative analysis. Antibody-based methods, including immunoblotting analysis, allow for a straightforward and cost-effective way of visually detecting proteins and their respective protein isoforms. For low-abundance proteins, there is the potential to initially enrich these proteins via immunoprecipitation before subsequently analyzing them in a qualitative or quantitative manner. Starting with immunoblot analysis, we employed four distinct pan-tropic antibodies to detect all p53 protein isoforms (Fig. 23a). These antibodies apparently recognize the DNA-binding domain (DBD) of p53. This conserved domain is available in all p53 protein isoforms. Using the antibodies PAb240, ab26, DO-12, and PAb421 resulted in the detection of multiple unspecific bands (Fig. 23b), which, except for FLp53, did not correspond to the expected size of the protein isoforms (Fig. 23c). Since it is known for all p53 protein isoforms, except for FLp53, to be significantly underrepresented, we attempted to enrich $\Delta 40p53$, $\Delta 133p53$, and $\Delta 160p53$ through immunoprecipitation.

Immunoprecipitation is a technique that involves the initial capture of the target protein through specific antibody-bead interactions. Subsequently, these proteins are separated from the heterogenous protein lysate by distinct precipitation procedures encompassing multiple centrifugation steps, gravity flow, or magnetic separation.

Results

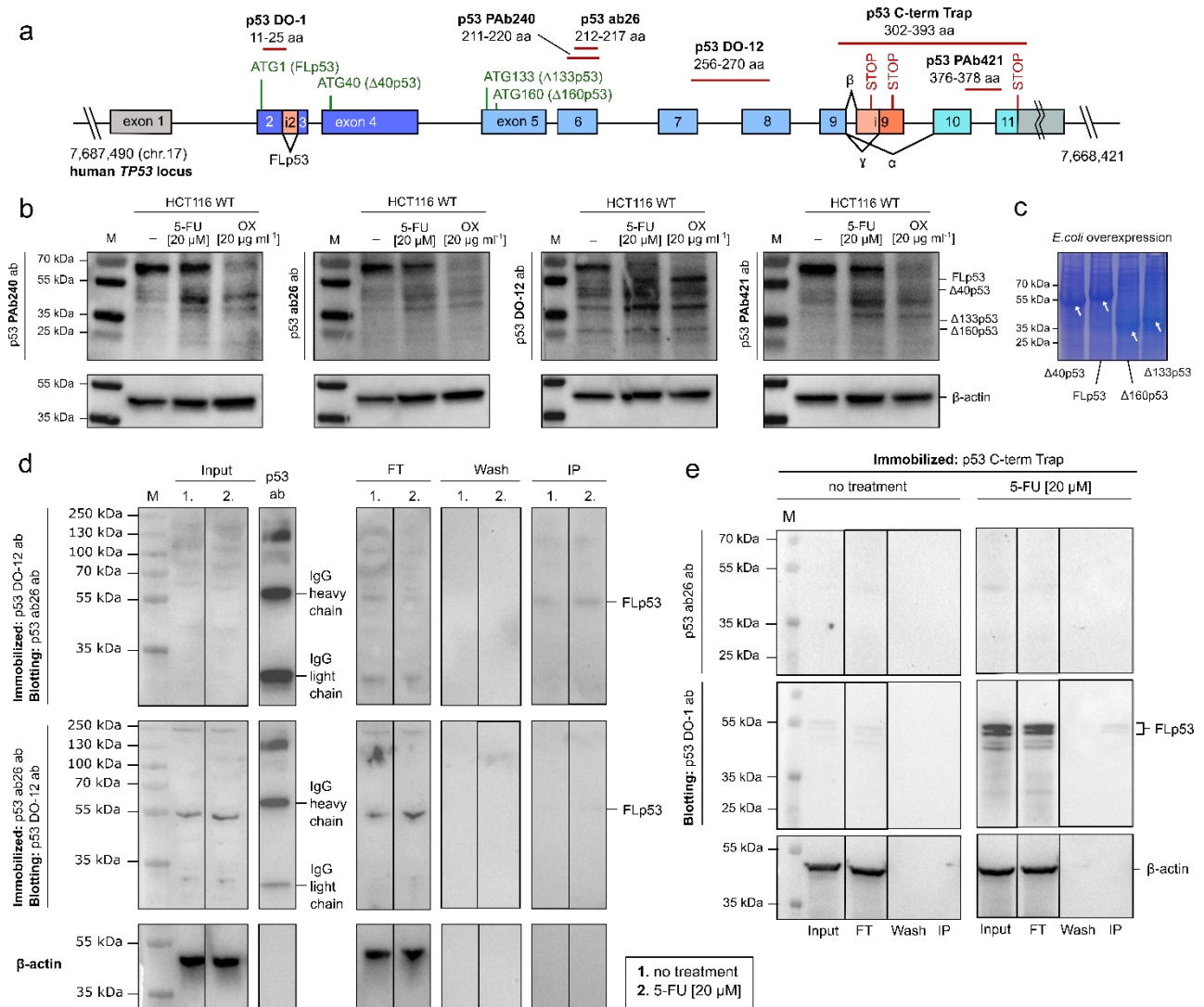


Figure 23: Western blot analyses (WB) display distinct limitations in detecting and quantifying specific p53 isoforms. **a**) Representation of the human *TP53* locus with the respective coding exons (blue bars) and the epitopes (red lines) for specific pantropic p53 antibodies. **b**) WB analysis of RIPA lysates derived from HCT116 WT cells, either 1) non-treated, 2) treated with 5-fluorouracil (5-FU) [30 μM], or 3) oxaliplatin (OX) [20 $\mu\text{g ml}^{-1}$]. p53 protein isoforms were analyzed with distinct pantropic primary antibodies, including ab26, PAb240, DO-12, and PAb421. HCT116 cells were lysed 24 h after treatment. p53 protein isoforms were detected using primary monoclonal mouse antibodies and secondary HRP-conjugated anti-mouse secondary antibodies. These data highlight the limitations of analyzing p53 isoforms by WB. The detected signals do not correspond to the molecular size of the distinct isoforms. The deviations in molecular weight are due to post-translational modifications and make it challenging to assign the signals to the corresponding isoforms. **c**) Overexpression of recombinant p53 protein isoforms in *E. coli* and validation of their molecular mass by SDS-PAGE. **d**) Immunoprecipitation of p53 protein isoforms using magnetic beads. RIPA lysates from HCT116 WT cells either non-treated or treated with 5-FU [20 μM] (24 h) were used as input. **e**) Immunoprecipitation of p53 protein isoforms using the Nanobead p53 C-term trap technology is shown. RIPA lysates from HCT116 WT cells either non-treated or treated with 5-FU [20 μM] (24 h) were used as input. p53 protein isoforms were immobilized with a Nanobead p53-term trap and blotted with the indicated primary antibodies.

Therefore, we crosslinked magnetic beads with ab26 pantropic antibodies. Again, cell lysates were isolated from HCT116 WT cells either treated with DMSO or 20 μM 5-FU (24 h). These cell lysates were incubated with crosslinked ab26-crosslinked magnetic

Results

beads and were magnetically separated from the heterogenic protein lysates. Thereafter, specifically bound proteins were eluted and detected with DO-12 p53-antibodies on western blot (Fig. 23d). We further excluded the chance of unspecific binding of p53 to non-crosslinked magnetic beads (additional pre-clearing step). We only detected signals for FLp53, mainly in the “input” and “flowthrough” fractions, which indicates a weak interaction between the ab26 antibody and p53. Vice versa, immobilizing DO-12 on magnetic beads and detecting precipitated p53 with ab26 resulted in larger quantities of p53, but again, exclusively FLp53 was detectable on western blot.

Subsequently, we applied another promising immunoprecipitation approach. The p53-C-term-Trap from chromotek utilizes single variable domains on a heavy chain (VHH), also referred to as “Nanobodies,” directed against the C-terminal chain of p53. These single-chain Nanobodies are commercially available as pre-coupled antibody-agarose beads. The p53-C-term-Trap chromotek kit conveniently precipitates and detects FLp53, $\Delta 40$ p53, $\Delta 133$ p53, and $\Delta 160$ p53 protein isoforms. On this account, we immunoprecipitated cell lysates from HCT116 WT cells treated with either DMSO or 20 μ M 5-FU. Thereafter, all fractions (input, wash, flowthrough, and immunoprecipitation) were analyzed by western blot (Fig. 23e). Again, pan-tropic ab26 antibodies could not detect any conclusive p53 protein isoform signals. Exclusively, DO-1 antibodies from Santa Cruz, directed against the N-terminal TA-domain, could detect FLp53 α , FLp53 β , and FLp53 γ . Strong signals only occurred for the input- and flowthrough-fractions of 5-FU pretreated HCT116 WT cells. In conclusion, all antibodies that we have commercially obtained and tested could not establish a specific antibody-p53 interaction.

Therefore, we found it helpful to stably insert a recombinant sequence tag with a high affinity to specific commercial antibodies. We decided to integrate a recombinant FLAG tag (amino acid sequence: DYKDDDDK) into the conserved DNA binding domain (DBD) of p53. The inserted sequence also contained an autonomous selection cassette with the PuroR- and the HSVtk-gene (Fig. 24a). The selection cassette itself did not affect p53's translation or functionality since, due to the flanking splice donor and splice acceptor sites, the selection cassette is post-transcriptionally spliced out as an intron but acting in an autonomous way (Fig. 24a, b). The recombinant FLAG-tag was then allocated in exon 6 between amino acid positions 198 and 199 (Fig. 24b). Genotyping of these genetically modified HCT116 cells resulted in two monoclonal cell

Results

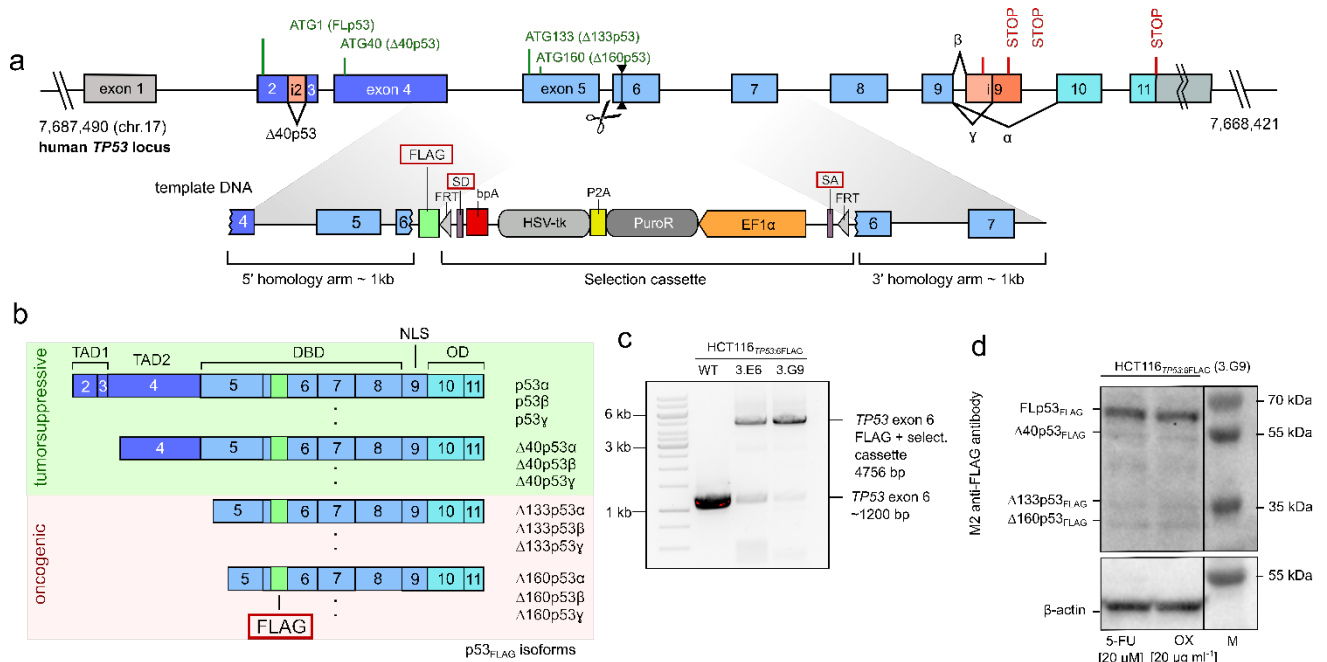


Figure 24: Stable integration of a recombinant FLAG into p53 for enhanced antibody-based detection. **a)** Scheme of the human *TP53* locus and the integration site of a recombinant FLAG-tag into coding exon 6. Template DNA and Cas9 coding sequence (with corresponding sgRNA sequence) were transfected into HCT116 WT cells as separate plasmids. **b)** Schematic of all p53 isoforms, carrying a recombinant FLAG tag within coding exon 6. The FLAG-tag was used for the detection of total p53 isoforms via WB. **c)** Agarose gel electrophoresis of PCR amplicons from genomic *TP53* locus is shown. Monoclonal HCT116 cells displayed stable integration of the FLAG-tag, proven by a 4756 bp fragment. *TP53* exon 6 PCR amplicons without genetic modification showed an amplification lane at 1200bp. Clone HCT116 3.G9 was chosen for p53 WB analysis. **d)** WB analysis of RIPA lysates from HCT116 3.G9 cells either treated with 20 μM 5-FU or 20 $\mu\text{g ml}^{-1}$ OX for 24 h. Anti-FLAG antibody (M2) was used to detect the specific p53 protein isoforms.

lines (HCT116 3.E6 and 3.G9) carrying the inserted FLAG tag (Fig. 24c). The PCR-amplicons were loaded onto agarose gels showing a band at 1,200 bp for isolated DNA from HCT116 WT cells and 4,756 bp for isolated DNA from stable cell lines with integrated FLAG tag. We isolated cell lysates of HCT116 3.G9 monoclonal cells, either treated with 20 μM 5-FU or 20 $\mu\text{g ml}^{-1}$ OX. Now that p53 contained the additional FLAG-tag, all corresponding protein isoforms visualized on western blot were shifted upwards for approximately 5.2 kDa (Fig. 24d). FLp53, representing the most abundant protein isoform, appeared at 60 kDa. $\Delta 40\text{p}53$, $\Delta 133\text{p}53$, and $\Delta 160\text{p}53$ all showed comparably weak signals and appeared at 55 kDa, 35 kDa, and 30 kDa, respectively. Conclusively, we increased the binding affinity of specific antibodies to FLAG tag carrying p53 protein isoforms, which markedly facilitated their antibody-based detection on western blot. One could continue with immunoprecipitation to enrich the underrepresented $\Delta 40\text{p}53$, $\Delta 133\text{p}53$, and $\Delta 160\text{p}53$ isoforms. However, to demonstrate the complexity of antibody-based detections without proper antibody specificity, we decided not to follow this strategy further. There is another antibody-

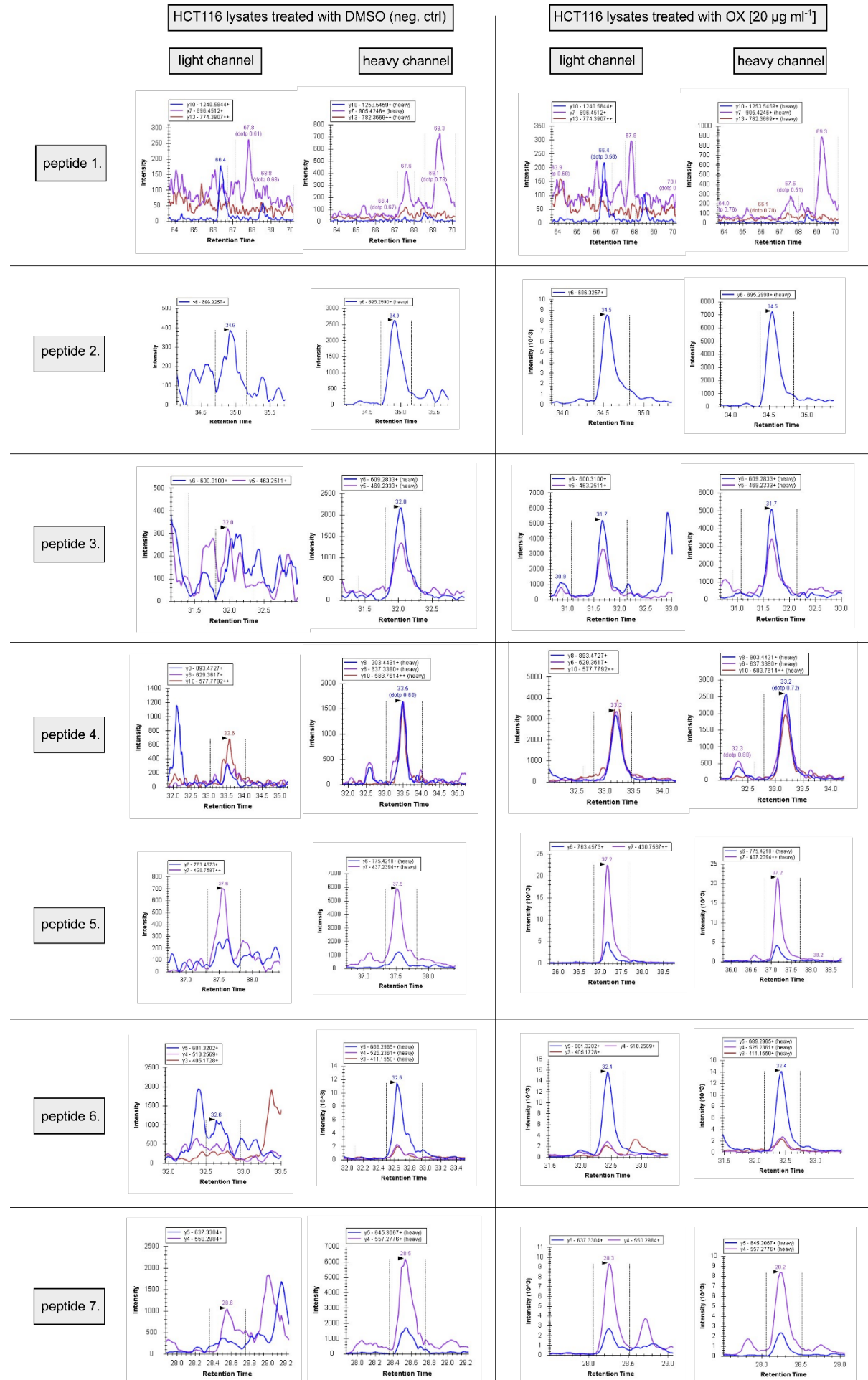
independent gold-standard method for protein isoform detection made possible by the broad applicability of mass spectrometry.

3.6 Detection and quantification of p53 isoforms via multiple reaction monitoring mass spectrometry

Mass spectrometry-based assays hold great promise in replacing protein immunoassays, especially in basic science and clinical research. Previous investigations have demonstrated the efficacy of assays employing multiple-reaction monitoring mass spectrometry (MRM-MS) for quantifying proteins in biological samples [191]. Targeted proteomic experiments, exhibited with MRM-MS, a technique with a longstanding clinical history in quantifying small molecules, offer the potential for accurate relative quantification of established proteins within complex mixtures. In the realm of targeted proteomics, peptides generated through protease digestion, typically utilizing trypsin, function as surrogate markers reflecting the specific protein abundance. MRM-MS assays provide distinct advantages over conventional immunoassays, including the ability to swiftly develop and validate MRM-based methods. Furthermore, these assays readily support multiplexing for the concurrent quantification of numerous proteins in a single analysis, spanning a broad range of relative concentrations, without encountering the cross-reactive interferences we often observe in our immunoassays [192].

To setup the quantitative measurement of the desired p53 protein isoform groups (FLp53, $\Delta 40$ p53, and $\Delta 133+\Delta 160$ p53), 0.7 fmol of ^{15}N -labeled and trypsin digested recombinant FLp53 protein were spiked into the mass spectrometer. Seven p53-related peptides were identified as suitable for quantifying their respective protein isoforms in a multiplexed manner (Fig. 25). Peptide 1, spanning from 1-24 aa, was the representative peptide for FLp53. Peptides 2, 3, and 4, spanning from 103-111 aa, 112-121 aa, and 122-133 aa, respectively, were representatives of FLp53 and $\Delta 40$ p53. Peptides 5, 6, and 7 spanning from 183-197 aa, 204-210 aa, and 269-274 aa laying in the conserved domain of p53, therefore, were representatives of all p53 isoforms (Fig. 26a). For the actual isoform quantification, HCT116 WT cells were treated with either 0.4 % DMSO (control), 20 μM 5-FU, or 20 $\mu\text{g ml}^{-1}$ OX for 24 h. Treated cells were then lysed with RIPA buffer, and cell lysates were sent to Polyquant (Bad Abbach, Germany) for sample preparation and measurement. Measurement of

Results



Results

Figure 25: Supplementary figure 4: MRM-Mass spectrometry chromatograms of p53 representative peptides. All mass spectrometry experiments and computational analyses as well as recombinant ^{15}N -isotope-labelled p53 expression and purification were conducted by Polyquant (Bad Abbach, Germany). Bacterial expression vector for recombinant FLp53 α as well as HCT116 WT cell treatment and cell lysis (with RIPA) were generated and provided by our laboratory. All samples were measured in targeted MRM mode. Differentially treated HCT116 cell lysates and ^{15}N -isotope (150 mM NaCl, 1,0 % IGEPAL® CA-630, 0,5 % Natriumdesoxycholat, 0,1 % SDS, 50 mM Tris, pH 8,0) labelled p53 were pre-digested with trypsin and analyzed via MRM-mass spectrometry. Seven p53 representative peptides were chosen for quantitative analysis. Representative peptides were measured in light channel (endogenous p53 from HCT116 WT cell lysates) and heavy channel mode (spiked ^{15}N -isotope labelled p53). Left column shows chromatograms of RIPA lysates from 0.2 % DMSO treated HCT116 WT cells (light channel) and ^{15}N -isotope labelled p53 as reference (heavy channel). Right column of chromatograms shows RIPA lysates from oxaliplatin-treated [$20\ \mu\text{g}\ \text{ml}^{-1}$] HCT116 WT cells (light channel) and ^{15}N -isotope labelled p53 as reference (heavy channel). Quantitative measurements were conducted with cell lysates from 1,000 HCT116 cells, in which 0.7 fmol of ^{15}N -isotope labelled p53 were spiked. Peptide 1 revealed low detectability in DMSO-, as well as in OX-treated cells and, thus, could not be quantified. Measurements were conducted in triplicates (n=3).

these heterogeneous cell lysates resulted in differential peptide quantification in response to the chemotherapeutics 5-FU and OX. Since peptide 1 is the only representative of FLp53, its low detection-specificity prevented the quantification of FLp53 in any sample (Fig. 25). Nevertheless, absolute peptide quantification of peptides 2, 3, and 4 (FL+ Δ 40p53, tumor suppressive isoforms) and peptides 5, 6, and 7 (Δ 133+160p53, oncogenic isoforms) allowed for quantitative discrimination of two p53 isoform groups (tumor suppressive vs. oncogenic) (Fig. 26b, c, d). The individual peptide quantifications (Fig. 26b) were averaged according to their respective p53 isoform assignment (Fig. 26c). On the one hand, these data demonstrate significant upregulation of p53 as a response to the 24 h treatment with both 5-FU and OX. On the other hand, the averaged values from peptides 2, 3, and 4 (representing tumor suppressive isoforms) and the values from peptides 5, 6, and 7 (representing all p53 isoforms) are at the same level. The *in silico* estimation of the relative FLp53+ Δ 40p53 (tumor suppressive) and Δ 133+ Δ 160p53 quantities revealed a significant underrepresentation of the truncated isoforms Δ 133+ Δ 160p53 (Fig. 26d). Consequently, the quantification of these protein isoforms proves to be nontrivial. Only after excessive upregulation due to OX treatment minimal amounts of Δ 133+ Δ 160p53 could be detected. Given the uniform amounts of peptide 2-7, none of the newly synthesized Δ 133+ Δ 160p53 isoforms accumulate but rather degrade rapidly. Further, the low specificity of peptide 1 can be attributed to its unusually long sequence. Larger peptides are more likely to be subjected to post-translational modifications. In the case

Results

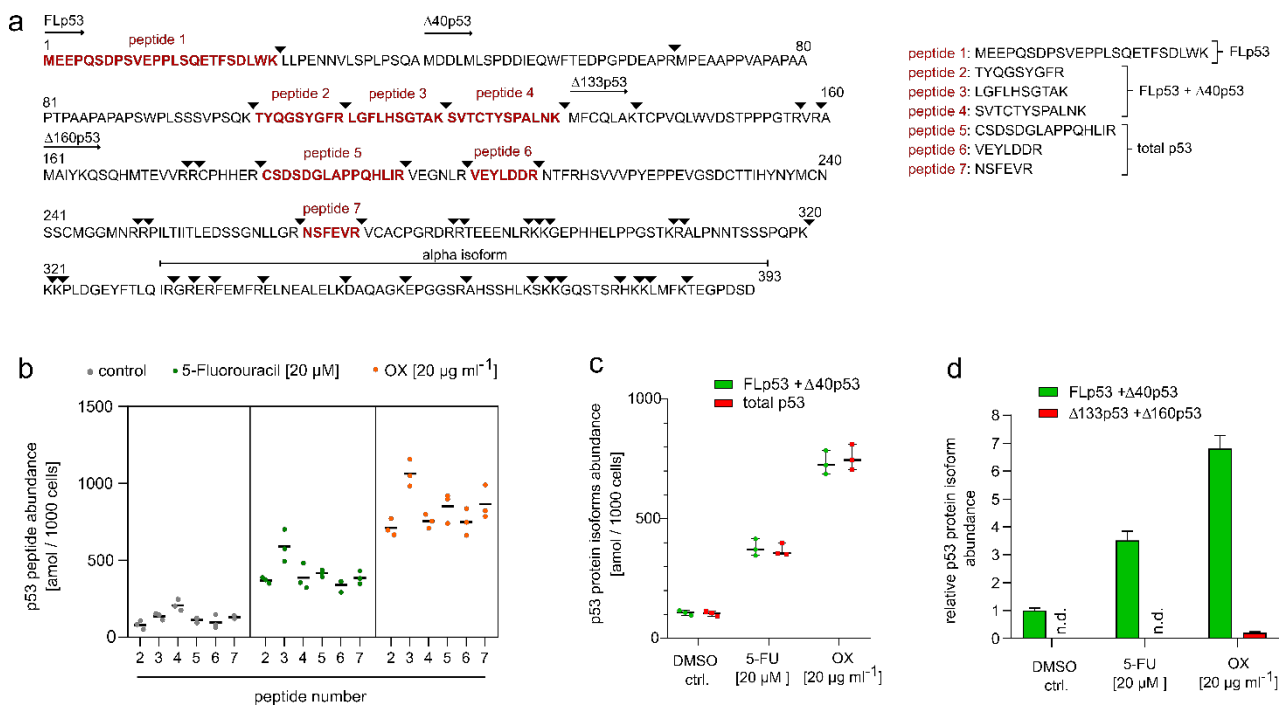


Figure 26: p53 protein isoform discrimination and absolute quantification via multiple reaction monitoring – mass spectrometry (MRM-MS). **a)** Protein sequence of p53 including the distinct translation start sites for FLp53, $\Delta 40$ p53, $\Delta 133$ p53, and $\Delta 160$ p53. Black triangles show potential trypsin digestion sites and resulting peptides. Sequences marked in red represent tryptic peptides concatenated for the synthesis of a heavy isotope-labelled protein internal standard for absolute quantification via multiple reaction monitoring on a triple quadrupole mass spectrometer. **b)** Absolute quantification of corresponding p53 peptides [amol per 1000 cells] for different treatment conditions, namely DMSO ctrl. (grey), 20 μ M 5-FU (green), and 20 μ g ml⁻¹ OX (orange), respectively, at timepoint 24 h. Measurements were conducted in triplicates (n=3). Horizontal bars indicate mean values. Peptide 1, representing FLp53 was not detectable. Quantification of peptides 5-7 is a measure of the total expression of p53. Quantification of peptides 2-4 is a measure of expression of FLp53+ $\Delta 40$ p53. **c)** Absolute quantification of p53 protein isoforms [amol per 1000 cells] from HCT116 WT cell lysates measured via mass spectrometry for different treatment conditions (n=3). Dots represent mean values of the corresponding peptides. Peptides 2-7 show equimolar levels, indicating that FLp53 and/or $\Delta 40$ p53 are predominantly expressed, while $\Delta 133$ p53+ $\Delta 160$ p53 isoforms are strongly underrepresented. **d)** Relative p53 protein isoform abundance of FLp53+ $\Delta 40$ p53 (calculated means from peptide-quantification 2-4) and $\Delta 133$ p53+ $\Delta 160$ p53 (calculated means from peptide-quantification 5-7 and subtracted from the means of peptide 2-4) (n=3). HCT116 cells were treated 48 h with DMSO [0.025%], 5-FU [20 μ M], or OX [20 μ g ml⁻¹] prior to cell lysis. FLp53+ $\Delta 40$ p53 values were normalized to the DMSO control. $\Delta 133$ p53+ $\Delta 160$ p53 values were normalized to the DMSO control and subsequently subtracted from the relative FLp53+ $\Delta 40$ p53 values. For distinct treatments with DMSO (ctrl.), 5-FU, and OX we did not detect considerable amounts of $\Delta 133$ p53+ $\Delta 160$ p53.

of p53, there are multiple phosphorylation sites, including Ser6, Ser9, Ser15, and Thr18. Depending on the activation status of p53, these amino acids are either phosphorylated or not. The varying molecular mass makes it challenging to choose a consistent detection window and, thus, to precisely quantify peptide 1. To some extent, the quantification of peptide 1 can be improved by optimizing peptide preparation or measurement settings. Chymotrypsin and Glut-C, for instance, are peptidases that generate a different peptide-digestions pattern. Therefore, the length of peptide 1 could be reduced to mitigate its susceptibility to potential post-translational effects by

Results

minimizing or eliminating their impact. Nevertheless, it remains unaltered that the cellular levels of $\Delta 133p53$ and $\Delta 160p53$ are minimal, making their detection and quantification via mass spectrometry extremely challenging. Hence, we further rely on p53 isoform quantifications via EXSISERS. Although the measured values provide relative protein isoform amounts, EXSISERS accurately determines temporal changes in protein expression. In addition, the following advantages should be considered:

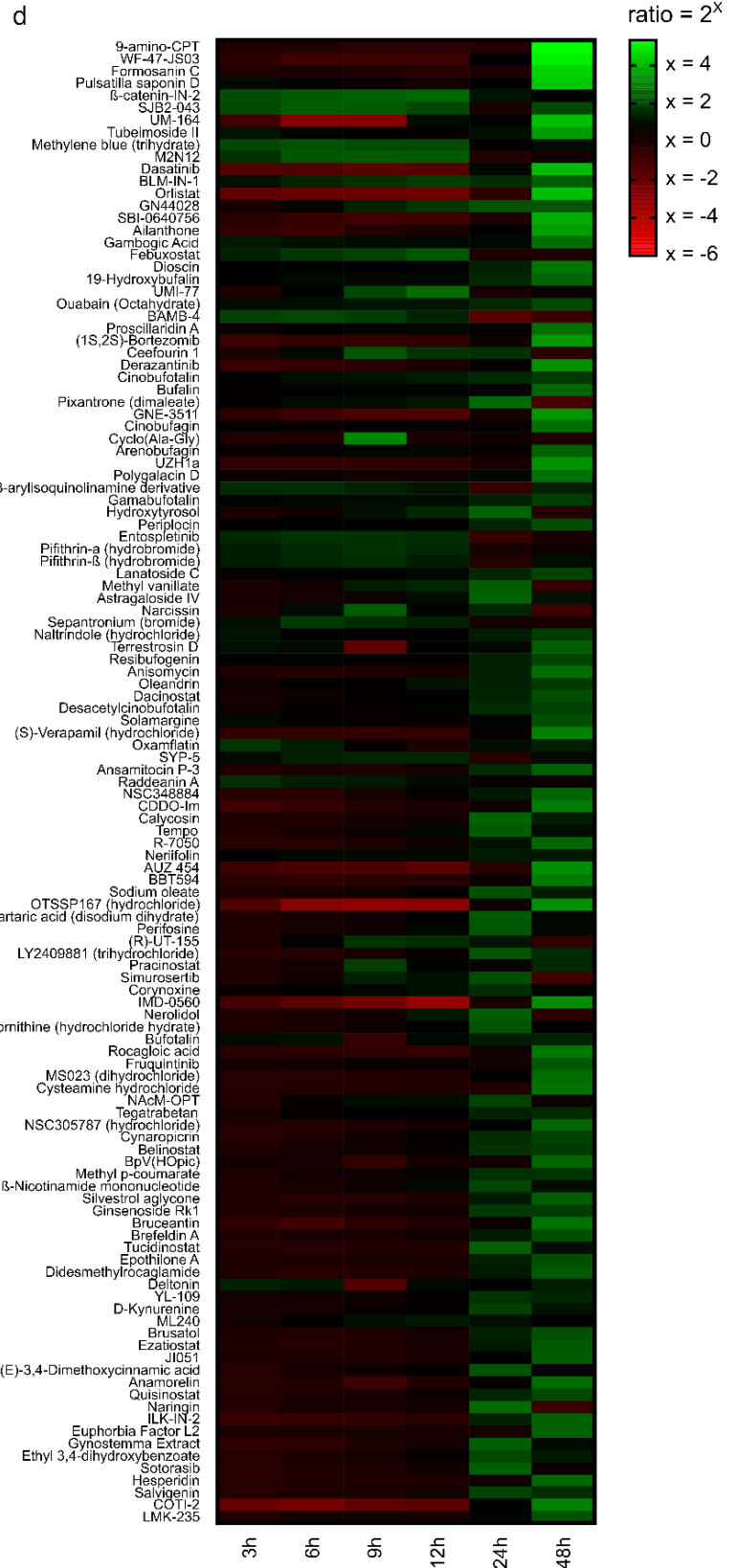
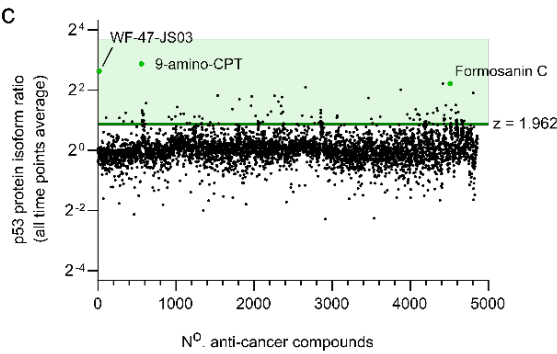
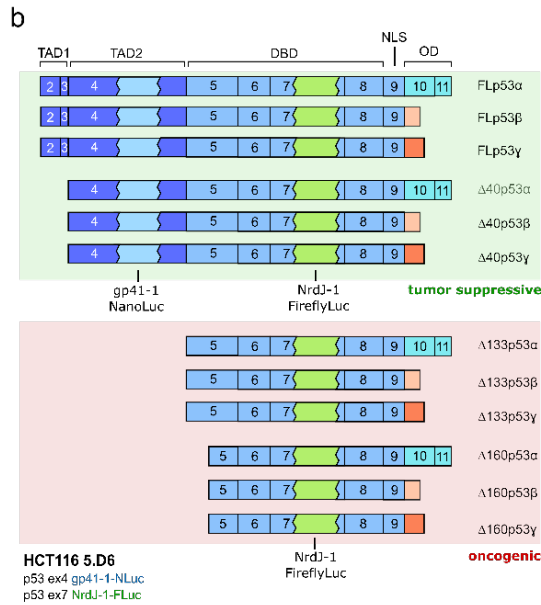
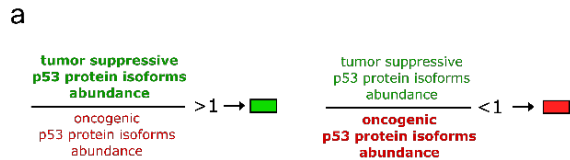
- 1) EXSISERS allows for translational quantification of any target protein,
- 2) differentiation of specific protein isoforms,
- 3) acquisition of time-series data,
- 4) measurement in living cells, and
- 5) high scalability with high-throughput screening applicability.

All listed EXSISERS characteristics would be elaborate or not feasible with mass spectrometry.

3.7 High-throughput screening of differential p53 isoform expression in response to 4,863 anti-cancer compounds.

Most commercial kits provide luciferase substrates dissolved in cell lysis buffer, making cytosolic luciferases accessible for measurements. Due to the cell membrane permeable character of endurazine (NanoLuc specific substrate) and D-luciferin ethylester (FireflyLuc specific substrate), cell lysis is not required. Therefore, EXSISERS applies to real-time protein quantification measurements in living cells. We used EXSISERS on a high-throughput drug screening to identify therapeutic agents that enhance p53-mediated tumor suppression and cell death induction while inhibiting p53 isoforms with oncogenic properties. To this end, we chose the dual-luciferase reporter cell line EXSISERS_{TP53:4NLuc-7FLuc}, which showed minor benefits in terms of p53 inducibility (Fig. 18b, c). This cell line primarily differentiates between tumor suppressive FLp53+ $\Delta 40p53$ and oncogenic $\Delta 133+\Delta 160p53$ isoforms (Fig. 27a, b). Calculating the ratio (tumor suppressive isoforms:oncogenic isoforms) allowed us to rank all drugs according to their p53-isoform-inducing properties. Cells were treated with an anti-cancer compound library (HY-L025) comprising 4,863 drugs. For each compound, p53 isoform ratios were measured and calculated as an average of six

Results



measured time points (3, 6, 9, 12, 24, 48 h) and plotted on an exponential scale (Fig. 27c). Based on this, we identified the 121 most significant drugs highly upregulating tumor suppressive p53 isoforms ($p < 0.025$), also referred to as p53-Tumor suppressor Isoform Enhancers (p53-TIEs; Fig. 27d). For the sake of completeness, we also included the 121 most significant drugs highly upregulating pro-oncogenic p53 protein

Results

Figure 27: Identification of anti-cancer compounds significantly inducing tumor suppressive p53 protein isoforms (p53-TIEs). **a)** Ratio between tumor suppressive and oncogenic isoforms were translated into color-codes. **b)** Schematic of all twelve p53 protein isoforms expressed in EXSISERS^{TP53:4NLuc-7FLuc} cell line. Luminescent measurements of stably integrated gp41-1-NLuc (exon 4) and NrdJ-1-FLuc (exon 7) enabled discrimination and quantification of tumor suppressive (FLp53+Δ40p53) and oncogenic (Δ133p53+Δ160p53) p53 protein isoforms. **c)** p53 protein isoform ratio (tumor suppressive : oncogenic) was calculated for 4,863 different anti-cancer compounds (provided by the anti-cancer compound library HY-L025, June 2022). Ratios for all timepoints (3 h, 6 h, 9 h, 12 h, 24 h, 48 h) were averaged and plotted on an exponential scale. These ratios were subjected to the Anderson-Darling test. All compounds significantly upregulating tumor suppressive p53 (**p53-TIEs**) are located in the green area above the z-value of 1.962 (highest 2.5 %). Top-three p53-TIEs are indicated as green dots. **d)** Heatmap represents multiple timepoint measurements, displaying p53 protein isoform ratios (tumor suppressive / oncogenic) in color codes for 121 compounds significantly upregulating tumor suppressive p53 protein isoforms (determined by Anderson-Darling test with z-values above 1.962).

isoforms ($p < 0.025$), also referred to as p53 Oncogenic Isoform Enhancers (p53-OIEs; Fig. 28). But either highly upregulating tumor suppressive or oncogenic p53 protein isoforms, does not necessarily harm the tumor cell. Out of the 4,863 anti-cancer compounds, we selected 108 compounds with the highest anti-tumor efficacy by studying their effect on cell morphology (phase-contrast microscopy) and cell viability (LIVE/DEAD staining; Fig. 29). The differential p53 isoform inducibility of these 108 drugs was set into ratio (tumor suppressive : oncogenic). The significance of being among the top 3 compounds that either most efficiently upregulate tumor suppressive (p53-TIE) or upregulate oncogenic p53 (p53-OIE) while still exhibiting high toxicity to tumor cells was calculated using the Anderson-Darling equation. The respective probabilities were reported as z-values (Fig. 30a).

As the top 3 most toxic p53-TIEs ($z \geq 1.962$, $p < 0.025$), we identified the ubiquitin-specific peptidase 1 (USP1) inhibitor SJB2-043, bloom syndrome protein inhibitor 1 (BLM-IN-1), and inhibitor of the anti-apoptotic Bcl-2 protein family, namely gambogic acid (Fig. 30b, c, d). Under the top 3 most toxic p53-OIEs ($z \leq -1.962$, $p < 0.025$), on the other hand, we identified Foxo1 inhibitor AS1708727, mitochondrial respiratory chain complex I inhibitor IACS-010759 hydrochloride (HCl), and protein arginine methyltransferase 5 (PRMT5) inhibitor JNJ-64619178 (Fig. 30b, c, d).

Given the information associated with each compound within the anti-cancer compound library, such as the cellular pathways influenced by the individual compounds, we conducted a comparative pathway analysis. Specifically, we sought to compare the pathway abundance and the percentage weighting of the identified p53-TIE (Fig. 27d) and p53-OIE (Fig. 28d) lists concerning the total anti-cancer compound.

Results

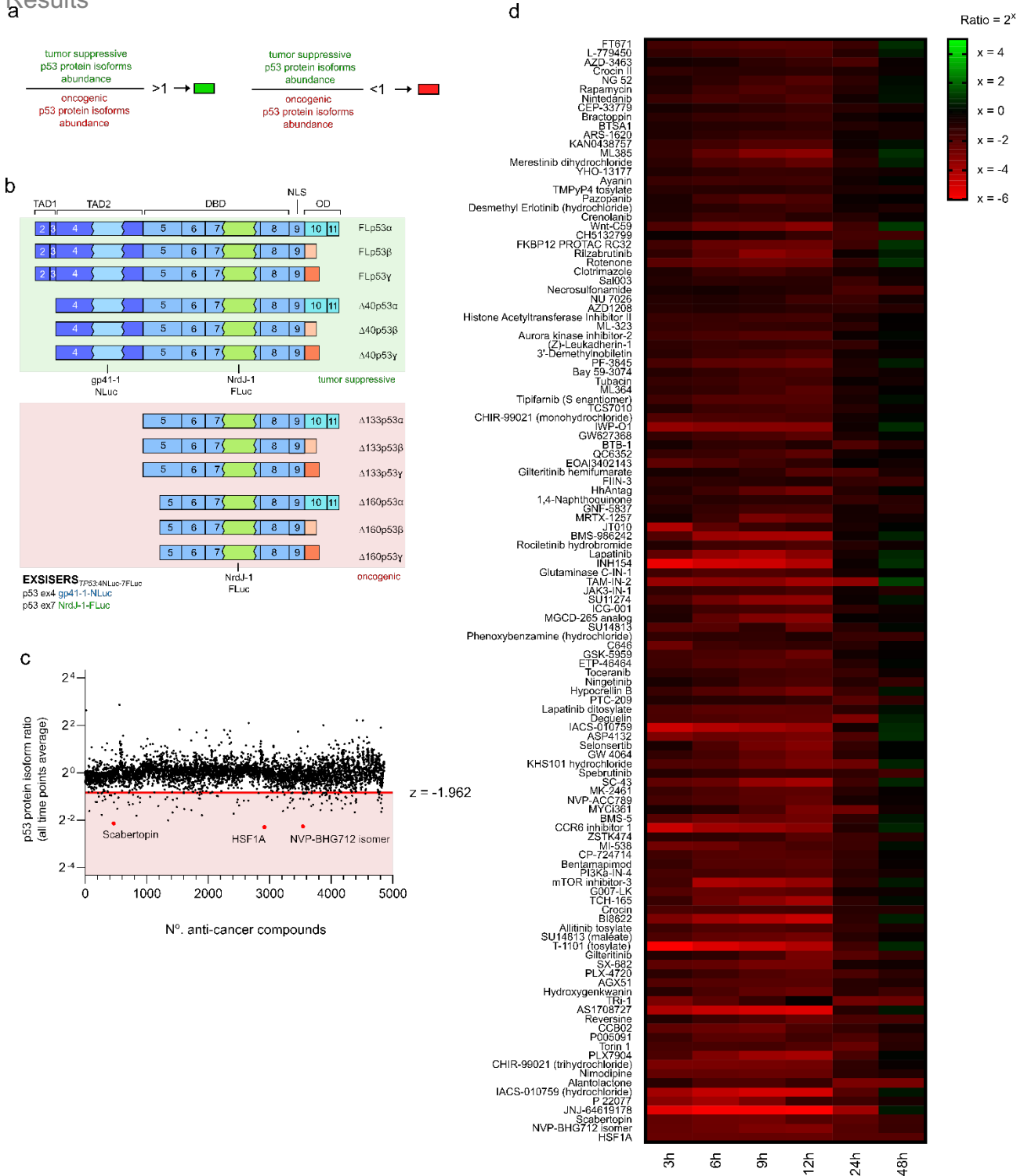
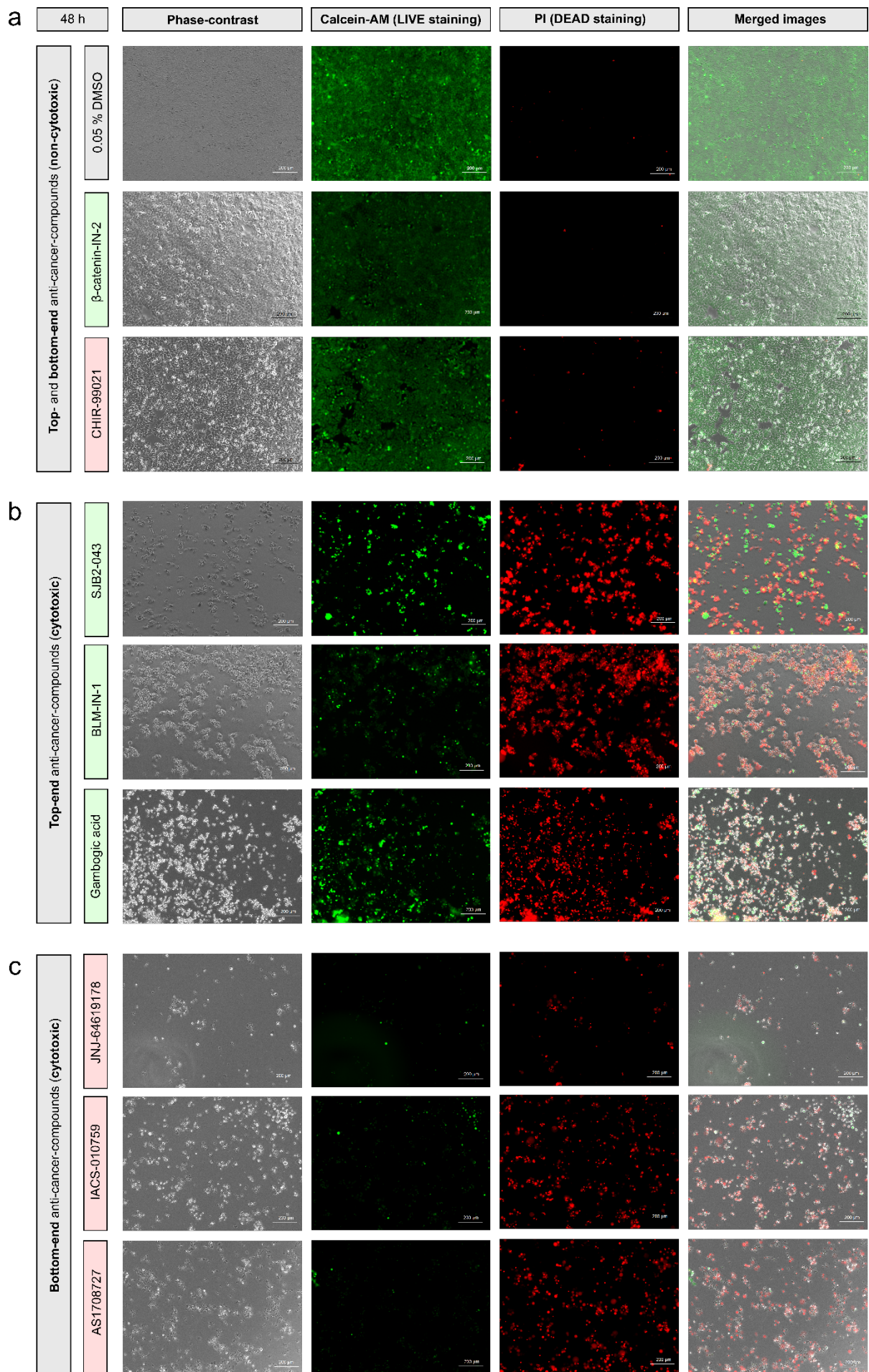


Figure 28: Identification of anti-cancer compounds which significantly induce oncogenic p53 protein isoforms (p53-OIEs). **a)** Ratio between tumor suppressive and oncogenic isoforms were translated into color-codes. **b)** Schematic of all twelve p53 protein isoforms expressed in EXSISERS_{TP53:4NLuc-7FLuc} Cell line. Luminescent measurements of stably integrated gp41-1-NLuc (exon 4) and NrdJ-1-FLuc (exon 7) enable to distinguish tumor suppressive (FLp53+Δ40p53) and oncogenic (Δ133p53+Δ160p53) p53 protein isoforms. **c)** p53 protein isoform ratio (tumor suppressive : oncogenic) was calculated for 4,863 different anti-cancer compounds (provided by the anti-cancer compound library HY-L025, June 2022). Ratios for all timepoints (3 h, 6 h, 9 h, 12 h, 24 h, 48 h) were averaged and plotted on an exponential scale. These ratios were subjected to the Anderson-Darling test. All compounds significantly upregulating tumor oncogenic p53 (**p53-OIEs**) are located in the red area below the z-value of -1.962 (lowest 2.5 %). Top-three p53-OIEs are indicated as red dots. **d)** Heatmap represents multiple timepoint measurements, displaying p53 protein isoform ratios (tumor suppressive : oncogenic) in color codes for 121 compounds significantly upregulating tumor oncogenic p53 protein isoforms (determined by Anderson-Darling test with z-values below -1.962).

Results



Results

Figure 30: The most potent cell death-inducing anti-CRC compounds were identified by phase contrast and calcein AM/PI fluorescence microscopy analysis. **a)** Phase contrast, Calcein AM- (LIVE-staining), and PI-fluorescence (DEAD-staining) microscopic images of DMSO (control), β -calcein-IN-2, and CHIR-99021 treated HCT116 WT cells (48 h). This section includes one representative of anti-cancer compounds each significantly upregulating tumor suppressive or oncogenic p53 protein isoforms without any cell death-inducing effects on HCT116 WT cells. **b)** Phase contrast, Calcein AM-, and PI-fluorescence microscopic images of SJB-043, BLM-IN-1, and Gambogic acid treated HCT116 WT cells. These compounds represent the top three anti-cancer compounds significantly upregulating tumor suppressive p53 protein isoforms (see Fig. 31d) while showing high cell death-inducing effects on HCT116 WT cells. **c)** Phase contrast, Calcein AM-, and PI-fluorescence microscopic images of JNJ-64619178, IACS-010759, and AS1708727 treated HCT116 WT cells. These compounds represent the top three anti-cancer compounds significantly upregulating oncogenic p53 protein isoforms (see Fig. 31d) while showing high cell death-inducing effects on HCT116 WT cells. All drugs were applied with a working concentration of 5 μ M. Scale bar represents 200 μ m.

library. The drug-related, absolute pathway-counts were determined using a custom-created Python script and converting the values into percentage quantities (Fig. 31a). This transformation allowed us to standardize pathway contributions across three distinct groups: the total library, p53-TIEs, and p53-OIEs. Notably, these percentages assume varying weightings across the different groups. For ease of comparison, we standardized all values and compared them with the normalized values of the "total library" (Fig. 31b). For the sake of simplicity, we excluded the last three pathways from the standardization process, given their absence in both p53-TIE and p53-OIE lists, resulting in absolute, percentage, and relative values of zero. Our analysis unveiled a remarkable pattern: compounds exhibiting a substantial upregulation of tumor suppressive p53 protein isoforms (p53-TIEs) predominantly engaged two specific pathways: apoptosis and the NF- κ B pathway. p53-TIEs related to apoptosis revealed a prevalence exceeding 6 % compared to both the "total library" and the "p53-OIE library" (Fig. 31a). The relative difference is approximately 0.4 (Fig. 31b). p53-TIEs related to the NF- κ B pathway exceeded 3.5 % compared to both the "total library" while this pathway no longer plays a crucial role for the p53-OIEs (Fig. 31a). In contrast, the identified p53-OIEs exhibited a prevalence in primarily influencing these three pathways: Protein Tyrosine Kinase/RTK, PI3K/Akt/mTOR, and JAK/STAT signaling. Surprisingly, the abundance significantly decreased in all three pathways within the p53-TIE library (Fig 31a, b). It becomes evident that the percentage disparity is mostly pronounced for the Protein Tyrosine Kinase pathway (5 %) when compared to the "total library" (Fig. 31a). Additionally, it is worth mentioning that all of these aforementioned

Results

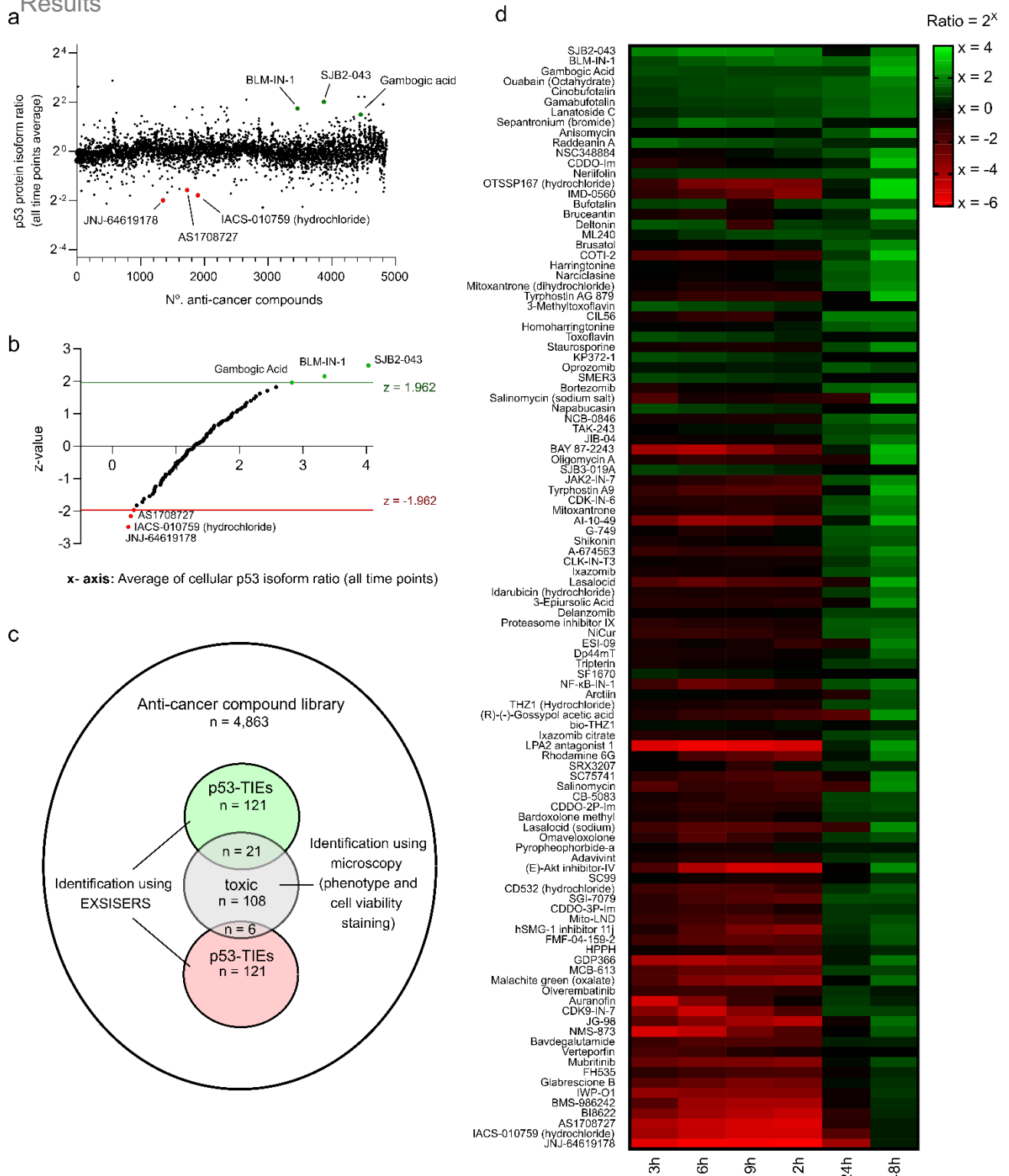


Figure 30: High-throughput screening of an anti-cancer compound library with EXISERS identifies new potential CRC therapeutics. **a**) The ratio of the p53 protein isoforms (tumor suppressive vs. oncogenic) was calculated for 4,863 different anti-cancer compounds (provided by the anti-cancer compound library HY-L025 from MCE) at multiple timepoints (3 h, 6 h, 9 h, 12 h, 24 h, 48 h), averaged and plotted on an exponential scale. Drug candidates of interest exhibiting high expression of either tumor suppressive or oncogenic p53 protein isoforms are indicated as green or red dots, respectively. **b**) Additionally we evaluated the toxicity of each compound by selecting according to their effects on the phenotype (phase-contrast) and cell viability (LIVE/DEAD-staining, fluorescence microscopy). Previously calculated ratios from in total 108 selected compounds were z-transformed. Significance ($z = \pm 1.962$; $p < 0.025$) was calculated to identify the most significantly drugs upregulating tumor suppressive (p53-Tumor suppressive Isoform Enhancers = p53-TIEs) or oncogenic p53 isoforms (p53-Oncogenic Isoform Enhancers = p53-OIEs) that additionally displaying high toxicity on CRC cells. **c**) Overview of the anti-cancer compound library and its high-throughput profiling using EXISERS and microscopic selection to identify TIEs ($n = 121$), OIEs ($n = 121$), and highly toxic compounds ($n = 108$). Among these, 21 p53-TIEs and 6 p53-OIEs overlap, additionally displaying significant toxicity to CRC cells. **d**) Heatmap represents time-dependent p53 protein isoform ratios (tumor suppressive vs. oncogenic) of the 108 compounds most efficiently inducing cell death in HCT116-EXISERS_{TP53:4NLuc-7FLuc} cells.

Results

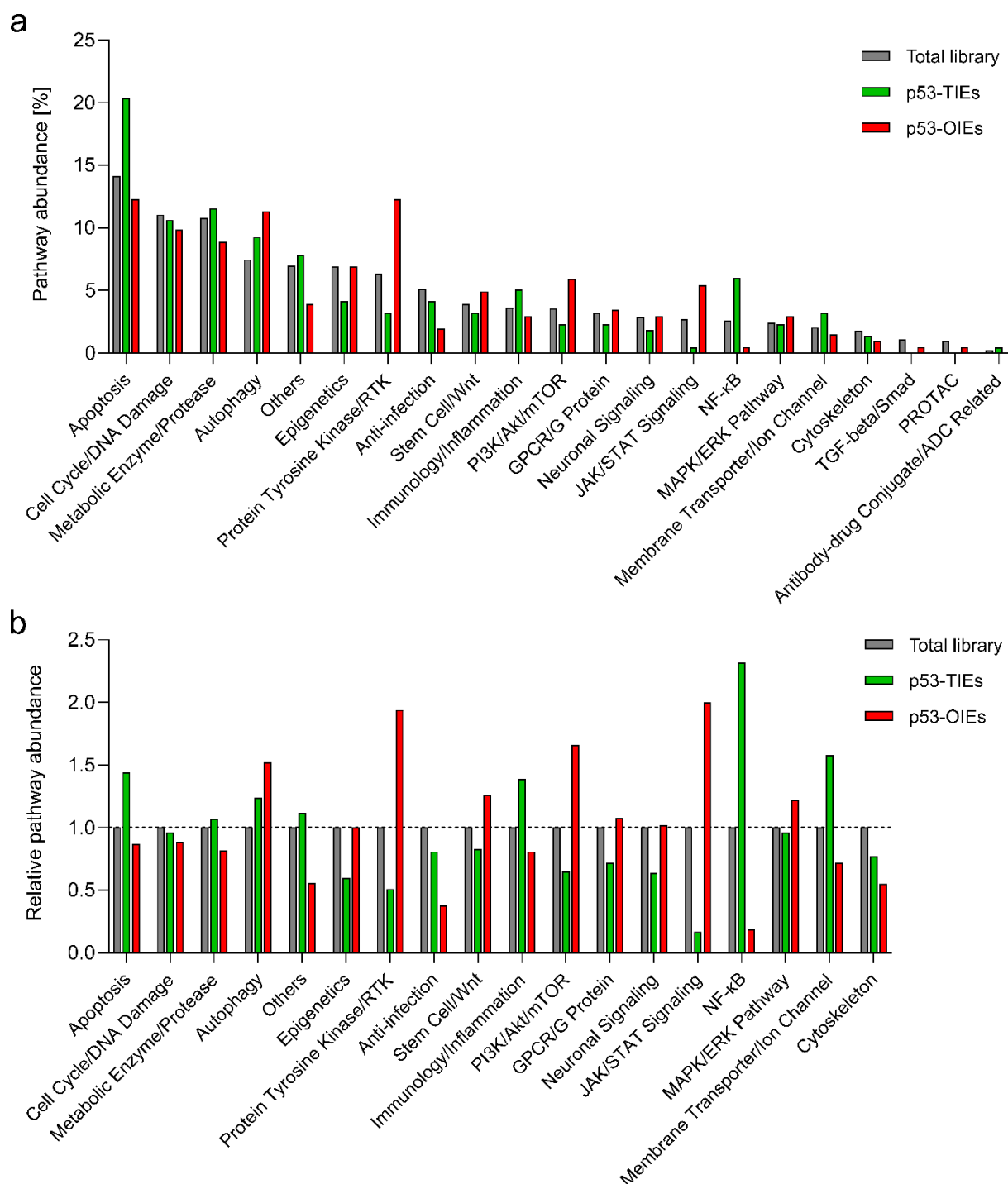


Figure 31: Pathway abundance of the total anti-cancer compound library compared to those of the identified p53-TIEs and p53-OIEs. a) Percentual abundance of the pathways in which the drugs (listed in total library, p53-TIEs = Fig. 27 and p53-OIEs Fig. 28) are interfering in. Total pathway counts were analyzed with a Python script showed in Supplementary Fig. 5. Total pathway counts were converted into percentual abundances. **b)** For comparative purposes, all pathway abundances determined for “total library” were normalized to 1. p53-TIE and p53-OIE pathway abundances were relativized. This perspective facilitates a more rigorous comparison of the individual pathways. TGF-beta/Smad, PROTAC and Antibody-drug Conjugate/ADC Related pathways were excluded in this context due to their absence either in the p53-TIE and p53-OIE lists (otherwise resulting in a calculated value of 0).

pathways predominantly represent signaling transduction pathways that are more frequently modulated by p53-OIEs. This pathway analysis elucidates intriguing

Results

interrelationships between the pathways and the p53 family. Specifically, it highlights potential associations between specific p53 isoforms and distinct pathways, thereby broadening the scope of p53 as a target for future therapeutic strategies. The 'Discussion' section will revisit and thoroughly discuss these interrelationships.

3.8 Identification of toxic anti-cancer compounds acting in an opposite p53-dependent manner.

USP1 is one of the best-characterized human deubiquitinases. It plays an important role in the cellular response to DNA damage and has been suggested as a target in cancer therapy [193]. USP1 inhibition through SJB2-043 has been shown to revert chemotherapeutic resistance in non-small cell lung cancer (NSCLC) cells [194].

BLM has been reported to be directly recruited to DNA-double strand breaks (DNA-DSB), promoting an accumulation of RAD51 and regulating the homologous directed repair [195]. BLM inhibition with BLM-IN-1 potentially amplifies p53-dependent cell-cycle arrest and apoptosis.

Gambogic acid has been reported to exhibit toxicity against tumor cells through the efficient activation of caspases. Gambogic acid displays varying levels of inhibition against all six human Bcl-2 family proteins, with the most pronounced inhibitory effects observed on anti-apoptotic Mcl-1 and Bcl-B [196].

From the top 3 toxic p53-TIEs, it becomes apparent that all compounds exert an anti-tumoral effect through their direct or indirect activating effects on tumor suppressive p53. Of note, the top 3 p53-OIEs also show strong toxic effects on cancer cells despite their strong activating influence on oncogenic p53 isoforms. Therefore, it is also important to take a closer look at their mechanisms of action.

JNJ-64619178, which is also referred to as Onametostat, is a selective PRMT5 type II methyltransferase inhibitor. PRMT5 symmetrically di-methylates arginine residues on proteins involved in signal transduction and cellular transcription. An elevated PRMT5 activity is known to promote the epithelial-mesenchymal transition of tumors, which has been correlated with poor survival of patients [197]. Therefore, PRMT5 inhibition with Onametostat (JNJ-64619178) has anti-tumoral effects by exhibiting anti-proliferative activity.

IACS-010759 is a selective mitochondrial respiratory chain complex I inhibitor. By blocking complex I, the regular electron flux is interrupted, which results in retrograde

Results

electron transport, during which electrons are transferred to oxygen species. At moderate ROS levels, we postulate for p53 to activate antioxidant genes, including hydrogen peroxidases, that preserve cell survival [198,199].

AS1708727 is a potent inhibitor of the forkhead transcription factor Foxo1. Foxo1, in turn, has an important role in regulating glucose and triglyceride metabolism. Its inhibition was shown to exert both anti-hypertriglyceridemic and anti-hyperglycemic effects. Originally meant to treat hyperglycemia in diabetes type II patients, AS1708727 also has anti-tumoral effects.

At first glance, these top 3 toxic p53-OIEs do not directly interfere with the p53 pathway. However, our data unequivocally demonstrate that the tumor cells likely initiate a compensatory effect by upregulating oncogenic p53 in response to the perturbation of metabolism and signal transduction. Therefore, we transitioned back to the triple-EXSISERS reporter system to conduct a more detailed study of p53-TIEs and p53-OIEs on the differential p53 protein isoform induction.

SJB2-043 and BLM-IN-1, which were found to be highly toxic p53-TIEs, effectively induced tumor suppressive p53 protein isoforms, revealing a higher FLp53: Δ 40p53 ratio (first 12 h of treatment) for the induction of cell cycle arrest just to transition into a higher Δ 40p53:FLp53 ratio at later time points (24 and 48 h) for the induction of apoptosis (Fig. 32a, b). The oncogenic p53 protein isoforms remained moderately (BLM-IN-1) to strongly (SJB2-043) downregulated over the entire treatment period. In contrast, IACS-010759 and JNJ-64619178 induced predominantly oncogenic p53, while tumor suppressive p53 protein isoforms remained low (Fig. 32c, d). Nevertheless, it should not be disregarded that the FLp53: Δ 40p53 ratio was shifted towards pro-apoptotic Δ 40p53 throughout the entire treatment period with both compounds, IACS-010759 and JNJ-64619178. However, we do not believe that Δ 40p53 induction is the predominant mechanism for initiating cell death in colorectal cancer cell lines.

We further studied the effects of SJB2-043 and BLM-IN-1 as p53-TIEs and IACS-010759 and JNJ-64619178 as p53-OIEs on various CRC-cell lines with differential p53 status. Corresponding compounds were titrated (concentration range: 0.2 nM – 5 μ M), and the viability of the different CRC cell lines in response to the varying dosages was measured with a luminescence-based assay. SJB2-043 and

Results

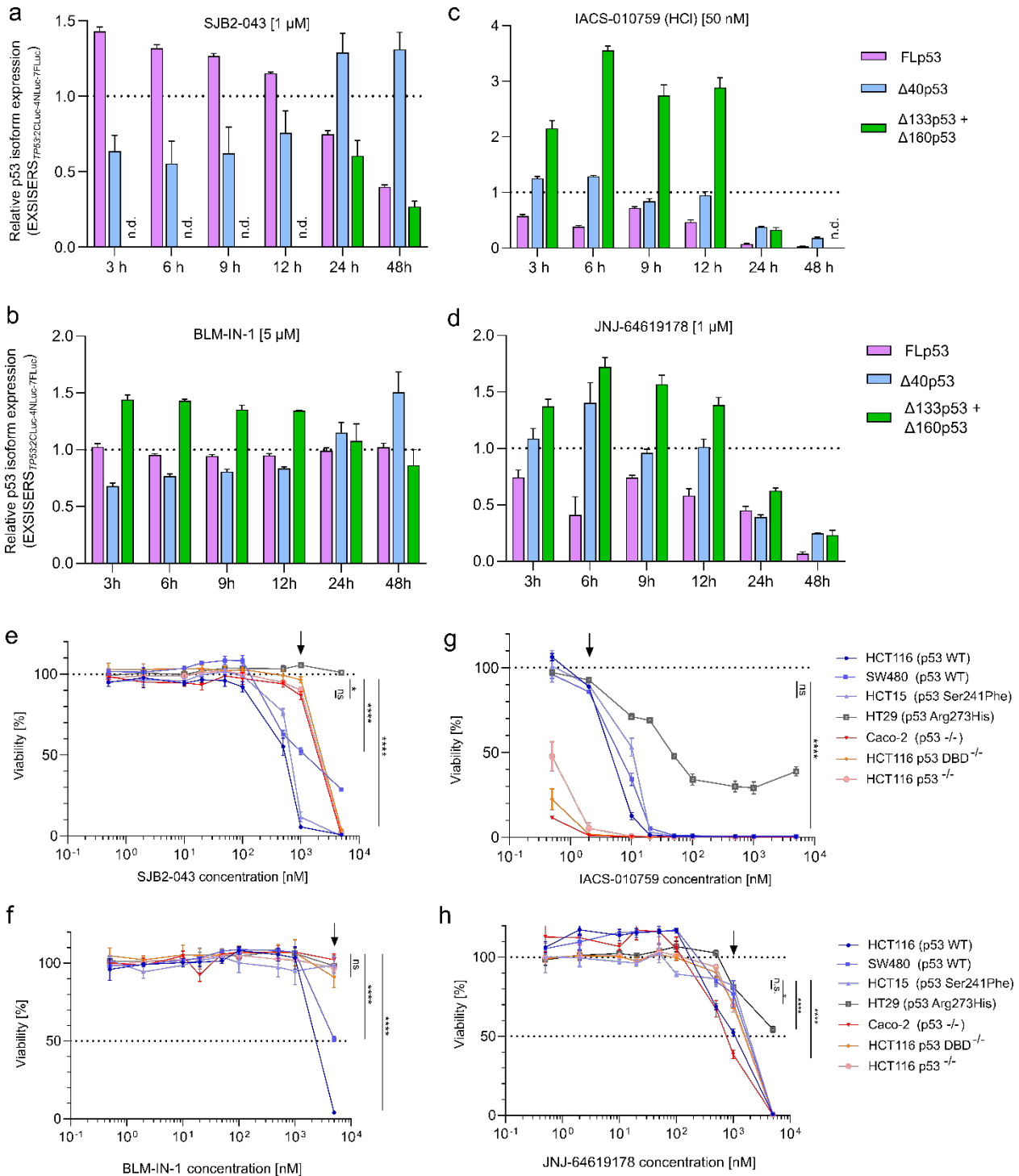
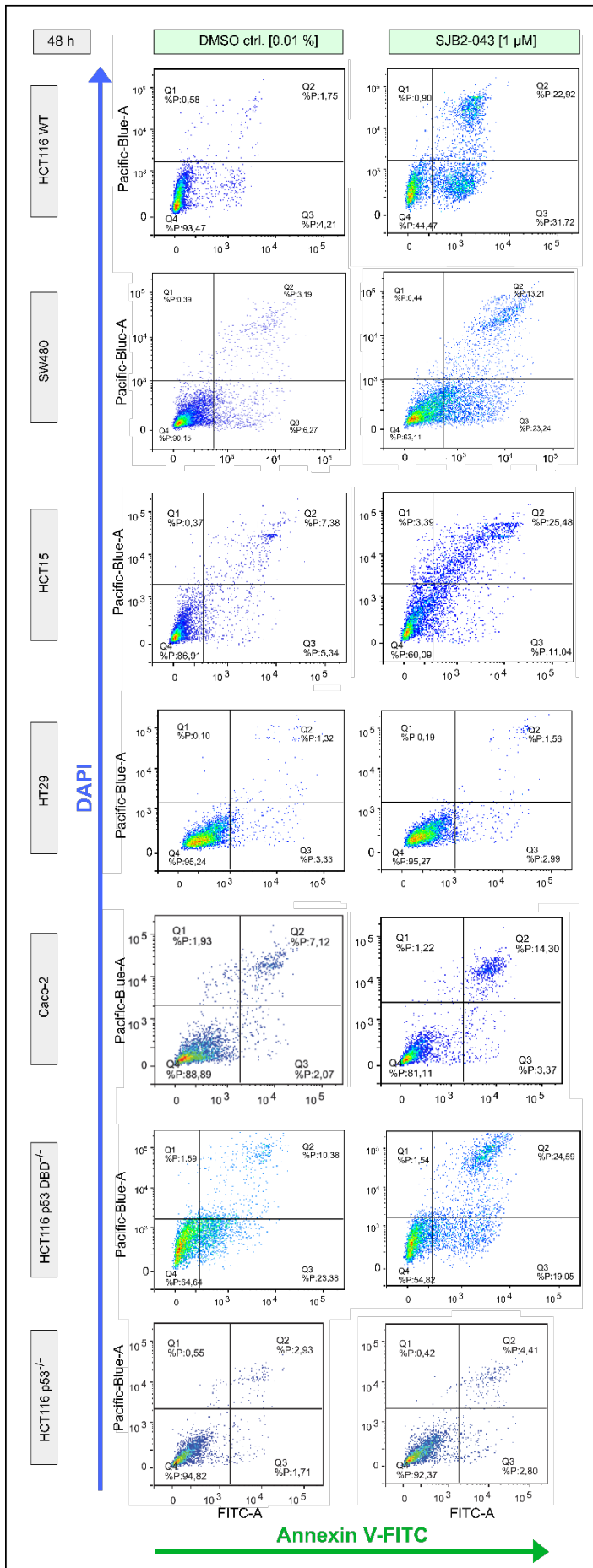


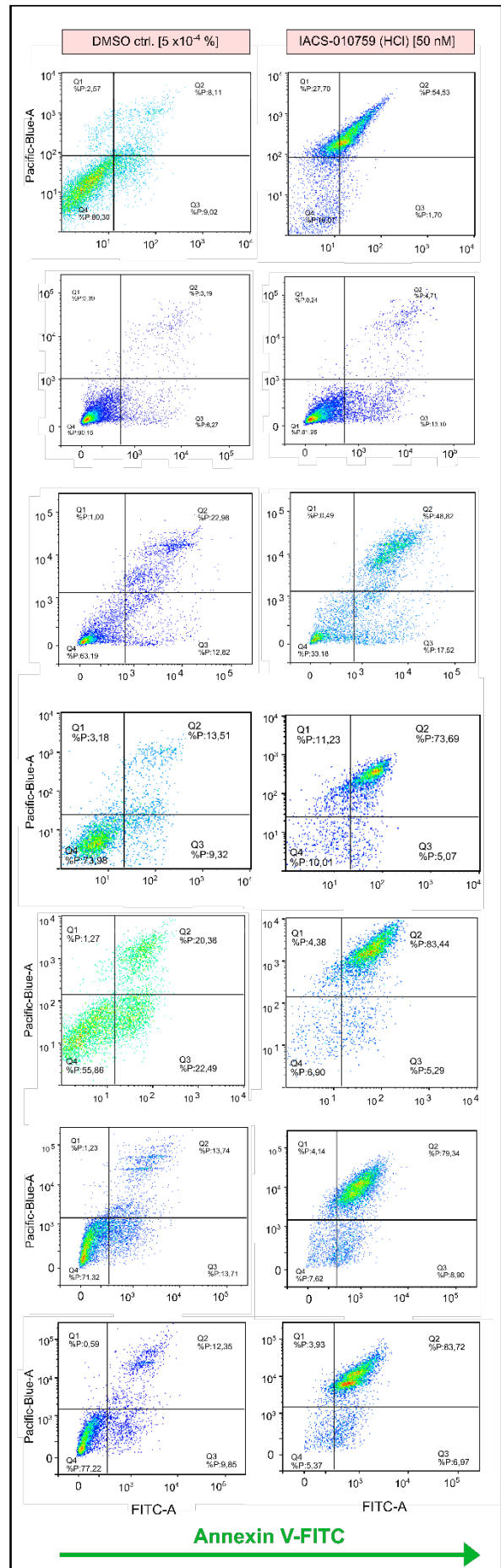
Figure 32: Differential effects of p53-TIEs and p53-OIEs on CRC tumor cell lines. **a)** Real-time and live-cell quantification of p53 protein isoforms (FLp53, Δ 40p53, and Δ 133p53+ Δ 160p53) using the EXSISERS_{TP53:2CLuc-4NLuc-7FLuc} cell line. Relative p53 protein isoform expression was determined for the USP1 inhibitor SJB2-043 [1 μ M], **b)** BLM-IN-1 [5 μ M], **c)** OXPHOS inhibitor IACS-010759 (HCl) [50 nM], and **d)** PRMT5 inhibitor JNJ-64619178 treatment [1 μ M] at 3 h, 6 h, 9 h, 12 h, 24 h, and 48 h. t=0 was used as a normalization control. DMSO-treated cells were used to normalize luminescent signals from treated cells (n=3). **e)** Luciferase-based cell viability assay using identified p53-TIE compounds SJB2-043 and **f)** BLM-IN-1, and the p53-OIE compounds **g)** IACS-010759 (HCl) and **h)** JNJ-64619178 for the treatment of distinct colorectal cancer cell lines (48h). Drug concentrations ranged from 0.5 nM to 5 μ M (n=3). Black arrows indicate the drug concentrations which were statistically evaluated using one-way ANOVA ($P > 0.05$ = n.s.; **** $p < 0.0001$) for all, SJB2-043 [1 μ M], BLM-IN-1 [5 μ M], IACS-010759 (HCl) [2 nM], and JNJ-64619178 [1 μ M] treatment. Cell viability was normalized to luminescent measurements obtained with 0.05 % DMSO control (dashed line). HCT116 p53 $^{-/-}$ cells were generated and kindly provided by Katja Neumeyer.

Results

a



b



Results

Figure 33: Flow cytometry analysis of distinct CRC cell lines upon SJB2-043 and IACS-010759 treatment. Annexin-FITC and DAPI signals were measured via flow cytometry to determine cell death rates of **a)** SJB2-043 [1 μ M] and **b)** IACS-010759.HCl [50 nM] treated CRC cell lines (HCT116 WT, SW480, HT29, HCT15, Caco-2, HCT116 p53 DBD^{-/-}, and HCT116 p53^{-/-}) after 24 h and 48 h of treatment. DMSO was used as a control treatment at the respective therapeutic dilution. Q4 quadrant represents viable cells, Q3 represents early apoptotic cells, Q1 and Q2 represent late apoptotic and necrotic cells. Each measurement was conducted in triplicates (n=3). HCT116 p53^{-/-} cells were generated and kindly provided by Katja Neumeyer.

BLM-IN-1 showed significant differences in efficacy depending on the genotypic status. In contrast to p53 WT cell lines, p53 mutated and p53 KO cell lines required higher doses to achieve the same or similar toxic effects (Fig. 32e, f). IACS-010759 and JNJ-64619178 revealed the opposite p53 dependency. In particular, p53 KO cell lines showed stronger susceptibility to these p53-OIEs. In the case of JNJ-64619178 treatment, this effect was not as pronounced as with IACS-010759 treatment, however it exhibited a clear tendency towards improved therapeutic response in p53-KO tumor cells (Fig. 32g). During IACS-010759 treatment, the differential therapeutic response between wild-type and p53-KO tumor cells showed highest significance at a 2 nM concentration (Fig. 32h).

However, it's important to note that cell viability does not necessarily equate to cell vitality. We also conducted a flow cytometric cell death assay to confirm the differential anti-tumoral effect of p53-TIEs and p53-OIEs on genotypically distinct CRC cell lines. As a result, we calculated the specific cell death induced by the respective therapeutics. Furthermore, we focused on one compound of each p53-TIE and p53-OIE group, namely SJB2-043 and IACS-010759.

Cell death assay of SJB2-043 treated HCT116 WT cells was conducted by Annexin-V-FITC and DAPI staining. Annexin-V-FITC preferentially binds to phosphatidyl serine exposed on the cell surface of early and late apoptotic cells. DAPI internalizes and interacts with the cell's genomic DNA as soon as the plasma membrane integrity is disrupted. Higher FITC and DAPI signals, therefore, indicate increased cell death rates.

SJB2-043 treatment [1 μ M] induced high cell death rates in HCT116, SW480 (*TP53* WT), and HCT15 (*TP53* S241F). In other p53-mutated or p53 knock-out cell lines, we observed deterioration to complete ineffectiveness (e.g., HT29, Caco-2) (Fig. 33a, Fig. 34a). This circumstance of differential SJB2-043 effect is due to the strong tumor suppressive p53 isoform induction leading to p53-dependent cell death.

Results

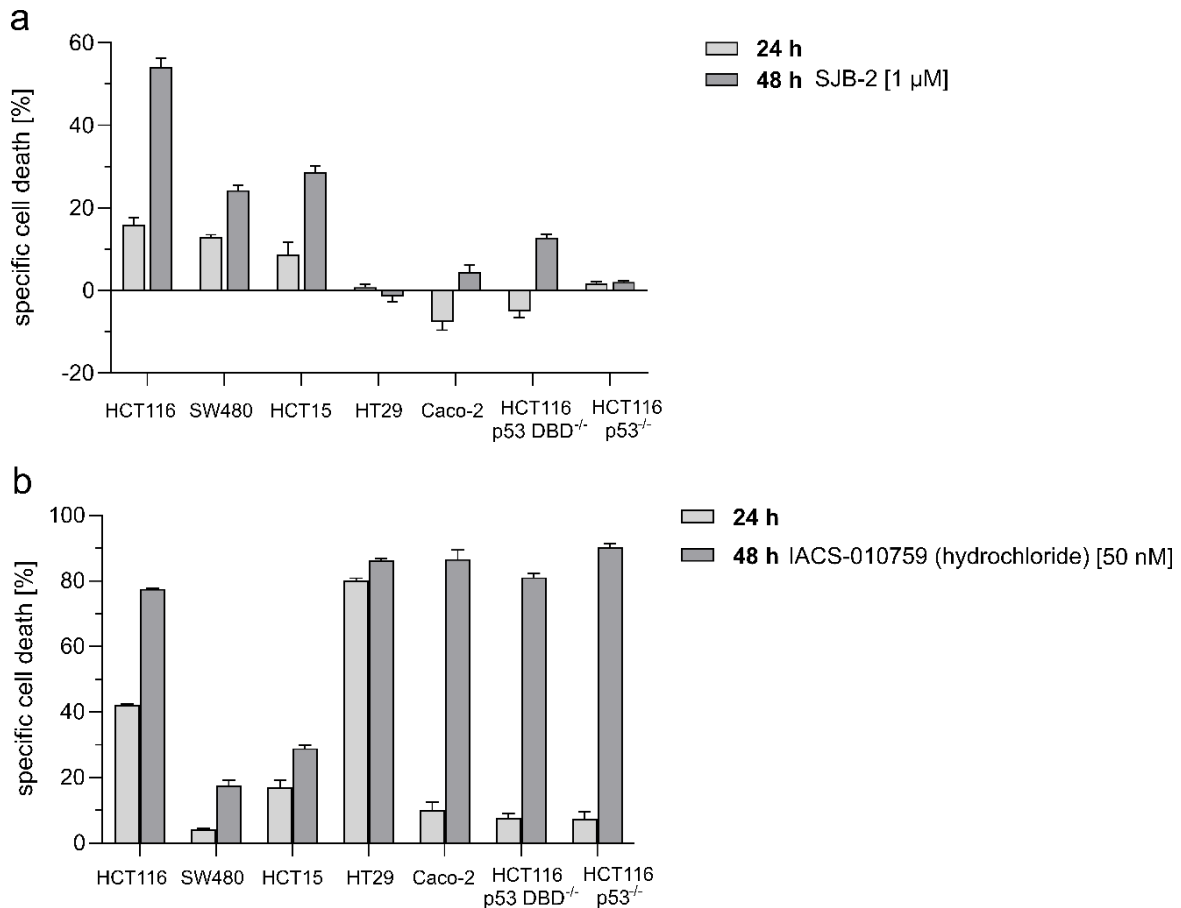


Figure 34: USP1 inhibitor SJB2-043 and OXPPOS inhibitor IACS-010759.HCl oppositely affect colorectal cancer cells depending on their genetic status of p53. a) Cell death rates were measured by flow cytometry to calculate the specific cell death of different CRC cell lines, treated with SJB2-043 [1 μM] and b) IACS-010759 (HCl) [50 nM] for 24 h and 48 h. Statistical significance was calculated using Brown-Forsythe and Welch ANOVA ($p > 0.05 = \text{n.s.}$, $*p < 0.05$; $p < 0.005$; $***p < 0.0005$; $****p < 0.0001$). HCT116 p53^{-/-} cells were generated and kindly provided by Katja Neumeyer.**

Contrarily, 50 nM IACS-010759 showed no additional effect on SW480 cells but maximized cell death rates in all other CRC-cell lines, especially including p53 KO cells (Fig. 33b, Fig. 34b). Here, oncogenic p53 isoform induction by IACS-010759 and other p53-OIEs caused tolerance to higher therapeutic concentrations in p53 WT cells. When p53 integrity is lost (loss-of-function mutations or KO), respective cells have an overall higher susceptibility to IACS-010759 treatment. We believe the two therapeutics acting in different p53-dependent manners have expanded the therapeutic opportunities for treating CRC.

3.9 Complex-I inhibitor IACS-010759 specifically targets colon cancer and is innocuous to healthy and surrounding colon tissue.

Lower drug concentrations are a strategic approach for minimizing the therapeutic burden and potential side effects in CRC patients. Thus, it is always the highest priority in medicine and research in drug development. Since the complex I inhibitor IACS-010759 exhibits anti-tumoral effects on various CRC cell lines, even at very low concentrations (2-50 nM), we expanded our experiments to include primary colonic cells from patients. Our primary emphasis was to assess the compound's efficacy in heterogeneous and 3-dimensional tumor structures and elucidate its tumor-specific effect.

In general, IACS-010759 is a mitochondrial respiratory chain complex I inhibitor blocking the forward electron flux [200] and promoting the release of reactive oxygen species (ROS) [201,202]. This reduces hypoxia-stimulated tumor progression and proliferation and increases induction of apoptosis [199,203]. Since blockage of the mitochondrial respiratory chain and the resulting energy depletion can potentially damage non-tumorigenic cells, we investigated the effect of IACS-010759 on healthy peripheral tissue, namely colonic fibroblasts. We isolated fibroblasts from patients with ulcerative colitis or Crohn's disease biopsies. Here, we also differentiated between inflamed (extracted from inflamed tissue) and non-inflamed tissue (extracted from non-inflamed/healthy tissue). These fibroblasts with distinct origins were treated with up to 50 nM IACS-010759 as a maximum tolerable dose for 2D cell culture. After 48 hours of treatment, fibroblasts were double stained with Annexin V-FITC/DAPI and analyzed by flow cytometry (Fig. 35a). Treatment with IACS-010759 for a total of 48 hours did not affect cell viability (Fig. 35b), nor did it result in increased specific cell death (Fig. 35c). Thereof we conclude, that up to 50 nM IACS-010759 treatment has minimal to no influence on healthy or chronic inflamed colonic fibroblasts at all.

Next, we investigated the tumor-specific effect of IACS-010759 on 3-dimensional colonic cell culture systems. Colon cancer organoids (PDM-46, PDM-47, PDM-50, No.80) and healthy colon organoids (induced pluripotent stem cells – iPSC, No.77, No.101, No.103, No.108) were seeded and cultivated in 3dGRO™ Human Colon Organoid Expansion Media and treated with 50 nM IACS-010759 for 48 h. Thereafter,

Results

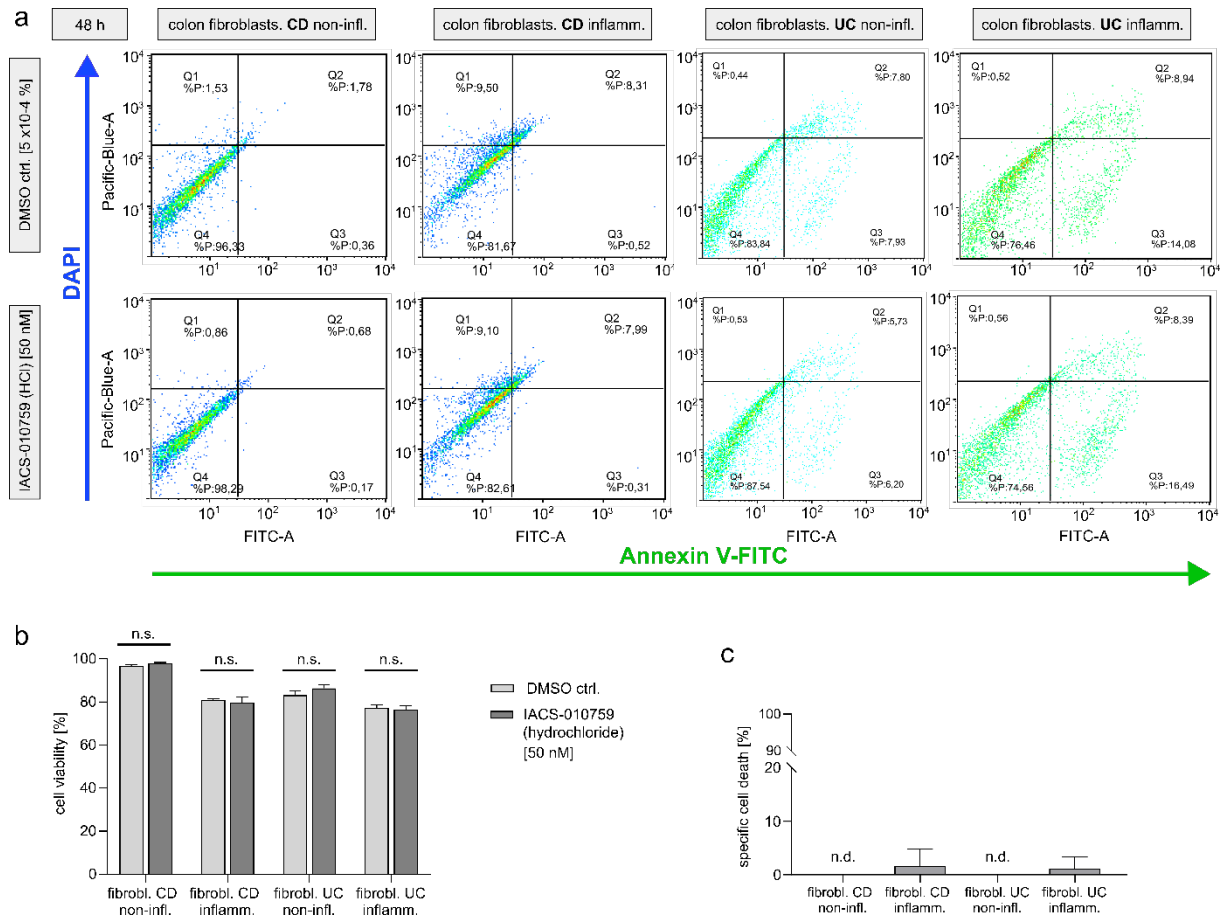


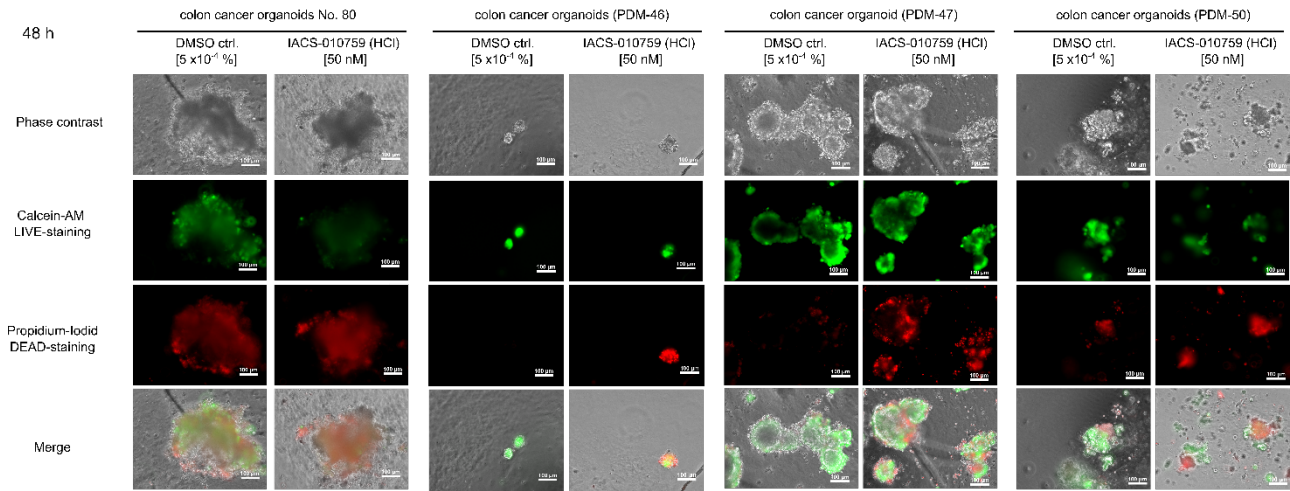
Figure 35: Flow cytometric analysis of primary colonic fibroblasts after treatment with IACS-010759 demonstrate minimal effects on non-tumor tissue. Annexin-FITC and DAPI signals were measured via flow cytometry to determine cell death rates of DMSO vs. IACS-010759.HCl [50 nM] treated primary fibroblasts. Cells were treated for 48 h prior to analysis. Fibroblasts were derived from patients with Crohn's disease (CD) or ulcerative colitis (UC). Q4 quadrant represents viable cells, Q3 represents early apoptotic cells, Q1 and Q2 represent late apoptotic and necrotic cells. Biopsies were either obtained from inflamed or non-inflamed tissue. Each condition was measured in triplicates (n=3). **b)** Cell viability and **c)** specific cell death rates of DMSO control and IACS-010759.HCl treated primary fibroblasts (48 h) were obtained by flow cytometry analyses. Differences in cell viability were statistically evaluated using Student's t-test (*p<0.05).

organoids were double stained with calcein-AM (LIVE stain) and propidium iodide (DEAD-staining) to determine the relative therapeutic effect on organoids. In metabolic active cells, calcein-AM, a substrate of esterases, is converted into fluorogenic calcein (green fluorescence). Propidium iodide intercalates with the genomic DNA and only passes the plasma membrane of damaged cells.

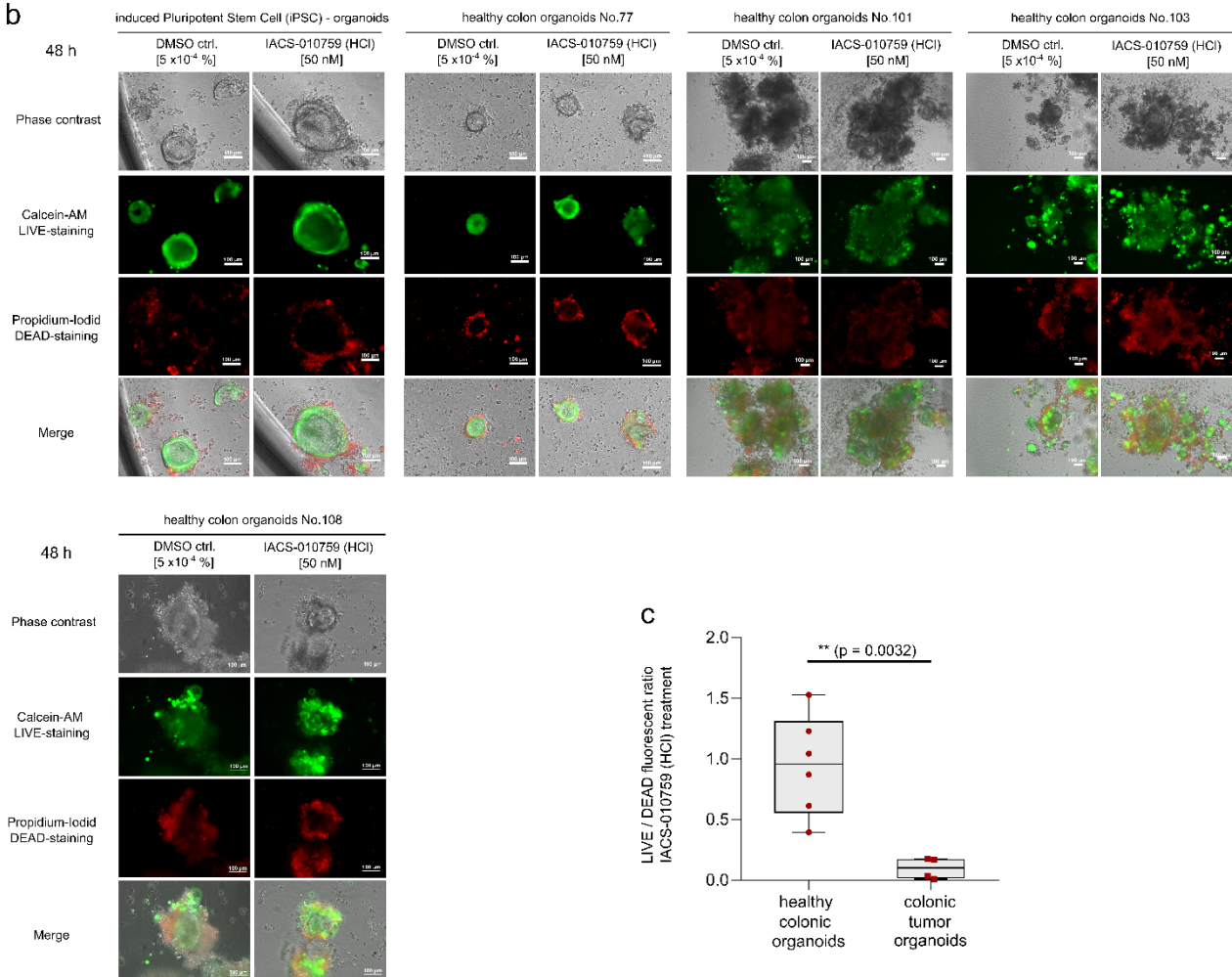
LIVE/DEAD-staining revealed that 50 nM IACS-010759 treatment marginally affected healthy colonic organoids. Fluorescent signals for LIVE- and DEAD-staining barely differed between control and IACS-010759 treatment (Fig. 36b). Colon cancer organoids, on the other hand, were strongly affected by 50 nM IACS-010759 treatment.

Results

a



b



c

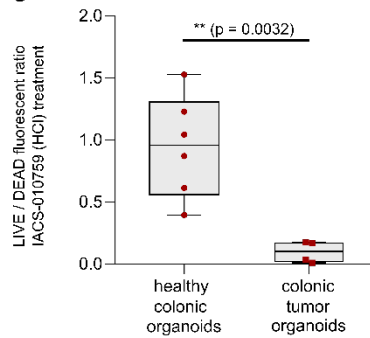


Figure 36: LIVE/DEAD staining of IACS-010759.HCl-treated healthy vs. colon cancer organoids reveals high tumor-specific effects. a) Colon cancer organoids (No. 80 obtained from colonic cancer biopsies at our clinics; PDM-46, PDM-47, PDM-50 obtained from ATCC) and b) healthy colon organoids (No. 76, 77, and 108 obtained from colonic biopsies at our clinics) were treated with DMSO ctrl. vs. IACS-010759.HCl [50 nM] for 48 h. After treatment, cells were stained with calcein-AM (LIVE-staining) and propidium iodide (DEAD-staining) and subsequently analyzed via fluorescence microscopy for life/death differentiation. Fluorescent images were taken with a 20x lens. Scale-bar indicates 100 μ m. c) Fluorescence intensities of the LIVE/DEAD fluorescence images (see a and b) with calcein-AM (green; LIVE) and propidium-iodide (red; DEAD) were quantified by fluorescence histograms and set into ratio. Fluorescence intensities obtained with IACS-010759 treatment were normalized to DMSO controls (set to $y=1$). Measurements and ratio calculations were conducted in triplicates ($n=3$).

Results

In contrast to the DMSO-treated control, fluorescent signals derived from LIVE-staining markedly decreased, whereas fluorescent signals derived from DEAD-staining significantly increased during IACS-010759 treatment (Fig. 36a). Furthermore, the fluorescence microscopic quantification and determination of the respective LIVE/DEAD-ratios demonstrated the tumor-specific potency of IACS-010759 in treating colon cancer organoids (Fig. 36c).

4. Discussion

Today, colorectal carcinoma (CRC) stands out as one of the most severe pathological progressions. Its high degree of malignancy and limitations of available therapeutic interventions contribute to its ranking as the third most prevalent neoplasm, accompanied by the second-highest mortality rate [14]. It is estimated that both the incidence and mortality rates will double by the year 2040. Certainly, it is imperative to consider the escalating population numbers. However, etiological environmental factors also substantially influence CRC's initiation and pathological progression. To prevent these incidence rates from continuously increasing, there is a pressing need to better understand and act on findings that elucidate this disease's onset and potential therapeutic strategies [35].

Current therapeutic regimes for treating CRC mainly involve the use of combinational chemotherapeutics, including folinic acid (FOL), oxaliplatin (OX), 5-fluorouracil (5-FU), and irinotecan (IRI). However, these treatments have severe drawbacks, including systemic toxicity, insufficient response rates, emerging therapeutic resistance, and low tumor-specificity [18,49]. Since p53 is the best-characterized tumor suppressor actively preventing tumor occurrence and further progression, it is reasonable to explore new compounds that induce the expression and stabilization, particularly of p53 isoforms with tumor-suppressive properties. This requires the precise quantification of the p53 protein isoforms to at least differentiate between the upregulation of tumor suppressive and oncogenic isoform species.

The precise regulatory mechanism of the expression of various p53 isoforms has been poorly defined. In general, most isoform networks harbor great complexity regarding their regulation and abundance in the cell. From a biological and medical point of view, it is essential to understand the regulatory mechanism between tumor suppressive and oncogenic p53 protein isoforms. Clarification of the regulatory mechanism is mandatory for the development of further targeted cancer therapies. Therefore, we introduced EXSISERS into *TP53*. As already stated, EXSISERS is an innovative intein-luciferase-based tool that allows for **1.** translational quantification of target proteins, **2.** differentiation of the specific protein isoforms, **3.** acquisition of time-series data **4.** measurement in living cells, and **5.** high scalability with high-throughput screening applicability. By introducing EXSISERS into *TP53* for the first time, we implemented a real-time and live-cell study of the mutual interplay between FLp53, $\Delta 40$ p53, $\Delta 133$ p53, and $\Delta 160$ p53, where conventional non-/antibody-based protein detection methods

quickly reach their limits. Through luminescent readout of the EXSISERS-reporters, we monitored the expression of p53 isoforms in response to distinct CRC-therapeutics. Understanding the tumor suppressor's regulative mechanisms is paramount for drugging p53 [121]. Especially in cancer cells carrying a p53 mutational background, EXSISERS elucidated the particular reliance of a therapeutic agent on functional p53. This, in turn, enabled the identification of p53-independent drugs to implement a p53-tailored therapy.

4.1 The journey towards an optimized triple-EXSISERS reporter system in *TP53*

One of the fundamental principles of the EXSISERS technology is the rapid and reliable measurement of luminescent signals, enabling the precise quantification of one or multiple proteins simultaneously. In contrast to contemporary gold-standard protein quantification methods, EXSISERS promises to preserve the structural and functional integrity of the protein of interest. The non-invasive character of EXSISERS ensures a natural and physiologically intact cell state.

The establishment of the novel triple-EXSISERS reporter system ultimately settled with choosing the proper split-intein and luciferase combination. The choice of the three split-inteins is predicated on their remarkable ultra-fast excision kinetics [166]. Notably, the split-inteins gp41-1 and NrdJ-1, in conjunction with their respective luciferase were previously described as optimized reporter systems [152] and, together with the third reporter, have additionally proven in our experiments the most substantial expression and splicing rates (Fig. 9).

The three luciferases, NanoLuc, FireflyLuc, and CypridinaLuc, firstly exhibit high substrate specificity with minimal cross-reactivity and, secondly, have never been described in that combination in a reporter system before.

Some approaches involve combining CLuc, FLuc, and Gaussia Luciferase (GLuc) [204]. GLuc is a naturally occurring and secreted protein isolated from the deep-sea copepod *Gaussia princeps*, which served as the basis for the development of NLuc. The discovery of new luciferases (such as hLuz - human codon-optimized luciferase originating from the mushroom *Neonothopanus nambi*) also contributed to the development of innovative triple-luciferase reporter assays [205]. Recently, even the possibility of a plasma membrane-anchored CLuc has been demonstrated [206].

Discussion

As the trend toward investigating increasingly complex phenomena continues, so does the demand for a growing number of concurrently measurable reporter systems. Although numerous approaches have been presented, the combination of NLuc, FLuc, and a membrane-anchored CLuc has never been considered before.

In contrast to cytosolic-resident luciferases, CLuc is typically secreted into the extracellular milieu and operates exclusively under oxidative conditions. Given that IMPDH-1-CLuc forms an integral component of the cytosolically synthesized p53, we devised a strategy for the co-translational introduction of CLuc into the endoplasmic reticulum (ER) while maintaining p53 within the cytosol (Fig. 11a). The integrated start- and stop-transfer sequences, which enabled the translocation of CLuc through the ER-translocon, also served as transmembrane domains anchoring IMPDH-1-CLuc to the ER-membrane. The subsequent transport to the plasma membrane led to the exposure of IMPDH-1-CLuc on the cell surface accessible for its specific luciferin substrate vargulin. The immunofluorescent labeling of p53 and IMPDH-1-CLuc in HCT116 cells transfected with recombinant FLp53-IMPDH-1-CLuc demonstrated efficient intein-splicing as evident from the spatial segregation of FLp53 (nucleus) and IMPDH-1-CLuc (ER) (Fig. 11b). Given the interconnected compartment protein quality control in mammalian cells [185,186], FLp53 had to retain structural integrity to be transported into the nucleus, which at least we have proven for recombinant FLp53. And stable EXSISERS_{TP53:2CLuc-4NLuc-7FLuc} cells lastly demonstrated successful spatial segregation of nuclear p53 and plasma membrane resident IMPDH-1-CLuc as well.

The CRISPR/Cas9-mediated knock-in of the EXSISERS reporters into *TP53* entailed a dual-selection strategy. Therefore, all EXSISERS reporters were integrated alongside a selection-cassette comprising two genes encoding the puromycin-N-acetyltransferase (PuroR) and the Herpes Simplex Virus thymidine kinase (HSVtk). Puromycin is a naturally derived amino nucleoside antibiotic that can interrupt protein synthesis. Puromycin is incorporated by ribosomes into the elongating amino acid chains, leading to the premature termination of translation. This antibiotic is widely used as a selection marker in cell lines that have undergone genetic modification [207]. As for the initial selection, we used puromycin as a selective antibiotic neutralized by PuroR in genetically modified HCT116 cell lines. The selection cassette was equipped with recognition sequences for DNA recombinases to facilitate the subsequent removal of the additionally integrated selection markers. NrdJ-1-FLuc

Discussion

was equipped with a selection cassette flanked by FRT sites, which are recognized by flippase recombinases. Gp41-1-NLuc was equipped with a selection cassette, having incorporated the Cre/LoxP system. Lastly, IMPDH-1-CLuc carried a selection cassette flanked by RoxP sites, which are recognized by Dre recombinases. Transfection of the respective recombinase-coding expression-plasmids ultimately led to the excision of the selection cassettes. The second selection step considered using ganciclovir, a nucleoside analog that is only phosphorylated and incorporated into DNA replication in the presence of HSV thymidine kinase [208]. The replication process is terminated once ganciclovir is incorporated into the DNA. For that reason, the HSVtk gene is also referred to as the suicide gene [209]. EXSISERS cells not having excised the selection cassette are selectively eliminated through the application of ganciclovir. Cells that have undergone positive selection with puromycin (after EXSISERS reporter knock-in) and negative selection with ganciclovir (after recombinase-mediated excision of the selection cassette) were considered for quantitative p53 isoform measurements. We have also ensured the EXSISERS reporters to be integrated in a homozygous manner. Thus, we sought to prevent a compensatory effect of unmodified over modified *TP53*, for example, due to differential gene strength.

The rapid splicing rates of the selected split-inteins, namely gp41-1, NrdJ-1, and IMPDH-1, result in the excision of the EXSISERS reporters occurring concomitantly with the translation of p53. Consequently, we hypothesize that protein folding of p53, and thereby the structure and function of p53 are unaffected by EXSISERS.

For the stable precursor cell lines EXSISERS_{TP53:7FLuc} and EXSISERS_{TP53:4NLuc-7FLuc}, which exhibit efficient intein-splicing and robust protein expression (Figure 16b, c), we indeed demonstrated the integrity of p53 as a transcription factor. After IMPDH-1-CLuc knock-in and generation of the final EXSISERS_{TP53:2CLuc-4NLuc-7FLuc} cell line, however, only a moderate splicing efficiency was observed (Fig. 16d). Of note, all EXSISERS reporters, inclusively p53, were expressed continuously.

However, insufficient intein splicing of IMPDH-1-CLuc may reduce the abundance of functional p53 transcription factors (Figure 18b). Furthermore, the phosphorylation of p53, especially at the N-terminus, is highly dependent on the IMPDH-1 splicing efficiency (Figure 18c). Given that IMPDH-1-CLuc is stably integrated between lysine 14 (Lys14) and serine 15 (Ser15), moderate IMPDH-1 intein splicing may result in restricted accessibility for serine/threonine kinases and reduced serine15-phospho-dependent p53 induction.

However, Ser15 is not the only amino acid phosphorylated by kinases upon activation. The phosphorylation of residues Ser15, Thr18, and Ser20 leads to diminished p53 interaction with its specific E3 ubiquitin ligase Mdm2 [210]. In addition to numerous other phosphorylation sites (Ser33, Ser37, Ser46, Ser55, Thr81, Thr155, Ser276), the C-terminal amino acids, notably Ser278, Ser315, and Ser392, have vital regulatory roles, enabling p53 tetramerization [211,212]. In its tetrameric form, p53 functions as a transcription factor [213]. Despite moderate intein splicing hindering Ser15 from phosphorylation, numerous other sites within the p53 sequence evoke similar or related regulatory functions.

Protein expression does not appear to be impaired by this integration. Since EXSISERS reflects the quantity of newly expressed p53 isoforms rather than the stability or activation of p53, EXSISERS_{TP53:2CLuc-4NLuc-7FLuc} can be safely employed for quantitative purposes. However, protein quantification is concurrently conducted with phenotypic studies (e.g., in response to specific drugs). We recommend the use of the EXSISERS_{TP53:4NLuc-7FLuc} precursor cell line. The data clearly demonstrated that integrating gp41-1-NLuc and NrdJ-1-FLuc did not impact p53's function and activatability. For this reason, we utilized EXSISERS_{TP53:4NLuc-7FLuc} cells for high-throughput screening of the anti-cancer compound library while exclusively employing EXSISERS_{TP53:2CLuc-4NLuc-7FLuc} cells for the analysis of differential p53 protein expression (FLp53, Δ 40p53, Δ 133+ Δ 160p53) in response to selected drugs.

4.2 Established protein analysis methods are challenging in terms of detection and quantification of the specific p53 isoforms.

p53 is reasonably referred to as the "guardian of the genome." The extensive functional repertoire of the tumor suppressor arises from the intricate post-translational modifications, accompanied by the diversity of its protein isoforms. The p53 isoforms remain inadequately explored, largely owing to the inherent challenges posed by certain limitations in today's protein detection methodologies. We integrated EXSISERS into *TP53* to investigate the intricacies of three essential p53 isoform subgroups (FLp53, Δ 40p53, and Δ 133+ Δ 160p53). Given that the N-terminal-variant isoforms are particularly attributed to distinct cellular functions, we aimed to examine their expression patterns in response to specific CRC drugs with known modes of

Discussion

action. Cellular signaling pathways that were activated by these drugs may then be associated with the upregulation of specific p53 protein isoforms.

The non-invasive character of EXSISERS allows for **1.** the translational quantification and **2.** differentiation of the specific target protein isoforms. **3.** Since our methodology does not require cell-lysis, luminescence signals can be acquired for a specific time interval with multiple measurement time points **4.** in the same living cells. **5.** The high scalability of genetically engineered tumor cells also offers high-throughput applicability. EXSISERS does not replace but complements existing gold-standard protein detection and quantification methods. For instance, real-time quantitative PCR (RT-qPCR) enables the relative quantification of short (50-200 bp long) amplicons from reverse-transcribed cDNA. Hence, using RT-qPCR allows for investigating a multitude of genes in terms of their transcriptional activity. As already stated, the transcriptional and translational regulation of genes do not necessarily coincide, as protein expression is also influenced by several factors, including translationally arrested mRNA [169], ribosomal frameshift regulation [170], and local mRNA translation [152,171,172]. It is worth mentioning that RT-qPCR is considered one of the more elaborate methods. Due to the highly invasive nature of sample preparation, each time point in a time series measurement has to be prepared separately. Additionally, increasing individual preparation steps raises the likelihood of bias, such as artificially induced cell stress reactions, that may reflect onto the (within seconds adjustable) RNA transcription. The opportunity of visually detecting p53 protein isoforms by antibody-based methods, including immunoblotting (Western blot) and immunofluorescence microscopy, heavily relies on the specificity of available antibodies. We have demonstrated that, to date, there are no commercial pan-tropic antibodies capable of specifically detecting all p53 protein isoforms. Furthermore, the cellular abundance of these isoforms strongly varies. Compared to FLp53 and $\Delta 40p53$, the anti-apoptotic isoforms $\Delta 133p53$ and $\Delta 160p53$ are minimally represented. Even the attempt to enrich these isoforms by immunoprecipitation did not increase protein signals. In summary, p53 protein isoforms cannot be enriched or visualized using antibody-dependent techniques, while RT-qPCR, although capable of quantifying at the transcriptional level, is usually elaborate and prevents longitudinal and large-scale experiments.

Discussion

Quantifying isoforms using mass spectrometry represents an antibody-independent approach, specifically when employing the selected reaction monitoring (SRM) or multiple reaction monitoring (MRM) technique. SRM/MRM uses the liquid-chromatography tandem mass spectrometry (LC-MS/MS) in which ions of a particular mass are selectively filtered by a liquid-chromatogram and two consecutively linked quadrupoles, which are finally detected in a quantitative manner. MS/MS offers the advantage of a high-resolution representation of peptide ions within a heterogeneous protein mixture. First attempts in distinguishing representative peptides for FLp53, $\Delta 40$ p53, and $\Delta 133+\Delta 160$ p53 only worked to a limited extent. The trypsin protease digestion of cell lysates from DMSO (control), 5 FU-, or OX-treated cells yielded a cleavage pattern that generated a single peptide representative for FLp53. Considering the p53 amino acid sequence, it becomes evident that peptide 1 (spanning from amino acid position 1 to 24, representing FLp53) is significantly larger than the other generated peptides (peptide 2-7, [Fig. 26](#)), which, in turn, exhibit an average length of 10 amino acids. Longer peptides are challenging to detect. The probability of a post-translational modification (e.g., acetylation, methylation, phosphorylation, glycosylation, etc.) increases with the length of a peptide. Especially, p53 becomes phosphorylated at Ser15, Thr18, and Ser20 upon activation. Additionally, alternative/non-consistent phosphorylation patterns make adjusting the setting for detecting peptides with varying masses nearly impossible. Consequently, MRM-MS/MS measurements with trypsin-digested lysates were able to detect peptide 2-7, which allowed differentiation between tumor suppressive (FLp53+ $\Delta 40$ p53) and anti-apoptotic protein isoforms ($\Delta 133$ p53 + $\Delta 160$ p53). However, we started another attempt using two proteases during sample preparation: trypsin and GluC endoproteinases. The rationale behind this approach was the generation of an N-terminal peptide, which is significantly shorter and less likely influenced by post-translational modifications. In addition, the cell lysates were treated with lambda phosphatases to ensure consistent peptide masses. Instead of a 24 aa long peptide, the double treatment with trypsin and gluC could generate a 7 amino acid long peptide spanning from Thr18 to Lys24.

Henceforth, we still have to ascertain whether the enhanced detection of a FLp53-representative peptide can be achieved through modified peptide preparations involving alternative proteases and an additional phosphatase step. The differentiation of the three isoform groups via mass spectrometry may underscore the significance of

the data acquired with EXSISERS while concurrently elucidating the similarities and disparities between absolute and relative isoform quantification.

Mass spectrometry offers the significant advantage of quantifying absolute peptide quantities. Analyses employing MRM-MS/MS have unequivocally revealed that, with proper sample preparation, the three p53 protein isoform groups FLp53, $\Delta 40$ p53, and $\Delta 133+\Delta 160$ p53 are also differentiable. Nonetheless, given the attainment of absolute quantities, the data demonstrated an almost negligible underrepresentation of $\Delta 133+\Delta 160$ p53. Very low amounts often prevent the comparison of isoform quantities between samples with distinct treatment conditions. Also, the sample preparation for mass spectrometry requires cell lysis. Its high invasiveness, therefore, does not allow for continuous time-series measurements of the same sample.

High-throughput screening, involving the screening of thousands of compounds, continues to be the primary approach for identifying active chemical substances. Mass spectrometry for high-throughput screenings, especially for differentiating the p53 protein isoforms, is a complex endeavor. Although recent technological advancements, such as automatization, have revolutionized the high-throughput character of mass spectrometry [214], these instruments generally entail substantial costs. They may not be financially feasible for every research facility. EXSISERS, in contrast, offers a cost-effective approach, facilitating high-throughput studies with minimal logistical overhead.

4.3 Enhancing insights into p53's expressional behavior through high-throughput screening of over 4,863 anti-cancer compounds with EXSISERS

The minimal invasiveness and high-throughput character of EXSISERS enable the classification of an unlimited number of drug compounds regarding their influence on the p53 isoform expression. This is made possible by the remarkable expandability of all genetically modified CRC cell lines. Through internal normalization to prior time points (before drug treatment, $t=0$), EXSISERS allows a continuous quantitative p53 isoform screening in the same living cells. This approach significantly reduces bias effects evoked by inter-cell variabilities (differences in seeded cell density, sample purification, etc.).

We deliberately chose to use the precursor cell line EXSISERSTP53:4NLuc-7FLuc for screening the Anti-Cancer Compound library. For a massive number of diverse assay

Discussion

conditions, the dual-luciferase reporter system offers several advantages. Firstly, the NLuc substrate Endurazine (a plasma membrane-permeable derivative of Furimazine) and FLuc substrate D-luciferin-ethyl-ester exhibit significantly greater thermostability than the CLuc substrate vargulin. Secondly, the primary focus is on the entire tumor suppressive and oncogenic p53 protein isoforms. This reduces both experimental and computational efforts and facilitates a rapid and reliable categorization of the analyzed compounds regarding their p53 inducibility.

The Anti-Cancer Compound Library (HY-L025, MCE) we have used for the EXSISERS screening comprises a compilation of thoroughly characterized compounds. Each compound is accompanied by precisely defined biological targets, the respective cellular pathways, and the biological activity of the individual agents. Therefore, we conducted simple pathway-analyses for each compound using simple bioinformatic assessments. Accordingly, we performed simple bioinformatic assessments to elucidate the type of pathways primarily modulated by the induction of tumor suppressive or oncogenic p53 isoforms.

p53 stands out as the most critical and efficient inducer of apoptosis. Therefore, it is not surprising that the apoptosis pathway predominates in the p53-TIE library (Fig. 31). In brief, p53 exhibits the capacity to initiate an irreversible induction of apoptosis through two distinct mechanisms: The first way of p53-mediated apoptosis induction is known as the BCL-2-regulated pathway, alternatively referred to as the intrinsic, mitochondrial, or stress pathway. It is activated in response to stress-inducing conditions such as cytokine depletion, endoplasmic reticulum (ER) stress, or DNA damage [215–217]. Conversely, the death receptor pathway, also known as the extrinsic pathway, is triggered by ligand binding to specific members of the tumor necrosis factor receptor (TNFR) superfamily, favoring the assembly of the intracellular death domain [215,216]. We found numerous drug candidates influencing the Bcl-2 pathway (Gambogic acid, UMI-77) [196,218], the TNFR- (extrinsic) pathway (R-7050, Cynaropicrin) [219–221], or saponin-like compounds suppressing the p53 specific E3-ubiquitin ligase Mdm2 and eventually activating p53 (Formosanin C, Pulsatilla saponin D, Dioscin, Tubeimoside II, Terrestrosin D, Raddeanin A) [222,223]. Indeed, numerous compounds within the p53-TIE library intervene in direct correlation with the p53-mediated apoptosis pathway.

Another pathway influenced by compounds prevalently upregulating tumor suppressive p53 protein isoforms is the NF- κ B pathway. Numerous studies have

Discussion

consistently demonstrated that p53 and NF- κ B frequently exert inhibitory effects on each other's capacity to activate gene expression, with this regulatory interplay being modulated by the relative abundance of each transcription factor [224–226]. In this context, we have identified a multitude of candidate compounds that exhibit inhibitory effects on NF- κ B signaling (Cynaropicrin, IMD-0560, Ginsenoside Rk1, Brusatol, (1S,2S)-Bortezomib) [221,227–232]. We postulate that inhibiting NF- κ B may increase the expression of transcriptionally active (tumor suppressive) p53. Consequently, our pathway analysis reaffirms the well-established hypothesis of the robust reciprocal regulation between these two pathways [224–226]. Of note, these confirmative findings provide substantial validation for the utility of high-throughput screening conducted with EXSISERS.

Based on our pathway analysis, p53-OIE compounds exhibit predominant involvement in signaling pathways such as Protein Tyrosine Kinase, JAK/STAT, and PI3K/Akt/mTOR. Emerging evidence from various studies indicates potential interconnections to the p53 pathway. The JAK/STAT signaling and the p53 pathway have been recurrently associated [233]. However, these interactions are increasingly implicated with oncogenic effects in distinct tumor types [234,235]. Also, for PI3K/Akt/mTOR, there was a close association with p53, since p53 can transactivate mTOR expression [236]. However, as already known, mTOR signaling promotes cellular proliferation and metabolic processes that contribute to the initiation and progression of tumors [237]. Additionally, a multitude of tyrosine kinases have been linked to p53 [238–240]. Remarkably, p53 appears to exert inhibitory effects on some tyrosine kinases while transducing others, thus leaving the precise characterization of p53's role (tumor suppressive or oncogenic) undecided. However, it is essential to acknowledge that the extensive regulatory range of p53 across various cellular signaling pathways underscores the intricate nature of this tumor suppressor.

Expanding our knowledge about the interrelationships of p53 and other crucial signaling pathways broadens the scope of developing new tumor targets that directly or indirectly induce p53-mediated cell death in tumor cells. Concurrently, this pathway analysis also has elucidated signal transduction pathways to avoid, as their activation may lead to unfavorable outcomes in cancer development. In summary, this correlation was established using EXSISERS, which identified key drugs that significantly upregulated p53 and unveiled the relationship between p53 and other cellular pathways.

The main scope of this study was the identification of pharmaceutical agents that effectively elicit cell death, particularly through the induction of tumor suppressive p53 protein isoforms. Notably, Gambogic acid, BLM-IN-1, and SJB2-043, all of which are known to have a strong impact on the p53-dependent pathway [194–196], exert their full efficacy in the presence of functional, non-mutated p53 (Fig. 32 and 34). With AS1708727, IACS-010759, and JNJ64619178 (Onametostat) being involved in either metabolism or signal transduction, these drugs exert their higher efficacy in the presence of mutated, non-functional p53. Our hypothesis suggests that p53-OIE compounds specifically lead to elevated cellular stress levels. p53 may partially mitigate the lethal cellular stress caused by upregulating oncogenic p53 isoforms. Loss-of-function mutations in p53, especially within its conserved domains, would impact all p53 isoforms, including the oncogenic ones. Consequently, we posit that the effect of p53-OIEs is potentiated when p53 is absent.

Aside from immunotherapy, which is increasingly finding its way into clinical use, the treatment sequence for CRC heavily relies on chemotherapy. Many studies focus on alternative combinations of chemotherapeutic agents to determine the optimal approach for patients based on their *RAS* or *BRAF* genotype [36]. However, in the case of p53, no individualized therapy is available, as virtually all chemotherapy treatments depend on p53 functionality [50–52]. Thus far, there has been no reference to a p53-tailored therapy. Identifying p53-TIEs and p53-OIEs and their contrasting p53 dependencies could pave the way for expanding the current therapeutic regimen.

Our primary focus was placed on one individual drug candidate from each group of toxic p53-TIEs and p53-OIEs, namely SJB2-043 and IACS010759. For the following reasons, we believe these compounds would constitute the best choice for CRC therapy.

4.4 USP1 specific inhibitor SJB2-043 as a therapy for tumors with wildtype p53.

The preservation of genomic integrity is essential to avoid oncogenesis in mammalian organisms. This relies on a complex network of DNA repair mechanisms [241]. Emerging research highlights the pivotal role of ubiquitin and SUMO modifications in regulating DNA repair processes [242,243]. Deubiquitinating enzymes like the ubiquitin-specific protease 1 (USP1) play a crucial role in removing ubiquitin from proteins involved in DNA repair, such as FANCD2 and PCNA [244,245] (Fig. 37). Inhibition of USP1, for example by the specific USP1 inhibitor SJB2-043, leads to the

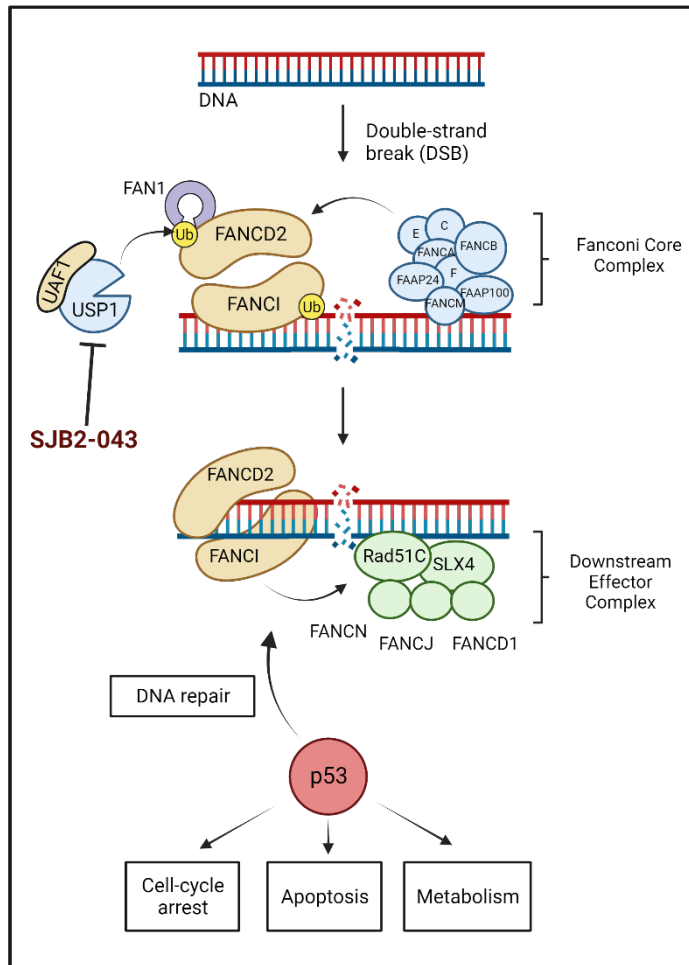


Figure 37: Inhibitory mechanisms of SJB2-043 a) The ubiquitin specific protein 1 (USP1) inhibitor SJB2-043 interferes with the DNA repair mechanism and obstructs the formation and association of the Fanconi Core Complex with damaged DNA. Over time, spontaneous or induced DNA damages accumulate, primarily leading to the induction of tumor-suppressive p53. The tumor suppressor either counteracts on the accumulation of the DNA damages by recruiting Rad51C and other DNA-repair factors, or induces cell-cycle arrest, cellular metabolic changes or apoptosis. This illustration was created with BioRender.

higher ubiquitinated FANCD2 and PCNA levels. In general, ubiquitinated proteins are more likely to be degraded by the proteasome. Lower levels of DNA-repair-recruiting factors like FANCD2 and PCNA enhance cellular vulnerability to DNA-damaging and crosslinking agents [246]. As most chemotherapeutic agents used in clinics cause severe DNA damage, we believe the simultaneous application of USP1 inhibitor SJB2-043 could potentiate the chemotherapeutic effect, which may evoke higher cell death rates with elevated tumor-specificity. However, SJB2-043 treatment requires wild-type p53. According to our data, inactivating mutations or a complete loss of p53 are associated with reduced SJB2-043 efficacy. Notably, up to 50 % of all tumor types come with a p53 mutation, of which approximately 30 % are miss-sense mutations mainly affecting 5 residues involved in DNA-binding (Arg273, Arg248, Arg175, Arg282, and Gly245) [122]. For this exact reason, we provide an alternative strategy for treating CRC.

4.5 Mitochondrial respiratory chain complex I inhibitor IACS-010759 as a therapy for p53-mutated tumors.

In contrast, IACS-010759 exploits the status of mutated and non-functional p53. IACS-010759 is a selective inhibitor of complex-I of mitochondrial oxidative phosphorylation (OXPHOS). Inhibition of complex-I promotes ROS release. Under moderate ROS levels, p53 is known to activate antioxidant genes to preserve cell survival [247,248]. Consequently, blocking OXPHOS in tumor cells bearing mutant p53 may enhance cellular ROS levels, leading to greater mitochondrial oxidative damage [249]. Further, cancer cells cover their energy needs by OXPHOS and not only by anaerobic glycolysis [250]. In summary, IACS 010759 is capable of inducing cell death in a p53-independent way (Fig. 34b). However, p53 loss-of-function mutations may also affect the anti-oxidative compensatory effect of $\Delta 133p53$ and $\Delta 160p53$. Therefore, ROS-elevation in concert with IACS-010759-mediated energy depletion represents a promising way to exploit p53-deficient and high-energy dependent tumor cells.

In recent years, IACS-010759 has received great attention due to its high targeting efficacy on solid tumors [199]. To our knowledge, IACS-010759 was not associated with CRC treatment before. Therefore, we evaluated its drug efficiency on patient-derived colon cancer organoids and further demonstrated its tumor-specific effect.

The tumor-specific effect of IACS-010759 may be attributed to various factors: High proliferative rates require high energy consumption. Moreover, rapid growth pushes the tumor to invade poorly vascularized tissue. The lack of nutrition and oxygen activates hypoxia-induced processes that further promote tumorigenic behavior.

These metabolic turnovers generate a higher intolerance to ROS-elevation and OXPHOS-related energy depletion [249,250]. Mitochondrial dysfunction through complex I inhibition also reduces hypoxia-derived tumor characteristics by destabilizing Hypoxia-inducible factor 1-alpha (HIF1- α) and the expression of its downstream targets [251]. IACS-010759 may address all these factors.

In vivo, IACS-010759 has demonstrated remarkable effects. In murine models, treatment with IACS-010759 robustly suppressed proliferation and induced apoptosis in brain cancer and acute myeloid leukemia (AML) models [199]. However, phase 1 clinical trials involving patients with AML and various solid tumors revealed that IACS-010759 could not be translated to clinical practice due to its significant neurotoxicity [252]. Scientists suspect an inadequately high dose was required to achieve anti-

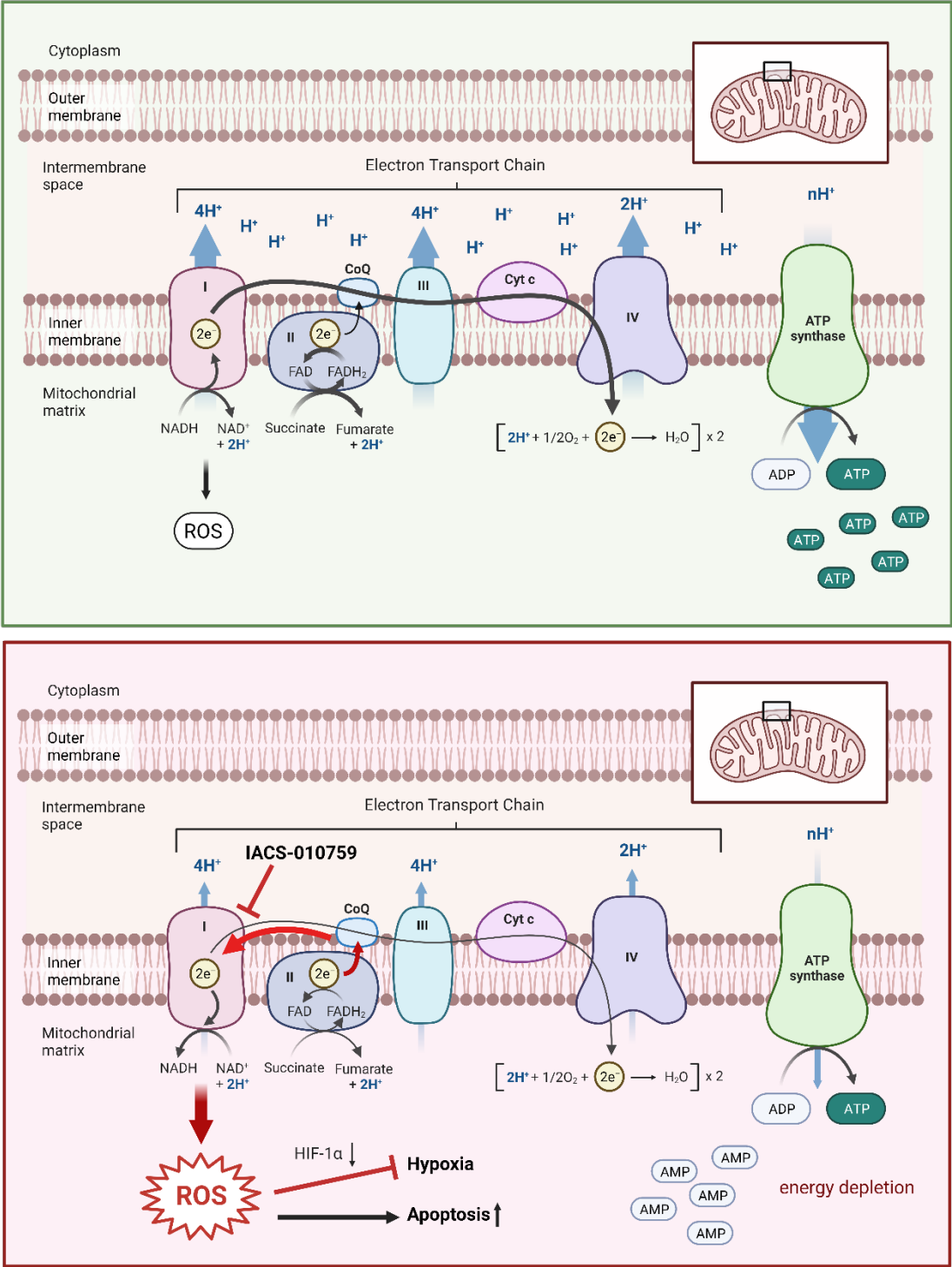


Figure 38: The OXPHOS complex I inhibitor IACS-010759 specifically targets highly proliferating and, thus, energy (ATP)-dependent colon cancer cells. Scheme of the mitochondrial respiratory chain under physiological condition (upper picture) and upon complex I inhibition with IACS-010759.HCl (lower picture). This image was created with BioRender.

tumoral effects [253]. Given that IACS-010759 can exert its full potential in p53-mutated tumors, thereby allowing for a significantly reduced effective dose, it may regain relevance for future clinical use.

4.6 Future perspectives

EXSISERS has revolutionized the multiplexed, quantitative determination of distinct proteins or protein isoforms. The use of plasma-permeable luciferin substrates additionally facilitates measurements with viable tumor cells. This minimal-invasive and high-throughput character of EXSISERS enabled the classification of a large number of anti-cancer compounds regarding their influence on p53. However, this represents just one of the many potential applications that EXSISERS can manage.

A large number of cellular stress signals induces activation of p53. However, the tumor suppressor gene *TP53* can also undergo transcriptional regulation by other gene regulators [254]. Studies that aim to identify additional master regulators of *TP53* (e.g., through whole-genome CRISPR/Cas9 gene-knockout or gene-induction libraries, siRNA libraries, etc.) could be easily conducted using EXSISERS_{TP53:2CLuc-4NLuc-7FLuc} cells. Beyond the scope of this particular thesis, EXSISERS holds huge potential for diverse applications in fundamental scientific research.

EXSISERS offers versatile applicability by being integrable into every protein of interest. Moreover, its adaptability extends to various tissue types and tumor cell lines. In light of our clinical department's hepatological orientation, we also plan to stably integrate EXSISERS into hepatocellular carcinoma (HCC) cell lines with wildtype p53. Given that HCC is one of the most prevalent and deadliest tumor types worldwide [14], with progressively increasing incidences and cancer-related deaths (55 % increment by 2040) [255], it is paramount to investigate novel therapeutic strategies. We believe that EXSISERS can significantly contribute to that.

In recent years, medicine has increasingly embraced personalized approaches. Returning to CRC, advancements in individualized strategies are exemplified by the approval of several immunotherapies (e.g., pembrolizumab) to especially address tumors with microsatellite instability [256].

With SBJ2-043 and IACS-010759, we believe to contribute to further individualized treatment strategies by providing a p53-genotype-tailored approach to current systemic therapies. Apart from these two therapeutics, our library has identified a multitude of agents acting in a p53-dependent manner. Especially concerning the neurotoxicity of IACS-010759 [252], it is advisable to avoid focusing on only a few drug candidates. Our future plans encompass broadening the clinical relevance of SJB2-043 and IACS-010759 and assessing the efficacy and tumor specificity of additional compounds cataloged in the drug library processed by EXSISERS.

5. Zusammenfassung

Heutzutage stellt das Kolorektale Karzinom (KRK) eines der schwerwiegendsten Erkrankungen dar. Um zu verhindern, dass die Inzidenzen kontinuierlich ansteigen, besteht ein dringender Bedarf an neuen therapeutischen Strategien zur effektiveren und individualisierten Behandlung dieser Erkrankung.

Das derzeitige therapeutische Regime sieht hauptsächlich den Einsatz verschiedener Kombinationen an Chemotherapeutika vor, darunter Folsäure (FOL), Oxaliplatin (OX), 5-FU (F) und Irinotecan (IRI). Allerdings sind diese Therapien oftmals mit systemischer Toxizität und unzureichenden Ansprechraten verbunden. Zudem hängt der therapeutische Erfolg stark vom der Aktivierbarkeit von Tumorsuppressor Proteinen wie z.B. p53 ab.

Der Tumorsuppressor p53, auch bekannt als „der Wächter des Genoms“, ist aufgrund seiner weitreichenden Regulationspanne eines der wichtigsten Proteine zur Erkennung und Bekämpfung pathogener Zell-Entartungen.

Die zelluläre Aktivität von p53 unterliegt einem präzisen Regulationsmechanismus und reagiert auf eine Vielzahl intrinsischer und extrinsischer Stressfaktoren. Als Reaktion darauf löst p53 entweder den Zellzyklusarrest aus, oder initiiert Apoptose. Andererseits kann p53 auch überlebens-fördernde Signalwege aktivieren. Der vorherrschende aktivierte Signalweg und das daraus resultierende Zellschicksal hängen somit stark von den differentiell exprimierten p53-Protein-Isoformen und ihren jeweiligen Verhältnissen in der Zelle ab.

Wir haben ein neuartiges **EX**on-**S**pezifisches **I**soform-**E**xpressions **R**epporter **S**ystem (EXSISERS) in *TP53* in einer Modellzelllinien des Kolorektalen Karzinoms (HCT116) etabliert, um eine umfassende Analyse des Zusammenspiels der einzelnen Protein-Isoformen FLp53, $\Delta 40$ p53 und $\Delta 133+\Delta 160$ p53 durchzuführen. EXSISERS verwendet ein Triple-Intein-Luziferase Reporter System, das die simultane Quantifizierung und Unterscheidung der vorliegenden p53-Isoformen über Lumineszenz-Signale in Echtzeit und lebenden Zellen ermöglicht. Unter Verwendung von EXSISERS konnten wir mithilfe klinisch bewährter Chemotherapeutika (5-Fluorouracil, Oxaliplatin) FLp53 als vorwiegend Zellzyklus-Arrest-induzierende Isoform und $\Delta 40$ p53 als Apoptose-induzierende Isoform identifizieren. EXSISERS ermöglichte zudem die systemische Studie neuer Tumor-Therapeutika in Bezug auf die differenzielle Induktion der p53-Isoformexpression im Hochdurchsatz-Verfahren. Das Hochdurchsatz-Screening einer Wirkstoff-Bibliothek mit 4.863 verschiedenen Anti-Tumor-Substanzen führte zur

Identifizierung von zwei hocheffizienten Wirkstoffkandidaten, die gegensätzliche p53-abhängige toxische Effekte hervorrufen:

Der Ubiquitin spezifische Protease 1 (USP-1) Inhibitor SJB2-043 erhöht hochsignifikant die Expression der tumorsuppressiven Isoformen FLp53 und $\Delta 40p53$ sowie den Zelltod in p53-wildtypischen Zellen.

IACS-010759 hingegen, ist ein selektiver Komplex 1 Inhibitor der mitochondrialen Atmungskette. IACS-010759 verstärkt die Expression von onkogenen $\Delta 133p53$ und $\Delta 160p53$ Isoformen und führt zu gesteigerten Zelltodraten in Zellen mit mutiertem p53.

Die erreichten Ziele lassen sich wie folgt stichpunktartig zusammenfassen:

- Ausbau EXSISERS-Technologie, die auf Lumineszenz-basierte Messungen die Quantifizierung von bis zu drei Protein-Isoform-Gruppen gleichzeitig ermöglicht.
- Stabile Integration von 3 EXSISERS-Reporter (IMPDH-1-CLuc, gp41-1-NLuc, NrdJ-1-FLuc) in das Tumorsuppressor-Gen *TP53* für die Echtzeit-Quantifizierung der Isoformen FLp53, $\Delta 40p53$ und $\Delta 133+\Delta 160p53$.
- Untersuchung der dynamischen Regulation der p53-Isoformen als Reaktion auf die Behandlung mit klinisch etablierten Chemotherapeutika. Untersuchung der Isoform-spezifischen Aktivierung p53-typischer Signalwege: FLp53: Zellzyklus-Arrest, $\Delta 40p53$: Induktion des Zelltods, $\Delta 133p53$ und $\Delta 160p53$: negative Regulatoren von FLp53 und Beschleunigung des $\Delta 40p53$ -vermittelten Zelltods.
- Nicht-invasives Hochdurchsatz Screening von 4.863 Anti-Tumor Substanzen in Bezug auf die differenzielle p53-Isoform-Expression. Identifizierung des Deubiquitinase-Inhibitors SJB2-043 als potenzielle Behandlungsoption für Tumore mit wildtypischem p53.
- Identifizierung von IACS-010759 als Komplex 1 Inhibitor der mitochondrialen Atmungskette als potenzielle Behandlungsoption für Tumore mit deaktivierenden p53-Mutationen oder -Deletionen.
- IACS-010759 zeigt Tumor-spezifische Wirkungen bei der Behandlung von gesunden und tumorösen Darmepithel-Organoiden.

Mithilfe von EXSISERS konnten wir im Hochdurchsatz-Verfahren eine Vielzahl von Anti-Tumor Substanzen in Bezug auf die Hochregulation der p53 Protein-Isoformen identifizieren und somit wertvolle Erkenntnisse für die p53-personalisierte Krebstherapie liefern.

6. Abbreviations

Δ 40p53	N-terminally (40 amino acid) truncated p53 protein isoform
Δ 133p53	N-terminally (133 amino acid) truncated p53 protein isoform
Δ 160p53	N-terminally (160 amino acid) truncated p53 protein isoform
3'HA	3 prime homology arm (downstream of the DNA double-strand break)
5'HA	5 prime homology arm (downstream of the DNA double strand break)
5-FU	5-fluorouracil
aa	amino acid
ab	antibody
Ago	Agonaute
APAF1	Apoptotic protease-activating factor 1
APC	adenomatous-polyposis-coli
APCs	antigen-presenting cells
Bak	BCL2-antagonist/killer 1 (member of the Bcl-2 family)
Bax	Bcl-2-associated X protein (member of the Bcl-2 family)
Bcl-2	B-cell lymphoma 2
Bcl-Xl	B-cell lymphoma-extra-large (member of the Bcl-2 family)
BLM IN 1	bloom syndrome protein inhibitor 1
BLU	bioluminescent light unit
CAPIRI	capecitabine + irinotecan
CAPOX	capecitabine + oxaliplatin
Cas9	CRISPR-associated protein 9
CD	Crohn's Disease
CIN	chromosomal instability
CIMP	CpG island methylator phenotype
crRNA	CRISPR RNA
CLuc	Cypridina luciferase
CRC	Colorectal carcinoma
CRISPR	Clustered regulatory interspaced short palindromic repeats

Abbreviations

CTLA-4	cytotoxic T lymphocyte antigen 4
DBD	DNA-binding domain
DBS	double-strand break
dCas9	dead Cas9 (nuclease inactive Cas9 protein)
DMSO	Dimethyl sulfoxide
DNA	deoxyribonucleic acid
ER	endoplasmic reticulum
ErbB	erythroblastosis oncogene B
ERK	extracellular signal-regulated kinase
EXSISERS	exon-specific isoform expression reporter system
FANCD2	Fanconi anemia group D2 protein
FDA	Food and Drug Administration
FGFR	fibroblast growth factor receptor
FLp53	full-length p53
FLuc	Firefly luciferase
FRT	Flippase-Recognition-Target
FOLFOX	folinic acid + 5-fluorouracil + oxaliplatin
FOLFOXIRI	folinic acid + 5-fluorouracil + oxaliplatin + irinotecan
FOXFIRI	5-fluorouracil + oxaliplatin + irinotecan
Foxo	forkhead transcription factor
GLuc	Gaussia luciferase
HDR	homologous direct repair
HER	human epidermal growth factor receptor
HGF	hepatocyte growth factor
HIF1 α	hypoxia-inducible factor 1 alpha
hLuz	human codon-optimized luciferase
HSVtk	Herpes Simplex Virus thymidine kinase
IgG	immunoglobulin G
iPSCs	induced pluripotent stem cells
JAK/STAT3	Janus kinase/signal transducer and activator of transcription 3
KI	Knock-in

Abbreviations

KO	Knock-out
LC-MS/MS	Liquide chromatography-tandem mass spectrometry
MEK	Raf-mitogen-activated protein kinase
MET	mesenchymal-epithelial transition factor
MHC	histocompatibility complexes
(d)MMR	(deficient) miss match repair
mNG	mNeonGreen
MRM	Multiple Reaction Monitoring
mRNA	messenger RNA
MSI	microsatellite instability
NHEJ	Non-homologous end joining
NLuc	Nano luciferase
NLS	nuclear localization factor
NP-1/2	neuropilin-1/2
NSCLC	non-small cell lung cancer
OD	Oligomerization domain
OS	overall survival
OX	oxaliplatin
OXPHOS	oxidative phosphorylation
p21	CDK-inhibitor 1
p53	tumor suppressor protein p53
p53 $\alpha/\beta/\gamma/\Psi$	C-terminally varying protein isoforms resulting from alternative splicing
p53-RE	p53-response element
p53-OIE	p53-oncogenic isoform enhancer
p53-TIE	p53-tumor suppressor isoform enhancer
P2a	peptide 2a
PARP	Poly ADP-Ribose Polymerase
PCNA	Proliferating-Cell-Nuclear-Antigen
PCR	polymerase chain reaction
PD-1	programmed cell death protein 1

Abbreviations

PDIA3	protein disulfide-isomerase A3
PDGFR	platelet-derived growth factor receptor
PFS	progression-free survival
PIGF	placental growth factor
POI	protein of interest
PRMT5	protein arginine methyltransferase 5
PUMA	p53 upregulated modulator of apoptosis (member of the Bcl-2 family)
PuroR	puromycin resistance (puromycin-N-acetyltransferase)
RNA	ribonucleic acid
RNAi	RNA interference
ROS	reactive oxygen species
rpm	rounds per minute
RT-qPCR	Reverse transcriptase – quantitative Polymerase Chain Reaction
sgRNA	single guide RNA
SDS-PAGE	sodium dodecyl sulfate polyacrylamide gel electrophoresis
SRM	Selective Reaction Monitoring
SV40	Simian virus 40
TAD	Transactivation domain
TALLEN	transcription activator-like enhancer nuclease
TKI	Tyrosine kinase inhibitors
TP53	Tumor suppressor gene p53
Tracr RNA	trans-activating crRNA
tRNA	transfer RNA
UC	Ulcerative colitis
USP1	Ubiquitin-specific peptidase 1
VHH	heavy chain
VPR	VP64-p65-Rta (composition of three transactivation factors)
WB	Western blot
WT	wild type
ZNF	zinc finger nuclease

7. References

1. Azzouz, L.L.; Sharma, S. Physiology, Large Intestine. In *StatPearls*; StatPearls Publishing: Treasure Island (FL), 2023.
2. Sulaiman, S.; Marciani, L. MRI of the Colon in the Pharmaceutical Field: The Future before Us. *Pharmaceutics* **2019**, *11*, E146, doi:10.3390/pharmaceutics11040146.
3. Precup, G.; Vodnar, D.-C. Gut *Prevotella* as a Possible Biomarker of Diet and Its Eubiotic versus Dysbiotic Roles: A Comprehensive Literature Review. *Br J Nutr* **2019**, *122*, 131–140, doi:10.1017/s0007114519000680.
4. Wang, Y.H.W.; Wiseman, J. Anatomy, Abdomen and Pelvis, Rectum. **2022**.
5. Bazira, P.J. Anatomy of the Caecum, Appendix, and Colon. *Surgery (Oxford)* **2023**, *41*, 1–6, doi:10.1016/j.mpsur.2022.11.003.
6. Guinane, C.M.; Tadrous, A.; Fouhy, F.; Ryan, C.A.; Dempsey, E.M.; Murphy, B.; Andrews, E.; Cotter, P.D.; Stanton, C.; Ross, R.P. Microbial Composition of Human Appendices from Patients Following Appendectomy. *mBio* **2013**, *4*, e00366-12, doi:10.1128/mBio.00366-12.
7. Bazar, K.A.; Lee, P.Y.; Joon Yun, A. An “Eye” in the Gut: The Appendix as a Sentinel Sensory Organ of the Immune Intelligence Network. *Medical Hypotheses* **2004**, *63*, 752–758, doi:10.1016/j.mehy.2004.04.008.
8. Mörbe, U.M.; Jørgensen, P.B.; Fenton, T.M.; von Burg, N.; Riis, L.B.; Spencer, J.; Agace, W.W. Human Gut-Associated Lymphoid Tissues (GALT); Diversity, Structure, and Function. *Mucosal Immunol* **2021**, *14*, 793–802, doi:10.1038/s41385-021-00389-4.
9. Salimoglu, S.; Kilinc, G.; Calik, B. Anatomy of the Colon, Rectum, and Anus. In *Colon Polyps and Colorectal Cancer*, Engin, O., Ed.; Springer International Publishing: Cham, 2021; pp. 1–22 ISBN 978-3-030-57273-0.
10. Kufe, D.W. Mucins in Cancer: Function, Prognosis and Therapy. *Nat Rev Cancer* **2009**, *9*, 874–885, doi:10.1038/nrc2761.
11. Schmitt, M.; Greten, F.R. The Inflammatory Pathogenesis of Colorectal Cancer. *Nat Rev Immunol* **2021**, *21*, 653–667, doi:10.1038/s41577-021-00534-x.
12. Provenzale, D.; Ness, R.M.; Llor, X.; Weiss, J.M.; Abbadessa, B.; Cooper, G.; Early, D.S.; Friedman, M.; Giardiello, F.M.; Glaser, K.; et al. NCCN Guidelines Insights: Colorectal Cancer Screening, Version 2.2020: Featured Updates to the NCCN Guidelines. *Journal of the National Comprehensive Cancer Network* **2020**, *18*, 1312–1320, doi:10.6004/jnccn.2020.0048.
13. Shaukat, A.; Levin, T.R. Current and Future Colorectal Cancer Screening Strategies. *Nat Rev Gastroenterol Hepatol* **2022**, *19*, 521–531, doi:10.1038/s41575-022-00612-y.
14. Sung, H.; Ferlay, J.; Siegel, R.L.; Laversanne, M.; Soerjomataram, I.; Jemal, A.; Bray, F. Global Cancer Statistics 2020: GLOBOCAN Estimates of Incidence and Mortality Worldwide for 36 Cancers in 185 Countries. *CA: A Cancer Journal for Clinicians* **2021**, *71*, 209–249, doi:10.3322/caac.21660.
15. Keum, N.; Giovannucci, E. Global Burden of Colorectal Cancer: Emerging Trends, Risk Factors and Prevention Strategies. *Nature reviews. Gastroenterology & hepatology* **2019**, *16*, 713–732.
16. Zhao, Q.; Wang, F.; Chen, Y.-X.; Chen, S.; Yao, Y.-C.; Zeng, Z.-L.; Jiang, T.-J.; Wang, Y.-N.; Wu, C.-Y.; Jing, Y.; et al. Comprehensive Profiling of 1015 Patients’ Exomes Reveals Genomic-Clinical Associations in Colorectal Cancer. *Nat Commun* **2022**, *13*, 2342, doi:10.1038/s41467-022-30062-8.

References

17. Rattray, N.J.W.; Charkoftaki, G.; Rattray, Z.; Hansen, J.E.; Vasiliou, V.; Johnson, C.H. Environmental Influences in the Etiology of Colorectal Cancer: The Premise of Metabolomics. *Curr Pharmacol Rep* **2017**, *3*, 114–125, doi:10.1007/s40495-017-0088-z.
18. Hossain, M.S.; Karuniawati, H.; Jairoun, A.A.; Urbi, Z.; Ooi, D.J.; John, A.; Lim, Y.C.; Kibria, K.M.K.; Mohiuddin, A.K.M.; Ming, L.C.; et al. Colorectal Cancer: A Review of Carcinogenesis, Global Epidemiology, Current Challenges, Risk Factors, Preventive and Treatment Strategies. *Cancers* **2022**, *14*, 1732, doi:10.3390/cancers14071732.
19. Parmar, S.; Easwaran, H. Genetic and Epigenetic Dependencies in Colorectal Cancer Development. *Gastroenterol Rep (Oxf)* **2022**, *10*, goac035, doi:10.1093/gastro/goac035.
20. Bakhoun, S.F.; Cantley, L.C. The Multifaceted Role of Chromosomal Instability in Cancer and Its Microenvironment. *Cell* **2018**, *174*, 1347–1360, doi:10.1016/j.cell.2018.08.027.
21. Lao, V.V.; Grady, W.M. Epigenetics and Colorectal Cancer. *Nat Rev Gastroenterol Hepatol* **2011**, *8*, 686–700, doi:10.1038/nrgastro.2011.173.
22. Zeinalian, M.; Hashemzadeh-Chaleshtori, M.; Salehi, R.; Emami, M.H. Clinical Aspects of Microsatellite Instability Testing in Colorectal Cancer. *Adv Biomed Res* **2018**, *7*, 28, doi:10.4103/abr.abr_185_16.
23. Mundade, R.; Imperiale, T.F.; Prabhu, L.; Loehrer, P.J.; Lu, T. Genetic Pathways, Prevention, and Treatment of Sporadic Colorectal Cancer. *Oncoscience* **2014**, *1*, 400–406.
24. Powell, S.M.; Zilz, N.; Beazer-Barclay, Y.; Bryan, T.M.; Hamilton, S.R.; Thibodeau, S.N.; Vogelstein, B.; Kinzler, K.W. APC Mutations Occur Early during Colorectal Tumorigenesis. *Nature* **1992**, *359*, 235–237, doi:10.1038/359235a0.
25. Esteller, M.; Sparks, A.; Toyota, M.; Sanchez-Cespedes, M.; Capella, G.; Peinado, M.A.; Gonzalez, S.; Tarafa, G.; Sidransky, D.; Meltzer, S.J.; et al. Analysis of Adenomatous Polyposis Coli Promoter Hypermethylation in Human Cancer. *Cancer Res* **2000**, *60*, 4366–4371.
26. Sparks, A.B.; Morin, P.J.; Vogelstein, B.; Kinzler, K.W. Mutational Analysis of the APC/Beta-Catenin/Tcf Pathway in Colorectal Cancer. *Cancer Res* **1998**, *58*, 1130–1134.
27. Schatoff, E.M.; Leach, B.I.; Dow, L.E. Wnt Signaling and Colorectal Cancer. *Curr Colorectal Cancer Rep* **2017**, *13*, 101–110, doi:10.1007/s11888-017-0354-9.
28. Liu, X.; Jakubowski, M.; Hunt, J.L. KRAS Gene Mutation in Colorectal Cancer Is Correlated With Increased Proliferation and Spontaneous Apoptosis. *American Journal of Clinical Pathology* **2011**, *135*, 245–252, doi:10.1309/AJCP7FO2VAXIVSTP.
29. Park, J.-I. Growth Arrest Signaling of the Raf/MEK/ERK Pathway in Cancer. *Front Biol (Beijing)* **2014**, *9*, 95–103, doi:10.1007/s11515-014-1299-x.
30. Huang, L.; Guo, Z.; Wang, F.; Fu, L. KRAS Mutation: From Undruggable to Druggable in Cancer. *Sig Transduct Target Ther* **2021**, *6*, 1–20, doi:10.1038/s41392-021-00780-4.
31. Nakayama, M.; Oshima, M. Mutant P53 in Colon Cancer. *J Mol Cell Biol* **2019**, *11*, 267–276, doi:10.1093/jmcb/mjy075.
32. Russo, A.; Bazan, V.; Iacopetta, B.; Kerr, D.; Soussi, T.; Gebbia, N. The TP53 Colorectal Cancer International Collaborative Study on the Prognostic and Predictive Significance of P53 Mutation: Influence of Tumor Site, Type of Mutation, and Adjuvant Treatment. *JCO* **2005**, *23*, 7518–7528, doi:10.1200/JCO.2005.00.471.

References

33. Iacopetta, B.; Russo, A.; Bazan, V.; Dardanoni, G.; Gebbia, N.; Soussi, T.; Kerr, D.; Elsaleh, H.; Soong, R.; Kandioler, D.; et al. Functional Categories of TP53 Mutation in Colorectal Cancer: Results of an International Collaborative Study. *Annals of Oncology* **2006**, *17*, 842–847, doi:10.1093/annonc/mdl035.
34. Chen, X.; Zhang, T.; Su, W.; Dou, Z.; Zhao, D.; Jin, X.; Lei, H.; Wang, J.; Xie, X.; Cheng, B.; et al. Mutant P53 in Cancer: From Molecular Mechanism to Therapeutic Modulation. *Cell Death Dis* **2022**, *13*, 1–14, doi:10.1038/s41419-022-05408-1.
35. Morgan, E.; Arnold, M.; Gini, A.; Lorenzoni, V.; Cabasag, C.J.; Laversanne, M.; Vignat, J.; Ferlay, J.; Murphy, N.; Bray, F. Global Burden of Colorectal Cancer in 2020 and 2040: Incidence and Mortality Estimates from GLOBOCAN. *Gut* **2023**, *72*, 338–344, doi:10.1136/gutjnl-2022-327736.
36. Xie, Y.-H.; Chen, Y.-X.; Fang, J.-Y. Comprehensive Review of Targeted Therapy for Colorectal Cancer. *Sig Transduct Target Ther* **2020**, *5*, 1–30, doi:10.1038/s41392-020-0116-z.
37. Schreuders, E.H.; Ruco, A.; Rabeneck, L.; Schoen, R.E.; Sung, J.J.; Young, G.P.; Kuipers, E.J. Colorectal Cancer Screening: A Global Overview of Existing Programmes. *Gut* **2015**, *64*, 1637–1649.
38. Sánchez-Gundín, J.; Fernández-Carballido, A.M.; Martínez-Valdivieso, L.; Barreda-Hernández, D.; Torres-Suárez, A.I. New Trends in the Therapeutic Approach to Metastatic Colorectal Cancer. *Int J Med Sci* **2018**, *15*, 659–665, doi:10.7150/ijms.24453.
39. van der Stok, E.P.; Spaander, M.C.W.; Grünhagen, D.J.; Verhoef, C.; Kuipers, E.J. Surveillance after Curative Treatment for Colorectal Cancer. *Nat Rev Clin Oncol* **2017**, *14*, 297–315, doi:10.1038/nrclinonc.2016.199.
40. Messersmith, W.A. NCCN Guidelines Updates: Management of Metastatic Colorectal Cancer. *Journal of the National Comprehensive Cancer Network* **2019**, *17*, 599–601, doi:10.6004/jnccn.2019.5014.
41. Brown, K.G.M.; Solomon, M.J.; Mahon, K.; O'Shannassy, S. Management of Colorectal Cancer. *BMJ* **2019**, *366*, l4561, doi:10.1136/bmj.l4561.
42. Seymour, M.T.; Maughan, T.S.; Ledermann, J.A.; Topham, C.; James, R.; Gwyther, S.J.; Smith, D.B.; Shepherd, S.; Maraveyas, A.; Ferry, D.R.; et al. Different Strategies of Sequential and Combination Chemotherapy for Patients with Poor Prognosis Advanced Colorectal Cancer (MRC FOCUS): A Randomised Controlled Trial. *Lancet* **2007**, *370*, 143–152, doi:10.1016/S0140-6736(07)61087-3.
43. Koopman, M.; Antonini, N.F.; Douma, J.; Wals, J.; Honkoop, A.H.; Erdkamp, F.L.; de Jong, R.S.; Rodenburg, C.J.; Vreugdenhil, G.; Loosveld, O.J.; et al. Sequential versus Combination Chemotherapy with Capecitabine, Irinotecan, and Oxaliplatin in Advanced Colorectal Cancer (CAIRO): A Phase III Randomised Controlled Trial. *Lancet* **2007**, *370*, 135–142, doi:10.1016/S0140-6736(07)61086-1.
44. Van Cutsem, E.; Cervantes, A.; Nordlinger, B.; Arnold, D.; ESMO Guidelines Working Group Metastatic Colorectal Cancer: ESMO Clinical Practice Guidelines for Diagnosis, Treatment and Follow-Up. *Ann Oncol* **2014**, *25 Suppl 3*, iii1-9, doi:10.1093/annonc/mdu260.
45. Falcone, A.; Ricci, S.; Brunetti, I.; Pfanner, E.; Allegrini, G.; Barbara, C.; Crinò, L.; Benedetti, G.; Evangelista, W.; Fanchini, L.; et al. Phase III Trial of Infusional Fluorouracil, Leucovorin, Oxaliplatin, and Irinotecan (FOLFOXIRI) Compared with Infusional Fluorouracil, Leucovorin, and Irinotecan (FOLFIRI) as First-Line Treatment for Metastatic Colorectal Cancer: The Gruppo Oncologico Nord Ovest. *J Clin Oncol* **2007**, *25*, 1670–1676, doi:10.1200/JCO.2006.09.0928.

References

46. Souglakos, J.; Androulakis, N.; Syrigos, K.; Polyzos, A.; Ziras, N.; Athanasiadis, A.; Kakolyris, S.; Tsousis, S.; Kouroussis, C.; Vamvakas, L.; et al. FOLFOXIRI (Folinic Acid, 5-Fluorouracil, Oxaliplatin and Irinotecan) vs FOLFIRI (Folinic Acid, 5-Fluorouracil and Irinotecan) as First-Line Treatment in Metastatic Colorectal Cancer (MCC): A Multicentre Randomised Phase III Trial from the Hellenic Oncology Research Group (HORG). *Br J Cancer* **2006**, *94*, 798–805, doi:10.1038/sj.bjc.6603011.
47. Goldberg, R.M.; Sargent, D.J.; Morton, R.F.; Fuchs, C.S.; Ramanathan, R.K.; Williamson, S.K.; Findlay, B.P.; Pitot, H.C.; Alberts, S.R. A Randomized Controlled Trial of Fluorouracil plus Leucovorin, Irinotecan, and Oxaliplatin Combinations in Patients with Previously Untreated Metastatic Colorectal Cancer. *J Clin Oncol* **2004**, *22*, 23–30, doi:10.1200/JCO.2004.09.046.
48. Cassidy, J.; Taberero, J.; Twelves, C.; Brunet, R.; Butts, C.; Conroy, T.; Debraud, F.; Figer, A.; Grossmann, J.; Sawada, N.; et al. XELOX (Capecitabine plus Oxaliplatin): Active First-Line Therapy for Patients with Metastatic Colorectal Cancer. *J Clin Oncol* **2004**, *22*, 2084–2091, doi:10.1200/JCO.2004.11.069.
49. Cho, Y.-H.; Ro, E.J.; Yoon, J.-S.; Mizutani, T.; Kang, D.-W.; Park, J.-C.; Il Kim, T.; Clevers, H.; Choi, K.-Y. 5-FU Promotes Stemness of Colorectal Cancer via P53-Mediated WNT/ β -Catenin Pathway Activation. *Nature Communications* **2020**, *11*, 5321, doi:10.1038/s41467-020-19173-2.
50. Müller, M.; Scaffidi, C.A.; Galle, P.R.; Stremmel, W.; Krammer, P.H. The Role of P53 and the CD95 (APO-1/Fas) Death System in Chemotherapy-Induced Apoptosis. *Eur Cytokine Netw* **1998**, *9*, 685–686.
51. Yang, C.; Zhou, Q.; Li, M.; Tong, X.; Sun, J.; Qing, Y.; Sun, L.; Yang, X.; Hu, X.; Jiang, J.; et al. Upregulation of CYP2S1 by Oxaliplatin Is Associated with P53 Status in Colorectal Cancer Cell Lines. *Sci Rep* **2016**, *6*, 33078, doi:10.1038/srep33078.
52. Yang, C.M.; Kang, M.-K.; Jung, W.-J.; Joo, J.-S.; Kim, Y.-J.; Choi, Y.; Kim, H.-P. P53 Expression Confers Sensitivity to 5-fluorouracil via Distinct Chromatin Accessibility Dynamics in Human Colorectal Cancer. *Oncology Letters* **2021**, *21*, 1–1, doi:10.3892/ol.2021.12487.
53. Oh, D.-Y.; Bang, Y.-J. HER2-Targeted Therapies - a Role beyond Breast Cancer. *Nat Rev Clin Oncol* **2020**, *17*, 33–48, doi:10.1038/s41571-019-0268-3.
54. Ferguson, F.M.; Gray, N.S. Kinase Inhibitors: The Road Ahead. *Nat Rev Drug Discov* **2018**, *17*, 353–377, doi:10.1038/nrd.2018.21.
55. Arteaga, C.L.; Engelman, J.A. ERBB Receptors: From Oncogene Discovery to Basic Science to Mechanism-Based Cancer Therapeutics. *Cancer Cell* **2014**, *25*, 282–303, doi:10.1016/j.ccr.2014.02.025.
56. Tebbutt, N.; Pedersen, M.W.; Johns, T.G. Targeting the ERBB Family in Cancer: Couples Therapy. *Nat Rev Cancer* **2013**, *13*, 663–673, doi:10.1038/nrc3559.
57. Vecchione, L.; Jacobs, B.; Normanno, N.; Ciardiello, F.; Tejpar, S. EGFR-Targeted Therapy. *Exp Cell Res* **2011**, *317*, 2765–2771, doi:10.1016/j.yexcr.2011.08.021.
58. Wang, Z. ErbB Receptors and Cancer. *Methods Mol Biol* **2017**, *1652*, 3–35, doi:10.1007/978-1-4939-7219-7_1.
59. Mendelsohn, J.; Prewett, M.; Rockwell, P.; Goldstein, N.I. CCR 20th Anniversary Commentary: A Chimeric Antibody, C225, Inhibits EGFR Activation and Tumor Growth. *Clinical Cancer Research* **2015**, *21*, 227–229, doi:10.1158/1078-0432.CCR-14-2491.
60. Jonker, D.J.; O’Callaghan, C.J.; Karapetis, C.S.; Zalcberg, J.R.; Tu, D.; Au, H.-J.; Berry, S.R.; Krahn, M.; Price, T.; Simes, R.J.; et al. Cetuximab for the Treatment of Colorectal Cancer. *N Engl J Med* **2007**, *357*, 2040–2048, doi:10.1056/NEJMoa071834.

References

61. Price, T.J.; Peeters, M.; Kim, T.W.; Li, J.; Cascinu, S.; Ruff, P.; Suresh, A.S.; Thomas, A.; Tjulandin, S.; Zhang, K.; et al. Panitumumab versus Cetuximab in Patients with Chemotherapy-Refractory Wild-Type KRAS Exon 2 Metastatic Colorectal Cancer (ASPECCT): A Randomised, Multicentre, Open-Label, Non-Inferiority Phase 3 Study. *Lancet Oncol* **2014**, *15*, 569–579, doi:10.1016/S1470-2045(14)70118-4.
62. Creasy, J.M.; Sadot, E.; Koerkamp, B.G.; Chou, J.F.; Gonen, M.; Kemeny, N.E.; Saltz, L.B.; Balachandran, V.P.; Peter Kingham, T.; DeMatteo, R.P.; et al. The Impact of Primary Tumor Location on Long-Term Survival in Patients Undergoing Hepatic Resection for Metastatic Colon Cancer. *Ann Surg Oncol* **2018**, *25*, 431–438, doi:10.1245/s10434-017-6264-x.
63. Ferrara, N.; Gerber, H.-P.; LeCouter, J. The Biology of VEGF and Its Receptors. *Nat Med* **2003**, *9*, 669–676, doi:10.1038/nm0603-669.
64. Hurwitz, H.; Fehrenbacher, L.; Novotny, W.; Cartwright, T.; Hainsworth, J.; Heim, W.; Berlin, J.; Baron, A.; Griffing, S.; Holmgren, E.; et al. Bevacizumab plus Irinotecan, Fluorouracil, and Leucovorin for Metastatic Colorectal Cancer. *N Engl J Med* **2004**, *350*, 2335–2342, doi:10.1056/NEJMoa032691.
65. Saltz, L.B.; Clarke, S.; Díaz-Rubio, E.; Scheithauer, W.; Figer, A.; Wong, R.; Koski, S.; Lichinitser, M.; Yang, T.-S.; Rivera, F.; et al. Bevacizumab in Combination with Oxaliplatin-Based Chemotherapy as First-Line Therapy in Metastatic Colorectal Cancer: A Randomized Phase III Study. *J Clin Oncol* **2008**, *26*, 2013–2019, doi:10.1200/JCO.2007.14.9930.
66. Passardi, A.; Nanni, O.; Tassinari, D.; Turci, D.; Cavanna, L.; Fontana, A.; Ruscelli, S.; Mucciarini, C.; Lorusso, V.; Ragazzini, A.; et al. Effectiveness of Bevacizumab Added to Standard Chemotherapy in Metastatic Colorectal Cancer: Final Results for First-Line Treatment from the ITACa Randomized Clinical Trial. *Ann Oncol* **2015**, *26*, 1201–1207, doi:10.1093/annonc/mdv130.
67. Cremolini, C.; Loupakis, F.; Antoniotti, C.; Lupi, C.; Sensi, E.; Lonardi, S.; Mezi, S.; Tomasello, G.; Ronzoni, M.; Zaniboni, A.; et al. FOLFOXIRI plus Bevacizumab versus FOLFIRI plus Bevacizumab as First-Line Treatment of Patients with Metastatic Colorectal Cancer: Updated Overall Survival and Molecular Subgroup Analyses of the Open-Label, Phase 3 TRIBE Study. *Lancet Oncol* **2015**, *16*, 1306–1315, doi:10.1016/S1470-2045(15)00122-9.
68. Giantonio, B.J.; Catalano, P.J.; Meropol, N.J.; O'Dwyer, P.J.; Mitchell, E.P.; Alberts, S.R.; Schwartz, M.A.; Benson, A.B.; Eastern Cooperative Oncology Group Study E3200 Bevacizumab in Combination with Oxaliplatin, Fluorouracil, and Leucovorin (FOLFOX4) for Previously Treated Metastatic Colorectal Cancer: Results from the Eastern Cooperative Oncology Group Study E3200. *J Clin Oncol* **2007**, *25*, 1539–1544, doi:10.1200/JCO.2006.09.6305.
69. Tang, P.A.; Cohen, S.J.; Kollmannsberger, C.; Bjarnason, G.; Virik, K.; MacKenzie, M.J.; Lourenco, L.; Wang, L.; Chen, A.; Moore, M.J. Phase II Clinical and Pharmacokinetic Study of Afibercept in Patients with Previously Treated Metastatic Colorectal Cancer. *Clin Cancer Res* **2012**, *18*, 6023–6031, doi:10.1158/1078-0432.CCR-11-3252.
70. Folprecht, G.; Pericay, C.; Saunders, M.P.; Thomas, A.; Lopez Lopez, R.; Roh, J.K.; Chistyakov, V.; Höhler, T.; Kim, J.-S.; Hofheinz, R.-D.; et al. Oxaliplatin and 5-FU/Folinic Acid (Modified FOLFOX6) with or without Afibercept in First-Line Treatment of Patients with Metastatic Colorectal Cancer: The AFFIRM Study. *Ann Oncol* **2016**, *27*, 1273–1279, doi:10.1093/annonc/mdw176.

References

71. Tabernero, J.; Yoshino, T.; Cohn, A.L.; Obermannova, R.; Bodoky, G.; Garcia-Carbonero, R.; Ciuleanu, T.-E.; Portnoy, D.C.; Van Cutsem, E.; Grothey, A.; et al. Ramucirumab versus Placebo in Combination with Second-Line FOLFIRI in Patients with Metastatic Colorectal Carcinoma That Progressed during or after First-Line Therapy with Bevacizumab, Oxaliplatin, and a Fluoropyrimidine (RAISE): A Randomised, Double-Blind, Multicentre, Phase 3 Study. *Lancet Oncol* **2015**, *16*, 499–508, doi:10.1016/S1470-2045(15)70127-0.
72. Argilés, G.; Saunders, M.P.; Rivera, F.; Sobrero, A.; Benson, A.; Guillén Ponce, C.; Cascinu, S.; Van Cutsem, E.; Macpherson, I.R.; Strumberg, D.; et al. Regorafenib plus Modified FOLFOX6 as First-Line Treatment of Metastatic Colorectal Cancer: A Phase II Trial. *Eur J Cancer* **2015**, *51*, 942–949, doi:10.1016/j.ejca.2015.02.013.
73. Grothey, A.; Van Cutsem, E.; Sobrero, A.; Siena, S.; Falcone, A.; Ychou, M.; Humblet, Y.; Bouché, O.; Mineur, L.; Barone, C.; et al. Regorafenib Monotherapy for Previously Treated Metastatic Colorectal Cancer (CORRECT): An International, Multicentre, Randomised, Placebo-Controlled, Phase 3 Trial. *Lancet* **2013**, *381*, 303–312, doi:10.1016/S0140-6736(12)61900-X.
74. Cheng, F.; Guo, D. MET in Glioma: Signaling Pathways and Targeted Therapies. *J Exp Clin Cancer Res* **2019**, *38*, 270, doi:10.1186/s13046-019-1269-x.
75. Demkova, L.; Kucerova, L. Role of the HGF/c-MET Tyrosine Kinase Inhibitors in Metastatic Melanoma. *Mol Cancer* **2018**, *17*, 26, doi:10.1186/s12943-018-0795-z.
76. Bradley, C.A.; Salto-Tellez, M.; Laurent-Puig, P.; Bardelli, A.; Rolfo, C.; Tabernero, J.; Khawaja, H.A.; Lawler, M.; Johnston, P.G.; Schaeysbroeck, S.V. Targeting C-MET in Gastrointestinal Tumours: Rationale, Opportunities and Challenges. *Nat Rev Clin Oncol* **2017**, *14*, 562–576, doi:10.1038/nrclinonc.2017.40.
77. Di Renzo, M.F.; Olivero, M.; Giacomini, A.; Porte, H.; Chastre, E.; Mirossay, L.; Nordlinger, B.; Bretti, S.; Bottardi, S.; Giordano, S. Overexpression and Amplification of the Met/HGF Receptor Gene during the Progression of Colorectal Cancer. *Clin Cancer Res* **1995**, *1*, 147–154.
78. Kammula, U.S.; Kuntz, E.J.; Francone, T.D.; Zeng, Z.; Shia, J.; Landmann, R.G.; Paty, P.B.; Weiser, M.R. Molecular Co-Expression of the c-Met Oncogene and Hepatocyte Growth Factor in Primary Colon Cancer Predicts Tumor Stage and Clinical Outcome. *Cancer Letters* **2007**, *248*, 219–228, doi:10.1016/j.canlet.2006.07.007.
79. El-Deiry, W.S.; Vijayvergia, N.; Xiu, J.; Scicchitano, A.; Lim, B.; Yee, N.S.; Harvey, H.A.; Gatalica, Z.; Reddy, S. Molecular Profiling of 6,892 Colorectal Cancer Samples Suggests Different Possible Treatment Options Specific to Metastatic Sites. *Cancer Biology & Therapy* **2015**, *16*, 1726–1737, doi:10.1080/15384047.2015.1113356.
80. Iveson, T.; Donehower, R.C.; Davidenko, I.; Tjulandin, S.; Deptala, A.; Harrison, M.; Nirni, S.; Lakshmaiah, K.; Thomas, A.; Jiang, Y.; et al. Rilotumumab in Combination with Epirubicin, Cisplatin, and Capecitabine as First-Line Treatment for Gastric or Oesophagogastric Junction Adenocarcinoma: An Open-Label, Dose de-Escalation Phase 1b Study and a Double-Blind, Randomised Phase 2 Study. *The Lancet Oncology* **2014**, *15*, 1007–1018, doi:10.1016/S1470-2045(14)70023-3.
81. Sharpe, A.H.; Freeman, G.J. The B7–CD28 Superfamily. *Nat Rev Immunol* **2002**, *2*, 116–126, doi:10.1038/nri727.
82. Jelinek, T.; Mihalyova, J.; Kascak, M.; Duras, J.; Hajek, R. PD-1/PD-L1 Inhibitors in Haematological Malignancies: Update 2017. *Immunology* **2017**, *152*, 357–371, doi:10.1111/imm.12788.

References

83. Chen, L.; Han, X. Anti-PD-1/PD-L1 Therapy of Human Cancer: Past, Present, and Future. *J Clin Invest* **2015**, *125*, 3384–3391, doi:10.1172/JCI80011.
84. Markman, J.L.; Shiao, S.L. Impact of the Immune System and Immunotherapy in Colorectal Cancer. *J Gastrointest Oncol* **2015**, *6*, 208–223, doi:10.3978/j.issn.2078-6891.2014.077.
85. Grivennikov, S.I.; Greten, F.R.; Karin, M. Immunity, Inflammation, and Cancer. *Cell* **2010**, *140*, 883–899, doi:10.1016/j.cell.2010.01.025.
86. Havel, J.J.; Chowell, D.; Chan, T.A. The Evolving Landscape of Biomarkers for Checkpoint Inhibitor Immunotherapy. *Nat Rev Cancer* **2019**, *19*, 133–150, doi:10.1038/s41568-019-0116-x.
87. Giancchetti, E.; Delfino, D.V.; Fierabracci, A. Recent Insights into the Role of the PD-1/PD-L1 Pathway in Immunological Tolerance and Autoimmunity. *Autoimmunity Reviews* **2013**, *12*, 1091–1100, doi:10.1016/j.autrev.2013.05.003.
88. Seidel, J.A.; Otsuka, A.; Kabashima, K. Anti-PD-1 and Anti-CTLA-4 Therapies in Cancer: Mechanisms of Action, Efficacy, and Limitations. *Frontiers in Oncology* **2018**, *8*.
89. Hoos, A.; Ibrahim, R.; Korman, A.; Abdallah, K.; Berman, D.; Shahabi, V.; Chin, K.; Canetta, R.; Humphrey, R. Development of Ipilimumab: Contribution to a New Paradigm for Cancer Immunotherapy. *Seminars in Oncology* **2010**, *37*, 533–546, doi:10.1053/j.seminoncol.2010.09.015.
90. Robert, C.; Schachter, J.; Long, G.V.; Arance, A.; Grob, J.J.; Mortier, L.; Daud, A.; Carlino, M.S.; McNeil, C.; Lotem, M.; et al. Pembrolizumab versus Ipilimumab in Advanced Melanoma. *N Engl J Med* **2015**, *372*, 2521–2532, doi:10.1056/NEJMoa1503093.
91. Herbst, R.S.; Baas, P.; Kim, D.-W.; Felip, E.; Pérez-Gracia, J.L.; Han, J.-Y.; Molina, J.; Kim, J.-H.; Arvis, C.D.; Ahn, M.-J.; et al. Pembrolizumab versus Docetaxel for Previously Treated, PD-L1-Positive, Advanced Non-Small-Cell Lung Cancer (KEYNOTE-010): A Randomised Controlled Trial. *The Lancet* **2016**, *387*, 1540–1550, doi:10.1016/S0140-6736(15)01281-7.
92. Motzer, R.J.; Escudier, B.; McDermott, D.F.; George, S.; Hammers, H.J.; Srinivas, S.; Tykodi, S.S.; Sosman, J.A.; Procopio, G.; Plimack, E.R.; et al. Nivolumab versus Everolimus in Advanced Renal-Cell Carcinoma. *N Engl J Med* **2015**, *373*, 1803–1813, doi:10.1056/NEJMoa1510665.
93. Robert, C.; Long, G.V.; Brady, B.; Dutriaux, C.; Maio, M.; Mortier, L.; Hassel, J.C.; Rutkowski, P.; McNeil, C.; Kalinka-Warzocha, E.; et al. Nivolumab in Previously Untreated Melanoma without BRAF Mutation. *N Engl J Med* **2015**, *372*, 320–330, doi:10.1056/NEJMoa1412082.
94. Brahmer, J.; Reckamp, K.L.; Baas, P.; Crinò, L.; Eberhardt, W.E.E.; Poddubskaya, E.; Antonia, S.; Pluzanski, A.; Vokes, E.E.; Holgado, E.; et al. Nivolumab versus Docetaxel in Advanced Squamous-Cell Non-Small-Cell Lung Cancer. *N Engl J Med* **2015**, *373*, 123–135, doi:10.1056/NEJMoa1504627.
95. Arrichiello, G.; Poliero, L.; Borrelli, C.; Paragliola, F.; Nacca, V.; Napolitano, S.; Corte, C.M.D.; Martini, G.; Martinelli, E. Immunotherapy in Colorectal Cancer: Is the Long-Awaited Revolution Finally Happening? *Cancer Treat Res Commun* **2021**, *28*, 100442, doi:10.1016/j.ctarc.2021.100442.
96. Lane, D.P. Cancer. P53, Guardian of the Genome. *Nature* **1992**, *358*, 15–16, doi:10.1038/358015a0.

References

97. Levine, A.J. P53: 800 Million Years of Evolution and 40 Years of Discovery. *Nat Rev Cancer* **2020**, *20*, 471–480, doi:10.1038/s41568-020-0262-1.
98. Vogelstein, B.; Kinzler, K.W. Cancer Genes and the Pathways They Control. *Nat Med* **2004**, *10*, 789–799, doi:10.1038/nm1087.
99. Haupt, Y.; Maya, R.; Kazaz, A.; Oren, M. Mdm2 Promotes the Rapid Degradation of P53. *Nature* **1997**, *387*, 296–299, doi:10.1038/387296a0.
100. Kunst, C.; Haderer, M.; Heckel, S.; Schlosser, S.; Müller, M. The P53 Family in Hepatocellular Carcinoma. *Translational Cancer Research* **2016**, *5*, 632–638.
101. Ho, T.; Tan, B.X.; Lane, D. How the Other Half Lives: What P53 Does When It Is Not Being a Transcription Factor. *International Journal of Molecular Sciences* **2020**, *21*, 13, doi:10.3390/ijms21010013.
102. Wang, H.; Guo, M.; Wei, H.; Chen, Y. Targeting P53 Pathways: Mechanisms, Structures, and Advances in Therapy. *Sig Transduct Target Ther* **2023**, *8*, 1–35, doi:10.1038/s41392-023-01347-1.
103. Müller, M.; Wilder, S.; Bannasch, D.; Israeli, D.; Lehlbach, K.; Li-Weber, M.; Friedman, S.L.; Galle, P.R.; Stremmel, W.; Oren, M.; et al. P53 Activates the CD95 (APO-1/Fas) Gene in Response to DNA Damage by Anticancer Drugs. *The Journal of experimental medicine* **1998**, *188*, 2033–2045, doi:10.1084/jem.188.11.2033.
104. Follis, A.V.; Llambi, F.; Ou, L.; Baran, K.; Green, D.R.; Kriwacki, R.W. The DNA-Binding Domain Mediates Both Nuclear and Cytosolic Functions of P53. *Nature structural & molecular biology* **2014**, *21*, 535–543, doi:10.1038/nsmb.2829.
105. Harris, C.C.; Hollstein, M. Clinical Implications of the P53 Tumor-Suppressor Gene. *N Engl J Med* **1993**, *329*, 1318–1327, doi:10.1056/NEJM199310283291807.
106. Müller, M.; Schleithoff, E.S.; Stremmel, W.; Melino, G.; Krammer, P.H.; Schilling, T. One, Two, Three--P53, P63, P73 and Chemosensitivity. *Drug Resist Updat* **2006**, *9*, 288–306, doi:10.1016/j.drug.2007.01.001.
107. Farkas, M.; Hashimoto, H.; Bi, Y.; Davuluri, R.V.; Resnick-Silverman, L.; Manfredi, J.J.; Debler, E.W.; McMahon, S.B. Distinct Mechanisms Control Genome Recognition by P53 at Its Target Genes Linked to Different Cell Fates. *Nat Commun* **2021**, *12*, 484, doi:10.1038/s41467-020-20783-z.
108. Jänicke, R.U.; Sohn, D.; Schulze-Osthoff, K. The Dark Side of a Tumor Suppressor: Anti-Apoptotic P53. *Cell Death Differ* **2008**, *15*, 959–976, doi:10.1038/cdd.2008.33.
109. Bourdon, J.-C.; Fernandes, K.; Murray-Zmijewski, F.; Liu, G.; Diot, A.; Xirodimas, D.P.; Saville, M.K.; Lane, D.P. P53 Isoforms Can Regulate P53 Transcriptional Activity. *Genes Dev* **2005**, *19*, 2122–2137, doi:10.1101/gad.1339905.
110. Steffens Reinhardt, L.; Zhang, X.; Groen, K.; Morten, B.C.; De Iuliis, G.N.; Braithwaite, A.W.; Bourdon, J.-C.; Avery-Kiejda, K.A. Alterations in the P53 Isoform Ratio Govern Breast Cancer Cell Fate in Response to DNA Damage. *Cell Death Dis* **2022**, *13*, 1–18, doi:10.1038/s41419-022-05349-9.
111. Jorruiz, S.M.; Bourdon, J.-C. P53 Isoforms: Key Regulators of the Cell Fate Decision. *Cold Spring Harb Perspect Med* **2016**, *6*, a026039, doi:10.1101/cshperspect.a026039.
112. Muller, M.; Scaffidi, C.A.; Galle, P.R.; Stremmel, W.; Krammer, P.H. The Role of P53 and the CD95 (APO-1/Fas) Death System in Chemotherapy-Induced Apoptosis. *European cytokine network* **1998**, *9*, 685–686.
113. Muller, M.; Schleithoff, E.S.; Stremmel, W.; Melino, G.; Krammer, P.H.; Schilling, T. One, Two, Three--P53, P63, P73 and Chemosensitivity. *Drug resistance updates reviews and commentaries in antimicrobial and anticancer chemotherapy* **2006**, *9*, 288–306, doi:10.1016/j.drug.2007.01.001.

References

114. Muller, M.; Volkmann, M.; Zentgraf, H.; Galle, P.R. Clinical Implications of the P53 Tumor-Suppressor Gene. *The New England journal of medicine* **1994**, *330*, 865.
115. Hafner, A.; Bulyk, M.L.; Jambhekar, A.; Lahav, G. The Multiple Mechanisms That Regulate P53 Activity and Cell Fate. *Nat Rev Mol Cell Biol* **2019**, *20*, 199–210, doi:10.1038/s41580-019-0110-x.
116. Hafsi, H.; Santos-Silva, D.; Courtois-Cox, S.; Hainaut, P. Effects of $\Delta 40p53$, an Isoform of P53 Lacking the N-Terminus, on Transactivation Capacity of the Tumor Suppressor Protein P53. *BMC Cancer* **2013**, *13*, 134, doi:10.1186/1471-2407-13-134.
117. Steffens Reinhardt, L.; Zhang, X.; Wawruszak, A.; Groen, K.; De Iulius, G.N.; Avery-Kiejda, K.A. Good Cop, Bad Cop: Defining the Roles of $\Delta 40p53$ in Cancer and Aging. *Cancers* **2020**, *12*, 1659, doi:10.3390/cancers12061659.
118. Candeias, M.M.; Powell, D.J.; Roubalova, E.; Apcher, S.; Bourougaa, K.; Vojtesek, B.; Bruzzoni-Giovanelli, H.; Fåhræus, R. Expression of P53 and P53/47 Are Controlled by Alternative Mechanisms of Messenger RNA Translation Initiation. *Oncogene* **2006**, *25*, 6936–6947, doi:10.1038/sj.onc.1209996.
119. Bernard, H.; Garmy-Susini, B.; Ainaoui, N.; Van Den Berghe, L.; Peurichard, A.; Javerzat, S.; Bikfalvi, A.; Lane, D.P.; Bourdon, J.C.; Prats, A.-C. The P53 Isoform, $\Delta 133p53\alpha$, Stimulates Angiogenesis and Tumour Progression. *Oncogene* **2013**, *32*, 2150–2160, doi:10.1038/onc.2012.242.
120. Fujita, K.; Mondal, A.M.; Horikawa, I.; Nguyen, G.H.; Kumamoto, K.; Sohn, J.J.; Bowman, E.D.; Mathe, E.A.; Schetter, A.J.; Pine, S.R.; et al. P53 Isoforms $\Delta 133p53$ and P53 β Are Endogenous Regulators of Replicative Cellular Senescence. *Nat Cell Biol* **2009**, *11*, 1135–1142, doi:10.1038/ncb1928.
121. Hassin, O.; Oren, M. Drugging P53 in Cancer: One Protein, Many Targets. *Nat Rev Drug Discov* **2023**, *22*, 127–144, doi:10.1038/s41573-022-00571-8.
122. Giacomelli, A.O.; Yang, X.; Lintner, R.E.; McFarland, J.M.; Duby, M.; Kim, J.; Howard, T.P.; Takeda, D.Y.; Ly, S.H.; Kim, E.; et al. Mutational Processes Shape the Landscape of TP53 Mutations in Human Cancer. *Nat Genet* **2018**, *50*, 1381–1387, doi:10.1038/s41588-018-0204-y.
123. Bourdon, J.-C. P53 and Its Isoforms in Cancer. *British journal of cancer* **2007**, *97*, 277–282, doi:10.1038/sj.bjc.6603886.
124. Dedeurwaerdere, F.; Claes, K.B.; Van Dorpe, J.; Rottiers, I.; Van der Meulen, J.; Breyne, J.; Swaerts, K.; Martens, G. Comparison of Microsatellite Instability Detection by Immunohistochemistry and Molecular Techniques in Colorectal and Endometrial Cancer. *Sci Rep* **2021**, *11*, 12880, doi:10.1038/s41598-021-91974-x.
125. Khalil, A.M. The Genome Editing Revolution: Review. *Journal of Genetic Engineering and Biotechnology* **2020**, *18*, 68, doi:10.1186/s43141-020-00078-y.
126. Stoddard, B.L. Homing Endonucleases: From Microbial Genetic Invaders to Reagents for Targeted DNA Modification. *Structure* **2011**, *19*, 7–15, doi:10.1016/j.str.2010.12.003.
127. Kim, Y.G.; Cha, J.; Chandrasegaran, S. Hybrid Restriction Enzymes: Zinc Finger Fusions to Fok I Cleavage Domain. *Proc Natl Acad Sci U S A* **1996**, *93*, 1156–1160, doi:10.1073/pnas.93.3.1156.
128. Urnov, F.D.; Rebar, E.J.; Holmes, M.C.; Zhang, H.S.; Gregory, P.D. Genome Editing with Engineered Zinc Finger Nucleases. *Nat Rev Genet* **2010**, *11*, 636–646, doi:10.1038/nrg2842.
129. Boch, J.; Scholze, H.; Schornack, S.; Landgraf, A.; Hahn, S.; Kay, S.; Lahaye, T.; Nickstadt, A.; Bonas, U. Breaking the Code of DNA Binding Specificity of TAL-Type III Effectors. *Science* **2009**, *326*, 1509–1512, doi:10.1126/science.1178811.

References

130. Christian, M.; Cermak, T.; Doyle, E.L.; Schmidt, C.; Zhang, F.; Hummel, A.; Bogdanove, A.J.; Voytas, D.F. Targeting DNA Double-Strand Breaks with TAL Effector Nucleases. *Genetics* **2010**, *186*, 757–761, doi:10.1534/genetics.110.120717.
131. Feng, R.; Patil, S.; Zhao, X.; Miao, Z.; Qian, A. RNA Therapeutics - Research and Clinical Advancements. *Frontiers in Molecular Biosciences* **2021**, *8*.
132. Oost, J. van der; Patinios, C. The Genome Editing Revolution. *Trends in Biotechnology* **2023**, *41*, 396–409, doi:10.1016/j.tibtech.2022.12.022.
133. Jinek, M.; Chylinski, K.; Fonfara, I.; Hauer, M.; Doudna, J.A.; Charpentier, E. A Programmable Dual-RNA-Guided DNA Endonuclease in Adaptive Bacterial Immunity. *Science* **2012**, *337*, 816–821, doi:10.1126/science.1225829.
134. Gasiunas, G.; Barrangou, R.; Horvath, P.; Siksnys, V. Cas9–crRNA Ribonucleoprotein Complex Mediates Specific DNA Cleavage for Adaptive Immunity in Bacteria. *Proceedings of the National Academy of Sciences* **2012**, *109*, E2579–E2586, doi:10.1073/pnas.1208507109.
135. Cong, L.; Ran, F.A.; Cox, D.; Lin, S.; Barretto, R.; Habib, N.; Hsu, P.D.; Wu, X.; Jiang, W.; Marraffini, L.A.; et al. Multiplex Genome Engineering Using CRISPR/Cas Systems. *Science* **2013**, *339*, 819–823, doi:10.1126/science.1231143.
136. Mali, P.; Yang, L.; Esvelt, K.M.; Aach, J.; Guell, M.; DiCarlo, J.E.; Norville, J.E.; Church, G.M. RNA-Guided Human Genome Engineering via Cas9. *Science* **2013**, *339*, 823–826, doi:10.1126/science.1232033.
137. Hwang, W.Y.; Fu, Y.; Reyon, D.; Maeder, M.L.; Tsai, S.Q.; Sander, J.D.; Peterson, R.T.; Yeh, J.-R.J.; Joung, J.K. Efficient Genome Editing in Zebrafish Using a CRISPR-Cas System. *Nat Biotechnol* **2013**, *31*, 227–229, doi:10.1038/nbt.2501.
138. Cho, S.W.; Kim, S.; Kim, J.M.; Kim, J.-S. Targeted Genome Engineering in Human Cells with the Cas9 RNA-Guided Endonuclease. *Nat Biotechnol* **2013**, *31*, 230–232, doi:10.1038/nbt.2507.
139. Jinek, M.; East, A.; Cheng, A.; Lin, S.; Ma, E.; Doudna, J. RNA-Programmed Genome Editing in Human Cells. *Elife* **2013**, *2*, e00471, doi:10.7554/eLife.00471.
140. Ishino, Y.; Shinagawa, H.; Makino, K.; Amemura, M.; Nakata, A. Nucleotide Sequence of the *lap* Gene, Responsible for Alkaline Phosphatase Isozyme Conversion in *Escherichia Coli*, and Identification of the Gene Product. *J Bacteriol* **1987**, *169*, 5429–5433, doi:10.1128/jb.169.12.5429-5433.1987.
141. Mojica, F.J.; Juez, G.; Rodríguez-Valera, F. Transcription at Different Salinities of *Haloferax Mediterranei* Sequences Adjacent to Partially Modified PstI Sites. *Mol Microbiol* **1993**, *9*, 613–621, doi:10.1111/j.1365-2958.1993.tb01721.x.
142. Mojica, F.J.M.; Díez-Villaseñor, C.; García-Martínez, J.; Soria, E. Intervening Sequences of Regularly Spaced Prokaryotic Repeats Derive from Foreign Genetic Elements. *J Mol Evol* **2005**, *60*, 174–182, doi:10.1007/s00239-004-0046-3.
143. Makarova, K.S.; Grishin, N.V.; Shabalina, S.A.; Wolf, Y.I.; Koonin, E.V. A Putative RNA-Interference-Based Immune System in Prokaryotes: Computational Analysis of the Predicted Enzymatic Machinery, Functional Analogies with Eukaryotic RNAi, and Hypothetical Mechanisms of Action. *Biol Direct* **2006**, *1*, 7, doi:10.1186/1745-6150-1-7.
144. Koonin, E.V.; Makarova, K.S.; Zhang, F. Diversity, Classification and Evolution of CRISPR-Cas Systems. *Curr Opin Microbiol* **2017**, *37*, 67–78, doi:10.1016/j.mib.2017.05.008.
145. Makarova, K.S.; Wolf, Y.I.; Iranzo, J.; Shmakov, S.A.; Alkhnbashi, O.S.; Brouns, S.J.J.; Charpentier, E.; Cheng, D.; Haft, D.H.; Horvath, P.; et al. Evolutionary Classification of

References

- CRISPR–Cas Systems: A Burst of Class 2 and Derived Variants. *Nat Rev Microbiol* **2020**, *18*, 67–83, doi:10.1038/s41579-019-0299-x.
146. Anzalone, A.V.; Koblan, L.W.; Liu, D.R. Genome Editing with CRISPR–Cas Nucleases, Base Editors, Transposases and Prime Editors. *Nat Biotechnol* **2020**, *38*, 824–844, doi:10.1038/s41587-020-0561-9.
 147. Jiang, F.; Doudna, J.A. CRISPR-Cas9 Structures and Mechanisms. *Annu Rev Biophys* **2017**, *46*, 505–529, doi:10.1146/annurev-biophys-062215-010822.
 148. Deltcheva, E.; Chylinski, K.; Sharma, C.M.; Gonzales, K.; Chao, Y.; Pirzada, Z.A.; Eckert, M.R.; Vogel, J.; Charpentier, E. CRISPR RNA Maturation by Trans-Encoded Small RNA and Host Factor RNase III. *Nature* **2011**, *471*, 602–607, doi:10.1038/nature09886.
 149. Adli, M. The CRISPR Tool Kit for Genome Editing and Beyond. *Nat Commun* **2018**, *9*, 1911, doi:10.1038/s41467-018-04252-2.
 150. Sansbury, B.M.; Hewes, A.M.; Kmiec, E.B. Understanding the Diversity of Genetic Outcomes from CRISPR-Cas Generated Homology-Directed Repair. *Commun Biol* **2019**, *2*, 1–10, doi:10.1038/s42003-019-0705-y.
 151. Katti, A.; Diaz, B.J.; Caragine, C.M.; Sanjana, N.E.; Dow, L.E. CRISPR in Cancer Biology and Therapy. *Nat Rev Cancer* **2022**, *22*, 259–279, doi:10.1038/s41568-022-00441-w.
 152. Truong, D.-J.J.; Phlairaharn, T.; Eßwein, B.; Gruber, C.; Tümen, D.; Baligács, E.; Armbrust, N.; Vaccaro, F.L.; Lederer, E.-M.; Beck, E.M.; et al. Non-Invasive and High-Throughput Interrogation of Exon-Specific Isoform Expression. *Nature Cell Biology* **2021**, doi:10.1038/s41556-021-00678-x.
 153. Delroisse, J.; Duchatelet, L.; Flammang, P.; Mallefet, J. Leaving the Dark Side? Insights Into the Evolution of Luciferases. *Frontiers in Marine Science* **2021**, *8*.
 154. White, E.H.; Steinmetz, M.G.; Miano, J.D.; Wildes, P.D.; Morland, R. Chemi-and Bioluminescence of Firefly Luciferin. *Journal of the American Chemical Society* **1980**, *102*, 3199–3208.
 155. Marques, S.M.; Esteves da Silva, J.C.G. Firefly Bioluminescence: A Mechanistic Approach of Luciferase Catalyzed Reactions. *IUBMB Life* **2009**, *61*, 6–17, doi:10.1002/iub.134.
 156. Shimomura, O.; Johnson, F.H.; Masugi, T. *Cypridina* Bioluminescence: Light-Emitting Oxyluciferin-Luciferase Complex. *Science* 1969, *164*, 1299–1300.
 157. Ruecker, O.; Zillner, K.; Groebner-Ferreira, R.; Heitzer, M. Gaussia-Luciferase as a Sensitive Reporter Gene for Monitoring Promoter Activity in the Nucleus of the Green Alga *Chlamydomonas Reinhardtii*. *Mol Genet Genomics* **2008**, *280*, 153–162, doi:10.1007/s00438-008-0352-3.
 158. Hall, M.P.; Unch, J.; Binkowski, B.F.; Valley, M.P.; Butler, B.L.; Wood, M.G.; Otto, P.; Zimmerman, K.; Vidugiris, G.; Machleidt, T.; et al. Engineered Luciferase Reporter from a Deep Sea Shrimp Utilizing a Novel Imidazopyrazinone Substrate. *ACS Chem Biol* **2012**, *7*, 1848–1857, doi:10.1021/cb3002478.
 159. England, C.G.; Ehlerding, E.B.; Cai, W. NanoLuc: A Small Luciferase Is Brightening Up the Field of Bioluminescence. *Bioconjugate chemistry* **2016**, *27*, 1175–1187, doi:10.1021/acs.bioconjchem.6b00112.
 160. Sato, W.; Rasmussen, M.; Deich, C.; Engelhart, A.E.; Adamala, K.P. Expanding Luciferase Reporter Systems for Cell-Free Protein Expression. *Sci Rep* **2022**, *12*, 11489, doi:10.1038/s41598-022-15624-6.

References

161. Shah, N.H.; Muir, T.W. Split Inteins: Nature's Protein Ligases. *Isr J Chem* **2011**, *51*, 854–861, doi:10.1002/ijch.201100094.
162. Hirata, R.; Ohsumk, Y.; Nakano, A.; Kawasaki, H.; Suzuki, K.; Anraku, Y. Molecular Structure of a Gene, VMA1, Encoding the Catalytic Subunit of H(+)-Translocating Adenosine Triphosphatase from Vacuolar Membranes of *Saccharomyces Cerevisiae*. *Journal of Biological Chemistry* **1990**, *265*, 6726–6733, doi:10.1016/S0021-9258(19)39210-5.
163. Aranko, A.S.; Wlodawer, A.; Iwaï, H. Nature's Recipe for Splitting Inteins. *Protein engineering, design & selection : PEDS* **2014**, *27*, 263–271, doi:10.1093/protein/gzu028.
164. Dong, F.; Gogol, E.P.; von Hippel, P.H. The Phage T4-Coded DNA Replication Helicase (Gp41) Forms a Hexamer upon Activation by Nucleoside Triphosphate. *J Biol Chem* **1995**, *270*, 7462–7473, doi:10.1074/jbc.270.13.7462.
165. Dassa, B.; London, N.; Stoddard, B.L.; Schueler-Furman, O.; Pietrokovski, S. Fractured Genes: A Novel Genomic Arrangement Involving New Split Inteins and a New Homing Endonuclease Family. *Nucleic Acids Res* **2009**, *37*, 2560–2573, doi:10.1093/nar/gkp095.
166. Carvajal-Vallejos, P.; Pallissé, R.; Mootz, H.D.; Schmidt, S.R. Unprecedented Rates and Efficiencies Revealed for New Natural Split Inteins from Metagenomic Sources. *Journal of Biological Chemistry* **2012**, *287*, 28686–28696, doi:10.1074/jbc.M112.372680.
167. Beyer, H.M.; Mikula, K.M.; Li, M.; Wlodawer, A.; Iwaï, H. The Crystal Structure of the Naturally Split Gp41-1 Intein Guides the Engineering of Orthogonal Split Inteins from Cis-Splicing Inteins. *FEBS J* **2020**, *287*, 1886–1898, doi:10.1111/febs.15113.
168. Katz, Y.; Wang, E.T.; Airoidi, E.M.; Burge, C.B. Analysis and Design of RNA Sequencing Experiments for Identifying Isoform Regulation. *Nat Methods* **2010**, *7*, 1009–1015, doi:10.1038/nmeth.1528.
169. O'Brien, J.; Hayder, H.; Zayed, Y.; Peng, C. Overview of MicroRNA Biogenesis, Mechanisms of Actions, and Circulation. *Frontiers in Endocrinology* **2018**, *9*.
170. Matsufuji, S.; Matsufuji, T.; Miyazaki, Y.; Murakami, Y.; Atkins, J.F.; Gesteland, R.F.; Hayashi, S. Autoregulatory Frameshifting in Decoding Mammalian Ornithine Decarboxylase Antizyme. *Cell* **1995**, *80*, 51–60, doi:10.1016/0092-8674(95)90450-6.
171. Anderson, P.; Kedersha, N. RNA Granules. *Journal of Cell Biology* **2006**, *172*, 803–808, doi:10.1083/jcb.200512082.
172. Baser, A.; Skabkin, M.; Kleber, S.; Dang, Y.; Gülcüler Balta, G.S.; Kalamakis, G.; Göpferich, M.; Ibañez, D.C.; Schefzik, R.; Lopez, A.S.; et al. Onset of Differentiation Is Post-Transcriptionally Controlled in Adult Neural Stem Cells. *Nature* **2019**, *566*, 100–104, doi:10.1038/s41586-019-0888-x.
173. Tümen, D.; Heumann, P.; Gülow, K.; Demirci, C.-N.; Cosma, L.-S.; Müller, M.; Kandulski, A. Pathogenesis and Current Treatment Strategies of Hepatocellular Carcinoma. *Biomedicines* **2022**, *10*, 3202, doi:10.3390/biomedicines10123202.
174. Chen, B.; Gilbert, L.A.; Cimini, B.A.; Schnitzbauer, J.; Zhang, W.; Li, G.-W.; Park, J.; Blackburn, E.H.; Weissman, J.S.; Qi, L.S.; et al. Dynamic Imaging of Genomic Loci in Living Human Cells by an Optimized CRISPR/Cas System. *Cell* **2013**, *155*, 1479–1491, doi:10.1016/j.cell.2013.12.001.
175. Brunak, S.; Engelbrecht, J.; Knudsen, S. Prediction of Human mRNA Donor and Acceptor Sites from the DNA Sequence. *J Mol Biol* **1991**, *220*, 49–65, doi:10.1016/0022-2836(91)90380-o.
176. Canny, M.D.; Moatti, N.; Wan, L.C.K.; Fradet-Turcotte, A.; Krasner, D.; Mateos-Gomez, P.A.; Zimmermann, M.; Orthwein, A.; Juang, Y.-C.; Zhang, W.; et al. Inhibition of 53BP1

References

- Favors Homology-Dependent DNA Repair and Increases CRISPR–Cas9 Genome-Editing Efficiency. *Nat Biotechnol* **2018**, *36*, 95–102, doi:10.1038/nbt.4021.
177. Jun-ichi, M.; Satoshi, T.; Kimi, A.; Fumi, T.; Akira, T.; Kiyoshi, T.; Ken-ichi, Y. Expression Vector System Based on the Chicken β -Actin Promoter Directs Efficient Production of Interleukin-5. *Gene* **1989**, *79*, 269–277, doi:10.1016/0378-1119(89)90209-6.
178. McCarty, N.S.; Graham, A.E.; Studená, L.; Ledesma-Amaro, R. Multiplexed CRISPR Technologies for Gene Editing and Transcriptional Regulation. *Nat Commun* **2020**, *11*, 1281, doi:10.1038/s41467-020-15053-x.
179. Chavez, A.; Scheiman, J.; Vora, S.; Pruitt, B.W.; Tuttle, M.; P R Iyer, E.; Lin, S.; Kiani, S.; Guzman, C.D.; Wiegand, D.J.; et al. Highly Efficient Cas9-Mediated Transcriptional Programming. *Nature Methods* **2015**, *12*, 326–328, doi:10.1038/nmeth.3312.
180. Wiśniewski, J.R.; Zougman, A.; Nagaraj, N.; Mann, M. Universal Sample Preparation Method for Proteome Analysis. *Nat Methods* **2009**, *6*, 359–362, doi:10.1038/nmeth.1322.
181. Kieβling, M.K.; Linke, B.; Brechmann, M.; Süss, D.; Krammer, P.H.; Gülow, K. Inhibition of NF- κ B Induces a Switch from CD95L-Dependent to CD95L-Independent and JNK-Mediated Apoptosis in T Cells. *FEBS Letters* **2010**, *584*, 4679–4688, doi:10.1016/j.febslet.2010.10.047.
182. Loening, A.M.; Wu, A.M.; Gambhir, S.S. Red-Shifted Renilla Reniformis Luciferase Variants for Imaging in Living Subjects. *Nature Methods* **2007**, *4*, 641–643, doi:10.1038/nmeth1070.
183. Rivlin, N.; Brosh, R.; Oren, M.; Rotter, V. Mutations in the P53 Tumor Suppressor Gene: Important Milestones at the Various Steps of Tumorigenesis. *Genes & cancer* **2011**, *2*, 466–474, doi:10.1177/1947601911408889.
184. Charles, J.P.; Fuchs, J.; Hefter, M.; Vishedyk, J.B.; Kleint, M.; Vogiatzi, F.; Schäfer, J.A.; Nist, A.; Timofeev, O.; Wanzel, M.; et al. Monitoring the Dynamics of Clonal Tumour Evolution in Vivo Using Secreted Luciferases. *Nat Commun* **2014**, *5*, 3981, doi:10.1038/ncomms4981.
185. Jones, R.D.; Gardner, R.G. Protein Quality Control in the Nucleus. *Curr Opin Cell Biol* **2016**, *40*, 81–89, doi:10.1016/j.ceb.2016.03.002.
186. Ravid, T.; Hochstrasser, M. Diversity of Degradation Signals in the Ubiquitin–Proteasome System. *Nat Rev Mol Cell Biol* **2008**, *9*, 679–689, doi:10.1038/nrm2468.
187. Eldeeb, M.A.; Zorca, C.E.; Goiran, T. Extracellular Protein Degradation via the Lysosome. *Commun Chem* **2020**, *3*, 1–3, doi:10.1038/s42004-020-00397-8.
188. Xie, K.; Minkenberg, B.; Yang, Y. Boosting CRISPR/Cas9 Multiplex Editing Capability with the Endogenous tRNA-Processing System. *Proceedings of the National Academy of Sciences* **2015**, *112*, 3570–3575, doi:10.1073/pnas.1420294112.
189. Pflaum, J.; Schlosser, S.; Muller, M. P53 Family and Cellular Stress Responses in Cancer. *Frontiers in oncology* **2014**, *4*, 285, doi:10.3389/fonc.2014.00285.
190. Zhao, L.; Sanyal, S. P53 Isoforms as Cancer Biomarkers and Therapeutic Targets. *Cancers* **2022**, *14*, 3145, doi:10.3390/cancers14133145.
191. Hoofnagle, A.N.; Becker, J.O.; Oda, M.N.; Cavigiolio, G.; Mayer, P.; Vaisar, T. Multiple Reaction Monitoring-Mass Spectrometric Assays Can Accurately Measure Many Protein Concentrations in Complex Mixtures. *Clin Chem* **2012**, *58*, 777–781, doi:10.1373/clinchem.2011.173856.
192. Anderson, N.L.; Anderson, N.G.; Pearson, T.W.; Borchers, C.H.; Paulovich, A.G.; Patterson, S.D.; Gillette, M.; Aebersold, R.; Carr, S.A. A Human Proteome Detection

References

- and Quantitation Project. *Mol Cell Proteomics* **2009**, *8*, 883–886, doi:10.1074/mcp.R800015-MCP200.
193. Fujiwara, T.; Saito, A.; Suzuki, M.; Shinomiya, H.; Suzuki, T.; Takahashi, E.; Tanigami, A.; Ichiyama, A.; Chung, C.H.; Nakamura, Y.; et al. Identification and Chromosomal Assignment of USP1, a Novel Gene Encoding a Human Ubiquitin-Specific Protease. *Genomics* **1998**, *54*, 155–158, doi:10.1006/geno.1998.5554.
194. Mistry, H.; Hsieh, G.; Buhrlage, S.J.; Huang, M.; Park, E.; Cuny, G.D.; Galinsky, I.; Stone, R.M.; Gray, N.S.; D'Andrea, A.D.; et al. Small-Molecule Inhibitors of USP1 Target ID1 Degradation in Leukemic Cells. *Molecular Cancer Therapeutics* **2013**, *12*, 2651–2662, doi:10.1158/1535-7163.MCT-13-0103-T.
195. Yin, Q.-K.; Wang, C.-X.; Wang, Y.-Q.; Guo, Q.-L.; Zhang, Z.-L.; Ou, T.-M.; Huang, S.-L.; Li, D.; Wang, H.-G.; Tan, J.-H.; et al. Discovery of Isaindigotone Derivatives as Novel Bloom's Syndrome Protein (BLM) Helicase Inhibitors That Disrupt the BLM/DNA Interactions and Regulate the Homologous Recombination Repair. *J Med Chem* **2019**, *62*, 3147–3162, doi:10.1021/acs.jmedchem.9b00083.
196. Zhai, D.; Jin, C.; Shiau, C.-W.; Kitada, S.; Satterthwait, A.C.; Reed, J.C. Gambogic Acid Is an Antagonist of Antiapoptotic Bcl-2 Family Proteins. *Mol Cancer Ther* **2008**, *7*, 1639–1646, doi:10.1158/1535-7163.MCT-07-2373.
197. Tao, H.; Yan, X.; Zhu, K.; Zhang, H. Discovery of Novel PRMT5 Inhibitors by Virtual Screening and Biological Evaluations. *Chem Pharm Bull (Tokyo)* **2019**, *67*, 382–388, doi:10.1248/cpb.c18-00980.
198. Protopopova, M.; Bandi, M.; Bardenhagen, J.; Bristow, C.; Carroll, C.; Chang, E.; Feng, N.; Gay, J.; Geck Do, M.; Greer, J.; et al. Abstract 4380: IACS-10759: A Novel OXPHOS Inhibitor Which Selectively Kill Tumors with Metabolic Vulnerabilities. *Cancer Research* **2015**, *75*, 4380, doi:10.1158/1538-7445.AM2015-4380.
199. Molina, J.R.; Sun, Y.; Protopopova, M.; Gera, S.; Bandi, M.; Bristow, C.; McAfoos, T.; Morlacchi, P.; Ackroyd, J.; Agip, A.-N.A.; et al. An Inhibitor of Oxidative Phosphorylation Exploits Cancer Vulnerability. *Nat Med* **2018**, *24*, 1036–1046, doi:10.1038/s41591-018-0052-4.
200. Tsuji, A.; Akao, T.; Masuya, T.; Murai, M.; Miyoshi, H. IACS-010759, a Potent Inhibitor of Glycolysis-Deficient Hypoxic Tumor Cells, Inhibits Mitochondrial Respiratory Complex I through a Unique Mechanism. *Journal of Biological Chemistry* **2020**, *295*, 7481–7491, doi:10.1074/jbc.RA120.013366.
201. Kamiński, M.; Kießling, M.; Süß, D.; Krammer, P.H.; Gülow, K. Novel Role for Mitochondria: Protein Kinase C θ -Dependent Oxidative Signaling Organelles in Activation-Induced T-Cell Death. *Mol Cell Biol* **2007**, *27*, 3625–3639, doi:10.1128/MCB.02295-06.
202. Kamiński, M.M.; Sauer, S.W.; Kamiński, M.; Opp, S.; Ruppert, T.; Grigaravičius, P.; Grudnik, P.; Gröne, H.-J.; Krammer, P.H.; Gülow, K. T Cell Activation Is Driven by an ADP-Dependent Glucokinase Linking Enhanced Glycolysis with Mitochondrial Reactive Oxygen Species Generation. *Cell Reports* **2012**, *2*, 1300–1315, doi:10.1016/j.celrep.2012.10.009.
203. Harris, A.L. Hypoxia — a Key Regulatory Factor in Tumour Growth. *Nat Rev Cancer* **2002**, *2*, 38–47, doi:10.1038/nrc704.
204. Maguire, C.A.; Bovenberg, M.S.; Crommentuijn, M.H.; Niers, J.M.; Kerami, M.; Teng, J.; Sena-Esteves, M.; Badr, C.E.; Tannous, B.A. Triple Bioluminescence Imaging for in Vivo Monitoring of Cellular Processes. *Mol Ther Nucleic Acids* **2013**, *2*, e99–e99, doi:10.1038/mtna.2013.25.

References

205. Mujawar, A.; Phadte, P.; Palkina, K.A.; Markina, N.M.; Mohammad, A.; Thakur, B.L.; Sarkisyan, K.S.; Balakireva, A.V.; Ray, P.; Yamplosky, I.; et al. Triple Reporter Assay: A Non-Overlapping Luciferase Assay for the Measurement of Complex Macromolecular Regulation in Cancer Cells Using a New Mushroom Luciferase–Luciferin Pair. *Sensors* **2023**, *23*, 7313, doi:10.3390/s23177313.
206. Moroz, M.A.; Zurita, J.; Moroz, A.; Nikolov, E.; Likar, Y.; Dobrenkov, K.; Lee, J.; Shenker, L.; Blasberg, R.; Serganova, I.; et al. Introducing a New Reporter Gene, Membrane-Anchored Cypridina Luciferase, for Multiplex Bioluminescence Imaging. *Molecular Therapy - Oncolytics* **2021**, *21*, 15–22, doi:10.1016/j.omto.2021.03.004.
207. Aviner, R. The Science of Puromycin: From Studies of Ribosome Function to Applications in Biotechnology. *Comput Struct Biotechnol J* **2020**, *18*, 1074–1083, doi:10.1016/j.csbj.2020.04.014.
208. Yamamoto, S.; Suzuki, S.; Hoshino, A.; Akimoto, M.; Shimada, T. Herpes Simplex Virus Thymidine Kinase/Ganciclovir-Mediated Killing of Tumor Cell Induces Tumor-Specific Cytotoxic T Cells in Mice. *Cancer Gene Ther* **1997**, *4*, 91–96.
209. Wang, J.; Lu, X.-X.; Chen, D.-Z.; Li, S.-F.; Zhang, L.-S. Herpes Simplex Virus Thymidine Kinase and Ganciclovir Suicide Gene Therapy for Human Pancreatic Cancer. *World J Gastroenterol* **2004**, *10*, 400–403, doi:10.3748/wjg.v10.i3.400.
210. Prives, C. Signaling to P53: Breaking the MDM2–P53 Circuit. *Cell* **1998**, *95*, 5–8, doi:10.1016/S0092-8674(00)81774-2.
211. Maclaine, N.J.; Hupp, T.R. The Regulation of P53 by Phosphorylation: A Model for How Distinct Signals Integrate into the P53 Pathway. *Aging* **2009**, *1*, 490–502, doi:10.18632/aging.100047.
212. Retzlaff, M.; Rohrberg, J.; Küpper, N.J.; Lagleder, S.; Bepperling, A.; Manzenrieder, F.; Peschek, J.; Kessler, H.; Buchner, J. The Regulatory Domain Stabilizes the P53 Tetramer by Intersubunit Contacts with the DNA Binding Domain. *Journal of Molecular Biology* **2013**, *425*, 144–155, doi:10.1016/j.jmb.2012.10.015.
213. Sullivan, K.D.; Galbraith, M.D.; Andrysiak, Z.; Espinosa, J.M. Mechanisms of Transcriptional Regulation by P53. *Cell Death Differ* **2018**, *25*, 133–143, doi:10.1038/cdd.2017.174.
214. Dueñas, M.E.; Peltier-Heap, R.E.; Leveridge, M.; Annan, R.S.; Büttner, F.H.; Trost, M. Advances in High-Throughput Mass Spectrometry in Drug Discovery. *EMBO Molecular Medicine* **2023**, *15*, e14850, doi:10.15252/emmm.202114850.
215. Aubrey, B.J.; Kelly, G.L.; Janic, A.; Herold, M.J.; Strasser, A. How Does P53 Induce Apoptosis and How Does This Relate to P53-Mediated Tumour Suppression? *Cell Death Differ* **2018**, *25*, 104–113, doi:10.1038/cdd.2017.169.
216. Strasser, A.; Harris, A.W.; Huang, D.C.; Krammer, P.H.; Cory, S. Bcl-2 and Fas/APO-1 Regulate Distinct Pathways to Lymphocyte Apoptosis. *EMBO J* **1995**, *14*, 6136–6147, doi:10.1002/j.1460-2075.1995.tb00304.x.
217. Czabotar, P.E.; Lessene, G.; Strasser, A.; Adams, J.M. Control of Apoptosis by the BCL-2 Protein Family: Implications for Physiology and Therapy. *Nat Rev Mol Cell Biol* **2014**, *15*, 49–63, doi:10.1038/nrm3722.
218. Abulwerdi, F.; Liao, C.; Liu, M.; Azmi, A.S.; Aboukameel, A.; Mady, A.S.A.; Gulappa, T.; Cierpicki, T.; Owens, S.; Zhang, T.; et al. A Novel Small-Molecule Inhibitor of Mcl-1 Blocks Pancreatic Cancer Growth in Vitro and in Vivo. *Mol Cancer Ther* **2014**, *13*, 565–575, doi:10.1158/1535-7163.MCT-12-0767.
219. Gururaja, T.L.; Yung, S.; Ding, R.; Huang, J.; Zhou, X.; McLaughlin, J.; Daniel-Issakani, S.; Singh, R.; Cooper, R.D.G.; Payan, D.G.; et al. A Class of Small Molecules That Inhibit

References

- TNF α -Induced Survival and Death Pathways via Prevention of Interactions between TNF α RI, TRADD, and RIP1. *Chem Biol* **2007**, *14*, 1105–1118, doi:10.1016/j.chembiol.2007.08.012.
220. King, M.D.; Alleyne, C.H.; Dhandapani, K.M. TNF-Alpha Receptor Antagonist, R-7050, Improves Neurological Outcomes Following Intracerebral Hemorrhage in Mice. *Neurosci Lett* **2013**, *542*, 92–96, doi:10.1016/j.neulet.2013.02.051.
221. Masutani, T.; Tanaka, Y.T.; Kojima, H.; Tsuboi, M.; Hara, A.; Niwa, M. Cynaropicrin Is Dual Regulator for Both Degradation Factors and Synthesis Factors in the Cartilage Metabolism. *Life Sci* **2016**, *158*, 70–77, doi:10.1016/j.lfs.2016.06.028.
222. Tu, Y.; Chen, L.; Ren, N.; Li, B.; Wu, Y.; Rankin, G.O.; Rojanasakul, Y.; Wang, Y.; Chen, Y.C. Standardized Saponin Extract from Baiye No.1 Tea (*Camellia Sinensis*) Flowers Induced S Phase Cell Cycle Arrest and Apoptosis via AKT-MDM2-P53 Signaling Pathway in Ovarian Cancer Cells. *Molecules* **2020**, *25*, 3515, doi:10.3390/molecules25153515.
223. Elekofehinti, O.O.; Iwaloye, O.; Olawale, F.; Ariyo, E.O. Saponins in Cancer Treatment: Current Progress and Future Prospects. *Pathophysiology* **2021**, *28*, 250–272, doi:10.3390/pathophysiology28020017.
224. Schneider, G.; Henrich, A.; Greiner, G.; Wolf, V.; Lovas, A.; Wieczorek, M.; Wagner, T.; Reichardt, S.; von Werder, A.; Schmid, R.M.; et al. Cross Talk between Stimulated NF- κ B and the Tumor Suppressor P53. *Oncogene* **2010**, *29*, 2795–2806, doi:10.1038/onc.2010.46.
225. Webster, G.A.; Perkins, N.D. Transcriptional Cross Talk between NF- κ B and P53. *Mol Cell Biol* **1999**, *19*, 3485–3495.
226. Carrà, G.; Lingua, M.F.; Maffeo, B.; Taulli, R.; Morotti, A. P53 vs NF- κ B: The Role of Nuclear Factor-Kappa B in the Regulation of P53 Activity and Vice Versa. *Cell. Mol. Life Sci.* **2020**, *77*, 4449–4458, doi:10.1007/s00018-020-03524-9.
227. Cho, J.Y.; Baik, K.U.; Jung, J.H.; Park, M.H. In Vitro Anti-Inflammatory Effects of Cynaropicrin, a Sesquiterpene Lactone, from *Saussurea Lappa*. *Eur J Pharmacol* **2000**, *398*, 399–407, doi:10.1016/s0014-2999(00)00337-x.
228. Tada, Y.; Kokabu, S.; Sugiyama, G.; Nakatomi, C.; Aoki, K.; Fukushima, H.; Osawa, K.; Sugamori, Y.; Ohya, K.; Okamoto, M.; et al. The Novel I κ B Kinase β Inhibitor IMD-0560 Prevents Bone Invasion by Oral Squamous Cell Carcinoma. *Oncotarget* **2014**, *5*, 12317–12330, doi:10.18632/oncotarget.2640.
229. Elshafay, A.; Tinh, N.X.; Salman, S.; Shaheen, Y.S.; Othman, E.B.; Elhady, M.T.; Kansakar, A.R.; Tran, L.; Van, L.; Hirayama, K.; et al. Ginsenoside Rk1 Bioactivity: A Systematic Review. *PeerJ* **2017**, *5*, e3993, doi:10.7717/peerj.3993.
230. Olayanju, A.; Copple, I.M.; Bryan, H.K.; Edge, G.T.; Sison, R.L.; Wong, M.W.; Lai, Z.-Q.; Lin, Z.-X.; Dunn, K.; Sanderson, C.M.; et al. Brusatol Provokes a Rapid and Transient Inhibition of Nrf2 Signaling and Sensitizes Mammalian Cells to Chemical Toxicity-Implications for Therapeutic Targeting of Nrf2. *Free Radic Biol Med* **2015**, *78*, 202–212, doi:10.1016/j.freeradbiomed.2014.11.003.
231. Adams, J.; Palombella, V.J.; Sausville, E.A.; Johnson, J.; Destree, A.; Lazarus, D.D.; Maas, J.; Pien, C.S.; Prakash, S.; Elliott, P.J. Proteasome Inhibitors: A Novel Class of Potent and Effective Antitumor Agents. *Cancer Res* **1999**, *59*, 2615–2622.
232. Kamalzadeh, Z.; Babanezhad, E.; Ghaffari, S.; Mohseni Ezhiyeh, A.; Mohammadnejad, M.; Naghibfar, M.; Bararjanian, M.; Attar, H. Determination of Bortezomib in API Samples Using HPLC: Assessment of Enantiomeric and Diastereomeric Impurities. *J Chromatogr Sci* **2017**, *55*, 697–705, doi:10.1093/chromsci/bmx023.

References

233. Hu, X.; Li, J.; Fu, M.; Zhao, X.; Wang, W. The JAK/STAT Signaling Pathway: From Bench to Clinic. *Sig Transduct Target Ther* **2021**, *6*, 1–33, doi:10.1038/s41392-021-00791-1.
234. Goyal, H.; Chachoua, I.; Pecquet, C.; Vainchenker, W.; Constantinescu, S.N. A P53-JAK-STAT Connection Involved in Myeloproliferative Neoplasm Pathogenesis and Progression to Secondary Acute Myeloid Leukemia. *Blood Rev* **2020**, *42*, 100712, doi:10.1016/j.blre.2020.100712.
235. Chan, M.P.; Plouffe, K.R.; Liu, C.-J.; Palanisamy, N.; Carskadon, S.; Zhao, L.; Nazarian, R.M.; Durham, A.B.; Johnson, T.M.; Andea, A.A.; et al. Next-Generation Sequencing Implicates Oncogenic Roles for P53 and JAK/STAT Signaling in Microcystic Adnexal Carcinomas. *Mod Pathol* **2020**, *33*, 1092–1103, doi:10.1038/s41379-019-0424-4.
236. Cui, D.; Qu, R.; Liu, D.; Xiong, X.; Liang, T.; Zhao, Y. The Cross Talk Between P53 and mTOR Pathways in Response to Physiological and Genotoxic Stresses. *Front Cell Dev Biol* **2021**, *9*, 775507, doi:10.3389/fcell.2021.775507.
237. Tian, T.; Li, X.; Zhang, J. mTOR Signaling in Cancer and mTOR Inhibitors in Solid Tumor Targeting Therapy. *Int J Mol Sci* **2019**, *20*, 755, doi:10.3390/ijms20030755.
238. Golubovskaya, V.M.; Cance, W. Focal Adhesion Kinase and P53 Signal Transduction Pathways in Cancer. *Front Biosci* **2010**, *15*, 901–912.
239. Butti, R.; Das, S.; Gunasekaran, V.P.; Yadav, A.S.; Kumar, D.; Kundu, G.C. Receptor Tyrosine Kinases (RTKs) in Breast Cancer: Signaling, Therapeutic Implications and Challenges. *Molecular Cancer* **2018**, *17*, 34, doi:10.1186/s12943-018-0797-x.
240. Ghosh, A.K.; Boysen, J.; Price-troska, T.; Secreto, C.; Zent, C.S.; Kay, N. Axl Receptor Tyrosine Kinase Signaling Pathway and the P53 Tumor Suppressor Protein Exist In A Novel Regulatory Loop In B-Cell Chronic Lymphocytic Leukemia Cells. *Blood* **2011**, *118*, 799, doi:10.1182/blood.V118.21.799.799.
241. Murai, J.; Yang, K.; Dejsuphong, D.; Hirota, K.; Takeda, S.; D'Andrea, A.D. The USP1/UAF1 Complex Promotes Double-Strand Break Repair through Homologous Recombination. *Mol Cell Biol* **2011**, *31*, 2462–2469, doi:10.1128/MCB.05058-11.
242. Bergink, S.; Jentsch, S. Principles of Ubiquitin and SUMO Modifications in DNA Repair. *Nature* **2009**, *458*, 461–467, doi:10.1038/nature07963.
243. Galanty, Y.; Belotserkovskaya, R.; Coates, J.; Polo, S.; Miller, K.M.; Jackson, S.P. Mammalian SUMO E3-Ligases PIAS1 and PIAS4 Promote Responses to DNA Double-Strand Breaks. *Nature* **2009**, *462*, 935–939, doi:10.1038/nature08657.
244. Huang, T.T.; Nijman, S.M.B.; Mirchandani, K.D.; Galardy, P.J.; Cohn, M.A.; Haas, W.; Gygi, S.P.; Ploegh, H.L.; Bernards, R.; D'Andrea, A.D. Regulation of Monoubiquitinated PCNA by DUB Autocleavage. *Nat Cell Biol* **2006**, *8*, 339–347, doi:10.1038/ncb1378.
245. Nijman, S.M.B.; Huang, T.T.; Dirac, A.M.G.; Brummelkamp, T.R.; Kerkhoven, R.M.; D'Andrea, A.D.; Bernards, R. The Deubiquitinating Enzyme USP1 Regulates the Fanconi Anemia Pathway. *Mol Cell* **2005**, *17*, 331–339, doi:10.1016/j.molcel.2005.01.008.
246. Xu, X.; Li, S.; Cui, X.; Han, K.; Wang, J.; Hou, X.; Cui, L.; He, S.; Xiao, J.; Yang, Y. Inhibition of Ubiquitin Specific Protease 1 Sensitizes Colorectal Cancer Cells to DNA-Damaging Chemotherapeutics. *Frontiers in Oncology* **2019**, *9*.
247. Srinivas, U.S.; Tan, B.W.Q.; Vellayappan, B.A.; Jeyasekharan, A.D. ROS and the DNA Damage Response in Cancer. *Redox Biology* **2019**, *25*, 101084, doi:10.1016/j.redox.2018.101084.

References

248. Perillo, B.; Di Donato, M.; Pezone, A.; Di Zazzo, E.; Giovannelli, P.; Galasso, G.; Castoria, G.; Migliaccio, A. ROS in Cancer Therapy: The Bright Side of the Moon. *Exp Mol Med* **2020**, *52*, 192–203, doi:10.1038/s12276-020-0384-2.
249. Cordani, M.; Butera, G.; Pacchiana, R.; Masetto, F.; Mullappilly, N.; Riganti, C.; Donadelli, M. Mutant P53-Associated Molecular Mechanisms of ROS Regulation in Cancer Cells. *Biomolecules* **2020**, *10*, 361, doi:10.3390/biom10030361.
250. Bost, F.; Decoux-Poullot, A.-G.; Tanti, J.F.; Clavel, S. Energy Disruptors: Rising Stars in Anticancer Therapy? *Oncogenesis* **2016**, *5*, e188–e188, doi:10.1038/oncsis.2015.46.
251. van Gisbergen, M.W.; Offermans, K.; Voets, A.M.; Lieuwes, N.G.; Biemans, R.; Hoffmann, R.F.; Dubois, L.J.; Lambin, P. Mitochondrial Dysfunction Inhibits Hypoxia-Induced HIF-1 α Stabilization and Expression of Its Downstream Targets. *Frontiers in Oncology* **2020**, *10*.
252. Yap, T.A.; Daver, N.; Mahendra, M.; Zhang, J.; Kamiya-Matsuoka, C.; Meric-Bernstam, F.; Kantarjian, H.M.; Ravandi, F.; Collins, M.E.; Francesco, M.E.D.; et al. Complex I Inhibitor of Oxidative Phosphorylation in Advanced Solid Tumors and Acute Myeloid Leukemia: Phase I Trials. *Nat Med* **2023**, *29*, 115–126, doi:10.1038/s41591-022-02103-8.
253. Zhang, X.; Dang, C.V. Time to Hit Pause on Mitochondria-Targeting Cancer Therapies. *Nat Med* **2023**, *29*, 29–30, doi:10.1038/s41591-022-02129-y.
254. Huang, Q.; Raya, A.; DeJesus, P.; Chao, S.-H.; Quon, K.C.; Caldwell, J.S.; Chanda, S.K.; Izpisua-Belmonte, J.C.; Schultz, P.G. Identification of P53 Regulators by Genome-Wide Functional Analysis. *Proceedings of the National Academy of Sciences* **2004**, *101*, 3456–3461, doi:10.1073/pnas.0308562100.
255. Rungay, H.; Arnold, M.; Ferlay, J.; Lesi, O.; Cabasag, C.J.; Vignat, J.; Laversanne, M.; McGlynn, K.A.; Soerjomataram, I. Global Burden of Primary Liver Cancer in 2020 and Predictions to 2040. *Journal of Hepatology* **2022**, *77*, 1598–1606, doi:10.1016/j.jhep.2022.08.021.
256. Casak, S.J.; Marcus, L.; Fashoyin-Aje, L.; Mushti, S.L.; Cheng, J.; Shen, Y.-L.; Pierce, W.F.; Her, L.; Goldberg, K.B.; Theoret, M.R.; et al. FDA Approval Summary: Pembrolizumab for the First-Line Treatment of Patients with MSI-H/dMMR Advanced Unresectable or Metastatic Colorectal Carcinoma. *Clin Cancer Res* **2021**, *27*, 4680–4684, doi:10.1158/1078-0432.CCR-21-0557.

8. Appendix

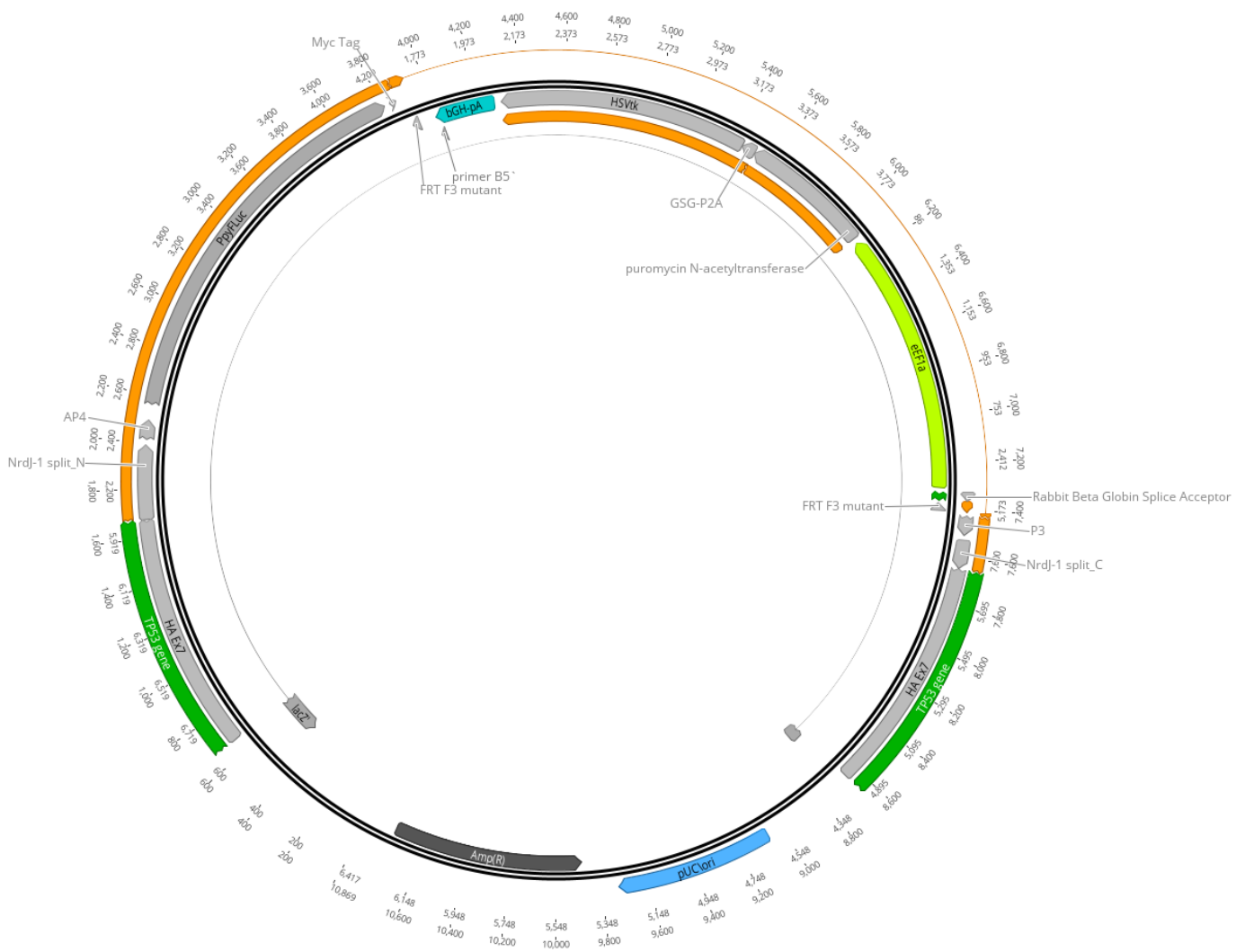
Table 1: Sequences of PCR- and analytical primer

T7 Endonuclease Assay		
Locus	Forward primer	Reverse primer
TP53 coding exon 2	AAGAAGTGCATGGCTGGTGAG	CCTTACCAGAACGTTGTTTTTCAGG
TP53 coding exon 4	AAGACCCAGGTCCAGATGAAG	TAGAGACGAGGTTTCATCATGTTACC
TP53 coding exon 7	ATCGAGACCATCCTGGCTAAC	ATGTGATGAGAGGTGGATGGG
TP53 coding exon 8	TAGGCTCCAGAAAGGACAAGG	TTGTCTTTGAGGCATCACTGC
Genotyping		
TP53 exon 2 (IMPDH-1-CLuc insertion)	AGTCAGATCCTAGCGTCG	ATCCACTCACAGTTTCCATAG
TP53 exon 4 (gp41-1-NLuc insertion)	AAGACCCAGGTCCAGATGAAG	CAAAAGCCAAGGAATACACGTGG
TP53 exon 6 (FLAG-tag insertion)	TCCTTCCTCTCCTACAGTACTC	ATGTGATGAGAGGTGGATGGG
TP53 exon 7 (NrdJ-1-FLuc insertion)	GCAAAGTAAATGGGTTTAACTATTGC	ATGTGATGAGAGGTGGATGGG
TP53 exon 7 to 8 (p53 DBD KO validation)	AAGACCCAGGTCCAGATGAAG	TTGTCTTTGAGGCATCACTGC
cDNA genotyping (transcript validation)		
TP53 exon 2 to 11	AGTCAGATCCTAGCGTCGAG	TGGTTAGTACGGTGAAGTGG
Real-time quantitative PCR (RT-qPCR)		
TP53 Ex2 - Ex4 (FLp53)	AGTCAGATCCTAGCGTCGAG	ATCATCCATTGCTTGGGACG
TP53 Ex4 - Ex5 (FLp53+Δ40p53)	TTCTGTCCCTTCCCAGAAAAC	AACATCTTGTTGAGGGCAGG
TP53 Ex5 - Ex6 (Total p53)	ATCTACAAGCAGTCACAGCAC	TCGGATAAGATGCTGAGGAGG
Homology arm amplification		
TP53 exon 2 (IMPDH-1-CLuc insertion)		
5'HA	AAGTATCAGACAATGTAAGTGCTATG	CAGAGGGGGCTCGACG
3'HA	AGTCAGGAAACATTTTCAGACCTATG	TGAAACAGGCTGGACACGC
TP53 exon 4 (gp41-1-NLuc insertion)		
5'HA	AGTTGTTCTTCCAGAAGCTTTGC	CAGGGGCCAGGAGGG
3'HA	TCATCTTCTGTCCCTTCCCAG	CCTTCCACTCGGATAAGATGC
TP53 exon 6 (FLAG-tag insertion)		
5'HA	TTCCATGAGACTTCAATGCC	TTCCACTCGGATAAGATGCTG
3'HA	GGAAATTTGCGTGTGGAGTATTG	AGTAAGGAAATCAGGTCTACC
TP53 exon 7 (NrdJ-1-FLuc insertion)		
5'HA	TCCTTCCTCTCCTACAGTACTC	GTTACACATGTAGTTGTAGTGGATG
3'HA	AGTTCCTGCATGGGCGGC	TAACACCATCGTAAGTCAAGTAGC
TP53 exon 7 to 8 (p53 DBD KO validation)		
5'HA	TCCTTCCTCTCCTACAGTACTC	GTTACACATGTAGTTGTAGTGGATG
3'HA	AGCACTAAGCGAGGTAAGC	GGAGGGTATAATGAGCTATGATCAC

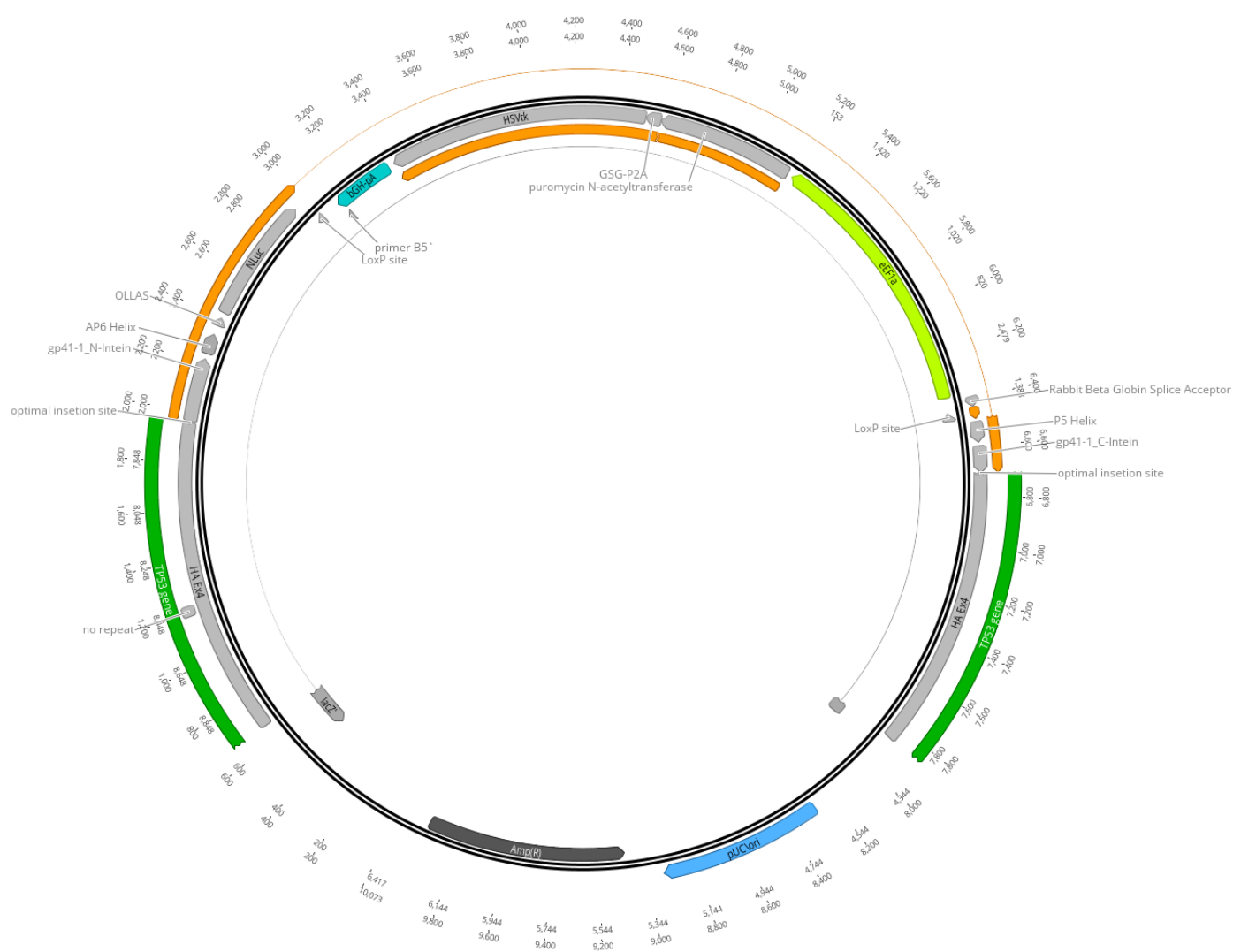
Appendix

Table 2: Sequences of the sgRNA sequences consisting of crRNA, loop and tracrRNA

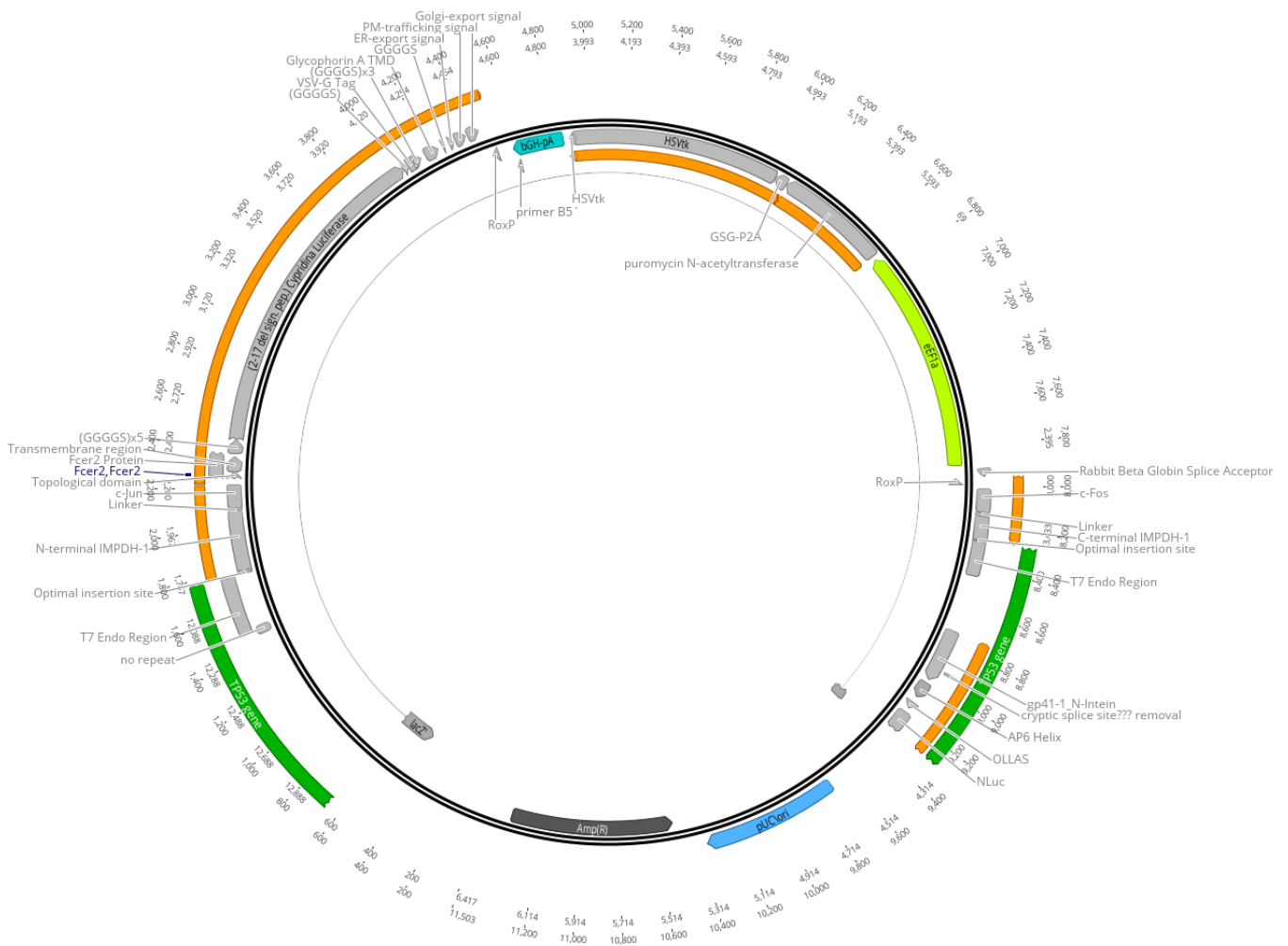
Locus (sgRNA)	crRNA	loop	tracrRNA
TP53 Exon 2 sgRNA 1	CGTCGAGCCCCCTCTGAGTCGTTAAGAGCTA	TGCTG	GAAACAGCATAGCAAGTTTAAA TAAGGCTAGTCCGTTATCAACTTGAAAAAGTGGCACCGAGTCGGTGCT
TP53 Exon 2 sgRNA 2	GAAAATGTTTCCTGACTCAGGTTAAGAGCTA	TGCTG	GAAACAGCATAGCAAGTTTAAAT AAGGCTAGTCCGTTATCAACTTGAAAAAGTGGCACCGAGTCGGTGCT
TP53 Exon 4 sgRNA 1	GAAGGGACAGAAGATGACAGGTTAAGAGCTA	TGCTG	GAAACAGCATAGCAAGTTTAA ATAAGGCTAGTCCGTTATCAACTTGAAAAAGTGGCACCGAGTCGGTGCT
TP53 Exon 4 sgRNA 2	GGGAAGGGACAGAAGATGACGTTAAGAGCTA	TGCTG	GAAACAGCATAGCAAGTTTAA ATAAGGCTAGTCCGTTATCAACTTGAAAAAGTGGCACCGAGTCGGTGCT
TP53 Exon 6 sgRNA 1	CAGCATCTTATCCGAGTGGAGTTAAGAGCTA	TGCTG	GAAACAGCATAGCAAGTTTAAA TAAGGCTAGTCCGTTATCAACTTGAAAAAGTGGCACCGAGTCGGTGCT
TP53 Exon 7 sgRNA 1	CCGGTTCATGCCGCCCATGCGTTAAGAGCTA	TGCTG	GAAACAGCATAGCAAGTTTAAA TAAGGCTAGTCCGTTATCAACTTGAAAAAGTGGCACCGAGTCGGTGCT
TP53 Exon 7 sgRNA 2	CATGTGTAACAGTTCCTGCAGTTAAGAGCTA	TGCTG	GAAACAGCATAGCAAGTTTAAAT AAGGCTAGTCCGTTATCAACTTGAAAAAGTGGCACCGAGTCGGTGCT
TP53 Exon 7 sgRNA 3	ATGTGTAACAGTTCCTGCATGTTAAGAGCTA	TGCTG	GAAACAGCATAGCAAGTTTAAAT AAGGCTAGTCCGTTATCAACTTGAAAAAGTGGCACCGAGTCGGTGCT
TP53 Exon 8 sgRNA 1	CTCACCACGAGTGCCCCCAGTTAAGAGCTA	TGCTG	GAAACAGCATAGCAAGTTTAAA TAAGGCTAGTCCGTTATCAACTTGAAAAAGTGGCACCGAGTCGGTGCT
TP53 Exon 8 sgRNA 2	TTACCTCGCTTAGTGCTCCCGTTAAGAGCTA	TGCTG	GAAACAGCATAGCAAGTTTAAAT AAGGCTAGTCCGTTATCAACTTGAAAAAGTGGCACCGAGTCGGTGCT



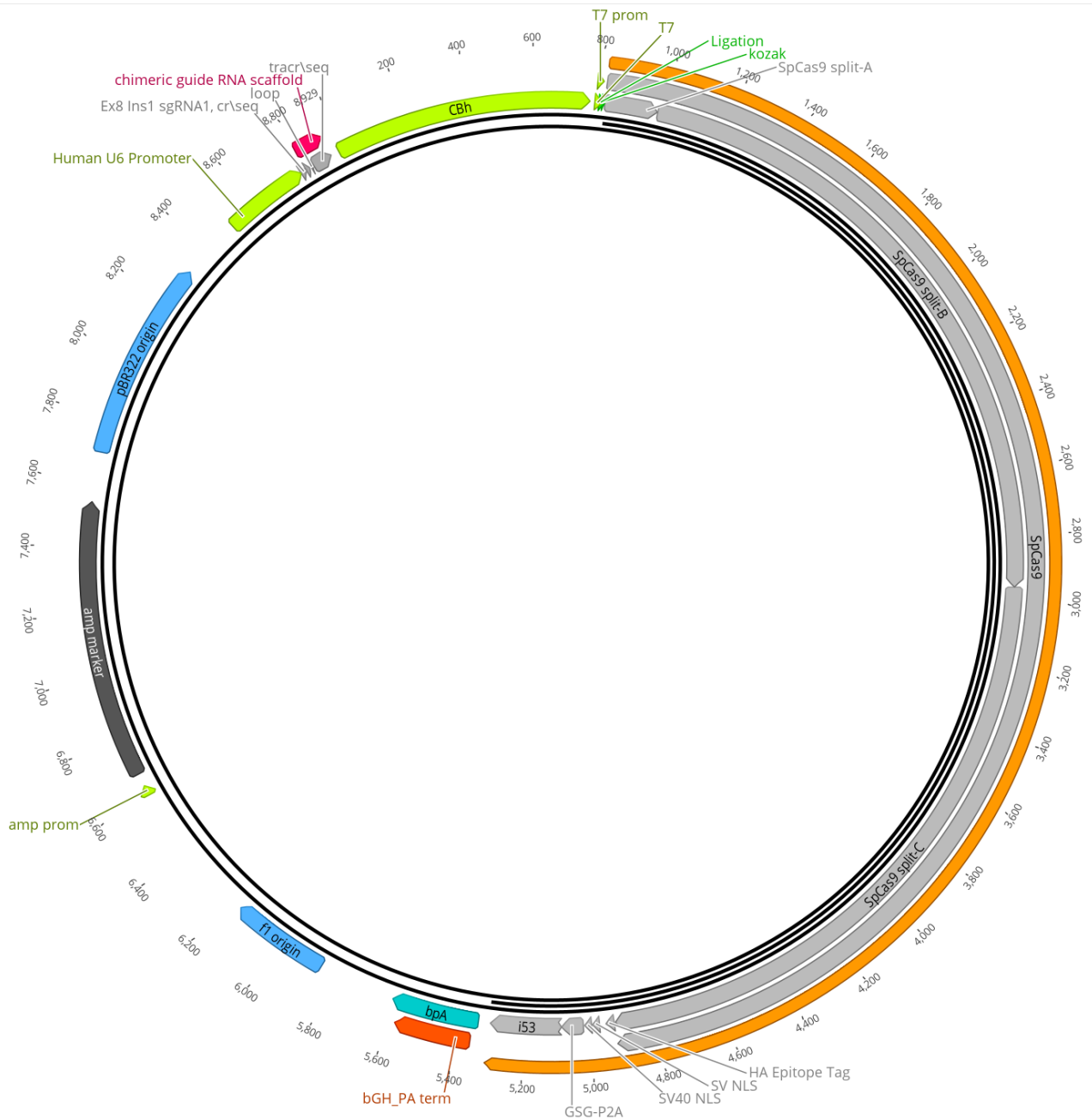
Supplementary Fig. 1: Schematic of the donor plasmid carrying the coding sequence for the EXSISERS reporter *NrdJ1-FLuc* (*PpyFLuc* = *Photinus pyralis* firefly luciferase). The EXSISERS reporter is disrupted by the selection cassette consisting of puromycin-N-acetyltransferase (*PuroR*) and Herpes simplex virus thymidine kinase (*HSVtk*) driven by *eF1 α* promoter. Green annotations depict the 5' and 3' homology arms containing the upstream and downstream sequences of the *TP53* exon 7 loci (obligatory for knock-in via Cas9-mediated DNA-double strand break and subsequent homologous direct repair). Lighter green = promoter, darker green = genome locus, lighter blue = transcription termination site, grey = functional domains and proteins, orange = open reading frame, darker blue = origin of replication, darker grey = ampicillin resistance gene.



Supplementary Fig. 2: Schematic of the donor plasmid carrying the coding sequence for the EXSISERS reporter gp41-1-NLuc. The EXSISERS reporter is disrupted by the selection cassette consisting of puromycin-N-acetyltransferase (PuroR) and Herpes simplex virus thymidine kinase (HSVtk) driven by eF1 α promoter. Green annotations depict the 5' and 3' homology arms containing the upstream and downstream sequences of the *TP53* exon 7 loci (obligatory for knock-in via Cas9-mediated DNA-double strand break and subsequent homologous direct repair). Lighter green = promoter, darker green = genome locus, lighter blue = transcription termination site, grey = functional domains and proteins, orange = open reading frame, darker blue = origin of replication, darker grey = ampicillin resistance gene.



Supplementary Fig. 3: Schematic of the donor plasmid carrying the coding sequence for the EXSISERS reporter IMPDH-1-CLuc, also including the start- and stop-transfer signals for ER- and plasma membrane anchoring, as well as an ER-export-, golgi-export- and plasma membrane trafficking-signal. The EXSISERS reporter is disrupted by the selection cassette consisting of puromycin-N-acetyltransferase (PuroR) and Herpes simplex virus thymidine kinase (HSVtk) driven by eF1 α promoter. Green annotations depict the 5' and 3' homology arms containing the upstream and downstream sequences of the *TP53* exon 7 loci (obligatory for knock-in via Cas9-mediated DNA-double strand break and subsequent homologous direct repair). Lighter green = promoter, darker green = genome locus, lighter blue = transcription termination site, grey = functional domains and proteins, orange = open reading frame, darker blue = origin of replication, darker grey = ampicillin resistance gene.



Supplementary Fig. 4: Schematic of the mammalian expression plasmid coding *Streptococcus pyogenes* Cas9 protein and the HDR-enhancer i53 protein, which both are translationally separated by a p2A peptide. The constitutive transcription is driven by a CBh promoter. Furthermore, this plasmid contains a transcription unit for the corresponding sgRNA, which is driven by a U6 promoter and terminated by 6xT. Lighter green = promoter, lighter blue = transcription termination site, grey = functional domains of proteins and RNA molecules, pink = chimeric guide RNA scaffold, orange = open reading frame, darker blue = origin of replication, darker grey = ampicillin resistance gene.

```

import openpyxl
# Function to split and count pathways in a cell
def process_cell(cell_value, pathway_counts):
    pathways = cell_value.split(";")
    for pathway in pathways:
        pathway = pathway.strip() # Remove leading/trailing spaces
        pathway_counts[pathway] = pathway_counts.get(pathway, 0) + 1

# Function to analyze an Excel file
def analyze_excel(input_file_path, output_file_path):
    workbook = openpyxl.load_workbook(input_file_path)
    sheet = workbook.active

    # Initialize pathway counts
    pathway_counts = {}

    row = 8 # Start from row 8 in column F
    while True:
        cell = sheet.cell(row=row, column=6) # Column F

        if cell.value is None or cell.value == "":
            break # Stop when an empty cell is encountered

        process_cell(cell.value, pathway_counts)
        row += 1

    # Create a new Excel file to store the results
    result_workbook = openpyxl.Workbook()
    result_sheet = result_workbook.active
    result_sheet.append(["Pathway", "Abundance"])

    # Write the pathway counts to the new file
    for pathway, count in pathway_counts.items():
        result_sheet.append([pathway, count])

    # Save the new file
    result_workbook.save(output_file_path)

if __name__ == "__main__":
    input_file_path = input("Enter the path and name of the Excel file to
be analyzed: ")
    output_file_path = input("Enter the path and name for the new Excel
file: ")

    analyze_excel(input_file_path, output_file_path)
    print(f"Analysis completed. Results saved to '{output_file_path}'")

```

Supplementary Fig. 5: Python script that counts the pathway abundance for all compounds listed within an Excel sheet. For comparative purposes, we counted the pathway abundance for the whole anti-cancer compound library and for two Excel sheets that list either the p53-TIE or p53-OIEs compounds. Prerequisite for a working count with this specific script is the first compound starting in row 8 and the pathways listed in column F of an Excel sheet. This script creates a new Excel sheet showing all pathways with their respective absolute abundance.

9. Declaration of Independence

I, Tümen Deniz, born on the 19th of November 1993 in Bad Säckingen, Germany, hereby declare that I have independently prepared the present work without improper assistance from third parties and without the use of any materials other than those indicated.

Data and concepts obtained directly or indirectly from other sources are indicated with the respective source. In particular, I have not sought or received any paid assistance from intermediary or advisory services.

The work has not been submitted in identical or similar form to any other examining authority in Germany or abroad.

Location, Date

Signature

10. Acknowledgement

I want to express my heartfelt gratitude to the following individuals for their invaluable contributions and unwavering support throughout my doctoral journey.

First and foremost, I extend my deepest appreciation to my doctoral supervisor, **PD. Dr. Karsten Gülow** for his exceptional guidance, leadership, and dedication to the project. I wouldn't have reached my current academic standing without his invaluable expertise. His readiness to listen, consistent support during challenging times, and the wealth of knowledge he has shared with me, have profoundly impacted my academic and personal growth.

I sincerely thank **Prof. Dr. Martina Müller-Schilling** for warmly welcoming me into the research group and for her continuous support throughout my doctoral work. Her tireless encouragement to visit (inter-)national conferences to exchange my knowledge with scientific and medical peers has been invaluable. I appreciate the privilege of being a part of the research group of Internal Medicine 1 and the opportunity to represent exceptional research throughout the years.

Prof. Dr. Herbert Tschochner deserves profound recognition for years of mentorship and guidance. As a respected scientist and mentor, he has been instrumental in this project's constructive advancement.

PD. Dr. Claudia Kunst merits immense appreciation for her remarkable project supervision. Her support, advice, and tireless assistance during every stage of the project, from interim reports to the final dissertation, have been instrumental to my success.

I am grateful to **Prof. Dr. Gil Gregor Westmeyer** and **Dr. Dong-Jiunn Jeffery Truong** for their knowledge and skills, which have enriched my doctoral journey. Their trust in me, particularly in handling the EXSISERS technology before its initial publication, laid the foundation for our interdisciplinary collaboration. I also deeply value their contributions and wish them the best in their future endeavors.

I am grateful to **Prof. Dr. Peter Oefner** for his valuable expertise and scientific contributions. His open-door policy and support as the graduate committee chair were pivotal during the final stages of my doctoral journey.

I thank **Prof. Dr. Anja Wege** for her support and relevant questions during scientific colloquia and the finalization of my doctoral thesis.

Lisa Aschenbrenner, you have been an unwavering presence in my academic journey. You stood by my side from day one, enriching my professional and personal life. You witnessed the highs and lows, celebrated my successes, and shared my challenges. Your steadfast support has left an indelible mark on my journey, no matter the workload. The extent of her contributions and support are inexpressible in words. Thank you for everything!

The team has played a crucial role in creating a warm, supportive, collaborative atmosphere. The camaraderie and unity in this environment were exceptional. I thank **Manuela Peisl-Gunckel** for her guidance and invaluable advice in organoid culturing and treatment. Her words, "You can either stumble or rise over the stones in your path; it's your decision," will forever remain etched in my memory. I extend my gratitude to **Kirstin Pollinger**, the FACS Diva, for her experimental assistance, especially in the final stages of my doctoral thesis. **Heidi Gschwendtner** especially enhanced my knowledge about RNA handling. In this context, she greatly contributed to my gain of knowledge. Also, she brightened my lab days with her warmth and happy spirits. **Martina Meisinger**, who may always have believed her contributions would go unnoticed, has significantly simplified the work of everyone in this research group. She is indeed a valuable asset. A true gem. I would also like to thank **Marika Haderer**, **Marlen Michalski**, and **Fabian Hölzl** for the unforgettable days of enjoyment, motivation, and mutual support.

A heartfelt thanks to the many **interns** from the Molecular Medicine master's program and the medical **doctoral students** I had the privilege of mentoring. Special thanks to Barbara Volz, Versuschka Albert, and Katja Neumeyer for their contributions.

I appreciate the entire clinical team for their medical and scientific expertise. In particular, I thank **Prof. Dr. Arne Kandulski** for providing biopsies from endoscopy and **Dr. Sophie Schlosser-Hupf** for her outstanding organization of conference visits.

I also thank **Dr. Florian Sigloch** from Polyquant for our pleasant and reliable collaboration. The mass spectrometric measurements significantly enriched the project.

I want to acknowledge the **AG Rehli research group** for their generous use of laboratory equipment.

The countless FACS sorting afternoons with **Irina Fink** are cherished memories. I wish her all the best for her future.

My family deserves a very special mention. **My parents** and **my sister** provided unwavering warmth, support, and understanding throughout the journey. I am deeply grateful for the emotional encouragement. To my beloved **wife**, I owe the strength, fortitude, and courage I consistently had to maintain. You have been my steadfast companion through every phase of this journey. No matter where the path ahead leads us, we can fearlessly confront any challenge with you by my side.



Deniz Tümen

Curriculum vitae (German)

Akademischer Werdegang

Promotion

Seit 2019

- Universitätsklinikum Regensburg, Innere Medizin 1
- Angestrebter akademischer Titel: Dr. rer. physiol.
- Thema: CRISPR/Cas9 basierte Gen-Editierung der p53-Familie

Studium

Masterstudium in Biochemie 2016 - 2018

- Technische Universität München
- Masterarbeit: Am Helmholtz-Zentrum München, Institut für Synthetische Biomedizin, Note: 1.0
- Abschlussnote: 1.3

Bachelorstudium in Molekulare Biotechnologie 2012 - 2016

- Technische Universität München
- Bachelorarbeit: Am Helmholtz-Zentrum München, Institut für strukturelle Biologie, Note: 1.7
- Abschlussnote: 2.1

Berufserfahrung / Praktika

- Roche Diagnostics GmbH, Abteilung für Enzyme-Engineering, Penzberg 2018
- Deutsches Zentrum für neurodegenerative Erkrankungen, LMU, München 2017
- Helmholtz-Zentrum München, Institut für Entwicklungsgenetik 2016

Mitgliedschaften

- Deutsche Gesellschaft für Innere Medizin seit 2022
- Gesellschaft für Biochemie und Molekularbiologie seit 2018
- Graduiertenprogramm BIOMEDIGS seit 2019

Zusatzqualifikationen

- 5-Euro Business – Praxisorientierte Existenzgründung 2023
- Python-Programmierung, Universität Regensburg 2022
- Scientific Writing, Uniklinikum Regensburg (UKR) 2021
- Mikroskopie-Kurs Zeiss, Freising 2020
- Versuchstierkunde und Tierschutz, FELASA, UKR 2019



Geboren:
am 19. Nov. 1993
in Bad Säckingen



Beruflich:
+49 941/944-17173
Privat:
+49 1577 0411198



deniz.tuemen@ukr.de



Paarstraße 72
93059 Regensburg



Sprachen

Deutsch ● ● ● ● ●

Bulgarisch ● ● ● ● ●

Englisch ● ● ● ● ●

Spanisch ● ● ● ○ ○

Französisch ● ● ○ ○ ○



EDV-Kenntnisse

MS Office ● ● ● ● ●

MS Excel ● ● ● ● ●

Powerpoint ● ● ● ● ●

Graph. Prism ● ● ● ● ●

Inkscape ● ● ● ● ●

Autodesk Fusion ● ● ● ● ●

Python ● ● ● ○ ○

Blender ● ● ● ○ ○

Forschungsprojekte

aktuell

- Entwicklung eines neuen Exon-spezifischen Reporter-systems zur Echtzeit-Analyse differenzieller Protein Isoform-Expressionen von p53

aktuell

- Genomweites CRISPR/Cas9 Knockout Screening zur Identifizierung Gen abhängiger Resistenzentwicklungen in kutanen T Zellymphomen bei DMF – Behandlung

aktuell

- P53 Knockout induzierte Inaktivierung der Flippase und Plasmamembran-Exposition von Phosphatidylserin – Ein neuer Mechanismus der Immunevasion von Tumoren?

aktuell

- Neuartige Strategie zur Unterscheidung von gesundem und tumorösem Gewebe durch Erkennung spezifischer DNA-Methylierungsmuster

Konferenzbesuche

Okt. 2023

- United European Gastroenterology – Poster – **Copenhagen**

Jan. 2023

- German Association of the Study of the Liver – Poster Präsentation – **Bochum**

Nov. 2022

- American Association for the Study of the Liver – Poster Präsentation – **Washington D.C.**

Okt. 2022

- United European Gastroenterology – Vortrag – **Wien**

Sep. 2022

- RIGeL Summerschool – Poster Präsentation

Sep. 2022

- Deutsche Gesellschaft für Gastroenterologie, Verdauungs- und Stoffwechselkrankheiten – Vortrag – **Hamburg**

Mai 2022

- Gesellschaft für Gastroenterologie in Bayern – Posterpräsentation – **Freising**

Apr. 2022

- Deutsche Gesellschaft für Innere Medizin – „Young Investigator Award“- **Vortrag – Wiesbaden**

Jan. 2022

- German Association of the Study of the Liver – **Vortrag – Heidelberg**

Preise / Auszeichnungen

Jul. 2023

- Erster Platz – 5-Euro Business Existenzgründung

Apr. 2023

- Wissenschaftlicher Posterpreis – DGIM

Mai. 2022

- Wissenschaftlicher Posterpreis – GFGB

Apr. 2022

- Nominierung für “Young Investigator Award” – DGIM

Anträge

aktuell

- Ethikantrag, Epigenetische Untersuchungen des Darmepithels zur Entwicklung Tumor-spezifischer Therapien, in Bearbeitung

Nov. 2022

- Wilhelm-Sander-Stiftung, Drittmittel, Mit Antragsteller

Jul. 2022

- S2-Antrag, „Rescuing“ von mutiertem p53 in Model-Zelllinien des CRC und HCC, Mit Antragsteller

Okt. 2020

- S2-Antrag, Genomweite CRISPR/Cas9 Knockout Studien in kutanen T-Zell Lymphozyten, Mit Antragsteller

12. Publications

Articles

- 1) **Deniz Tümen**, Dong Jiunn Jeffery Truong, Barbara Volz, Katja Neumeyer, Veruschka Albert, Jan P. Teubner, Patricia Mester Pavel, Mara Kießling, Katrin Heider, Carl Philipp Schilling⁴, Elisabeth Aschenbrenner, Manuela Gunckel, Kirstin Pollinger, Claudia Kunst, Stephan Schmid, Arne Kandulski, Herbert Tschochner, Peter J. Oefner, Gil Gregor Westmeyer, Karsten Gülow and Martina Müller. Non-invasive high-throughput monitoring of exon-specific p53 isoform expression via EXSISERS to identify novel therapeutic options for colorectal cancer, **in process**, planned journal: Nature Biotechnology
- 2) Truong, Dong-Jiunn Jeffery; Phlairaharn, Teeradon; Eßwein, Bianca; Gruber, Christoph; **Tümen, Deniz**; Baligács, Enikő, et al. (2021): Non-invasive and high-throughput interrogation of exon-specific isoform expression. In: Nature Cell Biology 23 (6), S. 652–663. DOI: 10.1038/s41556-021-00678-x.
- 3) Michalski M, Bauer M, Walz F, **Tümen D**, Heumann P, Stöckert P, Gunckel M, Kunst C, Kandulski A, Schmid S, Müller M, Gülow K. Simultaneous Inhibition of Mcl-1 and Bcl-2 Induces Synergistic Cell Death in Hepatocellular Carcinoma. Biomedicines. 2023 Jun 8;11(6):1666. doi: 10.3390/biomedicines11061666 Titel anhand dieser DOI in Citavi-Projekt übernehmen. PMID: 37371761; PMCID: PMC10295989.
- 4) Gisela Wölfel, Elisabeth Ostheim, Agnes Staub, **Deniz Tümen**, Philipp Heumann, Stephan Schmid, Sophie Schlosser, Martina Muller, Karsten Gülow, Claudia Kunst (2023): The p53 family of transcription factors represses the alpha-fetoprotein (AFP) gene expression in hepatocellular carcinoma (HCC); accepted, J Gastrointestin Liver Dis.

Reviews

- 5) **Tümen Deniz**, Philipp Heumann, Karsten Gülow, Cagla-Nur Demirci, Lidia-Sabina Cosma, Martina Müller, and Arne Kandulski. 2022. "Pathogenesis and Current Treatment Strategies of Hepatocellular Carcinoma" Biomedicines 10, no. 12: 3202. <https://doi.org/10.3390/biomedicines10123202>
- 6) Schlosser Sophie, **Tümen Deniz**, Volz Barbara, Neumeyer Katja, Egler N, Kunst Claudia, Tews Hauke C., Schmid Stefan, Kandulski Arne, Müller Martina and Gülow Karsten (2022) HCC biomarkers – state of the old and outlook to future promising biomarkers and their potential in everyday clinical practice. Front. Oncol. 12:1016952. doi: 10.3389/fonc.2022.1016952

- 7) Kunst C, Schmid S, Michalski M, **Tümen D**, Buttenschön J, Müller M, Gülow K. The Influence of Gut Microbiota on Oxidative Stress and the Immune System. *Biomedicines*. 2023 May 8;11(5):1388. doi: 10.3390/biomedicines11051388; PMID: 37239059; PMCID: PMC10216031.

Congress participations

- 8) **Tümen, D.**; T., D.J.J.; Volz, B.; Aschenbrenner, E.; Teubner, J.P.; Neumeyer, K.; Gunckel, M.; Pollinger, K.; Mester-Pavel, P.; Michalski, M.; Albert, V.; Kunst, C.; Gülow, K.; Müller-Schilling, M. Neues Exon-Spezifisches Isoform-Expressions Reporter System (EXSISERS) zur Hochdurchsatz-Quantifizierung von p53 Protein Isoformen in Echtzeit und in lebenden Zellen. *Deutsche Gesellschaft für Gastroenterologie (DGVS). Zeitschrift für Gastroenterol* 2023, 61, KV179, doi:10.1055/s-0043-1771877.
- 9) Neumeyer, K.; **Tümen, D.**; Aschenbrenner, E.; Kunst, C.; Kandulski, A.; Gülow, K.; Müller-Schilling, M. p53 – ein neuer Regulator für periphere Toleranz und Immunevasion beim kolorektalen Karzinom. *Deutsche Gesellschaft für Gastroenterologie (DGVS). In Proceedings of the Zeitschrift für Gastroenterologie; Georg Thieme Verlag, August 2023; Vol. 61, p. KV228.*
- 10) Seubert, M.; Volz, B.; **Tümen, D.**; Aschenbrenner, E.; Kunst, C.; Müller-Schilling, M.; Gülow, K. Ein neues Reportersystem zur Detektion von Zellen des kolorektalen Karzinoms anhand spezifischer Gen-Methylierungsmuster. *Deutsche Gesellschaft für Gastroenterologie (DGVS). In Proceedings of the Zeitschrift für Gastroenterologie; Georg Thieme Verlag, August 2023; Vol. 61, p. KV223.*
- 11) **Deniz Tümen**, Dong-Jiunn Jeffery Truong, Barbara Volz, Elisabeth Aschenbrenner, Jan-Peter Teubner, Katja Neumeyer, Manuela Gunckel, Patricia Mester, Veruschka Albert, Claudia Kunst, Karsten Gülow and Martina Müller-Schilling. Exon-specific isoform expression reporter systems (EXSISERS) – A novel system to monitor differential p53 protein-isoform expression in response to tumor-specific treatment. *Deutsche Gesellschaft für Innere Medizin (DGIM) 2023, Springer Verlag.*
- 12) Katja Neumeyer, **Deniz Tümen**, Elisabeth Aschenbrenner, Arne Kandulski, Claudia Kunst, Karsten Gülow und Martina Müller-Schilling. Eine neue Rolle von p53 in der Immunerkennung maligner Tumore – Induktion peripherer Toleranz am Beispiel des kolorektalen Karzinoms. *Deutsche Gesellschaft für Innere Medizin (DGIM) 2023, Springer Verlag.*
- 13) **Deniz Tümen**, Barbara Volz , Elisabeth Aschenbrenner , Jan-Peter Teubner , Katja Neumeyer, Manuela Gunckel , Kirstin Pollinger , Dong-JiunnJeffery Truong , Patricia Mester-Pavel , Veruschka Albert , Claudia Kunst , Karsten Gülow , Martina Müller-

Schilling (2023) Exon-specific isoform expression reporter systems (EXSISERS) – A novel reporter to monitor differential p53 protein-isoform expression in response to tumor-specific treatments. German Association of the Liver (GASL). Zeitschrift für Gastroenterologie. doi: 10.1055/s-0042-1760017

- 14) **Deniz Tümen**, Elisabeth Aschenbrenner, Barbara Volz, Jan-Peter Teubner, Katja Neumeyer, Manuela Gunckel, Kirstin Pollinger, Patricia Mester-Pavel, Marlen Michalski, Veruschka Albert, Dong-JiunnJeffery Truong, Claudia Kunst, Karsten Gülow, Martina Müller-Schilling (2023) Echt-Zeit-Quantifizierung von p53-Protein-Isoformen im Hochdurchsatz-Verfahren mit einem neuem Exon-spezifischen Luciferase-Reportersystem. Gesellschaft für Gastroenterologie in Bayern (GFGB). Zeitschrift für Gastroenterologie. doi: 10.1055/s-0043-1764087

- 15) Katja Neumeyer, **Deniz Tümen** , Elisabeth Aschenbrenner , Claudia Kunst , Arne Kandulski , Karsten Gülow , Martina Müller-Schilling (2023) Eine neue Rolle für p53 in der Induktion peripherer Toleranz beim Hepatozellulären und Kolorektalen Karzinom. Gesellschaft für Gastroenterologie in Bayern (GFGB). Zeitschrift für Gastroenterologie. doi: 10.1055/s-0043-1764088

- 16) **Deniz Tümen** , E Aschenbrenner , B Volz , D-JJ Truong , C Kunst , K Gülow , M Müller-Schilling (2022) Neuartiges Exon-spezifisches Reportersystem zur Quantifizierung von p53-Protein-Isoformen in Echtzeit in lebenden Zellen. Deutsche Gesellschaft für Gastroenterologie (DGVS). Zeitschrift für Gastroenterologie. doi: 10.1055/s-0042-1754893

- 17) **Deniz Tümen** , Jan-Peter Teubner , Elisabeth Aschenbrenner , Karsten Gülow , Martina Müller-Schilling (2022) Introduction of an novel exon-specific isoform expression reporter system (EXSISERS) into p53 for the study of differential protein-isoform expression. Gesellschaft für Gastroenterologie in Bayern (GFGB). Zeitschrift für Gastroenterologie. doi: 10.1055/s-0041-1740758

- 18) **Deniz Tümen** , Elisabeth Aschenbrenner , Jan-Peter Teubner , Dong-JiunnJeffery Truong , Claudia Kunst , Karsten Gülow , Martina Müller-Schilling (2022) Introduction of a novel triple intein-luciferase assay for real-time detection of differential protein isoforms by the example of the tumor suppressor p53. German Association of the Liver (GASL). Zeitschrift für Gastroenterologie. doi: 10.1055/s-0042-1745672

- 19) Jan Peter Teubner; **Deniz Tümen**; Elisabeth Aschenbrenner; Karsten Gülow; Martina Müller-Schilling (2022) Genomweites-CRISPR/Cas9 Knock-out Screening zur Identifizierung genabhängiger DMF-Resistenzen beim kutanen T-Zell-Lymphom. Deutsche Gesellschaft für Innere Medizin (DGIM), Springer Verlag.

- 20) **Deniz Tümen**, Elisabeth Aschenbrenner, Jan-Peter Teubner, Dong-Jiunn Jeffery Truong, Claudia Kunst, Karsten Gülow, Martina Müller-Schilling (2022) Entwicklung eines neuen Exon-spezifischen Reportersystems zur Echtzeit-Analyse differenzieller Protein Isoform-Expressionen am Beispiel von p53. Deutsche Gesellschaft für Innere Medizin (DGIM), Springer Verlag.
- 21) **D. Tümen**, B. Volz, E. Aschenbrenner, D.-J.J. Truong, C. Kunst, K. Gülow, M. Müller-Schilling (2022) Novel exon-specific reporter system for live-cell quantification of p53 protein isoforms in real-time. United European Gastroenterology (UEG). Journal of the United European Gastroenterology. doi: <https://doi.org/10.1002/ueg2.12293>
- 22) **Deniz Tümen**, Barbara Volz, Elisabeth Aschenbrenner, Dong-Jiunn Jeffery Truong, Claudia Kunst, Karsten Gülow and Martina Mueller-Schilling (2022) Introduction of a novel exon-specific isoform expression reporter system to analyze in real-time treatment-dependent induction of various p53 isoforms. American Association for the Study of the Liver (AASLD). Hepatology. doi: <https://doi.org/10.1002/hep.32697>
- 23) J. Teubner, **D. Tümen**, E. Aschenbrenner, M. Müller-Schilling, K. Gülow (2021) Genome-wide CRISPR/Cas9 knockout screening for the identification of critical resistance drivers in dimethyl fumarate treated tumors. United European Gastroenterology (UEG). Journal of the United European Gastroenterology. doi: <https://doi.org/10.1002/ueg2.12144>